Quantification and regionalization of geomorphic processes using spatial models and high-resolution topographic data: A sediment budget of the Upper Kauner Valley, Ötztal Alps.

by

Ludwig Hilger

A Dissertation Presented in Partial Fulfillment
Of the Requirements for the Degree
Dr. rer. nat.

at

Faculty of Mathematics and Geography
Catholic University of Eichstätt-Ingolstadt
Germany 2017

Submitted on: 09.01.2017
Date of the oral examination: 24.05.2017

Faculty Mentor and Chair: Prof. Dr. Michael Becht
Committee Member: PD Dr. Tobias Heckmann

Statement of originality
The work contained in this thesis has not been previously submitted for a degree or diploma at any other higher education institution. To the best of my knowledge and belief, the thesis contains no material previously published or written by another person except where due references are made.

_____ Eichstätt, _____

Signature Date

To my parents

Contents

List of Figures

List of Tables

List of acronyms and mathematical symbols

Acronyms

a.s.l. above sea level

ASCII American Standard Code for Information Interchange

BEV Bundesamt für Eich- und Vermessungswesen

CDF Cumulative Distribution Function

CIT Channel Initiation Threshold

CRS Coordinate Reference System

CS Coordinate System

DEM Digital Elevation Model

DFG Deutsche Forschungsgemeinschaft

dGPS differential Global Positioning System

DGSD Deep-seated Gravitational Slope Deformation

DJF December, January, February

DoD DEM of Difference

DPR Debris fall Production Rate

DSM Digital Surface Model

DTM Digital Terrain Model

EGNOS European Geostationary Navigation Overlay Service

EPOSA Echtzeit Positionierung Austria

ER Erosion Rate

ERT Electric Resistivity Tomography

ESRI Environmental Systems Research Institute

ETRS89 European Terrestrial Reference System 1989

FOV Field Of View

FWF Fonds zur Förderung der wissenschaftlichen Forschung

GCP Ground control point

GIS Geographic Information System

GNSS Global Navigation Satellite System

GPU Geomorphological Process Unit

GUI Graphical User Interface

h.a.e. height above ellipsoid

HCA Hydrological Contributing Area

ICP Iterative Closest Point

IDW Inverse Distance Weighting

IMCORR image correlation (software)

INS Inertial Navigation System

JJA June, July, August

LAN Local Area Network

LIA Little Ice Age

LiDAR Light Detection And Ranging

LIS Laser Information System

LoD Level of Detection

LSP Land Surface Parameter

MSA Multi Station Adjustment

N/A not available

NCA Northern Calcareous Alps

NIR Near Infrared

PC Personal Computer

PDF Probability Density Function

PhD Doctor of Philosophy

PPA Principal Point of Autocollimation

PPS Principal Point of Symmetry

RAM Random-Access Memory

RBF Radial Basic Functions

RMSE Root Mean Square Error

RTK Real Time Kinematic

SAGA System for Automated Geoscientific Analyses

SCA Sediment Contributing Area

SfM Structure from Motion

SSD Solid State Disk

STA Sediment Transporting Avalanche

TIN Triangulated Irregular Network

TIWAG Tiroler Wasserkraft AG

TLS Terrestrial Laser Scanning

UAV Unmanned Aerial Vehicle

UTM Universal Transverse Mercator

WLAN Wireless Local Area Network

Mathematical symbols and physical units (global meaning in this thesis)

α slope inclination [°]

β scaling exponent of the tail of the probability density function describing the magnitude-frequency relationship of mass wasting processes ($\beta > 0$)

β_0 regression intercept in linear regression of log_{10} transformed data for power law estimation of the planimetric area - volume relationship.

β_1 regression slope in linear regression of log_{10} transformed data for power law estimation of the planimetric area - volume relationship.

β_{thres} slope threshold of the rock fall process path model [°]

β_{ff} free fall threshold of the rock fall runout length model [°]

$\delta(z)$ Surface representation uncertainty in DEMs [m]

ϵ random error term in linear regression of log_{10} transformed data for power law estimation of the planimetric area - volume relationship.

η slope of the magnitude-frequency cumulative distribution function of mass wasting processes ($\beta - 1$)

γ exponent of power-law volume-area relationship

λ rate of sediment loss in the paraglacial sediment exhaustion model

μ_{rfm} friction coefficient of the rock fall runout length model

ν factor in power-law volume-area relationship

ρ persistence factor for the rock fall process path model

σ_{simple} p

σ_{DTM1} elevation uncertainty of DTM at timeslice t = 1 when differencing two DTMs [m]

σ_{DTM2} elevation uncertainty of DTM at timeslice t = 2 when differencing two DTMs [m]

σ_{DTM} standard deviation of cell differences in a DoD calculated from two point clouds of the same surface acquired under unchanged conditions. Approximation for $\delta(z)$.

σ_{sig} overall level of detection. DoD value below the absolute value of which all DoD values are considered as errors

σ_v	error in volume calculation (propagated from the individual errors of each DTM)
φ	vertical angle in a TLS device's own coordinate system
ϑ	horizontal angle in a TLS device's own coordinate system
a	dispersion exponent of the rock fall process path model
A_s	specific catchment area [m m^{-2}]
A_{sc}	sediment contributing area in equation 6.4.1
A_{sf}	area of slope failure depositional/erosional area [m^2]
C	normalization constant in magnitude-frequency relationships of mass wasting processes
c	speed of light in vacuum ($299\,792\,458\,m\,s^{-1}$)
d	grid cell size [m]
d_b	average bedrock density [t m^{-3}]
e	Euler's constant
L	catchment lowering rate [m yr^{-1}]
l	liter
M/D	mass-to-drag ratio of the rock fall range model
M_{sca}	mean yearly sediment yield from hill slope channels
n	number of cells with valid values in both DTMs during DoD calculation
Q_D	fluvial dissolved load sediment discharge at catchment outlet [t m^{-2} yr^{-1}]
Q_S	fluvial solid load sediment discharge at catchment outlet [t m^{-2} yr^{-1}]
r	correlation coefficient in correlation and regression analysis
R^2	coefficient of determination in correlation and regression analysis
R_{min}	vertical resolution of a LiDAR device. Minimum distance two targets need to be separated within an laser footprint to be discernible as two separate objects [m]
S_0	sediment available for mobilization at the moment of deglaciation in the paraglacial sediment exhaustion model
S_t	sediment available for mobilization at the time t since deglaciation in the paraglacial sediment exhaustion model
t	time since deglaciation in the paraglacial sediment exhaustion model
t_{min}	minimum time difference between two received echoes in order to be separable [s]

$tval_i$ t-value calculated for each DoD cell during two sided t-test in significance assessment of DoD values

$tval_{crit}$ t-value pertaining to the significance level used during significance assessment of DoD values

V_{sf} volume of a slope failure [m^3]

x quantity representing the magnitude of a mass wasting process event in magnitude-frequency relationships of mass wasting processes

$x_{\min}$ lower bound of power-law behavior in the magnitude-frequency probability distribution function of mass wasting processes

x_{sc} Percentage of avalanche surface area covered by sediment

Z_{Actual} True value of elevation in space that is approximated by Z_{DEM}

Z_{DoDrep} cell values of the DoD of repeat measurements acquired on the same date

z_{DTM1_i} z value of cell i in DTM at time slice t = 1 [m h.a.e.]

z_{DTM2_i} z value of cell i in DTM at time slice t = 2 [m h.a.e.]

dm decimeter

Ghz gigahertz ($= 1 \times 10^9\,\text{Hz} = 1 \times 10^9\,\text{s}^{-1}$)

GJ gigajoule

ha hectare

Hz hertz ($= 1\,\text{s}^{-1}$)

J joule

m meter

min minutes

mm millimeter

Mt megatons

nm nanometer

pt point

s second

W watt

yr Year

1 Introduction

Global warming is expected to cause rapid and systematic changes in environmental variables, most importantly temperature and precipitation. This might lead to follow-up adaptions of other environmental factors and processes (Beniston, 2005). On a global scale, for instance, it is expected that warming will enhance the hydrological cycle, implying an increase in evaporation and a higher proportion of rainfall in precipitation. This, in turn, is likely to affect groundwater supply, soil moisture and the magnitude-frequency relations of floods and droughts (Beniston, 2003).
Several studies have shown that climatic changes are amplified in the Alps in comparison to the lowlands or the global scale. This means that trends in climatic variables are more pronounced in high elevations (Beniston, 2005). Since the beginning of measurements, there has always been an about three-fold amplification of the global climate signal in high mountain areas in comparison to the global scale (Diaz and Bradley, 1997, as cited in Beniston 2005). Accordingly, a higher increase in average temperatures is expected for the European Alps in comparison to the global trend. During the 20th century, an increase of minimum temperatures of up to 2 °C and a moderate increase in maximum temperatures has been observed for the alpine region. There has been only a small trend in annual precipitation and a decrease of sunshine duration (Beniston, 2000, as cited in Beniston 2005). However, such trends do not precisely inform about the change in the form of magnitude-frequency relationships but give a mean impression of developments. For example, it has been reported that although mean precipitation values have not changed much, an increase of the proportion of high-intensity precipitation events was observed (Hartmann et al., 2013).
Prediction of climate change in the Alps is highly depending on the IPCC CO_2 scenario applied. These scenarios represent different greenhouse gas emission paths in the future. As the future greenhouse gas emission is a result of very complex interactions between social, economic, political and technological forecasts (Beniston, 2005), predictions are bound to have high error margins. Furthermore, it is still a very challenging task to correctly model climate specifically in high mountain areas on a large scale (Beniston, 2003, 2005). Despite such issues, there is consensus in the scientific community about general current and future trends in Alpine climate: It is very likely that there will be higher temperatures and more humid conditions in winter and much warmer summers with lower precipitation values (Beniston, 2005).
The rapid melt of glaciers almost all over the world has become a symbol of global warming in the public mind (Haeberli et al., 2013). Indeed, glaciers show a negative mass and length balance almost all over the world. For the Alps, glacier surface area is reported to have decreased from about 4500 km^2 at the end of the Little ice age (LIA) in AD 1850 to 1800 km^2 in AD 2010, while glacier ice volume has decreased from about 300 km^3 to about 80$\pm$ 25 km^3. Glacier melt rates seem to have accelerated over the years, probably due to positive feedback mechanisms (Levermann et al., 2012). This trend and future climate predictions are strong evidence that the glaciers of the Alps will vanish entirely during the

next 150 years (Haeberli et al., 2013).
Similar statements can be made about the ongoing permafrost melt all over the Alps (Kääb et al., 2007a). Mountain permafrost also reacts to temperature increase, but somewhat delayed and usually causing surface changes of low magnitudes. As a consequence, these are invisible for the naked eye most of the time (Schrott et al., 2012). Permafrost degradation can reduce the mechanical properties of rock walls and may therefore reduce their stability (Funk and Krautblatter, 2010, cited in Schrott et al. 2012), while melting permafrost in loose material is believed to increase the probability of other mass wasting processes, such as debris flows (Sattler et al., 2011). Geomorphic processes that can be induced by melting permafrost are only a special case of geomorphic processes whose magnitude-frequency relationships are being or are going to be altered by global warming. The future behavior of geomorphic processes in high-mountain areas is currently an important topic in geoscientific research (Chiarle and Mortara, 2008).
High-mountain areas are some of the most geomorphologically dynamic regions on earth. This is mainly due to their young age, their glaciation history and the (resulting) high topographic relief (Otto and Schrott, 2010). Recent geomorphic processes constantly work to reduce this relief. According to Slaymaker and Embleton-Hamann (2009), the major direct drivers of environmental change in mountains are (1) relief, (2) hydroclimate, and (3) land use. The authors point out that precisely which of these drivers is most important in any specific mountain setting and how they should be ranked individually and in combination, is a matter of research (Beylich et al., 2011, Beylich, 2016).
Independent of the relative importance of each of these factor complexes, it is inevitable that the characteristics of the Earth's high mountain geomorphic systems are going to be altered by climate change. One concrete and important reason is the altering of the hydrological regime through an upward shift of the snow line and the ratio of precipitation falling as rain or snow throughout the year.
In general, it is expected that global warming will increase intensities of geomorphic processes (Otto and Schrott, 2010). The exact nature of the reaction to global warming, however, is not known (Knight and Harrison, 2014). Where process magnitude and frequency change close to densely populated areas, this can result in an increased potential danger (e.g. Evans and Clague, 1994, Becht et al., 2003, Keiler et al., 2010, Beniston et al., 2011). Especially large moraine sediment stores in the areas that had still been covered by glacier ice at the end of the LIA (proglacial areas), in combination with huge water volumes available in future moraine-dammed proglacial lakes have been identified as a hazard (Clague and Evans, 2000, Huggel et al., 2002). It is also for this reason why research on sediment transfer in high mountain areas is important. Knowledge about the spatial distribution, potential magnitudes, recurrence interval and mechanisms of the respective processes can help in planning of protection measures.
As a result, quite some efforts have been undertaken to shed light on sediment transport in high mountain areas in general, and specifically in subareas regarded to be most susceptible to climate change. Research projects such as SEDAG (2000-2006), ClimChAlp (2006-2007), SediCouple (2008-2012), AdaptAlp (2010), SedALP (2012-2015) have not only investigated sediment transport in high mountain catchments in general, but also given information usable for

future landscape management and hazard mitigation.
In general, predictions with narrow error bands about the development of geomorphological systems based on deterministic physical models are very difficult as even the climatic component alone is hard to model with low uncertainty (cf. above). This is why statements on the further development of geomorphic systems are often based on studies applying space-for-time substitution. As this requires a spatially and temporally well defined baseline, opportunities for this approach are rare. Therefore, it is necessary to build a body of high-quality contemporary data on sediment fluxes and budgets in high-mountain areas (Beylich et al., 2011). In many cases, contemporary high mountain cold environments provide the opportunity to identify solute and sedimentary systems where anthropogenic impacts are still less important than the effects of climate change. Accordingly, it is still possible in such environments to develop a library of baseline fluvial yields and sedimentary budgets before the natural environment is completely transformed (Slaymaker, 2008, Beylich et al., 2015). The work presented here can be seen as contributing to the knowledge base modeling can be based on, as all relevant processes in a high-mountain catchment are being quantified to construct a sediment budget.

2 Sediment budgets: Current state of research

2.1 Sediment budgets in general

Catchment-wide denudation rates have traditionally been calculated from fluvial sediment transport rates measured at the outlet of the catchment (e.g. Tschada, 1975, Sommer, 1980, Dedkov and Moszherin, 1992, cited in Becht 1995b). As a result, there has been a strong emphasis on the analysis of export rates obtained from such measurements (Walling, 1983, Phillips, 1986, Warburton, 1990). These values are taken as "sediment budgets" in many publications. This only holds true if the catchment is conceptualized as a whole, i.e. as only one unit, a closed system, which receives no sediment input (at least when aeolian sedimentation is being neglected).
In the definition that has become established among geomorphic sediment budget studies, however, it is not more but a component of a complete budget. A complete sediment budget of a defined catchment does not only state how much sediment leaves a catchment at the outlet of it's main river. It also quantifies the production rates of sediment and the different processes mobilizing it, thereby enabling statements on the relative importance of different processes in sediment transport within the catchment and their proportionate contribution

to the overall sediment yield (defined as the amount of sediment removed from the catchment per unit area in one year) of that catchment (Dietrich et al., 1982, Warburton, 1990). It is for this reason, that many sediment budget studies focus on processes that directly contribute sediment to the main channels (such as fluvial erosion or rock fall), neglecting internal sediment production and transfer. Examples for a negligence of internal sediment transfer include the omission of sediment transfer in rock glaciers or solifluction lobes far above the fluvial system. These fluxes are often not looked at closer because they are often conceptualized as sediment transfer through one single storage element, which are, and not even always, the smallest units in sediment budget studies (Dietrich et al., 1982). Although a honoring of these processes is certainly desirable, at least the sediment transfer through the soil mantle or other low-intensity processes are often not looked into for time reasons, especially in large-scale studies. The same holds true for biogenic transport, i.e. transport by processes like tree throw or animal burrowing. In addition, a distinct identification of gravel roads as a potential sediment source is often not undertaken in sediment budget studies, although advocated by Dietrich et al. (1982).
Independent of the number of processes being accounted for in sediment budget studies, there is also an aspect in sediment budgets that makes them much more valuable than just provided by data on masses entering the main fluvial system of a catchment. Sediment budgets can provide information on the sediment transport system in the catchment (Walling, 1983). As a consequence, a broader definition of a sediment budgets has to be adapted. Following Swanson et al. (1982) and Warburton (p. 261 1990), a sediment budget is

> a quantitative statement of the rates of production, transport and discharge of detrius [...], and provides a useful framework for understanding the movement of sediment through a catchment or landscape unit.

This definition expands the notion of a sediment budget by a decisive internal system component that includes internal sediment transfer. It also decidedly includes sediment transfer on single landscape units. In fact, there is an extensive body of scientific studies concerned with budgeting sediment transfer on very small scales, often including one landscape unit only. Examples of these studies are presented below. Budgeting on the scale of a landscape unit, i.e. landform is by far less complex than on the scale of whole valleys or valley subsystems. This is because, in general, fewer different processes operate in smaller areas.
Sediment budgets have to be defined conceptually thoroughly before they can be established. Before measurements begin, it has to be decided which processes are relevant (see part 4 for the ones chosen in this study) and where sediment monitoring stations are to be maintained. Every sediment budget, therefore, is based on an a priori conceptual model of the sediment transfer system in a catchment (Warburton, 1990).
In general, sediment budgets can be constructed by spatially and temporally integrating the total amount of mobilized sediment by different sediment moving processes within a defined catchment (Dietrich et al., 1982, Becht et al., 2005). These processes operate at (quasi-)continuous scales and their occurrence is characterized by a very high spatial and temporal variability (e.g. Dietrich and Dunne, 1978, Becht et al., 2005, Carrivick et al., 2013). While some processes are more or less constantly active, but at different intensities throughout the

year, others can be seen as occurring as discrete events (Becht et al., 2005). As a result, an integration of those processes is no easy task. It requires a catchment-wide identification, mapping and quantification of all relevant sediment transport processes and a localization of their interaction areas as well as a recognition of storage elements through which the transport processes act (Dietrich and Dunne, 1978, Dietrich et al., 1982).
For a quantification of the mobilized sediment, it is necessary to acquire reliable measurements of sediment transfers within the area of interest, most desirably everywhere in the catchment. The extrapolation of data collected from only a few measurement locations to the scale of a whole catchment, however, usually yields less reliable results (Dietrich and Dunne, 1978). Although the development of new monitoring techniques (e.g. LiDAR) has facilitated a spatially and temporally better representation of the landscape (development), measurements of all relevant processes literally everywhere in the catchment are impossible. As a result, sediment budgets must be seen as condensation of relevant information on the sediment transfer system of studied catchments. As all processes are controlled by external factors, there is a theoretical way to quantify sediment fluxes using data on these factors. Such predictive sediment budgets, however, are impossible to construct reliably due to the number and complex interaction of these factors. This is why virtually all sediment budgets are constructed for a specific and defined interval only (Dietrich et al., 1982, see below for the interval chosen in this study).
A localization of process interaction areas leads to the establishment of the topological form of a sediment budget in form of a flow chart, representing the sediment budget as a system of processes (see 2.3 for a more thorough discussion of this representation) (Dietrich and Dunne, 1978). Otherwise, it is not possible to separate sediment being added to the total discharge from transport of the same material along its sequential path to the basin outlet (i.e. in the main fluvial channels). In other words, spatial identification of process links is the only way to discriminate between contributions by different slope processes quantitatively (Dietrich et al., 1982).
The existence of such link locations and, as a consequence, the relative importance of a certain process to the sediment budget, however, is highly dependent on the magnitude and frequency of the process in question at a certain location. A debris flow, for example, might reach the process area of another process in one year, but not in the following one. Most of the time, it is not possible to fit a regression model between process events (such as a debris flow event) and the recurrence interval of their most important driving factors (such as a thunderstorm of very high intensity) because the interaction of these driving factors is decisive and often very complex. This is prevented by too many other, site-specific factors on both sides of the model and lag effects from previous events (such as refilling of sediment bodies available for mobilization) (Dietrich et al., 1982). Especially the influence of fluvial sediment transport is characterized by a very high temporal variability, whereby the missing of high magnitude-low frequency events in a measurement campaign can lead to significant underestimations of long-term sediment delivery (Kirchner et al., 2001, Carrivick et al., 2013). Another problem is constituted by episodically moving sediment bodies as deep-seated slope failures or other non-fluvial processes with relatively long recurrence intervals on hill slopes (such as debris flows) (Warburton, 1990). In cases of studies of short temporal duration, a determination of recurrence in-

tervals is especially difficult (Dietrich et al., 1982, Knight and Harrison, 2014). With reference to the influence of extreme events with (unknown) long recurrence intervals, the importance of such research on recent geomorphic processes is sometimes challenged. The definition of what an extreme event is in this context, however, is not clear (Becht, 1995b). It is a characteristic of many sediment budget studies that they are of limited temporal duration. Although it is very obvious that data on sediment transfers are more reliable the bigger the database is, many studies are set up for only a few years. In order to reduce the potential error in process measurements due to a short project duration, it is common practice to produce measurement rates from either historical imagery (e.g. Dietrich and Dunne, 1978, Schiefer and Gilbert, 2007, Staines et al., 2015) or by adopting a sedimentological approach, i.e. by qualitatively and quantitatively looking into the stratigraphy of the sediments in the catchment. In addition to the usually short total monitoring project durations, another cause for the missing of the measurement of critical events is the frequency of field work conducted by research teams during the total duration of a sediment budget project. It is impossible to be present in the study area continuously at all times. Where some processes or their proxies can be measured (quasi-)continuously (e.g. fluvial sediment transport), it is not possible for others (e.g. rock fall). Often, it is the remoteness or difficult accessibility of high mountain study sites that prohibit high frequency measurements. Available data at weekly or even higher temporal resolution is, therefore, not often available (see (Krautblatter, 2004) for a notable exception).
A recognition of storage elements has been an integral part of all sediment budgets. A quantification of all these storages, however, often requires a lot of work and is almost impossible on the scale of a whole catchment (Otto, 2006). This is why storages are often assumed as being in a steady state on the temporal scale of the scientific investigation. Often this assumption underestimates the recurrence interval of disturbing events. Since the advent of ALS data, however, rates can be calculated for each storage element with a high temporal resolution, alleviating this problem.

2.2 Sediment budgets in high mountain environments

Sediment budgets in high mountain environments show some marked differences to budgets in lowland areas. The impressive relief of high mountain areas is testimony of their comparatively young age, their past or present glacial history and (often) the erosive power of glaciers (O'Farrell et al., 2009). It has been shown that erosion rates in glaciated landscapes are significantly higher than in unglaciated ones (Parks and Madison, 1985, cited in O'Farrell et al. 2009).
Despite Jäckli (1957) and Rapp (1960)'s seminal work, it was only until two to three decades ago that the importance of different processes in high mountain areas was discussed, especially among German geomorphologists, predominantly

qualitatively (Beylich, 2000). A quantitative approach has been on the rise since then, in Germany mainly fostered by the work of the working groups in Heidelberg/Bonn as well as Michael Becht's and Achim Beylich's working groups. Other early work on glacio-fluvial sediment transport system, either integrating several processes or even just monitoring the fluvial sediment yield at the catchment outlet, has been completed by Church (1972), Maizels (1979), Hammer and Smith (1983), Fenn (1983), Gurnell and Clark (1987, cited in Warburton (1990)), for example.

Many studies working on sediment budgets in high mountain areas have only worked on a scale much smaller than a whole catchment, e.g. a single slope. This is also why relatively little is know about the relative importance of the different processes for the overall sediment budget of a catchment (Beylich, 2000). It is natural that sediment budget studies in high mountain areas are facing the same challenges as sediment budgets in general as touched upon in chapter 2.1. Quite some studies have calculated high mountain sediment budgets as the export from a catchment at the outlet, either by direct measurement of fluvial sediment transport or by quantifying sedimentation rates in lakes at the catchment outlet (e.g. Müller, 1999). As studies occupied with the measurement of sediment transport in the stream draining the catchment acquire one value integrating all processes, it does not help in understanding the processes operating within the catchment to form a sediment budget. It is therefore desirable to unravel the contributions of each process active in the area of interest. Otherwise, the catchment investigated must be considered as a "black box" (Warburton, 1990, Carrivick et al., 2013). To achieve the goal of a process distributed sediment budget, it would be necessary to measure processes everywhere in the catchment. As this is usually not possible, field campaign planning is very important. Generally one has to lower one's sights regarding as the field campaign time is limited by snow cover or weather conditions.

The event of both terrestrial and airborne light detection and ranging technology (cf. 5.4.1.2) becoming applicable to geomorphology has led to significant improvements regarding the problem of spatial variability being an uncontrollable factor in sediment budgeting. Whole catchments can now be surveyed in a few days. In addition, ALS data can be combined with TLS data to alleviate the shortcomings of the respective measurement geometries. LiDAR data has therefore already been used in geomorphological studies in alpine catchments, also for sediment budgeting purposes. Carrivick et al. (2013), for example, combined repeat TLS surveys with ALS data of an density of $2\,\mathrm{pt\,m^{-2}}$ to produce erosion rates of the proglacial area of Ödenwinkel Glacier in the Hohe Tauern mountain range, Austria.

According to Carrivick et al. (2013, p. 2), however, the ability of LiDAR to "determine geomorphological changes within alpine catchments is presently limited" because LiDAR data is usually "acquired on a campaign basis, rather than as part of routine monitoring strategies". In addition, it is often stated that the volume and complexity of such data further inhibits the successful application of spatially and temporally highly resolved laser scans in high mountain environments. Nevertheless, Carrivick et al. (2013) and Orwin et al. (2010) state that a direct differencing of repeated high-frequency topographical surveys are the best way to quantify geomorphological activity, although Carrivick et al. (2013) asserts that LiDAR data has "yet to be exploited for holistically examining multi-scale sediment fluxes within highly dynamic alpine catchments [...

and] alpine catchment-wide use of ALS and TLS datasets is still new and developing." The study presented here not only aims at working at exactly this methodological frontier (cf. 2.4 and 5.1), but also makes use of catchment-wide LiDAR data in the quantification of multiple processes (cf. 5.7).
Where more than one sub-system of a geomorphic system in a high-mountain area are investigated quantitatively using LiDAR data, processes are not separated by mapping but all surface change is lumped together in many studies (e.g. Staines et al., 2015, Rascher and Sass, 2016). In addition, a detailed identification of areas of dead ice or permafrost melt ("thermoerosion") is missing, a step that is necessary to separate actual sediment transport from ice melt. The importance of such as distinction has been shown by Irvine-Fynn et al. (2011) who attribute a discrepancy of 12.5 to 60 % in LiDAR-detected erosion to fluvial sediment output for their study area to ice melt and proceed to apply different models to examine the role of thermoerosion in their budgeting of a lateral moraine of Midtre Lovénbreen, Svalbard. Studies not taking care of such factors cannot be successful in establishing a sediment budget. However, DEMs of difference are often calculated for the whole study area indiscriminately. A process distinction is not undertaken most of the time, probably because it requires a lot of additional work.

2.3 Catchment as a system

In general, the landscape can be seen as a system where different landscape elements or landforms constitute the elements of that system and processes that transport material from one landform to another can be seen as links between the elements. In this context, the output from one landform constitutes the input for the subsequent one until the sediments leave the catchment, thereby forming a "landsystem" (sensu Geilhausen et al., 2012, Carrivick et al., 2013). The landscape representation as a system has become popular since Chorley and Kennedy (1971), is the prevalent one in geomorphology (e.g. Ballantyne, 2002b) and has also been termed "morphosystem analytical approach" (Beylich, 2000) or "landsystem approach" (Carrivick et al., 2013). Within every landsystem, some subsystems are not linked to the main sediment transport strand, thereby representing decoupled subsystems or, on the landform scale, decoupled landforms or storages. Most sediment transport systems (on the catchment scale at least) contain more elements not coupled to others than vice versa and much sediment produced on landforms high above the main channels (such as rock walls) does not reach the outlet but is stored along the way. This is what Walling (1983) has called the "sediment delivery problem" (delivery with respect to the catchment outlet) and why Fryirs (2013) has attributed most landscape systems as ineffective. The configuration of the landsystem is highly dependent on time and every study making use of this conceptualization must define an explicit temporal (and spatial) scale for which the landsystem representation is constructed (e.g. Schrott et al., 2006, Fryirs, 2013).
Landscape elements can serve as sediment sources (e.g. a rock wall), (interme-

diate) storages (e.g. a talus cone that is being reworked by frost creep or debris flows) or sediment sinks (e.g. a lake) on a defined time scale. The classification of such landforms as either source, link or sink is therefore crucial before a sediment budget can be calculated. A catchment wide systematic approach for an identification of sources, links and sinks is often not undertaken, especially not on the landform scale. As Carrivick et al. (2013) states, the localization of sediment sources, storages and sinks is one of the most demanding tasks of alpine sediment budgeting, the main reason being that catchment-wide models are generally qualitative and conceptual (Caine, 1974, Dietrich and Dunne, 1978, Carrivick et al., 2013). As the classification into source, link and sink is process based, it is not enough to locate the landforms, i.e. the landscape elements. The sediment pathways linking the landscape elements need to be known as well. As sediment is usually moved not only by one process, the identification of such pathways must be further addressed.

Each of the processes active in the landscape can be ascribed a distinctive process domain, that is the zones within the catchment where it is active and alters the earth's surface. These process domains can further be differentiated into zones of erosion, transport and deposition. Where such process zones overlap, material can be passed from one process domain to another (Becht, 1995b).

Ultimately, whole chains of process can form, thereby constituting a sediment cascade that, in turn forms cascading systems when chains of processes form a network (Becht et al., 2005). As a result, accumulation landforms can be seen as storage elements in interrupted sediment cascades, that is, at terminal places in a sediment cascade or where erosion rates of the landform do not reach the accumulation rates. In contrast to Ballantyne (2002b), non-bedrock landforms are not defined as sediment sources in this study but as intermediate storages as all sediment will ultimately reach the catchment outlet and therefore constitute intermediate storages. Sediment is generated in and mobilized from bedrock-areas (Ballantyne, 2002b). Cascades can be established topologically, that is by finding locations of unique process zones overlap (which have been termed "Geomorphological Process Units" (GPUs) by Bartsch et al. (2002)) and thereby identify important process combinations for sediment transport in a catchment (e.g. Wichmann et al., 2009, Heckmann and Schwanghart, 2013).

As stated by Slaymaker (1991) and Becht et al. (2005), it is desirable to enrich the identified process chains and process links between landforms with data derived from balances of the single landforms, thereby quantifying the mass of sediment being transported along the links of a cascading system. Quantification of a single process can be relatively straightforward if only one process with limited transport range and two landforms are involved (termed macro-scale by Becht (1995b)). On the meso-scale, however, this is still a challenging task, or as Becht (1995b) puts it: "Coupling the measured sediment transport rates with the modeled process domains, however, remains a challenging problem and is subject to further research." On the meso-scale, it is just as crucial to know the GPUs accurately to obtain correct sediment budgets of the landforms (or larger spatial units) involved (Becht, 1995b). The spatial domain of each process can either be determined by field mapping, rule-based classification from remote-sensing data (Bartsch et al., 2002) or by using numerical spatial process models(Becht et al., 2005, Wichmann et al., 2009). But as a landsystem on the meso-scale (i.e. on the scale of a whole Alpine Valley) typically consists of hundreds to thousands of different landscape elements, the task of representing

it on a level of detail that includes single landforms has almost never been undertaken.
Nevertheless, there is an increasing trend towards more quantitatively oriented studies which aim at (i) representing the cascading system of whole alpine valleys and, to a lesser degree, (ii) quantifying the element links, i.e. processes quantitatively based on measurements. Sanders et al. (2013), for example, develop a theoretical framework for the sediment budget of a glaciated alpine cirque in the Canadian Rocky Mountains. They distinguish sources, sediment pathways and sinks/storage elements and proceed to quantify each sediment budget component using different measurement techniques. Their study area is small, morphologically simply configured and with only a small variety of different active processes (in comparison to a meso-scale catchment stretching over several morpho-climates). But the authors present a very detailed and analyzed sediment budget for several sub-processes in an almost optimal setting for testing new approaches towards a higher resolved model of alpine sediment budgets and cascades.
One of the most detailed analyzes of the configuration of an alpine landsystem was presented by Heckmann and Schwanghart (2013) and explores steps on how the landsystem could be modeled for a meso-scale catchment based on numerical spatial process models for different processes. They also present a methodological solution to one of the main problems in both the quantitative and qualitative analysis of landsystems on the meso-scale. Where it had been impossible to keep track of thousands of landforms as elements and the process links between them in an alpine cascading system, both in terms of whether links between them exist or not and the masses transferred along them, the representation of the landsystem in the data structure of a directed graph does not only allow fast sub-setting of elements and processes but also offers new and fast methods for the analysis of this system on the landform- and all larger scales.
Figure 2.3.1 shows a corresponding conceptualization of high mountain sediment transport system used in this thesis. Most studies, as stated above, are only aiming at a quantification of one process and often on only one hill slope. This holds true independently of the methodology used, but is especially conspicuous when it comes to repeated topographic surveys as with LiDAR or dGPS:
Studies that have aimed at a quantification of rock fall of various sizes using such methods include Haas et al. (2009), Abellán et al. (2010), Heckmann et al. (2012a), Strunden et al. (2015). Debris flows have been quantified, among many others, by Bull et al. (2010), Bremer and Sass (2012) and sediment transfer by rock glaciers has been determined by Gärtner-ÂRoer and Nyenhuis (2010), Gärtner-Roer (2012).
As it was also pointed out by Beylich and Laute (2015), there has been a decidedly strong focus on the sediment transport processes in the main streams of high mountain catchments (e.g. Milan et al., 2007, Bertoldi et al., 2010, Carrivick et al., 2013). One reason is the fact that sediment transport measurement in the main fluvial system can provide the overall gross sediment output, which is very often substituted as a sediment budget (as mentioned above). A second reason is certainly the dominance in geomorphological activity of the fluvial system in many high mountain valley systems (Carrivick et al., 2013, Orwin et al., 2010).
The direct measurement of sediment transport in (proglacial) high mountain

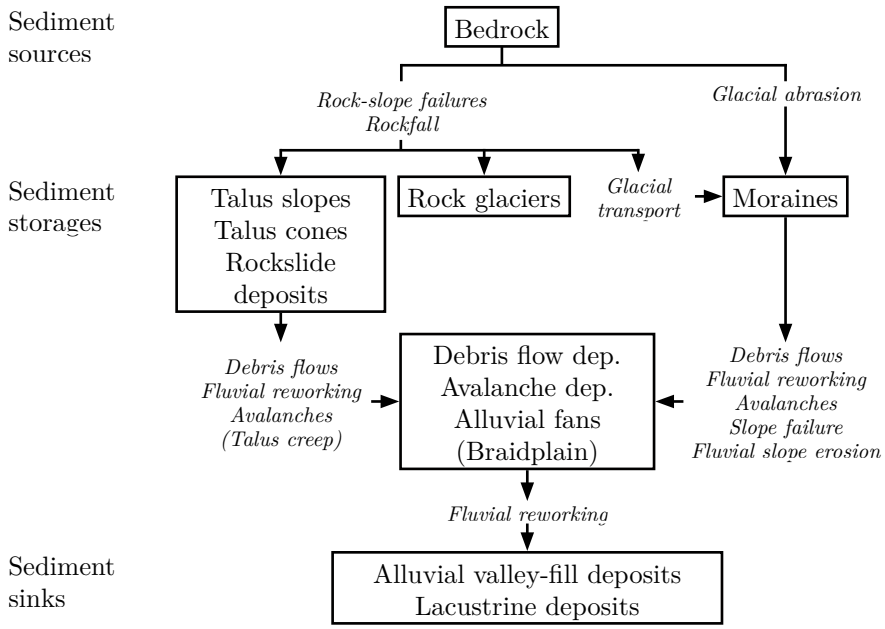

Figure 2.3.1: System view of the high mountain landscape used in this study.

streams is often hampered by the high variability in flow and sediment transfer rates on the one hand (Orwin et al., 2010) and unstable channel layouts on the other. A thorough study involving point cloud data stemming from photogrammetry and LiDAR was presented by Staines et al. (2015), who monitored surface change of the Sólheimajökull glacier foreland (Iceland). Due to the configuration and geomorphology of their study site, the focus of their work was also mainly on the development of the proglacial fluvial system. Their works can serve as an excellent example of how historical aerial imagery can be taken into account to extend the temporal data basis for studying sediment dynamics in proglacial areas.

Only few studies are available shedding light on the sediment production by glacial processes, the main reason being the difficulty of monitoring the glacial sedimentary processes below or within the ice masses (Warburton, 1990). As a result, there is a very limited number of studies informing about the absolute and relative importance of glacial versus non-glacial processes with respect to sediment supply to the main streams of mountain catchments although there has been an ongoing debate this topic for a long time in the scientific literature (Brocklehurst and Whipple, 2002, Spotila et al., 2004, Beylich et al., 2015). Most published rates on erosion of high mountain glaciers rely on the measurement of sediment yield in proglacial rivers (see Hallet et al., 1996, for a review), thereby neglecting the fact that these rates integrate also the fluxes of processes delivering sediment to the glacier from above or the sides. In addition, such rates cannot distinguish between sediment produced by glacial erosion at the glacier bed and material stemming from storages below the ice or next to the glacier margins (Warburton, 1990, Harbor and Warburton, 1993, O'Farrell et al., 2009).

It is therefore of utmost importance to gain knowledge about the sediment input by other processes to the glacial process area. Taking a downstream sandur and its sedimentological characteristics as a data basis, there is evidence that sediment input from the valley slopes (e.g. via rock fall or debris flows) is much more important than sediment flux directly from the glacier in the catchment studied by Carrivick and Rushmer (2009). A dedicated and detailed study on the relative importance of glacial erosion to hill slope processes was presented by O'Farrell et al. (2009). Using cosmogenic nuclide erosion rates for bedrock erosion, a combination of field measurements to quantify slope processes and suspended measurements from tributary glacial and non-glacial streams, they were able to juxtapose glacial (approximated by fluvial yield in the proglacial area) and non-glacial processes for the timescale of the Holocene at Matanuska Glacier, Alaska. A comparison of glacial bedrock erosion and rock wall retreat rates has been presented by Sanders et al. (2013), who conclude that rates are roughly equivalent.

Fortunately, there is an increasing body of studies incorporating measurements of more than one process into an analyzed sediment budget of high mountain catchments. It was not after 1990 that Warburton (1990) presented a quantitative sediment budget of the proglacial zone of The Bas Glacier d'Arolla, Val d'Hérens, Switzerland. He could show that fluvial sediment transport in the main braidplain was by far the most important process in the geomorphic system of his study area, i.e. that hillslope processes and tributary channels contributed only small amounts of sediment. However, no information on the system internal transfer rates was obtained. He could also show that short low-frequency, high-magnitude hydrological events had an enormous impact on the overall sediment budget. In fact, 95 % of the sediment eroded in the proglacial zone he studied had been mobilized by a meltwater flood event that lasted only three days. Nevertheless, also Warburtons seminal study lacks information on glacial sediment production and is based on a short duration (two months) field campaign only. In general, there are not many studies providing a comprehensive image of the sediment transfer system in high mountain basins. Some studies, at least, differentiate between surface change within the fluvial system and geomorphic work on valley slopes. An example is Irvine-Fynn et al. (2011), who use ALS data from two different dates to quantify surface change on a lateral moraine on the one hand, and the fluvial system on the other. However, they make no process distinction, as this is not possible with the low spatial resolution ($< 1\,\mathrm{pt\,m^{-2}}$) of their data sets. An integration of different methods has helped O'Farrell et al. (2009) to produce a sediment budget of the proglacial area of Matanuska Glacier, Alaska. They do not differentiate between single processes but use volume measurements of two classes of sediment fans and cosmogenic nuclide measurements on bedrock ridges to come up with three different process zones which they quantify separately and extrapolate to the whole study area using morphometry rules. Suspended sediment measurements are then compared to the rates obtained for the other landscape classes to facilitate a comparison of glacial and non-glacial processes.

In many cases, the scientific focus on streams draining high mountain catchments also implies a focus on the proglacial areas of these catchments, i.e. these parts of the catchment located between the current glacier margin and its LIA extent about 160 years ago as defined by the lateral and terminal moraines

observable in the landscape.[1] As these locations that had been covered by a glacier very recently (in geological time scales), a significant imbalance between sediment production and transport can be observed due to over-steepened topography, large unconsolidated sediment storages ready for remobilization and a complex drainage pattern (e.g. O'Farrell et al., 2009, Carrivick et al., 2013). As a result, sediment transport rates are generally multiple times higher inside the LIA moraine arc than outside and sediment yield from glaciated basins is often multiple times higher than long-term exhumation rates (O'Farrell et al., 2009). This is one of two main reasons why there is often a focus on proglacial areas in high mountain sediment budget studies although it is these high rates and the resulting complex landscape configuration that make the compilation of a sediment budget even more demanding (Carrivick et al., 2013). This landscape complexity is the second reason why proglacial areas are often studied in high mountain geomorphology: Despite a special interest on these areas, there are still several research gaps in these complex environments often regarding the dependence of sediment flux on time since deglaciation.
Qualitatively it has been observed very often that process activity is decreasing with distance from the current glacier margins (e.g. Curry et al., 2006). While debris flows, rotational debris slides and rock fall are typically operating at very high intensities close to the glacier, it is often only the fluvial system transferring masses close to the LIA terminal moraines (Carrivick et al., 2013). Few sediment budget studies concerned with meso-scale catchments and rates based on recent process measurements have taken time since deglaciation as a possible explaining variable into quantitative sediment budget studies. Doing so, has been identified as a desirable step by several authors (e.g. Carrivick et al., 2013).

2.4 Research problems

"The only way to generalize from a few measurement sites to a landscape is to develop predictive models of the relation of each transport process to its controls" (Dietrich et al., 1982). Today, this statement does not hold true in all cases anymore, as airborne laser scanning (ALS) as a survey method allows the quantification of at least some geomorphological processes in the whole catchment. Although ALS had been an available method for the generation of terrain representation for at least 20 years now (Kraus and Pfeifer, 1998), the quality of the data acquisition and processing was not good enough and the cost not low enough for small-scale morphological differencing for sediment budget determination. With the quality of the data now being good enough, sediment movement can be monitored to a satisfying degree on the meso-catchment scale. Point cloud processing is still demanding but can be accomplished given the right methodology and a huge investment of manpower (cf. 5.4.4). As a

[1] There has been a considerable amount of confusion even in the scientific literature about the differentiation of the terms "proglacial", "paraglacial" and "periglacial" (e.g. Slaymaker, 2009, 2011). Therefore, it can not be assumed that the reader has the same understanding of theses terms. As a result, I will give definitions when appropriate.

consequence, the share of mass transfers measured directly is rising while only the low-magnitude sediment transfer processes need to be modeled. As every model result is associated with an error bigger than the errors of the measurements the model is based on, this can be seen as a step forward.
Earlier studies on sediment cascades in high mountain areas successfully determined and visualized sediment pathways, i.e. links in the landsystem (e.g. Wichmann et al., 2009). These studies, however, developed models without the incorporation of the masses transported and could therefore only give topological information on the sediment transport between spatial units. As a result, the incorporation of measured sediment masses in such or related models would constitute a step forward in sediment budget and cascade research.
As Carrivick et al. (2013) state:

> ... a holistic discrimination of sediment sources, quantification of sediment fluxes, characterization of geomorphological activity by substrate class and the inter- and intra-annual spatial and temporal variability in these has hitherto been unreported.

The study presented here can certainly not meet all these requirements, but it should be considered as a step in this direction. But what this study can certainly give is a contribution to the closure of a second research gap identified by Carrivick and colleagues:

> High-resolution changes to individual landforms have been measured on an episodic campaign basis, but this technique has not been applied to entire proglacial areas. Quantification of geomorphological work within alpine catchments has been restricted to hydrological gauging of total suspended sediment.

They go on to specifically demand features of future research projects:

> Future studies should look to i) utilise repeated ALS to determine geomorphic changes over a whole catchment, ii) quantify the spatial organisation/fragmentation of geomorphological activity, and iii) quantify sediment supply with land surface age; i.e. with deglaciation.

The reader will notice that the study presented here tries to take these demands to heart.
After looking at the current state of sediment budget research in high mountain areas, it is clear where more work has to be done to improve our understanding of high mountain sediment transport systems. In summary, the main research goals of this study are:

- To show that spatially and temporally highly resolved catchment-wide LiDAR data can be successfully applied as a main source to establish a sediment budget of a meso-scale high mountain catchment.
- To quantify sediment transport rates of all relevant sediment transporting processes in close collaboration with the relevant working groups from the PROSA project (cf. part 1).
- To use the results of the quantification efforts of the other working groups in PROSA as a basis for a (model-based) regionalization of sediment transport rates to the catchment scale to obtain a sediment budget.

- To use methods for an identification of process coupling to establish an analyzable representation of the landsystem or fragmented high mountain landscape with landforms or process areas as system elements and quantified sediment pathways as links between system elements and combine this with transport rates to establish a sediment budget.
- To investigate whether the landscape inherited by the LIA has affected process rates since its deglaciation.
- To identify changes of process rates over sub-recent and present-day time scales.

2.5 The PROSA project

The research project, the framework of which this thesis has been completed in, is called "PROSA", which stands for "High-resolution measurements of morphodynamics in rapidly changing **PRO**glacial **S**ystems of the **A**lps". It is funded by the German Science Foundation (DFG) and the Austrian Science Fund (FWF) since early 2012. In total, working groups from five universities are part of this project. Most of the time, each university represents one sub-project and each sub-project is concerned with a set of tasks. See figure 2.5.1 for the organizational structure and a rough delineation of the project responsibilities. The overall research goal of this project is to quantify sediment transport processes and to regionalize/upscale these process rates to establish a sediment budget of the Upper Kauner Valley, Ötztal Alps, Austria (Heckmann et al., 2012b). As a result, it is often the case that a sub-project is concerned with providing data for the construction of this sediment budget. In general, the staff of each sub-project is responsible for the quantification of a certain set of sediment transporting processes (sub-projects one to four), while the staff of sub-project five is responsible for data acquisition and processing on the scale of the whole study area and for a regionalization of the process rates determined by the other sub-projects. Operational work in the five sub-projects was and is mainly managed by six PhD students from the five universities. In addition to the five universities forming the PROSA-project, a commissioned scientist from the University of Western Australia conducted geophysical surveys two times during the project time (January 2012 to February 2017). The size of the studied catchment and the availability of both terrestrial and airborne LiDAR data were key to the research design used in this study 5.1. Remote sensing techniques in general are the method of choice when it comes to the investigation of of sediment transport in meso-scale morphological systems (Slaymaker, 1991).
All landforms can be conceptualized as sediment sources if the time scale is long enough. LIA lateral moraines, for example act as sediment storages on a short timescale, but as intermittent sediment sources on a medium timescale and as permanent sources on a longer time scale (Carrivick et al., 2013). It is therefore very important to define the timescale a specific geomorphological project or study is limited to before any results can be of use. The timescale for this study was defined as encompassing a few years, that is about three years (2012–2014), as this is the time period for which ALS data is available for the whole study area and measurements by the sub-projects had been undertaken. As the data

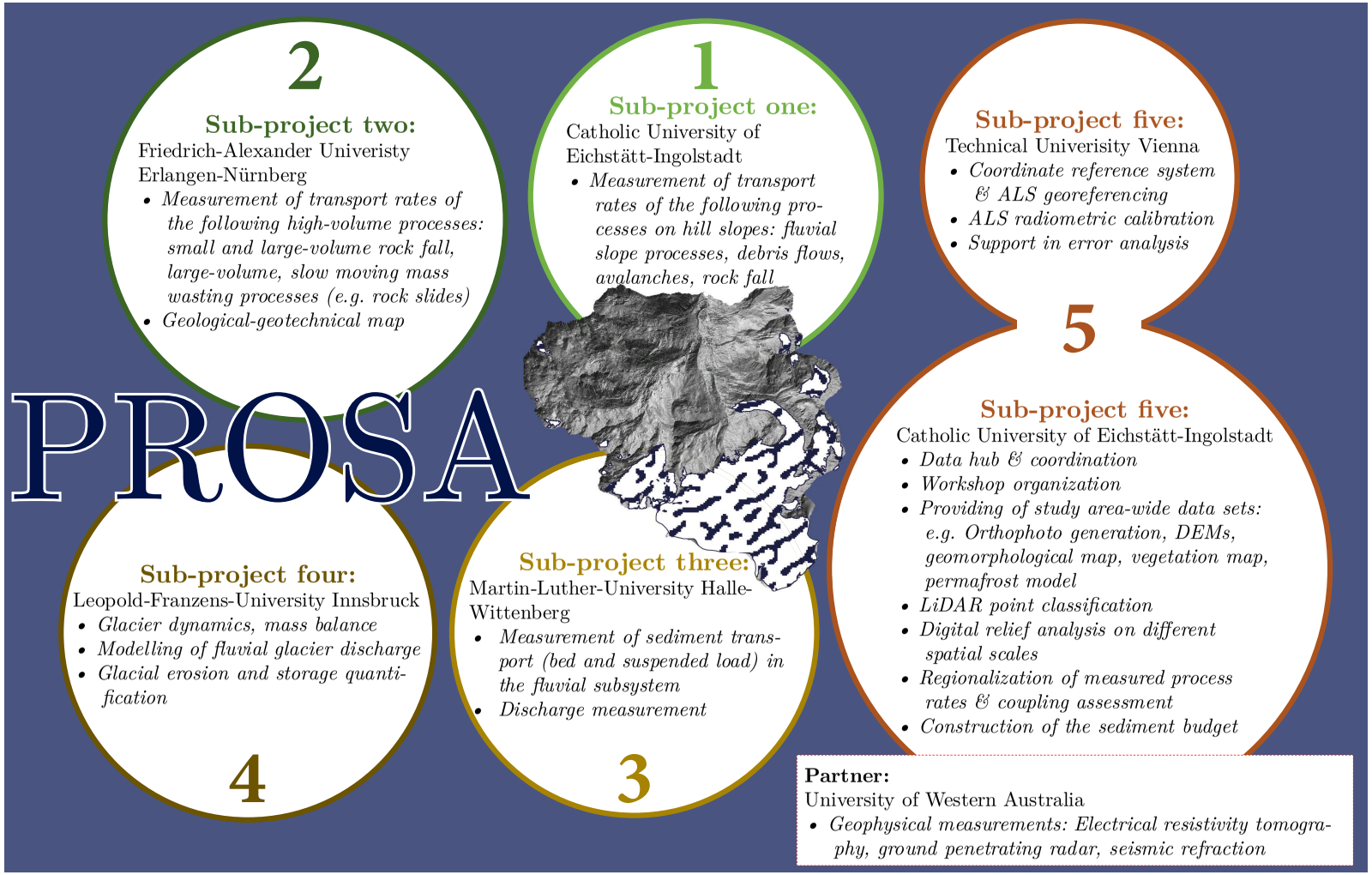

Figure 2.5.1: Organizational structure of the PROSA project

available for the quantification of different processes are of different quality and temporal resolution, however, the reference time period will have to be slightly different for each process. While debris flows could consistently be quantified for the whole catchment for a time period longer than the one mentioned above, data of avalanches was only available for the winters 2012/2013 and 2013/2014. As a result, reference time periods will always be reported together with sediment transfer rates.

3 Study area

3.1 Localization

The study area is located at the upper end of the Kauner Valley (which is a tributary to the Upper Inn river) within the Ötztal Alps. These are part of the Austrian Central Alps and the central-alpine dry region (Fliri, 1975, (as cited in Abermann et al. 2009)). The south-north trending valley is located at around 47° N and 11° E, and the southern border of the study area constitutes the main alpine divide.
The study area was defined by the author as the hydrological contributing area (HCA) of a cross-section at the mouth of the Fagge river into the Gepatsch reservoir, which has been built between 1961 and 1964 (Tschada and Hofer, 1990). The exact borders of the investigation area was determined using a hydrologically corrected, ALS-derived 1 m DEM using a series of standard GIS methods (Wang and Liu, 2006). The boundary derived this way was later corrected by the Innsbruck sub-project for current ice divides. Subsequently, an area of almost exactly 62 km^2 was defined as PROSA's area of interest.
The study area has a relief of circa 1773 m. The Fagge river mouth is located at an elevation of 1810 m h.a.e.[1] and constitutes the lowest point in the study area, whereas the highest peak in the study area is Hochvernagtspitze summit at 3583 m h.a.e.
The Austrian-Italien border runs close and north of the south-western study area limit. The study area is well known among ski enthusiasts as the Kauner Valley ski region is located in its south-western part.

3.2 Geology

The study area is part of the Eastern Alps crystalline zone and the Ötztal-Stubai complex. This complex is bordered by the Sill valley fault/High Tauern in the east, the Schneebergerzug with southern Tyrolean "Mittelostalpin" in the south, the Engadin window in the west and the Inn valley fault/Northern Calcareous Alps in the north (Purtscheller, 1978). The mass of the east-alpine

[1] Please see chapter 5.3 for the difference of a.s.l. and h.a.e.

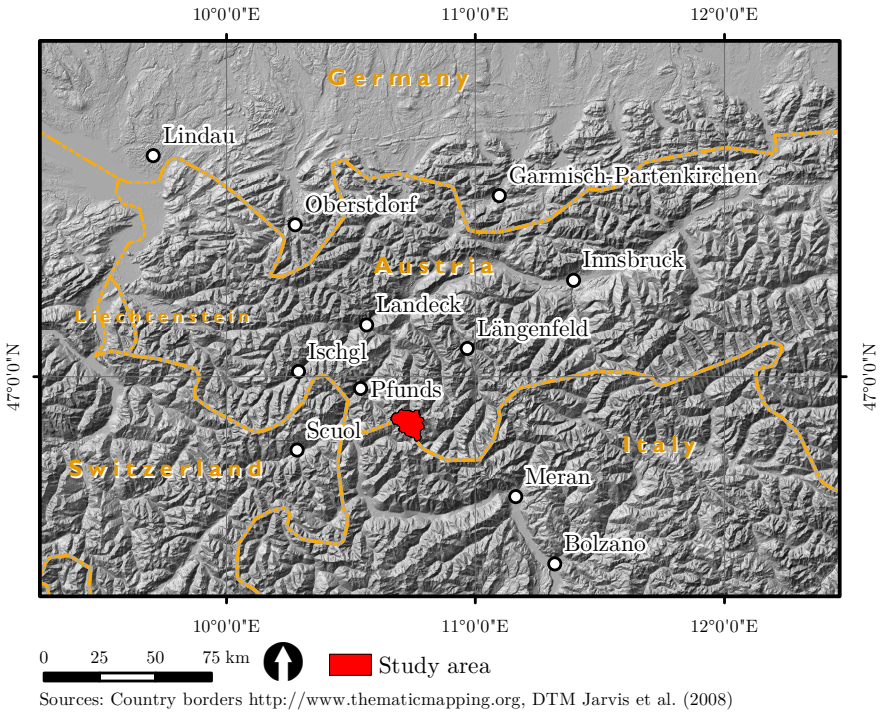

Figure 3.1.1: The location of the study area in western Austria.

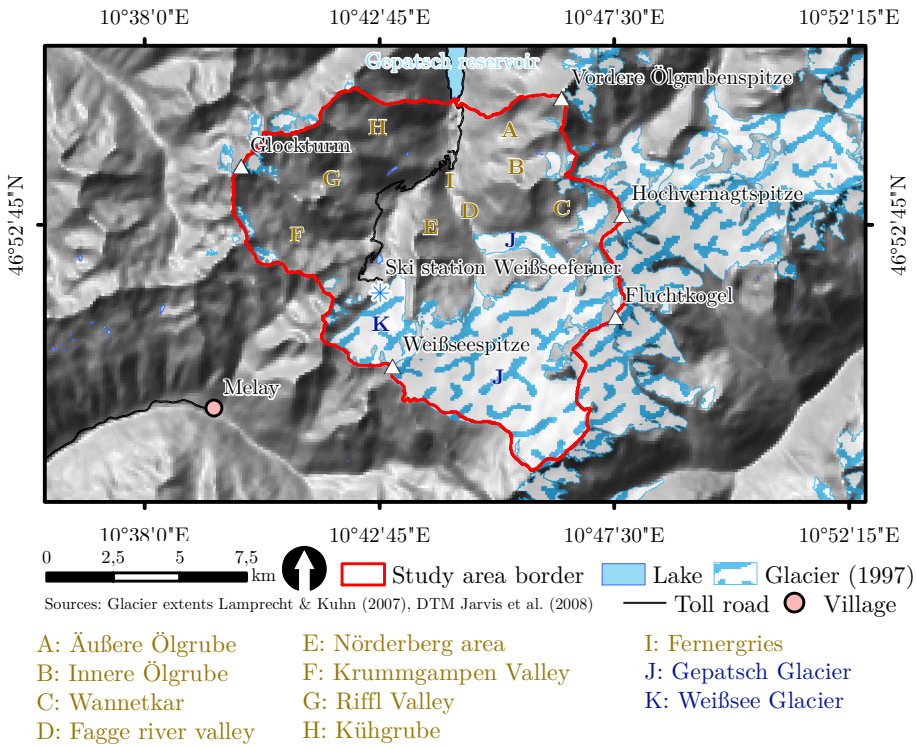

Figure 3.1.2: The study area and conspicuous natural and anthropogenic landmarks.

basal complex and a pack of sedimentary rocks was moved onto penninic nappes during the Alpine orogeny. The rocks of the Ötztal Alps in the Kauner Valley region have undergone at least two metamorphic phases (during the Caledonian and Variscian orogenies). At these times, sediments and volcanic rocks from late precambrian and early paleozoic times were altered to crystalline rocks (Bögel and Schmidt, 1976, Tollmann, 1977, Thöny et al., 2008, McCann, 2008, Zanon and Pergher, 2013). As a result, dominant rock types in the study area are different varieties of paragneiss, orthogneiss and amphibolite. Mica shist, quartzite and diabase dykes also occur, but are of lower importance. Especially the paragneisses display high spatial variability in orientation of their foliated structure and range from strongly foliated paragneiss with a high content of biotite to massive orthogneiss with high contents of quartz (Vehling et al., 2013b, Zanon and Pergher, 2013). The most frequent rock type in the study area "is a mostly coarse-grained biotite-plagioclase paragneiss with marked folitation (local name: "Schiefergneis")" (Heckmann et al., 2016). Mineral enrichments are mainly pyrite, pyrrhotite and chalcopyrite. Other minerals worth mentioning are arsenopyrite, cobaltite, sphalerite, mackinawite, ilmenite and rutile (Vavtar, 1981). Figure 3.2.1 gives an overview of the geology of the study area. Since the beginning of the latest (Alpine) orogeny, the rock bodies are altered again by tectonic stress (Pfiffner, 2010). The tectonic structure "is dominated by a variable, but mainly east-west striking, steep dipping foliation. Significant tectonic structures are several large NE-SW and NW-SE striking lineaments" (Heckmann et al., 2016).

Generally speaking, it is especially the metamorphic rocks stemming from igneous rocks (i.e. orthogneiss and amphibolite) that form rock walls and constitute the high ridges in the Ötztal Alps and the study area (Bögel and Schmidt, 1976). Nevertheless, the rock walls display a high degree of variability in rock mass properties. Not least, this is due to the Quaternary geomorphic history of the study area. Research by Vehling (2016) applying the rock mass classification scheme after Selby (1980, which ranges from 25 (very weak) to 100 (very strong)), to 70 different and representative rock bedrock sections has found the rock mass strength ranging from 42 to 93 (median: 65). His work has also shown that strong rock masses tend to show non-continuous joins with average openings below 1 mm, while weaker rock masses have high joint densities, with joint openings larger than 5 mm. Within weak rock masses, several joint sets are often present, leading to unfavorable intersections with respect to the rock surface. This constellation often produces wedge failures (Vehling et al., 2015, Heckmann et al., 2016).

3.3 Geomorphology

A wide variety of high-mountain landforms is present in the study area. Often they can be related to the spatial domains of different sediment transporting processes. In the course of this thesis, landforms and process areas where mapped detailed and on a small scale (cf. 5.6.1). Where absolute areas or area percent-

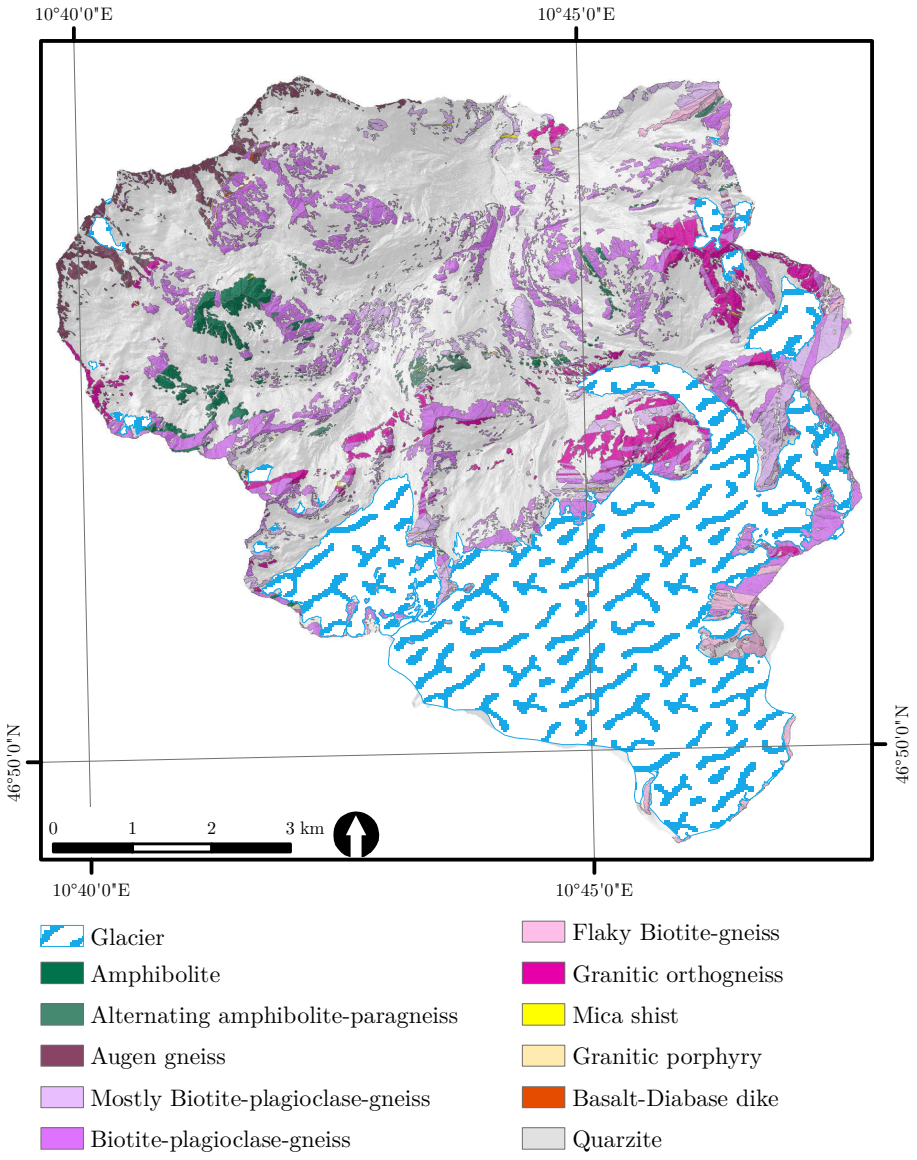

Figure 3.2.1: Geological map of the study area.

ages of different landform classes will be given in the following rough description of the study area's geomorphology, they were derived from this map.
The study area can roughly be separated into three different zones: i) The currently glaciated area, mainly Gepatsch and Weißsee Glaciers, ii) the proglacial zones of the glaciers and iii) the remainder of the study area. Not surprisingly, geomorphic activity is much higher in the proglacial zones than in the remainder of the catchment. Especially the Gepatsch Glacier forefield is reworked at very high intensities. This is mainly due to the high relief, steep slopes, heterogeneous valley width and surface diversity within the Gepatsch proglacial area, also in comparison to the Weißsee proglacial area.

The study area is in various parts anthropogenically modified as a popular mountain road traverses the catchment in its eastern part. Even more important, there are several skiing tracks in the Weißsee area. The maintenance of these two main features leads to earth works every summer, thereby influencing the sediment movement in the catchment significantly.
No definitions of the high-mountain landscape elements (such as glaciers, rock walls, moraines, debris cones, etc.) will be given here. In general, the reader is referred to the relevant literature (e.g. Stahr and Hartmann, 1999, Ahnert, 2003, Zepp, 2004). Where necessary, specific literature will be cited accordingly.
Remnants from former and larger glaciations can be found virtually everywhere in the study area. They cover circa 14 km^2 or 22.5 % of the planimetric study area. Moraines dating to times before AD 1855 can be found at many places of the catchment outside or above the LIA lateral and terminal moraines. Among these, the greatest share of both area and volume is occupied by lateral moraines from the Daun (older) and Egesen (younger, Younger Dryas cold period) advances, with the Daun moraines displaying a more pronounced superimposed relief, which is probably the result of periglacial reworking (Kerschner, 1979). The Egesen lateral moraines can be found in many parts of the catchment about 130 m above the AD 1855 moraines very close to the Daun moraines and cover circa 3.11 km^2 of the study area's planimetric area. In the lower parts of the catchment, heavily modified moraine material, probably from the Egesen advance, makes up the valley slopes. Having lost their characteristic form, these zones were recorded as an original class in the geomorphological map. They cover approximately 1.65 km^2. Other lateral and terminal moraines from pre-LIA times (but younger than Daun/Egesen) can also be found. They are rare as most of these landforms have been destroyed by erosion. Interesting is an undated moraine ring located circa 550 m downstream the Weißsee glacier AD 1855 terminal moraines. The AD 1855 lateral moraines, in turn, are found in relative proximity to today's glacier extent. In the Gepatsch Glacier forefield, they reach heights of 220 m, in the Weißsee glacier forefield 66 m. Corresponding terminal moraines are located circa 2500 (Gepatsch Glacier) and circa 1400 m (Weißsee glacier) downstream of the 2012 glacier extents. Younger lateral and terminal moraines of significantly smaller sizes are nested on the inter slopes of the LIA lateral moraines. Most conspicuous today are the deposits by the glacier advance in the late 1980s, especially on the east facing moraine slope facing today's Gepatsch Glacier snout. In sum, lateral and terminal moraine deposits pertaining to the LIA and younger glacier extents cover approximately 2.29 km^2 of the study area's projected surface. Also ground moraine material covers a large portion of the study area, mainly in the higher reaches of the tributary valleys. About 2 km^2 of these ground moraine surfaces is located outside the proglacial areas and can therefore be interpreted as ground moraine older than 161 years. These areas can mainly be found at protected locations far from hill slopes, such as in the broad valley bottom upstream of the lowest lift station and directly outside the LIA terminal moraine ring in the Upper Krummgampen Valley. The moraine surface is typically pierced by geomorphologically inactive whalebacks. Quite naturally, it has been modified to some degree, mainly by periglacial processes and some soil formation, but not enough to be classified as another landform class or process area. Ground moraines younger than the LIA is, quite naturally, widespread in the study area, mainly due to the recent melting history. The large, gently undulating ground moraine

surfaces cover 4.89 km^2 of the planimetric study area. They are almost absent in the rocky, steep and heavily reworked proglacial zone of Gepatsch Glacier and ski tracks replace them in the Weißsee Glacier counterpart, but vast young ground moraine areas can be found in the proglacial zones of the glaciers at the heads of the tributary valleys, especially, Krummgampen and Riffl valleys. In addition to moraines, the whole landform ensemble typical for the Central Alps is present in the study area.

Talus slope and talus cones can be found under all high rock walls outside the proglacial areas. Talus cones form where rock fall is spatially concentrated, i.e. below gullies in the rock walls. Most of the time, a cone shape is not achieved as neighboring cones tend to grow together to form more sheet-like surfaces. Rock fall accumulation landforms cover about 3.98 km^2 or approximately 6.4 % of the study area. It is conspicuous that large talus cones and sheets are concentrated in an elevation band between circa 2600 and 3000 m h.a.e. This fact reminds of observations by Höllermann (1964, cited in Becht 1995b) who reports the biggest and most active talus landforms below rock walls whose contributing areas end above the local snow line. This statement, however, needs to be taken with a grain of salt as the occurrence of vegetation might not only reflect the activity statuses or talus landforms but also be a result of natural vegetation change with increasing elevation (see also Becht, 1995b). Working in the Central Alps, Becht (1995b) has also found that talus landforms are more conspicuous at higher elevations and attributes this fact to increased debris production due to a longer duration of glaciation, firn and permafrost in the late Pleistocene and more recent glacier advances.

As the process area of low magnitude rock fall is often the same as that of larger magnitudes, with the larger magnitudes reaching the bases of the talus, debris from a bergsturz can be found at one location in the study area, at the foot of the rock glacier in the Riffl Valley (see subsection 6.1.1.2).

Block slopes are found extensively above the Daun moraines (they cover about 4.9 % of the planimetric study area). In using the term "block slopes", I largely follow the definition by Otto (2006). They are the "rectilinear slopes" of Höllermann (1983b) and the debris-mantled slopes of Ballantyne and Harris (1994). While they are associated with periglacial conditions, they are often found in the vicinity or a similar elevation zone as rock glaciers.

These impressive landforms dominate the landscape of whole cirques in the Upper Kauner Valley (e.g. Innere Ölgrube, where the arguably largest rock glacier of the Eastern Alps is located). There is a number of rock glaciers of all activity statuses present in the study area. In addition, there are several locations that are indicative of creeping permafrost in coarse material but are not big enough to be classified as rock glaciers or could be addressed as push moraines. Together, these landforms cover about 1.86 km^2 or 3 % of the study area.

Fluvial sediments can be found in the current active floodplain, as terraces a few meters above the floodplains, but also in form of alluvial fans and former meltwater stream beds which are now located high above the main fluvial system. In addition, fluvial sediments can be found in hill slope channels and at the toe of hillslope reworked primarily fluvially. Due to the high relief, alluvial fans are rare. A notable exception is a large exemplar just south-east of the Gepatsch mountain hut, having formed below the true left side of the main valley.

3.4 Glaciology

About 31 % of the study area are currently (2012) covered by glacier ice, not all parts of which can be classified as pertaining to glaciers. Glaciers are defined here as ice masses which cover an area of at least 0.01 km^2. Following this definition, the study area is home of twelve glaciers (as of 2012), the biggest of which (Gepatsch Glacier) being the second largest glacier of Austria (see Tab. 3.4.1). In the Ötztal Alps, the elevation of maximum ice-cover is circa 200 m

Name	**Area [km^2]**	**Name**	**Area [km^2]**
Gepatschferner	15.729	Krummgampenferner	0.060
Weißseeferner	2.388	Hinterer Ölgrubenferner	0.056
Östlicher Wannetferner	0.548	Weißseejochferner	0.045
Westlicher hinterer Ölgrubenferner	0.140	Weißseeferner W1	0.025
Rifflferner	0.088	N/A	0.016
Westlicher Wannetferner	0.066	N/A	0.012

Table 3.4.1: Glaciers and their areas within the study area (2012).

higher than the average for all Austrian glaciers. This is mainly due to the central-alpine climate and the relatively large area in high altitudes (Abermann et al., 2009). Gepatsch Glacier is the best example and probably the main cause for this observation as its average elevation is 3120 m h.a.e. (as of fall 2012).
In spite of a short advance phase in the 1980s, the glaciers located in the Ötztal Alps have in general experienced thickness, volume and length loss in the years after 1969 and also after the end of the little ice age (LIA) in AD 1855. This trend has continued through more recent times. The minimum altitude of ice cover has risen from 2060 m a.s.l to 2120 m a.s.l in 2006, for example. The relative area loss becomes smaller with increasing glacier area although the mean absolute annual area loss has decelerated for very small glaciers (0.01–0.1 km^2) in recent times. This is probably due to the retreat of their ice masses in relatively shadowed and sheltered high cirques. Looking at all glacier size classes at once, it cannot be doubted that glacier retreat has been accelerating and that these smallest glaciers are an exception to the rule. Expectedly, glacier area losses have increased less at higher elevations than at lower ones. It should also be noted that mean annual volume and mean annual thickness changes have increased more than mean annual area changes across all size classes (Abermann et al., 2009). More information on glacier retreat in the Ötztal Alps can be found in Abermann et al. (2009).
The mentioned general trends also hold true for the glaciers within the study area. There is a good correlation between the observed temperature increase and the length change of the Gepatsch Glacier tongue, while change in precipitation seems to be of minor importance (Hartl, 2010). Hartl's work has also shown that ice losses in the upper regions of Gepatsch Glacier are increasing in importance when it comes to overall ice losses and that the rate of volume loss is about

double the rate of loss in area in recent years.
Studies in length and volume changes of Gepatsch- and Weißsee Glaciers have been undertaken irregularly since 1887 (Finsterwalder and Schunck, 1888) and regularly since 1969 (Abermann et al., 2009) (see chapter 3.8). After historical aerial photos had been orthorectified (cf. 5.4.2.1) and historical maps had been georeferenced, glacier extents of at least the tongue areas where mapped by the author and the sub-project from Innsbruck. As a result, glacier extents (at least for the Gepatsch Glacier tongue) were finally available from 20 time steps. The data show that Gepatsch Glacier has lost about 2.5 km of length since the end of the LIA and that between 2003 and 2009, the glacier tongue shortened by about 30 m yr^{-1}. The change in the relationship between area and elevation of all glaciers within the study area for the time from 2006 to 2012 is visualized in figure 3.4.1. The lowest elevations covered by glacier ice (at Gepatsch Glacier) has risen from 2170 m h.a.e. in September 2006 to 2189 m h.a.e. in fall 2012, which corresponds to a length reduction of circa 215 m. A thorough study of

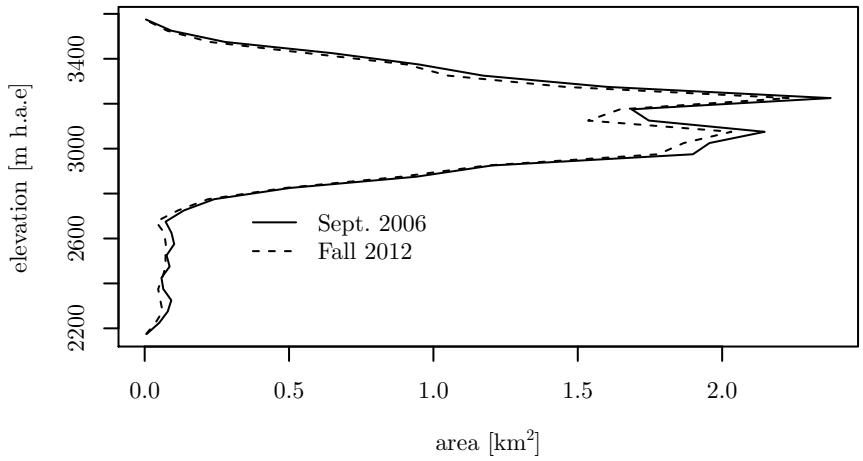

Figure 3.4.1: Area-elevation distribution in 50 m intervals for all glacier ice surfaces in the study area (September 2006 until fall 2012).

the Gepatsch Glacier and its volume and length changes between 1850 and 2006 has been presented by (Hartl, 2010). The glaciers in the study area have a long history of receding and advancing phases that can be traced through the whole Holocene. According to Nicolussi and Patzelt (2000), there have been multiple phases during the early Holocene in which the Gepatsch Glacier was shorter than in 1950. He has succeeded in reconstructing a temporally highly resolved image of the glacial history of Gepatsch Glacier.

3.5 Climate and hydrology

The study area's present climate can be described as a dry intramontane one with low annual precipitation values. In fact, the area is part of the driest part of the Austrian Alps. This is mainly due to rainshadowing effects by the surrounding mountain ranges. Relative low cloudiness and, as a result, unobstructed radiation lead to strong diurnal and seasonal temperature amplitudes (Fliri, 1975, Kilian et al., 1994). Figure 3.5.1 show two hygrothermal climate diagrams after Walter and Lieth for two locations of different elevation within the study area (data by courtesy of Tyrolean Waterpower AG (TIWAG), Innsbruck). The data represent a period from 2009 to 2015 (Gepatschalm, 1941 m h.a.e.) and 2006 to 2015 (Weißsee, 2516 m h.a.e.)[1]. While a value of circa 2.8 °C can

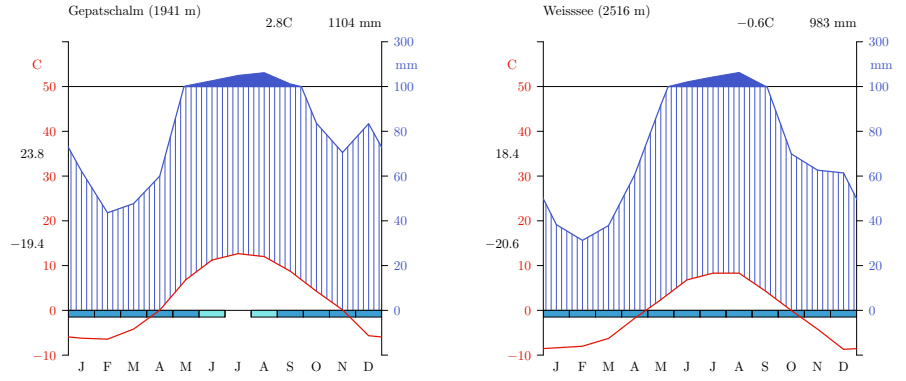

(a) (b)

Figure 3.5.1: Climate diagrams for two locations within the study area: Gepatschalm (a) and Weißsee (b).

be determined to the climate station at Gepatschalm (1941 m h.a.e.), an average annual temperature of −0.6 °C has been measured at Weißsee (2516 m h.a.e.). Using a temperature gradient of −0.65 °C per 100 m elevation change as determined by Thomas (1994), a range for the whole study area can be estimated. Thus, average annual temperatures should range between −7.53 °C at Hochvernagtspitze summit at 3583 m h.a.e. and 3.65 °C at the basin outlet 1810 m h.a.e. Mean annual temperatures at Gepatschalm show a higher variability (standard deviation: 2.7 °C) than mean winter temperatures (DJF, standard deviation: 1.55 °C) and mean summer temperatures (JJA, standard deviation: 0.91 °C). As no long-term temperature data is available for a measurement station within the study area, temperature data of Obergurgl-Vent (1938 m, c. 14 km air-line distance from the study area) provided by HISTALP was used for a trend analysis. The data and the result of a simple trend analysis is plotted in figure 3.5.2.

[1] I am fully aware of the fact that the time series of both stations are too short to obtain valid climate parameters, for which at least data of 30 years were necessary. In the absence of other stations within the study area I have calculated these statistics nevertheless.

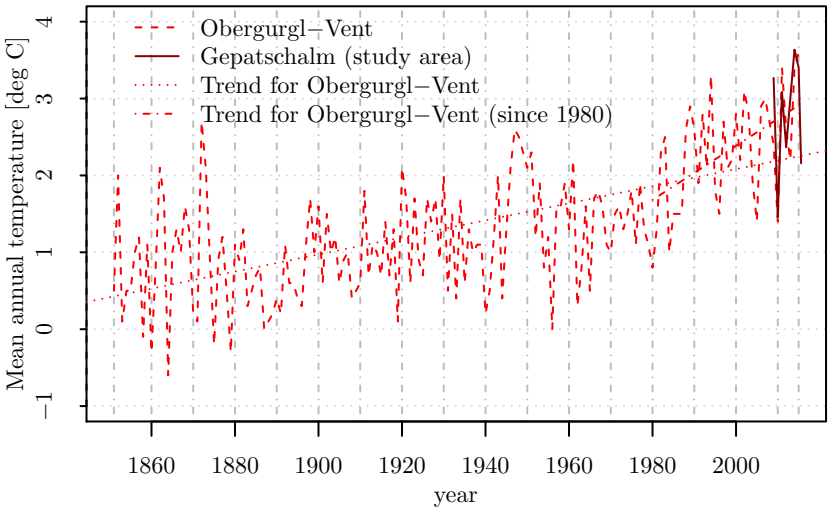

Figure 3.5.2: Temperature development over the last 164 years in Obergurgl-Vent.

In general, the Eastern Central Alps are characterized by a clear precipitation maximum in summer and relatively dry winters (Veit, 2002).
The annual precipitation shows an interannual variation between ca. 1030 mm and 1180 mm (Gepatschalm, mean 1100 mm and standard deviation 67 mm) and circa 730 mm and 1170 mm (Weißsee, mean 920 mm and standard deviation 128 mm), respectively. The seasonal precipitation variability is relatively high as can also be seen in figure 3.5.1 (Thomas, 1994). Rainfall mainly occurs during summer (maximum in August) in form of thunderstorms. These events potentially lead to extreme rainfall intensities capable of triggering debris flows (cf. 4.1.2) or initiating fluvial sediment transport in hill slope channels (cf. 4.4).
As no long-term precipitation data is available for a measurement station within the study area, precipitation data of Landeck or Obergurgl-Vent (798 m, circa 29 km air-line distance from the study area) provided by HISTALP was used for a trend analysis. The data and the result of a simple trend analysis is plotted in figure 3.5.3. A slight increase in annual precipitation sums has occurred in the region (see also Näher, 2013, Baewert and Morche, 2014).
The trends evident in temperature development and precipitation have a direct impact on discharge in the main channels of the study area. Discharge of the Fagge river has been measured continuously since 1971 by the TiWAG close to the Gepatschalm, some 3 km downstream of Gepatsch Glacier. The data show that while discharge maxima in the Fagge river have been generally increasing during the last 27 years, this trend cannot be observed for precipitation, which has been decreasing. It is very likely, that the increase in discharge maxima is to be attributed to increased glacier melt within the study area.
The discharge in the study area's main channels displays strong diurnal and

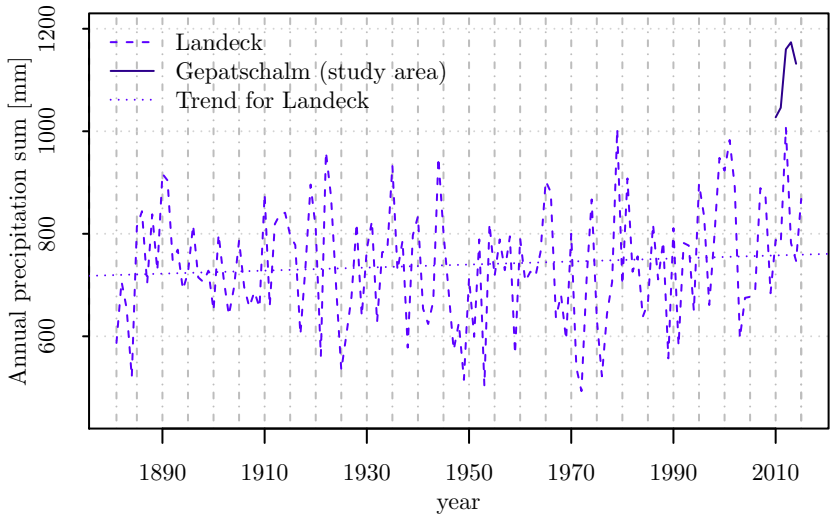

Figure 3.5.3: Yearly precipitation sum development over the last 164 years in Landeck.

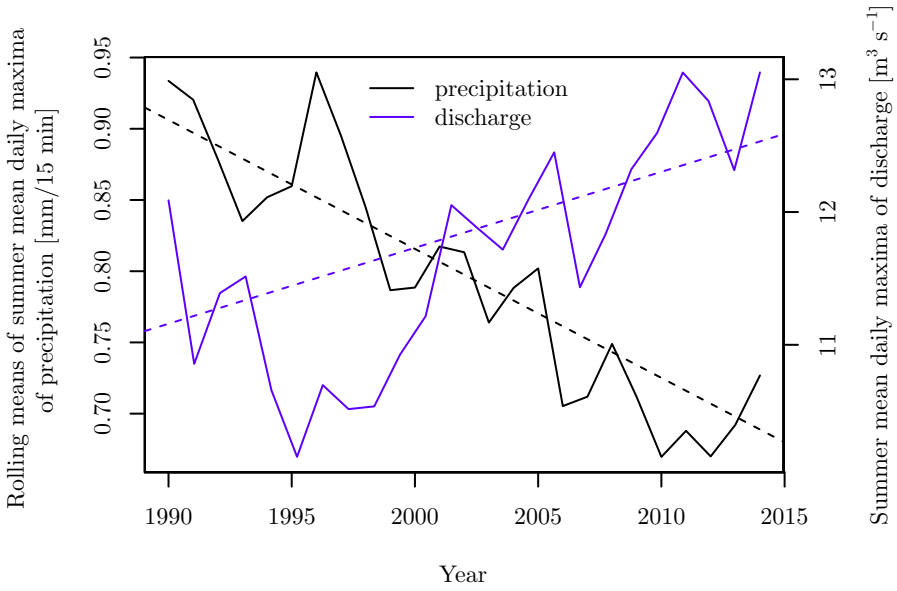

Figure 3.5.4: Discharge vs. precipitation trends. Discharge data from measurement station Gepatschalm. Precipitation data from climate station Dammfuss (circa 7.5 km north of the discharge measurement station).

seasonal variability as typical for glacial streams. From 1971 to 2015, the mean monthly discharge of Fagge river at Gepatschalm station varied from 0.17 m^3 s^{-1} in February to 9.46 m^3 s^{-1} in July (cf. 3.5.5). The highest discharge ever

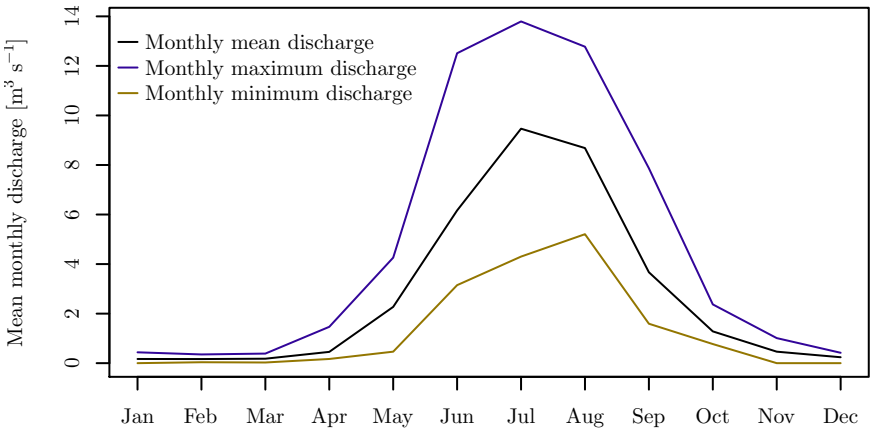

Figure 3.5.5: Distribution of monthly minimum, mean and maximum discharge at the measurement station Gepatschalm/Fagge river.

recorded was 59.18 $m^3 s^{-1}$ on August 24th, 1987, while the lowest discharge of 0.06 m^3 was recorded on March 22nd, 1992. The lion's share (c. 90 %) of discharge is occurring from May to September, while the months from December to February see only one to two percent of a year's discharge (Thomas, 1994).

3.6 Soils

Soil types predominant in the central alpine zone are acidic cambisols and leptic (semi-)spodosols. Leptic semispodosol can mainly be found on nutrient-poor crystalline rocks. Due to the relative dryness of the study area, the lower climatic elevation threshold for podosols occurrence is probably comparatively high. As a result of the influence of coniferous trees growing at relatively high altitudes and the high general elevation of the study area, spodosols are present in the lower elevations of the study area. At higher elevations, it is dystric leptosols and ranker soils that can be found (cf. Kilian et al., 1994, Harlaar, 2015).
Even when it comes to soils, the proglacial areas are a special case. Due to their recent deglaciation, their soils are in a initial stage of development. Soils found within the proglacial area were hyperskeletic leptosol (seldom), skeletic regosol, skeletic cambisol and spodosol (Harlaar, 2015, Temme et al., 2016). First signs of soil development in the Gepatsch Glacier proglacial area can generally be found at locations that have been deglaciated at least 40 years ago and soil formation seems to progress relatively fast (Harlaar, 2015).

3.7 Vegetation

Due to the generally high elevation of the study area, only a comparatively small percentage is covered by vegetation other than lichen. As a result of the study area's intramontane dry climate and high temperature amplitude, the tree-line is elevated (Kilian et al., 1994). It is mainly constituted by the Austrian stone pine (Pinus cembra) and located at about 2245 m a.s.l. It has been rising since the end of the little ice age. Krummholz can be found in elevations up to 2370 m a.s.l. (Nicolussi et al., 2005).
Of the nine vegetation elevation zones that can be delineated in Austria (taking information from Kilian et al. (1994) and Ellenberg and Leuschner (2010) to do so), only the four upper ones have a share in the Upper Kauner Valley. Table 3.7.1 gives an overview of the altitudinal vegetation zonation in the study area. In general, especially the Upper subalpine zone is modified by human activity

Altitudinal zone	**Elevation range**	***Plant communities* and species**
Nival zone	$>$ 3000 m	Low pioneer vegetation, e.g. Androsacion vandelii, Androsacion alpinae
Alpine zone	2300-3000 m	Alpine meadow and heath: *Caricetalia curvulae (Caricion curvulae, Festucion variae, Loiseleurio-Vaccinion), e.g. Vaccinium spp.*
Upper subalpine zone	2000-2300 m	Mainly Pinus cembra and Larix decidua, some Alnus viridis at rather wet locations, at higher elevations locally Rhododendron ferrugineum, Pinus mugo and Juniperus communis
Lower subalpine zone	1700-2000 m	Picea abies forest, interspersed Pinus cembra, Larix decidua, Salix spp. and Betula spp., some Pinus sylvestris L. at sunny and flat locations

Table 3.7.1: Altitudinal zonation of vegetation in the study area after Kilian et al. (1994), Ellenberg and Leuschner (2010) and Dubberke (2014)

(alpine farming) in the central Alps (Kilian et al., 1994). Alpine grazing in this vegetation zone is also common within the study area and has probably led to an altered composition in the vegetation. Very likely, the proportion of alpine meadows has been increased as a result.
Also when it comes to vegetation (succession), proglacial areas are a special case. As soil development and vegetation are interacting, reasons and factors are very similar to the ones discussed by Harlaar (2015) for soils. After these areas had become deglaciated, they were populated successively by pioneer vegetation.

It was observed that such vegetation (e.g. Linaria alpina, Saxifraga aizoides, Achillea moschata) can be found on surfaces only a few years old (Dubberke, 2014). Although slope and wetness are influencing factors, it could be shown that the time since deglaciation (which is, admittedly, a correlate to the other mentioned factors) is a meaningful factor for the quality and quantity of the vegetation in such areas, also in the study area. This could be shown by Pfaller (2011), who also mapped and identified a high number of different species within the proglacial zone of Gepatsch Glacier.
No vegetation map has been generated in the course of the PROSA project as the exact composition of the vegetation in the study area is not of interest for the sediment budget. As vegetation can influence erosional and deposition processes, though, a vegetation cover map comprising coarse classes of vegetation cover and height has been compiled for large parts of the study area. The spatial distribution of these different vegetation cover classes is depicted in figure 3.7.1 (cf. 5.6.2 for more information on the mapping) and the surface ratios of these different classes are reported in table 3.7.2.

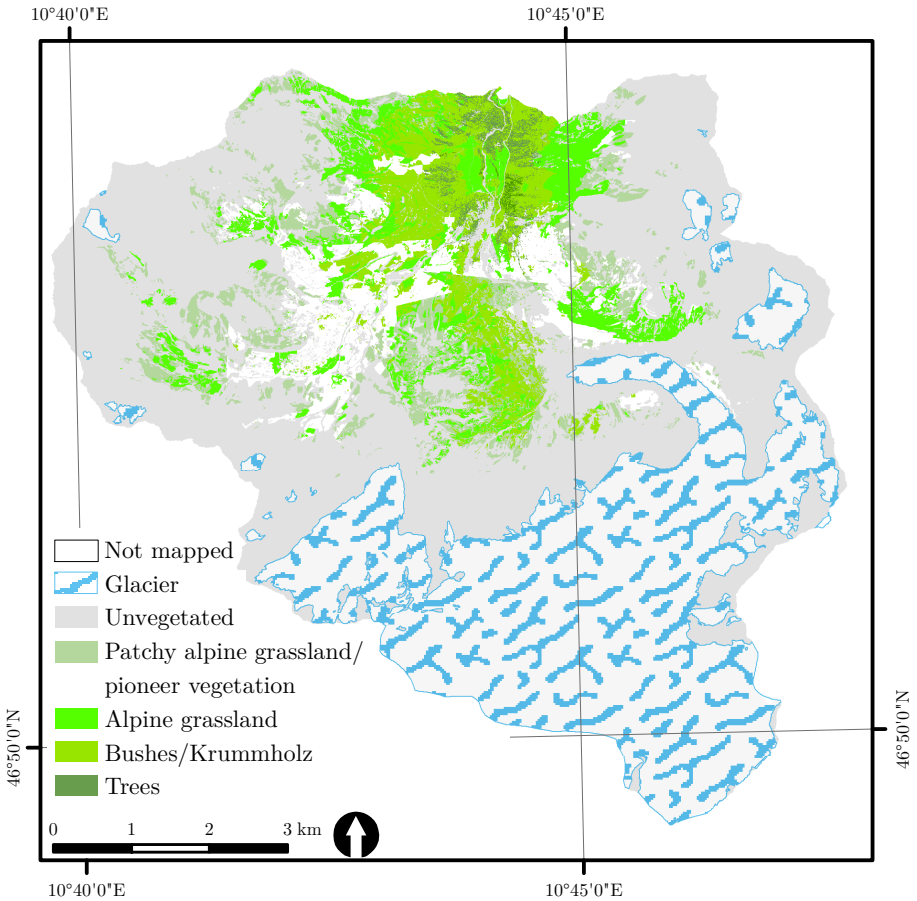

Figure 3.7.1: Vegetation cover map of the Upper Kauner Valley.

Although the map could not be finished before the final submitting of this thesis

(see section 5.6.2), it is complete enough to give an impression of the spatial distribution of vegetation in the study area.

Vegetation cover class	Not mapped	Not vegetated	Patchy alpine grassland or pioneer vegetation	Alpine grassland	Bushes or Krummholz	Trees
Percentage	6.55	74.06	6.34	6.34	5.78	0.93

Table 3.7.2: Surface percentages for the different classes in figure 3.7.1

3.8 Previous geoscientific work in the study area

Looking at the geomorphological setting of the study area, it is not surprising that some scientific work had been conducted by several working groups before the start of PROSA. A first outline of Gepatsch Glacier can be found in the Atlas Tyrolensis, published by Peter Anich and Blasius Hueber in 1774 (Hartl, 2010). First scientific investigations of the area were conducted by Sonklar (1860), who also presented a map showing the extent of Gepatsch Glacier at the time of the LIA maximum (Hartl, 2010). Early specific research was decidedly focused on glaciology and documentation of ice mass gain and loss of the Gepatsch Glacier. This research was significantly driven by the famous mathematician and glaciologist Sebastian Finsterwalder. After the Gepatsch Glacier had been professionally surveyed for the first time in 1887/1888 by him and H. Schunck (Finsterwalder and Schunck, 1888), and a second time by Kerschensteiner (1892) (see also Kutta (1901)), the glaciological work using geodetic and photogrammetric techniques at Gepatsch Glacier became a Finsterwalder family enterprise. Sebastian's research at the Gepatsch (Finsterwalder, 1897, 1928) was continued by his son Richard (Finsterwalder, 1953), who also compiled an informative review on the history of Gepatsch Glacier surveys (Finsterwalder, 1951). After him, his nephew Rüdiger Finsterwalder took over (Finsterwalder and Rentsch, 1976, Finsterwalder, 1978, Finsterwalder and Rentsch, 1980, 1991/92). After the Finsterwalder dynasty ceased to work in the area, methodologically similar work on glacier balances of the glaciers in the study area was accomplished by Kurt Brunner and colleagues (Munich and Karlsruhe) (Brunner, 1978, Henninger, 1985, Brunner, 1987, 1988) and later Axel Thomas' working group at Mainz and Gießen Universities (Keutterling and Thomas, 2006a,b, Erdmann, 2009). Kurt Nicolussi and colleagues focused on holocene glacier and climate development based on dendrochronology (Nico-

lussi and Patzelt, 2000). Work on the development of Gepatsch Glacier since AD 1855 includes Gross (1987) and Hartl (2010). Contributions to other glacier related topics in study area, including mass balances, are Kinzl (1929), Ebster (1951), Morawetz (1954), Klebelsberg (1964) and Kinzl (1966). Ice thickness of the Gepatsch Glacier was determined by Giese (1963) and Massimo (1997). Hoinkes (1954) worked on katabatic winds, amongst other locations, at Gepatsch Glacier. Research specifically in moraines has been undertaken by Heuberger (1966) and Kerschner (1979). Axel Thomas has also looked at climate and hydrology at Gepatsch Glacier (Thomas, 1994).
The geology of the Upper Kauner Valley has been investigated by Purtscheller (1978), Thöny et al. (2008), whereas the geologists Heißel and Weber (2000) took a closer look at the combined rock-glacier mass movement at the Weißseespitze. Data on the sediment discharge from the study area is available from Tschada and Hofer (1990).
Quite some work has been done on the dynamics (Finsterwalder, 1928, Pillewizer, 1957, Berger, 2002, Berger et al., 2004, Krainer and Mostler, 2006, Hausmann et al., 2007, Girstmair et al., 2013, Bremer et al., 2013), internal structure (Hausmann et al., 2012), genesis and dating (Gerhold, 1963, 1967, 1969) and hydrology (Krainer et al., 2007) of rock glaciers in the study area. The Krummgampen Valley has been subject to geophysical sediment thickness measurements and permafrost distribution modeling for the purpose of modeling the hydrological regime under climate change conditions (Hausmann et al., 2008, 2009, 2010, 2013).
Other relevant work on geomorphology and/or geology of the area include Krainer (2010). Recent and ongoing work focuses on the identification of spring water sources in perennial streams for an identification of dead ice in sediments (Kraushaar et al., 2014). Paleoclimate and tree-line evolution in the Kauner Valley was investigated by Krapf (2001), Nicolussi et al. (2005).

4 Processes relevant for the sediment budget

It cannot be the goal of a scientific study concerned with the sediment budget of a 62 km^2 large catchment to measure all processes shaping the landscape in high mountain areas. It is necessary to focus on the processes dominating the sediment transport (system). Although processes like biogenic transport, for example, have been traditionally subsumed under creep processes it has not been studied in the PROSA project. Animal burrowing by marmots has been observed several times in the study area. It is however, negligible if compared to other processes in the study area. The choice which processes were looked at closer was largely based on field observations made during the first visits in the study area and the insights gained during the preparation of the

geomorphological-geological map (Becht, 1995b).
The processes that were identified as being relevant to the sediment transport system in the Upper Kauner Valley and, as a consequence, were being investigated by the PROSA project and author in more detail will be introduced in the remainder of this chapter.
In the following remarks, processes were grouped into mass wasting processes (see chapter 4.1), which includes rock fall of all magnitudes (4.1.1), debris flows (4.1.2)[1] and slides of all magnitudes (4.1.3 and 4.1.4) on the one hand and the remainder of processes, which includes creeping permafrost (4.2), avalanches (4.3) and fluvial slope processes (4.4).
Sediment transport by the glaciers and in the main fluvial system are not going to be referred to in this part of the thesis or in chapter 5.7 as the author was almost not at all involved in the determination of respective transport rates as opposed to the other processes. Results obtained by sub-projects three and four will be reported and discussed in chapter 7.1 as they were used to finalize the sediment budget. For more information on these processes and corresponding data and methods, please see Stocker-Waldhuber and Kuhn (2016) and Baewert et al. (2012), Baewert and Morche (2014), Morche et al. (2014).

4.1 Mass wasting processes

I equate the term "mass wasting process" (the term that will be used in the following) with "slope failure" and "landslide" as used in the bulk of anglophone literature (e.g. Bennett et al., 2012). In comparison to other sediment transporting processes (fluvial transport or avalanches), mass wasting processes are characterized by a relatively high proportion of sediment in the total mass that is moved, i.e. no significant amount of extra medium (i.e. water) is present for the transport of the sediment (as during fluvial transport) (Laatsch and Grottenthaler, 1972, Tognacca, 1999).
Mass wasting processes are defined here as to encompass rock falls of all magnitudes (see section 4.1.1), debris flows (section 4.1.2), rock slides and deep-seated gravitational slope deformations (section 4.1.4) and shallow soil slips (section 4.1.3). Many authors, such as Carson and Kirkby (1972) also include creeping processes such as gelifluction/creeping permafrost under the term. This can be justified, however, as also sediment transfer by rock glaciers has been investigated in this study, frost creep has been subsumed together with rock glaciers under "creeping permafrost" in an original thesis chapter (4.2).
As most mass wasting processes operate as discrete events discontinuously and at various magnitudes, their occurrence can be described statistically by magnitude-frequency distributions, volume-area relationships and land surface parameter combinations favoring the process. Such analyzes can help to understand the nature of these processes and can, therefore, be used in predictions or for data gap filling in mass wasting process inventories that are used to estimate sediment

[1] I am aware that the high water content in debris flows places this process in the border region between mass wasting processes and mass transport processes.

production of such processes (Bennett et al., 2012) as a basis for a sediment budget. This is why related information will be presented for the respective mass wasting processes if possible.

4.1.1 Rock fall

Rock falls are slope failures occurring on usually pre-fracture bedrock, whereas most of the other mass movement processes addressed below occur in loose sediment and soils (Bennett et al., 2012). As a result, rock fall can also be seen as the first step in a sediment cascade (Burt and Allison, 2010) of a high mountain valley (cf. figure 2.3.1). As the rock fall process area is, naturally, on and close to steep rock walls at the valley sides or heads, only a small portion of the sediment actually transported by rock fall is delivered directly to the fluvial system. Over thousands of years, however, sediment storages in form of talus slopes/sheets and talus cones develop in the accumulation area, which can be coupled to the fluvial system via other sediment transporting processes such as debris flows (cf. 4.1.2) or frost creep (cf. 4.2.1) (Schrott et al., 2003, Heckmann and Schwanghart, 2013). Where it is deposited onto a glacier, it constitutes a non-glacial input to the glacial sediment budget. The contribution of rock fall to sediment budgets in comparison to other processes has been investigated in a number of studies in high mountain and other "cold environments", such as the (sub-)arctic (Rapp, 1960, Warburton, 1990, Becht, 1995b, Beylich, 2000, Johnson and Warburton, 2002, Beylich and Kneisel, 2009, O'Farrell et al., 2009, Sanders et al., 2013).
rock fall can occur at a wide range of magnitudes from small pebbles to millions of cubic meters. As a result, the methodology used for the quantification of these different magnitudes has to be chosen carefully. In the remainder of this thesis, the volumetric classification introduced by Whalley (1974, 1984) and also used by Krautblatter et al. (2012) will be adopted. Accordingly, rock fall will be referred to as either "debris fall" ($< 10\,m^3$), "boulder fall" (10–100 m^3), "block fall" (100–10^4 m^3), "cliff fall" (10^4–10^6 m^3) or "bergsturz" ($> 10^6$ m^3), depending on the volumetric magnitude.

4.1.1.1 Debris fall

Debris fall can manifest itself as material detaching directly from the rock wall (primary debris fall) or as material mobilized from sediment stores on ledges within the rock wall (secondary debris fall). The quantification of low-magnitude rock fall was seen especially important, given the long-standing controversial debate over its relative contribution to sediment budgets in high mountain areas. In addition, it is suspected, that existing (historical) inventories and the statistics derived from them are probably biased towards medium and high magnitudes due to undersampling of debris fall (see Krautblatter et al., 2012). Debris fall has been observed multiple times by the author in the study area, and accumulation landforms such as talus slopes or cones are witness to the great importance of debris fall in the Upper Kauner Valley. Therefore, great efforts have been undertaken to quantify and regionalize resulting debris fall rates in this study (see 5.7.1.1.1 and 6.1.1.1).

4.1.1.2 Block fall, cliff fall and bergsturz

Sediment transfer rates for rock falls larger than $100\,m^3$ for the whole study area were presented by Vehling (2016). As these processes are an important component of the sediment budget, his results and the methods used by him are summarized in subsection 6.1.1.2.

4.1.2 Debris flows

Many different definitions of "debris flow" can be found in the scientific literature. Tognacca (1999) defines debris flows as "multi-phase, nonsteady, terrestrial mass moving processes that can have a wide range of appearances, display fluid-like behavior due to their water content and can show different rheological behavioral patterns" (translated by the author). Although other criteria are just as relevant (cf. 4.1 and (Coussot and Meunier, 1996)), debris flows often are distinguished from other mass wasting processes on the basis of the proportion of transported sediment to water (Zepp, 2004). A sediment mass content of between 70 to 90 % has been used to distinguish debris flows from rock slides and soil slips on the one side and fluvial sediment transport on the other (Stiny, 1910, Hutchinson, 1988, Johnson and Rodine, 1984, cited in Gegg 2010).
Debris flows themselves have further been differentiated using either the morphological situation of the triggering area or the triggering mechanism as criteria (cf. Tognacca, 1999). Hence, debris flows were classified as either slope or channel type debris flows on the one hand and/or as resulting from concentrated overland flow or slope instabilities on the other.
Disregarding the complex interaction of various factors influencing the triggering of debris flows, it can be stated that the initiation of debris flows is restricted to areas where the following requirements are met: High slope inclination, sediment available for mobilization and presence of enough water for transport. Slope inclinations in areas of slope type debris flow initiation are usually in a range of 20° to 40° as lower inclinations cannot build up enough shear stress, while not enough sediment can be stored in steeper areas. As a certain amount of sediment is necessary for a debris flow to occur, this mass wasting process is predominantly found on sediment storage landforms, such as lateral moraines or talus cones and sheets. Debris flows are often triggered by thunderstorms of high intensity. Quite some research has been completed on identifying rainfall intensity threshold for debris flow initiation and a negative trend for necessary intensities has been observed from the Northern Calcareous to the Central Alps (Hagg and Becht, 2000). Authors give rainfall intensity thresholds of circa 60–90 $mm\,h^{-1}$ for the NCA and 30–40 $mm\,h^{-1}$ for the Central Alps (Hagg and Becht, 2000, Veit, 2002).
In the study area, debris flow starting zones were found at locations with loose sediment and a slope inclination $> 25°$. Visual inspections shows that there seems to be no correlation between debris flow occurrence and aspect or elevation. Debris flows are mainly occurring on the AD 1855 lateral moraines of the Gepatsch and Weißsee glaciers. This is not surprising as these areas display steep inclinations and huge amounts of reworkable sediment. They are slope-type debris flows ("type one", (Wichmann, 2006)) caused by saturation of the debris. At other locations (e.g. Riffl Valley), initiation zones are often located

below bedrock couloirs concentrating water flow onto the talus surface below. These slope-type debris flows are therefore of the "mobilized" (Takahashi, 1981, cited in Sattler et al. 2011)/"fire hose" (Godt and Coe, 2007)/"type two" (Wichmann, 2006) subtype. Some debris flows seem to have developed directly from small translational slides, which is not unusual (Tognacca, 1999, Godt and Coe, 2007).
It is characteristic of debris flows, that material is moved in discrete successive waves several seconds or many minutes apart. This behavior is indicative of different sediment storages being eroded. Once the sediment transport has started, it is often the case that more sediment is entrained as long as conditions are favorable. As a result, the part of a debris flows' total process area where this is predominantly the case is termed the "erosional zone". Being capable of depositing material along its way, debris flows can leave predefined channels on a debris cone and form new ones by depositing levées (Mittelsten Scheid, Timm M., 2011). During this process, water is lost and where the slope inclination is low and/or when no water is left to drive the process any more, the debris flow stops, thereby depositing all remnant sediment in the so-called "accumulation zone". Zones of the process area where neither erosion or deposition are predominant and sediment is only transported through is termed the "transport zone".
After the first visit to the study area, it had been clear that debris flows are common in many parts of the study area and it had been suspected that they play an important role in transporting sediment to the main fluvial system. Information on the data and methods used to quantify sediment transport by debris flows can be found in subsection 5.7.1.2, while results are presented in section 6.1.2.

4.1.3 Shallow soil slips

There is a number of different definitions of shallow soil slips to be found in the literature. In this thesis, the author is following the definition used by Betz (2016). Traces of shallow soil slips can be found spatially concentrated in various parts of the study area. This process acts on hill slopes vegetated by alpine grassland and often constitutes a problem in areas used economically because it implies erosion of soil material (Wiegand and Geitner, 2010, cited in Betz 2016). In addition, scars left behind by shallow soil slips can act as starting or erosion zones for more effective sediment transport processes (such as debris flows or avalanches) (Wiegand and Geitner, 2013, cited in Betz 2016). In the Upper Kauner Valley, these failing shallow translational sediment bodies form erosional features termed "Blaike" in German geomorphology.[1]
None of the erosional scars observed in the study is located close enough to the main fluvial system as it is likely that material has been transported by the translational slide to the main fluvial system. Nevertheless, sediment is moved by this process within the study area, which is why a quantification of the sediment moved by shallow soil slips is desirable. Methods to obtain this are reported in subsection 5.7.1.3, while results are presented in section 6.1.3.

[1] The term "shallow soil slip scar" will be used synonymously to "Blaike" in the remainder of this thesis, just as "shallow soil slip" will be used to consistently refer to the translational sediment movement having formed a "Blaike".

4.1.4 Rock slides and Deep-seated Gravitational Slope Deformations

Although they do not deliver sediment to the main fluvial system, rock slides and deep-seated gravitational slope deformations need to be treated in this thesis for two reasons: i) They constitute an important factor of system internal sediment movement in the Upper Kauner Valley and ii) they are important in preparing sediment masses for secondary processes (such as rock fall, cf. section 4.1.1). These large mass movement complexes can be grouped into two overall classes. This is why rock slides (ger. "Felsgleitungen", see Vehling (2016)) and deep-seated gravitational slope deformations (ger. "Großhangbewegungen, kombinierte Prozesse", "Fels-Schutt-Gleitungen", see Vehling (2016)) will be treated separately. Deep-seated Gravitational Slope Deformations (DGSDs) are distinguished from rock slides by the fact that sliding process do occur, but also lateral drifting and flowing processes are present. Therefore, they belong to the type of combined processes (Vehling, 2016). Some of these DGSDs do not incorporate bedrock, but also substantial amounts of sediment, which is another reason for a differentiation from pure rock slides. Many of these processes act as multiple interlaced sliding bodies, while (most of the time) the near-surface bodies display significant activity. All results are from Vehling (2016) and his findings will only be reported in this thesis (section 6.1.4) for reasons of completeness of the sediment budget and clarity. Vehling (2016) gives detailed geotechnical descriptions of all of these mass movements in the study area.

4.2 Creeping Permafrost

4.2.1 Talus creep

In addition to debris flows, it is also frost creep that transports sediment on talus slopes and talus sheets. Please see Dietrich et al. (1982) for a relevant definition of this process. Evidences for bound creep had been observed by the author on his very first visit to the study area in the Riffl Valley and indicators for unbound creep have been observed multiple times during various field visits. The methodology used to estimate the sediment transfer by frost creep in the Upper Kauner Valley is presented in subsubsection 5.7.1.5.1, while results are reported in section 6.2.1.

4.2.2 Rock glaciers

Although it is unlikely that rock glaciers contribute much to the sediment exported from the study area (because they are decoupled from the main channels), it had been clear from the beginning that the internal sediment transfer accomplished by them is probably not to be scoffed at and that they need to be

addressed.
Rock glaciers are landforms pertaining the process complex of creeping permafrost. Active individuals move due to internal ice deformation as a result of gravity (Berger et al., 2004). In the Alps, active rock glacier creep velocities range from a few centimeters to a few meters per year (Humlum, 2000, Frauenfelder, 2004, Krainer and Mostler, 2006, cited in Dusik 2013). There is a great number of different rock glacier definitions and classifications (focusing on different aspects) found in the literature (e.g. Capps, 1910, Wahrhaftig and Cox, 1959, Johnson, 1974, Haeberli, 1985, Hamilton and Whalley, 1995). In this study, rock glaciers were defined by their morphology rather than by their thermal conditions as they pass through several activity phases during their lifetime (Berger et al., 2004). Therefore, three different classes were used to reflect different activity statuses in this study (Dusik, 2013): i) Active rock glaciers, which contain ice and move at least a decimeter per year. They are not vegetated and display a steep front, ii) Inactive rock glaciers, which still contain ice, but do not move. Their fronts are less steep and initial vegetation can be observed on their surface and iii) relict/fossil rock glaciers, which do not contain ice any more and therefore display a subsided surface. Only active rock glaciers transfer sediment and therefore have a share in the sediment budget. In the context of climate change, massive acceleration accompanied by surface subsidence in root zones or fast growing transversal crevasses have been observed on many rock glaciers in recent years (Kääb et al., 2007b, Roer et al., 2008, Avian et al., 2009). This also holds true for the well-studied rock glaciers in the study area.
The three most prominent active rock glaciers in the catchment are the multilobe Riffl Valley and Ölgrube rock glaciers and the single-lobe Krummgampen rock glacier. In their function concerning the sediment transport system of the Upper Kauner Valley, they are representative and will therefore be introduced (see Dusik (2013), Dusik et al. (2015) for a more differentiated discussion of these rock glaciers concerning multiple lobes, geology, genesis, etc.).
The Innere Ölgrube rock glacier seems to have lost its connection to the debris source area. As it displays high flow velocities, has a very well-developed rock glacier surface morphology and incorporates LIA till, this very large and famous rock glacier is believed to contain an ice-core and to have formed from debris-covered glacier tongues. Berger et al. (2004), Dusik (2013) and Neugirg (2013) report that it is still active, based on low spring water temperatures, BTS-measurements and high surface velocities (maximum of $2.5\,\mathrm{m\,yr^{-1}}$ and being temporally variable) (see also Berger (2002), Krainer and Mostler (2006), Hausmann et al. (2012)). Nevertheless, it is neither supplied with ice or debris from its root zone. Deep melt water lakes in the upper part of the rock glacier tongue are evidence for intense melting (Berger et al., 2004). The rock glacier effective blocks all coarse sediment transfer from the Innere Ölgrube cirque. It is drained by the small Schilti torrent running through a steep channel towards the Fernergries area. This torrent, however, carries no coarse sediment from the rock glacier (personal communication Dusik, August 22, 2016).
The well studied rock glacier in the Riffl Valley, covers an area of circa $0.26\,\mathrm{km^2}$. It separates two large parts of the Riffl Valley, thereby blocking the sediment from the upper part (cf. below). The rock glacier tongues enter a flat valley section characterized by the accumulation mass of the bergsturz discussed in subsection 6.1.1.2, which has caused the generation of a fluvial deposition area in its upstream area. The small river draining from the rock glacier front runs

through the sedimentation area and often below debris from the Bergsturz event (Dusik, 2013, Neugirg, 2013, Dusik et al., 2015). This prevents even relatively fine sediment from exiting the upper section of the Riffl Valley.
A less well known and smaller rock glacier covers an area of about 0.1 km^2 in the Krummgampen Valley at an altitude from circa 2515 to 2780 m h.a.e. It is by far not known about this multi-lobate rock glacier than it is about the two already discussed. The rock glacier has served as a methodological test site for Bremer et al. (2013). It is of great interest to this thesis as it is the only rock glacier located close enough to the main fluvial system to directly deliver coarse sediment to it and will therefore be discussed in the following.
Although it is probable that almost no sediment is transported into the main fluvial system in the Upper Kauner Valley, the sediment transfer by rock glaciers is of utmost importance for the sediment budget as a comparatively huge amount of sediment is moved by rock glaciers internally. Rock glaciers have repeatedly been reported as being among the processes moving the most sediment in high mountain areas (e.g. Barsch, 1977, Nyenhuis, 2006, Müller et al., 2014). The strategy used to estimate sediment transfer by rock glaciers in the Upper Kauner Valley is presented in subsubsection 5.7.1.5.2. Corresponding results can be found in section 6.2.2.

4.3 Avalanches

No discussion of avalanche definitions will be undertaken here, as there is an extensive body of relevant literature. Analogously, none of the various classification schemes based on avalanche dynamics, starting zones (morphology), snow texture, etc. will be adopted (De Quervain, 1966, McClung and Schärer, 1993, Lackinger and Gabl, 2000, Heckmann, 2006b). As the focus of this work is on the construction of a sediment budget, also avalanche genesis (metamorphic processes within the snow pack, etc. (cf. McClung, 1975, Langham, 1981, Bader and Weilenmann, 1992)) and morphology of avalanche deposits and impact forms (e.g. Matthes, 1938, Rapp, 1959, Peev, 1966, Corner, 1980, Luckman et al., 1994, Owen et al., 2006, Johnson and Smith, 2010) or mechanisms of sediment entrainment by avalanches (Barbolini et al., 2005, Confortola et al., 2012) are not discussed here. The reader is referred to the publications mentioned above.
It has been repeatedly shown, that some avalanches do not only transport snow, but also other material like vegetation and, most relevant in the context of sediment budget work, sediment. Corresponding research dates back to the first half of the 20th century (Allix, 1924, Matthes, 1938). Important work on sediment transport by avalanches has been completed (among others) by Gardner (1970b, 1983b), Luckman (1977, 1978), Bell et al. (1990), Becht (1995b), Jomelli (1999), Ackroyd (1986, 1987), Heckmann et al. (2002, 2005), Sass et al. (2010), Freppaz et al. (2010), Ceaglio et al. (2010), Confortola et al. (2012), Moore et al. (2013), Korup and Rixen (2014). Most of all avalanches transport not very much sediment. It is especially full-depth avalanches and slush avalanches

occurring late in winter or early in spring that are relevant for sediment transport (Sæmundsson et al., 2008), also in the study area. Although comparatively slowly moving due to a high content of water, full-depth snow avalanches have a high potential of sediment transport as snow volumes available for avalanching in late winter/early spring are high.
The amount of material transported by wet snow avalanches should not be underestimated. This is underlined by the terminology in English scientific literature, where the term "dirty avalanche" has become vernacularized (Moore et al., 2013, cited in (Näher, 2013)). In fact, sediment transporting avalanches can lo-

Figure 4.3.1: Sediment transporting avalanche accumulation in the Riffl valley, early June 2014.

cally be the dominating geomorphic process (Rapp, 1960, Luckman, 1977). The amount of sediment transported is a function of many factors. It is obvious that the composition of the substrate a avalanche traverses influences the amount of sediment transported. Where deep channels concentrate avalanche flow, sediment transport seems to be more intensive than on open, linear hill slopes although the erosional force can be very high at such location as well, given loose sediment is available for mobilization (Luckman, 1978, André, 1990b). In cases of vegetation covering the avalanche process area, less sediment is mobilized, while certain vegetation conditions can foster the entrainment of sediment. Last but not least, sediment transport is also highly dependent on the volume and speed, that is the kinetic energy of an avalanche (Barbolini et al., 2005). Where large snow masses travel at high speeds, vegetation can be destroyed and

sediment entrained at the same time.
While many authors limit the ability of sediment transport to full-depth and slush avalanches, this cannot be adopted for the current study. In the Upper Kauner Valley, it has been repeatedly observed that it is also surface layer avalanches transporting sediment. This occurs after the avalanche traversed hill slope areas already snow-free in early spring. In addition, debris falling onto the snow surface during winter are moved by surface layer avalanches (cf. Jomelli and Bertran, 2001). This also implies that avalanche starting zones must not be congruent with erosional zones, a fact that also holds true for full-depth and slush avalanches, which tend to entrain a large share of the transported sediment in their transit zones (Heckmann et al., 2002, Freppaz et al., 2010). Independent of the type of avalanche, transported sediment is accumulated together with the snow masses in lobate deposition zones. In order to prevent unnecessary terminological distinctions without difference in regard to sediment budgeting, the term "sediment transporting avalanche" will be used in this study to refer to all types of avalanches relevant for sediment transport, independent of their genesis or movement mechanism.
The methodology used to obtain sediment transfer rates by sediment transporting avalanches is introduced in section 5.7.2, while the results are brought forward in chapter 6.3.

4.4 Fluvial hill slope sediment transport

Slope erosion by surface runoff on hill slopes can manifest itself either as slope wash, linearly as rill or gully erosion or in the subsurface as piping. Aquatic slope erosion is considered being of great importance in the Upper Kauner Valley due to several reasons. First, a large portion of the study area is free of vegetation.
Second, it is mainly the small channels draining the slopes that negotiate the landscape often fragmented by landforms running parallel to contour lines (such as lateral moraines or bedrock outcrops, cf. 2.2). In comparison to other processes, they have the ability to connect sediment sources relatively far above the main channels more or less directly to the main fluvial system.
Surface parallel erosion by true sheet wash is probably of lower importance in the study area. Talus cones and slopes (which cover a considerable part of the catchment that is not covered by bedrock or glacier ice) are composed of too coarse debris to allow either Hortonian or saturation overland flow. This assessment is supported by Dunne (1979), Becht (1995b). Exceptions are steep vegetation-free areas on moraine deposits more or less impermeable to water. In the study area, such surfaces can be found on the lateral slopes of the channel heads of highly active 1855 lateral moraines and on erosion scars caused by shallow soil slips.
Results on this process are presented in chapter 6.4 and the methods used to obtain these results will be introduced in section 5.7.3.

5 Data and Methods

5.1 Research design

The methodological concept to quantify and/or regionalize rates in this study is as follows: Processes were either measured at monitoring sites of scales of either test plots or whole slopes (the "topische Dimension" of Becht (1995b)) or from ALS data covering the whole catchment (the "chorische Dimension" of Becht (1995b)).
Most of the time, the number of test sites was limited due to the large size of the catchment and difficult high mountain terrain even including glacier surfaces to be traversed for monitoring site access. The monitoring sites varied in geomorphological land surface parameters like aspect, altitude, but also in geology and lithology. Data acquisition and initial processing were mainly accomplished by the relevant sub-projects (cf. 2.5). Data compiled by the sub-projects served as an input for the work presented here and represented various states of processing states, from just after pre-processing to averaged sediment production rates. This data served as a basis of further processing or direct input for model-based regionalization.
In some cases (e.g. 5.7.2), regionalization was the basis for a calculation of values representative for the whole study area, thereby applying values obtained on a smaller scale (and smaller support) to a large-scale area (upscaling) (Blöschl and Sivapalan, 1995, Blöschl and Grayson, 2001, cited in Heckmann 2013b).
In this thesis, "test plot scale" will be used to refer to areas of a size of up to circa $40\,000\,\mathrm{m}^2$ as measurements used for a regionalization and up-scaling spanned over areas of up to that size: Test plots on avalanches were only of a size of $0.25\,\mathrm{m}^2$, hydrological catchments of fluvial hill slope channels sampled using sediment traps were of sizes of several thousand square meters, while sections of hill slopes up to $40\,000\,\mathrm{m}^2$ were surveyed via TLS to obtain measurements for fluvial hill slope erosion or debris flow quantification.
Including project preparatory work by Pfaller (2011) and Brandlmeier (2011), field work was done over a period from Summer 2010 to 2016. Due to the high alpine setting of the study area, field work involving remote sensing methods was only possible from mid-June to mid-October, whereas work on avalanche sediment transport, reservoir sedimentation and fluvial hillslope processes usually started a month earlier. Processes operating quasi-continuously with low magnitudes (e.g. debris fall, fluvial hill slope erosion) were measured on LiDAR test plots or with permanent sediment traps (rock fall collector nets, sediment traps in the hill slope channels). Processes occurring less often but operating at greater magnitudes (e.g. avalanches) were balanced using an event-based strategy (see also Becht, 1995b).
As most of the data was of spatial nature, of high data volume and was to be analyzed statistically, it was very important to establish and administer spatial postgres databases (cf. 5.4.4.1) or GIS (Geographic Information Systems). Fig-

ure 5.1.1 represents a simplified flow chart of the most important data sources or measurement devices and software packages that were used to establish data analysis for this study. Interfaces between otherwise incompatible software packages were established by self-written R scripts.

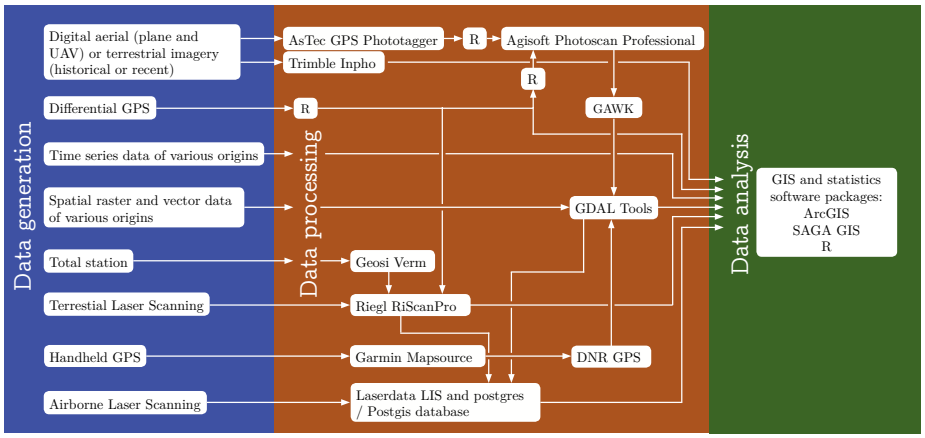

Figure 5.1.1: Most important data sources and software packages used in this study.

One of two main methodological backbones of the PROSA project and the work presented here are point clouds of diverse provenance that are being used for morphological budgeting (cf. 5.2). Essentially all point clouds were acquired using one of two basic remote sensing methods. Active methods encompassed different LiDAR sensors, producing point clouds directly. Passive sensors used different optical cameras, the images of which were used as input for a photogrammetric work flow to produce point clouds. While photogrammetry has been applied extensively in high mountain geomorphology and glaciology since at least 1913 (cf. Finsterwalder and Pillewizer, 1939), LiDAR has experienced a sharp increase in popularity in the geosciences. Recently, advances in computing technology and unmanned aerial vehicles (UAV) have, in turn, triggered a likewise sharp rise in applications of full-automated photogrammetry ("Structure from Motion" (SfM)) for point cloud generation. All methods mentioned have specific advantages and disadvantages. These will be discussed in the respective sections presenting the methods and measurement systems used.
In addition to the data acquired by working groups of the PROSA project, there are several sources from which relevant time series data on meteorology and hydrology were acquired. Precipitation, temperature, snow height and total radiation data of 15 min temporal resolution were available for two within and one station close to the study area. Monthly precipitation data were available for ten stations, four of which being located within and six close to the study area. All these data were provided by TIWAG.
In the following, general information on the overall methodology will be given. This comprises data and methods relevant for the work concerning all processes. The process-specific methodology will be presented and discussed in the respective sections dealing with these processes (chapter 5.7).

5.2 Budgeting using topographic data of different time steps

The above mentioned remote sensing methods are capable of generating point clouds in projected coordinate reference systems that can be conceptualized as discrete samples from a random field. The differencing of these point clouds or their derivatives to obtain the locations and volumes of sediment movement is generally seen as the most feasible method to establish sediment budget of various scales in different cold environments (cf. 2.2). This strategy of measuring sediment movement is widely known as the "morphological method" in the English literature (Wheaton, 2008). Although the general concept has been used in geomorphology a long time, the used techniques for acquiring the single point measurement used were generally too time-consuming and labor intensive as to allow for a survey of more than valley cross sections or single points that were thought to be representative of a whole landform. The advent of automatable total stations or dGPS constituted a step forward, but usage was historically confined to investigations in braided river systems (Brewer and Passmore, 2002, Wheaton, 2008, Carrivick et al., 2013). The sensors mainly used in this study, that is, TLS and ALS are introduced in section 5.4.1.

5.3 Coordinate reference system

As one of the requirements of the PROSA project is to measure geomorphic changes in high spatial and temporal resolution, it was important to choose a suitable projected coordinate reference system. After sub-project five of PROSA, dealing with geodetic questions, made the recommendation to use the European Terrestrial Reference System 1989 (ETRS89) / Universal Transverse Mercator zone 32 north coordinate reference system (EPSG-code: 25832), all data sets used in this work, having been acquired within the project (e.g. dGPS (cf. 5.4.3), LiDAR (cf. section 5.4.1) or photogrammetry (cf. 5.4.2.2)) or obtained from third parties, were ultimately projected into this coordinate reference system. As a result, all elevations derived from own data and given in this work represent ellipsoidal heights and are given as "height above ellipsoid" (h.a.e.) instead of "altitude above sea level" (a.s.l.). Details on the chosen projected CRS are given in table 5.3.1. The CRS was realized in the field by the establishment of five fixed points, measured by global navigation satellite system (GNSS) raw data logging and subsequent correction using the EPOSA-reference station network. This work was accomplished by the Vienna working group. The established fixed points were later used by the author as reference stations for real time kinematic (RTK) dGPS measurements and the measurement of TLS reflectors (see subsection 5.4.3.1).

Aliases	ETRF89/UTM zone 32N (EPSG: 25832)
Area of use	Europe-6°E to 12°E (EPSG: 2126)
Base geodetic CRS	ETRS89 = ETRF89 = EUREF89 = ETRS89-GRS80 (EPSG: 4258)
	Geodetic Datum: ETRS89 (EPSG: 6258)
Conversion	UTM 32N (EPSG: 16032)
Cartesian CS	Cartesian 2D CS
	Axes: easting, northing (E,N)
	Orientations: east, north (EPSG: 4400)

Table 5.3.1: Details on the CRS ETRS89/UTM 32N (EPSG: 25832) used throughout this work (International Association of Oil & Gas Producers, 2015).

5.4 Point data acquisition and processing

5.4.1 LiDAR

The most important data source for this study was acquired using LiDAR. LiDAR is a remote sensing method applying an active sensor. In principle, it is very similar to RADAR, however applying a smaller wavelength. Most laser measurement devices operate at wavelengths from 400 to 1600 nm (Beraldin et al., 2010). There are two different building classes for laser measurement devices: pulse lasers and continuous-wave lasers. In general, continuous-wave laser measurement systems have higher data rates, but lower range (< 100 m). As only pulse laser devices were applied in this study, only those will be addressed in the following. More information on the short range / continuous-wave laser technology can be found in Beraldin et al. (2010). Long range laser measurement devices calculate the distance by measuring the travel time of the laser light to the object and back, thereby most of the time setting up the emitter and receiver at the same distance to the object (see Beraldin et al. (2010) for more information, including the components and mechanics of laser scanners). As light waves travel withing a specific medium with a known velocity, the distance to the scanned object can then easily be calculated. No measurements are possible below the water surface as IR light cannot travel trough water. This results in measurement gaps at such locations.
The footprint of a laser beam becomes wider with increasing distance. Due to the divergence of the laser beam, the signal entering the receiver is an average of the surface within the beam footprint. If the footprint illuminates targets of varying distance from the measurement device (e.g. branch of a tree and rock face behind the tree), a single laser shot will result in multiple signal returns. The received signal, will therefore display a multimodal distribution with each mode corresponding to a different target.
Modern LiDAR measurement devices are capable of recording these distinct modes and discretizing them at a Ghz rate (so-called full-waveform devices).

As a result, it is not uncommon for a measurement point to be associated with an attribute specifying the return number of a laser shot it represents (as with almost all ALS data used in this study). Nevertheless, it is necessary for multiple targets within a laser beam's path to be separated by a minimum distance to be discerned as different targets. This minimum distance (R_{min}) represents the vertical resolution of a LiDAR device (cf. 5.4.1).

$$R_{min} = c \cdot \frac{t_{min}}{2} \tag{5.4.1}$$

with c being the speed of light and t_{min} the minimum time difference between two received echoes in order to be separable. Consequently, in order for a target object's echo to be registered as valid by the receiver, a minimum amount of energy needs to be returned from the target. The amount received is dependent on the distance, the area illuminated by the laser beam, pulse length, and, most importantly, the reflectivity of the target (Baltsavias, 1999, Beraldin et al., 2010). The amplitude of energy pulse at the receiver is generally recorded as a measurement point attribute (often also called "intensity"). The reflectivity of an object, in contrast, is an attribute of the scanned material, therefore independent from the distance, and can be calculated from the amplitude. It is dependent on the wavelength of the laser scanner, which is why different wavelengths have differing suitability for various surfaces (Beraldin et al., 2010). The availability of both multiple returns from one laser shot and object reflectivity as measurement point attributes can be very helpful in surface classification and was also used in this study (cf. 5.4.4).
Only the most important basics of LiDAR could be presented here. For more information on principles in LiDAR (e.g. specific of ALS, swath width, along ALS track point spacing, return pulse separation, formulas for all relations, etc.), the reader is referred to the relevant literature, such as Baltsavias (1999), Petrie and Toth (2008), Shan and Toth (2008) and Vosselman (2010).

5.4.1.1 Terrestrial Laser Scanning

While ALS systems have strong limitations in measuring the surface of steep terrain (cf. 5.4.1.2), TLS can fill these gaps. On the contrary, it is usually quite cumbersome to obtain an occlusion free point cloud of large areas of rather flat terrain (as accomplished in Hilger et al., 2015b). This is why most applications of TLS in geomorphology apply TLS to the monitoring of rock walls (e.g. Abellán et al., 2006, Haas et al., 2012b), steep hill slopes (e.g. Dunning et al., 2009, Aryal et al., 2012), active rock glacier fronts(Bauer et al., 2003, Avian et al., 2009) or steep river banks (e.g. Jaboyedoff et al., 2009, O'Neal and Pizzuto, 2011).
TLS instruments typically consist of a transmitter and receiver of laser pulses (typically in the infrared section of the electromagnetic spectrum), a scanning device, i.e. an internal system of oscillating and rotating mirrors and an automatically moving casing. TLS devices show very high data acquisition speeds with newer devices being able to measure up to 220,000 pt s^{-1} (e.g. Riegl Laser Measurement GmbH, 2014), which is a significant advantage over alternative surveying methods (e.g. total stations or dGPS-devices). The data is acquired in the TLS device's own coordinate system which uses the optical center of the

device as the origin. Coordinates of laser measurement points are stored in polar coordinates (ρ, horizontal angle, vertical angle φ). Most devices also record intensity or, especially some newer devices, reflectance as a point attribute.
During the course of the PROSA project, two different TLS devices were used for data acquisition, both by the Austrian manufacturer Riegl (http://www.riegl.com, see table 5.4.1) and both being panoramic scanners. Riegl terrestrial laser scanners have widely been used in geomorphological research (e.g. Bauer et al., 2003, Avian et al., 2009, Sanders et al., 2013) and offer satisfying fields of view (FOVs), precision and range. During the first monitoring year in the study area the device model LMS-Z420i was used. After July 2013, the newer and more advanced model VZ-4000 was applied. Both devices maintain complete eye safety (Laser Class one) as their wavelength can be absorbed by the water in eyeballs (Beraldin et al., 2010). Figure 5.4.1 shows both devices during field work. The

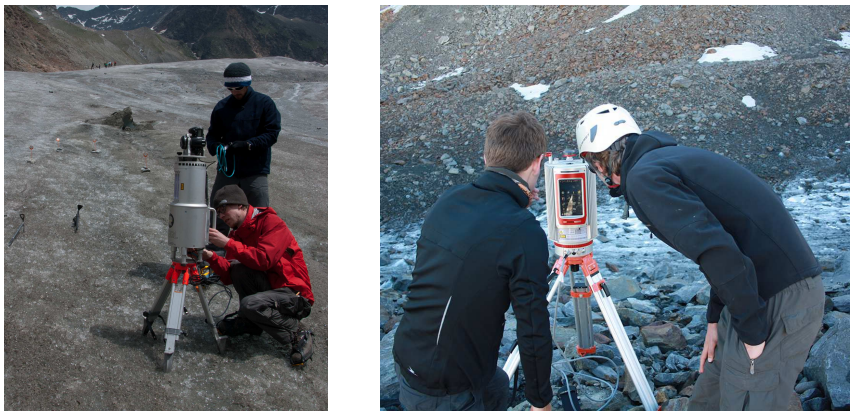

(a) (b)

Figure 5.4.1: TLS devices used for the acquisition of TLS point clouds: Riegl LMS Z-420i (left) and Riegl VZ-4000 (right).

LMS-Z420i is operated from a personal computer via a USB port. The software "RiScanPro" (supplied by the manufacturer) was used for this purpose (Riegl Laser Measurement GmbH, 2011). Due to the rough climatic conditions in the high Ötztal Alps, a Fujitsu Siemens tablet PC was employed in the field. The LMS-Z420i can be equipped with a Nikon D70 camera. After the laser and camera have been registered using a mounting procedure, photorealistic point clouds can be produced for visualization or further processing (see 5.4.4.2).
The VZ-4000 is a long-range TLS measurement device and does not need an external PC for operation. It possesses an internal 5-megapixel digital camera, which renders the camera mounting procedure unnecessary. Just as the Z420i, a vertically oscillating and/or rotating mirror mounted on a stable 360° rotating mechanism ensures relatively quick data acquisition (Riegl Laser Measurement GmbH, 2014). All TLS point clouds used in this study were georeferenced using control points (cf. subsection 5.4.4.2). Just as the LMS-Z420i, the VZ-4000 is powered by external 11-32 V DC batteries. In order to minimize shadowing effects, high tripods were used when accessibility allowed. During each measurement, a low resolution overview scan was acquired prior to the proper

Parameter	LMS-Z420i	VZ-4000
Maximum range*	1000 m	4000 m
Precision	up to 4 mm (average)	up to 10 mm
Accuracy**	10 mm	15 mm
Max. measurement rate	110 000 pt s^{-1}	222 000 pt s^{-1}
Max. FOV	80 °· 360°	60 °· 360°
Laser wavelength	near infrared	near infrared
Beam divergence	0.25 mrad	0.15 mrad
Minimum angle measurement resolution	0.002°	0.0005°

Table 5.4.1: Most relevant parameters for the TLS devices LMS-Z420i and VZ-4000 used in this work (Riegl Laser Measurement GmbH, 2010, 2014).
* Only under test conditions: Highly dependent on target reflectivity; only valid with flat targets bigger than the laser beam and vertical to the scanning direction; with good atmospheric conditions (high atmosphere clarity and overcast sky); also dependent on measurement rate selected.
** dependent on range

measurement. This served then as a basis for the selection of the area to be measured in detail. In doing so, battery power and time could be saved. The actual measurement scans were acquired using angle resolutions of 0.05° (all LMS-420i measurements) and 0.02° (all VZ-4000 measurements). Measurements were generally acquired using the last pulse detection mode, i.e. only last returns of a given laser pulse were recorded by the device (cf. 5.4.4.2).
A total number of 35 different areas have been surveyed by the Eichstätt working groups. To do so, 42 different scan positions have been set up and were visited at least once a year since summer 2012. Due to long snow cover some scan positions could be surveyed only once a year (e.g. 19–21), while others could be surveyed up to three times a year. A map of the scan positions in the study area is given in figure 5.4.2. The acquisition of the TLS scans in the field reported here was mainly accomplished by PROSA sub-project one. As all the data was extensively used in this study and the author was involved in the processing and data management of almost all and the acquisition of about a third of the data, the TLS data base is reported in the appendix. Only an outline is given, most notably, registration and georeferencing errors (cf. 5.4.4.2) or distances to target (ca. 40 to 250 m, depending on the scan position) are not given here. For values of each single scan, see Dusik (2016). Information on the georeferencing of some of the scans via reflective targets and dGPS and total station surveys can be found in section 5.4.3.

5.4.1.2 Airborne Laser Scanning

As it is impossible to monitor all 62 km^2 of the study area via TLS, ALS data for (almost) all of the catchment was acquired about two times a year by a third party company. An average point density of 10 pt m^{-2} had been demanded for each of these survey flights. Ideally, the whole study area should have been surveyed during one day per survey. Weather conditions and organizational problems on part of the commissioned company, however, prevented this. As

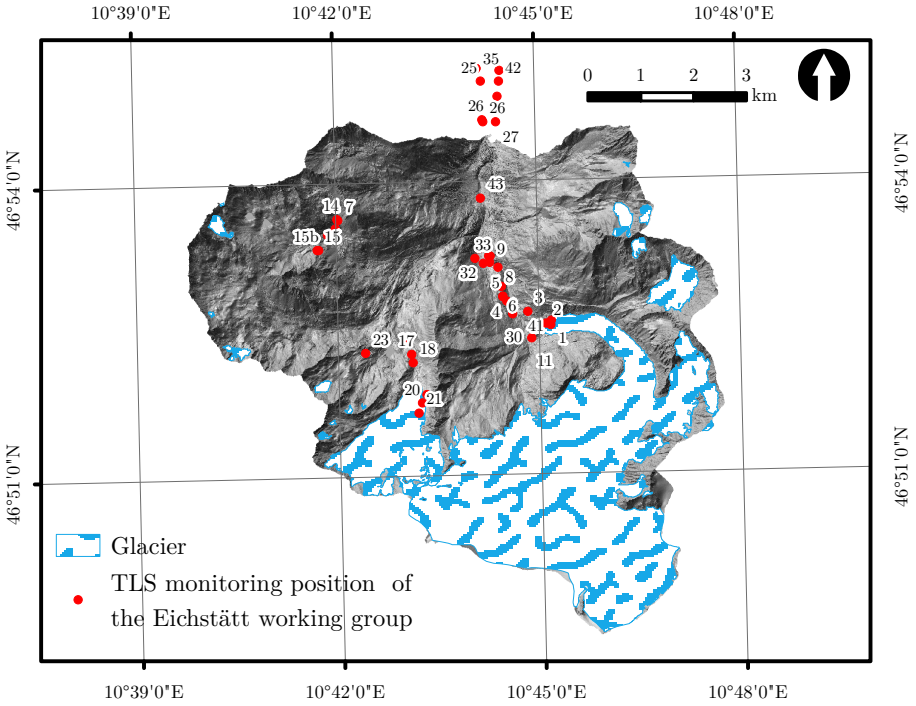

Figure 5.4.2: TLS scan positions maintained by the Eichstätt working groups.

a result, surveys of different parts of the study area, which should have been undertaken in a preferably small temporal interval, were conducted in as much of almost four weeks from each other (cf. surveys from fall 2012, table 5.4.2). Between ca. 112 and ca. 645 million points were generated on each of the survey days listed in table 5.4.2, totaling to 3.348 billion ALS points (as of June 2016) available for this study. As all aerial data, restrictions in measurement performance arise when the surveyed area contains steep sections such as rock walls as their surface is invisible from the airborne platform. As a result, a combination of both ALS and TLS measurements was desirable if a processes in a high mountain area shall be monitored extensively in both time and space as done in the PROSA project and Ruiz et al. (2004), Bremer and Sass (2012). To our knowledge, there has been no geomorphological study so far, that could resort to a data base as highly resolved temporarily and spatially on a scale as within the PROSA project.

5.4.2 Photogrammetry

The second, but less important source of topographic point cloud data was photogrammetry. While it has recently been used more extensively in sub-project one, the usage of topographic data from photogrammetry in sub-project five was almost exclusively limited to point clouds generated from historical aerial images from the 1950s. Digital elevation models derived from these images were used in the calculation of long-term sediment yield rates for the whole catch-

Flight date	Percent (area) of study area covered	Total nr. of points acquired	Average point density [pt m^{-2}]*	Scanner	Wave length	Operator
September 5, 2006	100	c. $400 \cdot 10^6$	c. 4.6	N/A	N/A	N/A
2008	c. 40	c. $112 \cdot 10^6$	c. 3.25	N/A	N/A	N/A
July 4, 2012	c. 64.5	c. $645 \cdot 10^6$	c. 11.9	Riegl LMS-Q680i-S	1064 nm	Milan Geoservice GmbH
July 5, 2012	c. 47.1	c. $326 \cdot 10^6$	c. 7.2	Riegl LMS-Q680i-S	1064 nm	Milan Geoservice GmbH
July 18, 2012	c. 68.2	c. $485 \cdot 10^6$	c. 7.9	Riegl LMS-Q680i-S	1064 nm	Milan Geoservice GmbH
September 28, 2012	c. 49.2	c. $533 \cdot 10^6$	c. 10.76	Riegl LMS/Q 680/400	1550 nm	Milan Geoservice GmbH
October 25, 2012	c. 69.2	c. $574 \cdot 10^6$	c. 9.6	Riegl LMS/Q 680/400	1550 nm	Milan Geoservice GmbH
July 18, 2014	c. 44.7	c. $271 \cdot 10^6$	c. 9.6	Riegl LMS-VQ580	1064 nm	Milan Geoservice GmbH

Table 5.4.2: Available ALS data and corresponding flight mission attributes (current as of June 6th, 2016) as used in this study.
* Within study area, referring to the area that was actually surveyed.

ment (see chapter 7.1) and for an investigation of long-term sediment movement by rock glaciers (see 5.7.1.5.2).
In addition to generating point clouds, photogrammetric techniques were applied to obtain orthorectified aerial images of different time steps since the 1950s. These were very important for mapping past processes (as with debris flows in subsubsection 5.7.1.2.1) and facilitated the mapping efforts in all PROSA sub-projects (cf. chapter 5.6 and Vehling (2016), for example).

5.4.2.1 Classical photogrammetry

The use of aerial images in geomorphological studies has been increasing steadily since the 1970s (Kondolf and Piegay, 2003). While this fact is mainly due to the increasing availability of such data and the development of more user friendly evaluation techniques, historical aerial images are of great value for sediment

budget studies. To be able to assess the intensity of geomorphic processes during the past decades and arrive at more reliable estimates of magnitude-frequency relationships of acting processes, historical aerial images covering the study area were to be acquired and orthorectified, whereby an average position precision of less than one meter was sought. Analogue aerial images of the study area or parts of it exist from the year 1953 onwards. The area of interest has been covered in time intervals of one to 16 years by different companies commissioned by different ordering parties. The uncompressed greyscale 8 bit scanned images were acquired from the Austrian federal office of geodesy (Bundesamt für Eich- und Vermessungswesen (BEV)). Table 5.4.3 gives an overview of the acquired images.

Flight date	Percent of study area covered by resulting orthophoto	Number of purchased images	Purpose	Source	Camera	Focal length [mm]	Scanning resolution [μm]	Average flying height [m a.s.l]*	Ground resolution of resulting orthophoto [m]
June 5th, 1953	60**	4	Forest condition estimation; Flight C	BEV	N/A	210.11	15	ca. 4700	0.4
August 31st, 1953	60**	36	Forest condition estimation; Flight C	BEV	N/A	210.11	15	ca. 8300	0.4
September 8th, 1953	60	48	Forest condition estimation; Flight C	BEV	N/A	210.11	15	ca. 7550	0.4
September 1st, 1954	10, reservoir	17	Forest condition estimation; Flight D	BEV	N/A	210.23	15	ca. 10130	0.55
October 7th, 1969	> 95	7	Austrian glacier inventory taking	BEV	Wild RC5/RC8	152.05	15	ca. 7120	0.45
September 29th, 1970	45	10	Tyrolean state surveying flight	BEV	Wild RC5/RC8	210.43	12	ca. 8665	0.2
August 18th, 1971	60	16	Tyrolean state surveying flight	BEV	Wild RC5/RC8	209.48	12	ca. 5025	0.25
August 14th, 1979	80	8	Hintereisferner	BEV	Wild RC5/RC8	152.59	15	ca. 8395	0.55

Continued on next page

Table 5.4.3 – continued from previous page

Flight date	Estimated percent of study area covered by resulting orthophoto	Number of purchased images	Purpose	Source	Camera	Focal length [mm]	Scanning resolution [μm]	Average flying height [m a.s.l]*	Ground resolution of resulting orthophoto [m]
September 13th, 1982	80	2	Tyrolean state high altitude surveying flight	BEV	Wild RC10	152.58	15	N/A	0.5
October 10th, 1990	100	5	N/A	BEV	Wild RC10	152.60	15	N/A	0.5
September 11th, 1997	85	4	N/A	BEV	Wild RC10	152.70	15	N/A	0.5

Table 5.4.3: Attributes of the image flights, the images of which were used for the generation of orthophotos and/or point clouds via structure from motion.
*As given on the images.
**This number is a sum of the coverages of all flights from 1953.

The data in table 5.4.3 show that the images were of scales ranging from circa 22300^{-1} to about 55000^{-1}. The complete work flow of orthophoto generation from the historical aerial images was accomplished in Trimble's Inpho software package (http://www.trimble.com/Imaging/Inpho.aspx) and corresponds to the classical work flow of digital stereo photogrammetry (cf. Schulz and Dornblut (2002) for more information). As a result, it is not referred here in great detail: After all images of a single image volume were oriented to north and pyramid layers were calculated for each single image, the internal orientation was established by providing data like focal length, principal point of symmetry (PPS), principal point of autocollimation (PPA) coordinates and fiducial mark coordinates from camera calibration reports (where available) in camera files and measuring of fiducial marks. Where no calibration report was available, the fiducial mark coordinates were determined.
External orientation was accomplished using ground control points mapped from an ALS-derived DEM, image projection center coordinates (x and y were estimated, z was read from the images) and aircraft pitches. The realization of a field measurement campaign with dGPS was taken into consideration as coordinates taken from remote sensing data are in general of inferior quality to coordinates acquired directly in the field and the GCPs could have been distributed at the most suitable positions over the image block. Several factors, however, opposed such a field campaign. First, a great portion of the study area are in a highly alpine environment with either steep rock faces or glacier surfaces. These were either inaccessible for a person with DGPS rover or would have required a financial and temporal expenditure that was not justified given that spatially high resolved LiDAR data was available. Second, for a measurement using GPS with a precision better than the one provided by an interpolation of ALS data, a certain degree of topographic openness is required to receive a sufficient number of satellite signals. Experience had shown that this is a difficult task, especially in the steep alpine valleys. Tests in the field have shown that measurements at the valley sides can take over half an hour or might not be possible at all, even after setting up a base station or using the live EPOSA correction service. This evaluation has also been reported by others (e.g. Schulz and Dornblut, 2002). Third, measuring rugged (valley side) locations with total station was no solution as the required precision could only have been achieved using a reflective prism. This would also have required a person to enter the dangerous zones. In addition to the ruggedness of the terrain, it was the extent of the study area that made a dGPS and/or total station measurement campaign at it's the margins, where the points are most important, unfeasible. Several locations would have been accessed from different neighboring valleys. Even under optimal weather conditions and with perfectly working equipment, the GCPs measurement campaign would easily have taken two weeks. Using an ALS-derived DEM, a total of 56 GCPs were prepared and subsets of these were used for orthophoto generation for the different image volumes. The GCP coordinates were measured with a position precision of ca. $\pm$ 30 cm and an elevation accuracy of ca. $\pm$ 40 cm. In addition, 20 to 100 tie points were established per image block. Image 5.4.3 gives a map of the projection center coordinates for each image volume.
Later, tie points were found automatically (usually between 2 and 28 per image) and measured iteratively before aerial triangulation (using the bundle adjustment procedure) was used for solving for intrinsic and extrinsic orientation

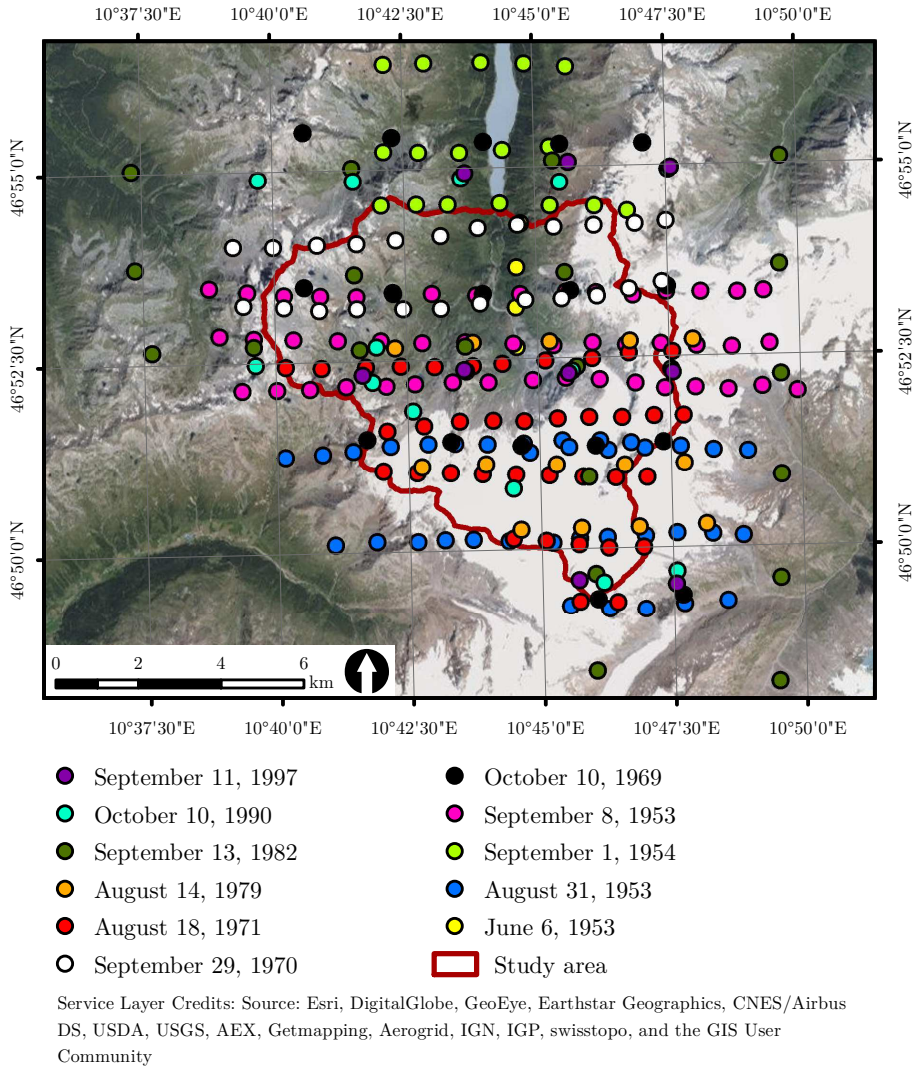

Figure 5.4.3: The image projection centers of the aerial images used for orthophoto generation.

parameters. In doing so, a whole image mosaic corresponding to one flight campaign and occasionally composed of several flight lines was oriented all at once and the camera coordinate system of each image was transformed to the PROSA project coordinate system. The high number of ground control and tie points was necessary as the image block itself was not stable enough to be supported by only a few points. Reasons for this obstacle could include suboptimal acquisition geometries and, of course, the extreme relief within the area of interest (cf. Schulz and Dornblut, 2002). To achieve a satisfactory overall solution, different combinations of GCPs used for each image block were tested. This procedure resulted in a global accuracy of between 0.4 and 0.5 pixels for

the different image blocks. Depending on the resolution of the input images, the ground resolution of the resulting orthophotos was fixed between 20 and 55 cm. The positioning accuracy of the images ranges below 50 cm in most cases, with the worst part showing discrepancies of up to 1.5 m. The images from the years of 1953 and 1954 were also used in the generation of four point clouds representing the surface of the respective flying dates (cf. subsection 5.4.2.2) using Structure from Motion methodology.
In addition to the orthophotos generated from aerial images for the study, several volumes of ready-made orthophotos were purchased from different suppliers. While the images from AD 1997 and older were all panchromatic, the purchased orthophotos were multispectral (r,g,b). They are listed in table 5.4.4.

Flight date	**Estimated percent of study area covered**	**Source**	**Ground resolution [m]**
September 5th, 2003	95	BEV	0.2
September 9th, 2009	80	BEV	0.2
July 31st, 2010	30	BEV	0.2
September 2010	70	BEV	0.2
2010	reservoir	BEV	0.1
July 18th, 2014	33	Milan Geoservice GmbH	0.1

Table 5.4.4: Attributes of purchased orthophotos used in this study.

5.4.2.2 Structure from Motion

The fact that previous work (cf. 5.4.2.1) had shown that orthophoto generation based on historical aerial images of the study area was feasible with small enough errors, the endeavor to generate a point cloud representing the study area's geomorphological state of the years 1953 and 1954 was undertaken as such data can be of value to investigate process intensities on the time scale of several decades. Previous work (Schiefer and Gilbert, 2007) had shown that a resulting terrain model can reach accuracies good enough for such purposes.
The images from the flights of 1953 and 1954 were used for a point cloud construction. The used images and their location are illustrated in figure 5.4.4.
All SfM processing steps were performed in the Agisoft Photoscan Professional software (http://www.agisoft.com/features/professional-edition/) on a very capable work station desktop machine:
In a first step, the external camera orientation had to be found. This includes image matching, feature correspondence analysis, image alignment, a successive adding of new cameras and a determination of relative camera positions followed by the actual "Structure from Motion" step, i.e. solving for intrinsic and extrinsic orientation parameters. In an Agisoft Photoscan Professional work flow, these steps correspond to the "Align photos" work flow step:

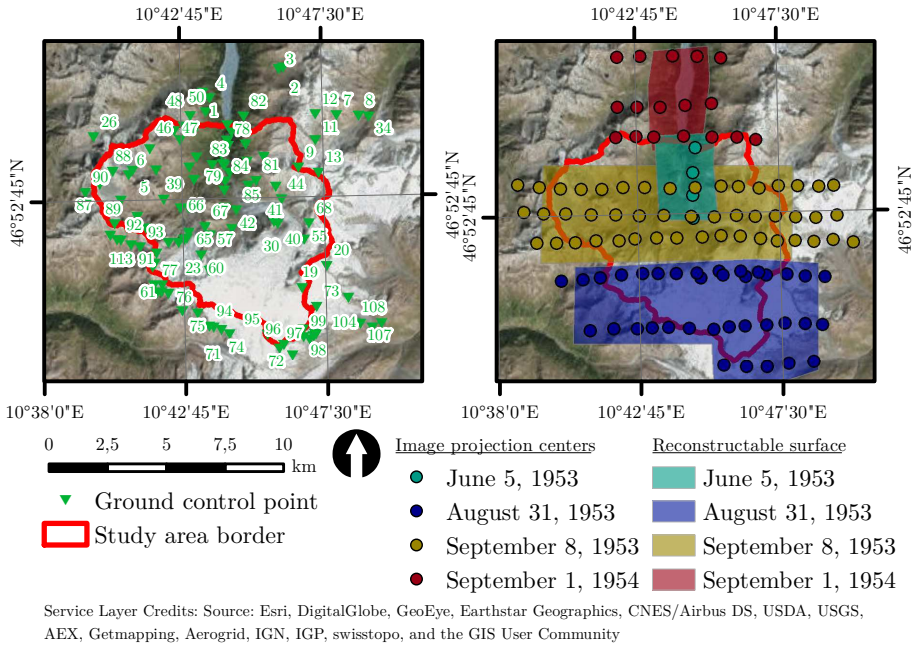

Figure 5.4.4: The flight missions and location of the image principle points of all aerial images used for point cloud generation using structure from motion.

After a masking of scratches, fractures, fungi and errors resulting from the scanning of the original analogue images, the quality and contrast of the images were found to be good enough to permit omission of a radiometric editing. The images were then matched using digital image correlation applying pixel gradients calculated on different resampling levels. A detailed description of the algorithm is given in Lowe (2004).
The relative camera orientations were then determined using the obtained feature correspondences using algorithms similar to the ones published in Fischler and Bolles (1981), Haralick et al. (1994), Nistér (2004). This is an iterative process, with new cameras being added to the model during processing.
Also bundle adjustment is performed automatically, solving for the intrinsic and extrinsic orientation parameters ("Structure from Motion"). Papers relevant to the algorithms used in by Agisoft Photoscan Professional are probably Pollefeys et al. (2002), Oliensis (1999), Lourakis and Argyros (2004), Brown and Lowe (2005).As the quality of this matching step is mainly dependent on the radiometric properties of the used images and only one eight bit greyscale band was available in the images, a comparatively high amount of manual intervention was necessary to align aerial images satisfactorily. Eventually, with the images covering almost exclusively the snow covered collecting basin of Gepatsch Glacier, the flight mission dating to August 31st, 1953 could not be aligned and was therefore dismissed.

As digital photos are a central projection of the objects they display, each image pixel corresponds to an object point. The amount of image pixels used for point cloud generation, and therefore the resulting point density, can be adjusted in the software. As the software interface only allows for a qualitative

parametrization, this parameter was always set to the second highest point density. Given the high amount of pixels in each image, no calculation of the highest density was possible with the computing system available.Due to unsatisfactory user-control, no DEMs were generated in Agisoft Photoscan Professional. The so-called "dense point cloud" was exported and further processed in the LIS software package, instead (cf. subsection 5.4.4.4).
The image block, and the consequential point clouds were georeferenced to the CRS used in the project (cf. chapter 5.3) via ground control points. As no ground control points had been placed on the surface during the flight missions in the 1950s, conspicuous natural and non-moving landmarks (like centers of boulder tops or similar) were used as GCPs, as contemplated in Bauer et al. (2003) and performed in Schiefer and Gilbert (2007).
A direct measurement of the GCPs to be used for SfM-point cloud generation was not possible for the same reasons why no GCPs were measured directly for orthophoto generation (see subsection 5.4.2.1). As the SfM-derived point cloud data was to be set off against ALS data to ultimately obtain sediment transport data, a much more elaborate work flow was developed for GCP coordinate determination in comparison to the one followed for historical orthophoto generation: First, the GCPs used for orthophoto generation and mapped on orthophotos were buffered and the resulting area was used to sample from the 2012 ALS point cloud data. Second, the point cloud was colored to conspicuously show the GCP, which revealed the mis-georeferencing between the orthophoto and the ALS data. Third, the location of the GCP was mapped directly in the ALS point cloud data and the coordinates of the closest ALS point was used as coordinates of the ground control point. This approach would also be preferable for orthophoto generation (subsection 5.4.2.1). However, the ALS data had not been available in the same quality and were not as readily accessible during the time when the orthophotos were generated. Figure 5.4.5 shows this correction procedure for GCP number 19. The GCPs acquired using this procedure were used for a georeferencing of all SfM image blocks and, among others, were also used in Dubberke (2014) and Wiggenhauser (2015). Most geomorphological studies working with SfM data report neither data on precision nor accuracy. What is being reported in most cases is the root mean square error of the GCPs used for georeferencing, which is calculated as follows:

$$RMSE = \sqrt{\frac{\sum_{i=1}^{n}(z_{pc_i} - z_{gcp_i})^2}{n}} \tag{5.4.2}$$

where n is the number of GCPs used for georeferencing the image block, z_{pc_i} the elevation of the point cloud at the location of the i-th GCP and z_{gcp_i} the actual (measured) elevation of the i-th ground control point. As can easily be seen, the RMSE is a global model-internal measure. Therefore, it is not possible to assess the local variation of accuracy over the resulting point cloud. Another look at equation 5.4.2 also reveals that the RMSE value decreases with decreasing number of used GCPs. As a result, a low RMSE value does not automatically imply a good accuracy or precision of the point cloud. Consequently, one should not use the RMSE value as a single quality measure of any point cloud or other digital surface representation (cf. below, pers. communication Stuart Lane, Oct. 2015). As the RMSE is the only error measure provided by many Sfm software packages and also by the widely-used software Agisoft Photoscan Professional,

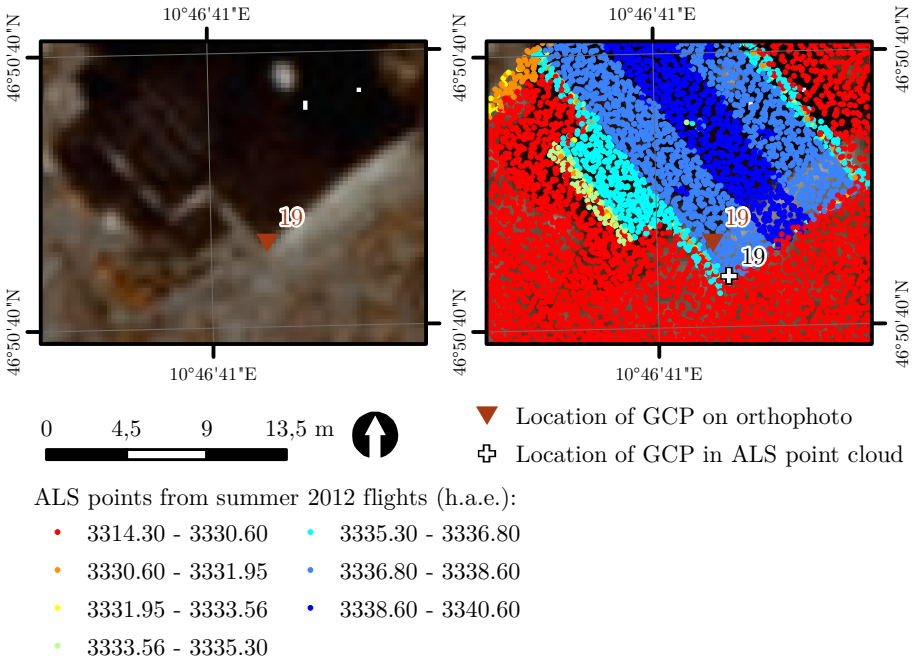

Figure 5.4.5: SfM ground control point number 19, being the south-western corner of the roof of the Brandenburger Haus mountain hut. The mis-georeferencing of the orthophoto can clearly be seen (circa 2.4 m xy space in this case). It is evident that such an amount of mis-registration can lead to significant problems in volume calculations if non-corrected GCP coordinates were used, especially in steep areas.

Flight	**Total nr. of points**	**Av. point density [pt m^{-2}]**
June 5th, 1953	ca. 38 Mio.	ca. 5.2
September 8th, 1953	ca. 300.5 Mio.	ca. 6.4
September 1st, 1954	ca. 2.6 Mio.*	ca. 3.6

Table 5.4.5: Total number of points and average point density of the point clouds generated with SfM. See figure 5.4.4 for the approximate areas of the study area covered by the reconstructed surfaces.
*Already clipped to the area of interest (cf. chapter 7.1).

however, this is the quality measure given in most geomorphological works published. As it is the only measure available to assess the quality of georeferencing of photogrammetric point cloud without comparisons to data obtained with other devices and gives some information on the model-internal quality, it was also used by the author as an indicator for GCP exclusion decisions. Different GCP combinations were tested until the RMSE was lower than one meter (the RMSE obtained for the image block of September 1954, for example, was 0.46 m (Wiggenhauser, 2015)). Later, DEMs obtained from the point cloud data were generated and compared to ALS data to exclude any grief systematic georeferencing errors.
The resulting point clouds were of different density and quality. Data quality was spatially highly variable, which is why only spatial subsets of the reconstructed surface could be used for geomorphological investigations. Table 5.4.5 gives some important attributes of the point clouds constructed by SfM.

5.4.3 Differential GPS and total station

Other sources for topographic point data were measurements with dGPS and total station. Before the advent of TLS and ALS, point clouds used for DTM construction were generated from painstaking fieldwork with dGPS (e.g. Brasington et al., 2000, Baptista et al., 2008, Young, 2012). Although both dGPS and total station measurements are of higher accuracy than LiDAR or photogrammetric data (Young, 2012), data from both devices were mainly used for registration and georeferencing of TLS point clouds via surveyed reflector discs and did not contribute to the overall surface topography point data base in this study. This is widespread and standard in studies based on high-density topographic data (e.g. Mora et al., 2003, Moretto et al., 2013).
In order to both facilitate and enhance the precision of TLS point cloud registration and to enable a georeferencing of TLS point clouds to the global coordinate reference system, reflective targets (discs with a diameter of 10 cm) were fixed to non-moveable objects or surfaces (big boulders, but mainly bedrock outcrops) within the scanned areas (see figure 5.4.6). 22 different scan positions were equipped with, in total, 87 reflector discs. The reflectors were left at their fixed location in the field for the duration of the whole project and were used for the registration and georeferencing of TLS scans acquired after the placement of the reflectors. Where possible, reflector discs were placed at different distances, and

Figure 5.4.6: Reflector discs with a diameter of 10 cm (left) were fixed to non-moveable objects (2nd from left) and used for a better registration and georeferencing of TLS point clouds. These reflector discs were later surveyed exactly using a differential GPS device (2nd from right) and a total station (right).

at different vertical and horizontal angles from the TLS device location as this is beneficial for an exact registration (see figure 5.4.7). During each TLS survey, as many reflector discs as possible were scanned with the highest possible point density. Where the TLS data was to be set off against ALS data, the global coordinates of the reflective disc centers were determined exactly with either dGPS or a combination of dGPS and total station measurements (see below).

5.4.3.1 Differential GPS

One possibility to determine global coordinates of reflector disc centers was a direct survey with a differential global positioning device (dGPS). As the

Figure 5.4.7: Reflector discs were placed at different distances and angles from the TLS scan positions. This image shows the location of reflector discs at scan position 16.

reception the European Geostationary Navigation Overlay Service (EGNOS) signal was often poor in the study area, the surveys were conducted in real time kinematic (RTK) mode. In doing so, the points surveyed by the Vienna working group served as reference stations (cf. section 5.3). This made it possible to measure both reflectors and anchorage points for successive total station measurements (see subsection 5.4.3.2) with a 3D-precision of 0.01–0.02 m. All dGPS measurements were completed in a geodetic CRS (EPSG: 4979) and later converted to UTM. For all dGPS measurements, a Leica Geosystems GS09 GNSS system was used (see figure 5.4.6). Due to the high precision requirements for this study, the fact that reflector discs were located in steep hill slopes, the high relief in the study area and the minimum number of six GNSS satellites necessary for RTK operation (cf. Young, 2012), dGPS measurements were in general rather time consuming or even impossible in areas close to the valley slopes. In the later case, discs were surveyed using a total station.

5.4.3.2 Total station

The total station survey of the reflector discs in the field was conducted together with field work help from sub-project one and theoretical support from the Vienna working group. In total, nine different total station positions were established. A Leica Geosystems TCRM1205 device was used for all surveys. The coordinates of the total station positions were determined by surveying at least three anchorage points with known coordinates from each total station position. These had been surveyed by dGPS and had been placed at different azimuths and distances of five to 50 m around each total station position. These anchorage points had been marked permanently by steel nails or small drilling holes. All anchorage points and reflector discs were then surveyed using a circular reflector prism (GPH1P) to allow for higher precision in comparison to measurements without prism and because measurement distance were sometimes very high. For the survey of the anchorage points, a 1.3 m reflector pole was used, while the prism was set onto the face of TLS reflector discs for their survey. In cases where the center of the prism was not visible from the total station position, distance and angle were measured separately and combined afterwards. For reflector disc measurement, the thickness of the prism housing was accounted for during post-processing by adding its value to the measured

reflector disc distances. All anchorage points and reflector discs where measured in both instrument faces, thereby enabling total station measurement error control.
Anchorage point dGPS coordinates and total station data (angles and distances) were combined and processed in the GEOSI VERM Large software package (http://www.idc-edv.at/geosi-software/). The reflector disc coordinates obtained where then projected to UTM and later used for a georeferencing of TLS scans in sub-project one.
After two years of measurement and up to nine time slices (ALS and TLS combined) Carrivick et al. (2013) have stated that their data sets were novel as they are "unrestricted to specific landforms and of multiple temporal intervals". After presenting the point data base above, it must be stated that, to my knowledge, there has been (by far) no other geomorphological study (independent of conceptual focus) with a point measurement data base as extensive, highly resolved spatially and temporally as the one presented here and used for this thesis.

5.4.4 Point cloud processing

After acquisition, most point cloud data must be processed before measurements or modeling concerning sediment movement is possible. Where the points are not acquired directly in the global CRS, they need to be georeferenced. In other cases, point clouds from different time steps or scan positions need to be transformed to the same local CRS. Independent of the point provenance, erroneous and non-ground points need to be removed from the data sets in order to be able to monitor sediment movement.

5.4.4.1 Point cloud storage and management

With about 3.346 billion ALS measurement points (as of February 2016), more than one billion TLS measurement points (as of August 2016) and 341 million points derived from historical aerial images (as of February 2016, cf. 5.4.2.2), data storage and management had to be ensured in a way that made a fast and both spatial and temporal flexible access of the data possible. To make this feasible, a PostgreSQL database with PostGIS support was maintained on a server (see Rieg et al. (2013) for another study making use of this management system). A interface to the database was provided by the "Laser Information System" (LIS) software package, a commercial extension of SAGA GIS (Conrad et al., 2015) provided by Laserdata (http://www.laserdata.at) whose team also provided valuable technical support.

5.4.4.2 TLS point clouds

As an offsetting of point clouds for volume calculations requires the data to be referenced to the same CRS, it is necessary to register the TLS point clouds to each other, either in a local or in a global CRS. In the PROSA-project, TLS data was referenced both to local and global CRSs, depending on the slope of the surface scanned at the different TLS monitoring stations: Monitoring sites with slope angles exceeding circa 50°, that is, scanned rock faces were referenced to a local CRS ("registration") as a projection to the UTM 32N system would

have prohibited to measure differences on these surfaces. Scans originating from other monitoring sites (e.g. moraines) were georeferenced in an additional step to the UTM 32N system using reflector coordinates obtained by dGPS and total station ("georeferencing", see section 5.4.3). To which of the two groups a monitoring station pertains is indicated in column "CRS" of the table in appendix three.
Both registering and georeferencing of the point clouds was performed in Riegl's software RiScanPro. As all of this work was performed within sub-project one, no great details on the work flow are given here and the reader is referred to the literature cited in the next paragraph.
Registration of TLS scans was accomplished using, Riegl's Multi Station Adjustment (MSA) feature, an algorithm very similar to the well known iterative closest point (ICP) algorithm (cf. Rusinkiwicz and Levoy, 2001, Sharp et al., 2002, Riegl Laser Measurement GmbH, 2011). Usage of MSA, ICP or similar algorithms is wide spread for registration and suitable for most environments (Gruen and Akca, 2005, Carrivick et al., 2013, e.g.). The transformation usually resulted in standard deviations of the surface distances (which is a measure of the registration error) between 0.4 and 5.0 cm. This work flow was followed for a registration of scans that were to remain in a local CRS.
Point clouds in which enough surveyed reflectors were available (i.e. those that should be set off against ALS data), precise registration could be achieved via reflector matching, minimizing the distances of corresponding reflectors (cf. Riegl et al., 2003). Transformation using this approach usually resulted in standard deviations of reflector coordinate residuals of a few millimeters. After all such scans were registered relatively to each other, they were georeferenced to the global UTM system using the global coordinates of the reflectors (cf. 5.4.3). Depending on the monitoring station, this resulted in standard deviations of the reflector coordinate residuals of 0.8 to 5.0 cm (Jana-Marie Dusik, oral communication). Finally, in order to facilitate the data management in the spatial database, all measurement points were assigned an integer time stamp attribute representing its acquisition date for data management on the server.
After the TLS point clouds were registered and georeferenced and a time stamp attribute was assigned, all point clouds were channeled through a work flow to remove erroneous points, remove redundant data and classify each measurement point as representing vegetation or ground. Due to the capability of the laser measurement systems used in the project to record several returns from one pulse (see section 5.4.1), this information could theoretically be used to distinguish ground from non-ground points (cf. 5.4.1.1). This information, however, is by far not enough to achieve this goal satisfactorily. On the one hand, some areas in the study area are vegetated so densely that also last return points represent vegetation. On the other hand, there are many surfaces in the study area displaying a high range of distances in direction of the laser beam (e.g. steep rock walls in case of ALS, ridges and edges within a rock wall in case of TLS) that multiple returns are generated from a single laser shot and ground returns are recorded as non-last returns. As a result, a much more sophisticated work flow comprising a number of different algorithms was applied to all georeferenced LiDAR measurement points acquired in sub-projects one and five. TLS scans only registered to a local reference system were processed manually by deleting the respective points. A sophisticated automatic work flow was not regarded as necessary because these scans mainly represent steep rock walls without much

vegetation. The work flow presented in the following and visualized for ALS data in figure 5.4.8 was applied in a very similar fashion to both georeferenced ALS and TLS data sets and will therefore be outlined only once. Differences to ALS data processing will be pointed out in section 5.4.4.3. Almost all processing steps beyond the registration or georeferencing of the raw point clouds were accomplished semi-automatically using tools in the GIS software package SAGA GIS, it's commercial extension LIS, ESRI ArcGIS and the Python and R programming environments.

A prerequisite of the semi-automated classification of measurement points is the keeping of the data in the spatial data base. Independent of the original file format and attributes, all point clouds were imported to the PostGIS database (cf. 5.4.4.1). All corresponding necessary processing steps were performed using LIS tools in the GUI. Data management in the data base facilitated an automatic performance of the following processing steps export, thinning, segmentation, classification and attribute drop using bash scripts. All these steps were performed using LIS tools and much of the information on the mode of operation of these tools is taken from their description pages in the LIS software package. In a first step, a TLS scan (i.e. of a unique monitoring area and point in time) is exported from the data base with all relevant attributes.

Second, all outliers in z-direction are found and removed using information on the deviance of each point from the mean elevation in its (x,y)-neighborhood: For an identification of negative outliers, the z-value differences of all points in a neighborhood of the 20 nearest points (to the current point) to the mean z-value of these points were calculated before they were ranked by this z-value difference. Then all points showing a minimum z-value difference to the mean of at least one meter and belonging to the four percent of highest z-value differences were deleted. Positive outliers were removed using a z-value difference threshold only: All points with a z-value four meters higher than the neighborhood mean were deleted.

The measurement points close to the scan position represent redundant data and could also lead to inconsistencies in subsequent data evaluation. In addition, this leads to impractical computation times in the following processing steps. As a result, it was decided to cap the maximum point density of georeferenced TLS scans in the project at $400\,\mathrm{pt\,m^{-2}}$. To achieve this, a 2D block thinning algorithm with a horizontal spacing of 0.05 m was applied. In doing so, the TLS measurement points closest to the nodes of a 0.05 m grid (one point per grid cell) were retained.

In a fourth step, the point cloud was segmented by robust neighborhood plane fitting (Fischler and Bolles, 1981, Ying Yang and Förstner, 2010). For each point, the 30 k nearest neighbors in a maximum distance to the current point of two meters were selected for plane fitting. The plane was fit using robust plane fitting, thereby excluding outliers from the computation: Only points closer than 0.3 m to the plane were included, while at least 75 % of all points in the neighborhood had to comply to this requirement. In case the current point was not included in the best fit plane, the point was skipped. In case, a plane was successful fit to the point and its neighborhood, the normal vector of that plane was computed and stored as a attributed of that point. After robust plane fitting, region growing was applied to group all points featuring approximately the same normal vector orientation into segments. A search radius of 1.5 m was used for region growing. Finished and valid segments were required to contain

a minimum of 30 points. Segments were allowed to merge if their maximum offset was smaller than 0.3 m. Segment size (in number of points) and segment ids were stored as point attributes for further processing.
Segment information served as input to a ground classification algorithm following the principle of progressive TIN densification. The process can be divided into several sub-routines: First, secure ground points are identified for usage as region growing seeds. Seed selection is an iterative, hierarchical process and starts with the identification of the lowest points in each cell of a low resolution raster. With each new iteration, the cell size is halved and corresponding additional lowest points are found. After each iteration, the ground points found so far are combined to form a triangulated irregular network. A new point is only added to the pool of ground seeds if the TIN facet theoretically resulting from the inclusion of that point is not steeper than 35° and the point is not higher than 0.5 m above the facet formed in the previous iteration. As a basic principle, only projected TIN edges shorter than 0.15 m were allowed. The iterations continued until the raster reached a cell size of 0.5 m. Second, after TIN densification is finished, all points closer to the TIN than 0.3 m are classified as ground. Finally, all points belonging to a valid segment as determined in the previous processing step are also classified as ground as long as at least one point of that segment has been classified as ground.
After completed classification, point cloud attributes representing intermediary results (i.e. segment id and segment size) were removed from the points to limit data volume. In addition, the class attribute was reclassified to the official ASPRS code scheme (American Society for Photogrammetry and Remote Sensing, 07.03.2005).
As the algorithms used mainly depend on the spatial variability in the z values of the measurement point clouds and a relatively aggressive calibration had been chosen, suboptimal results had been expected and were obtained in areas of very high topographic roughness such as coarse-grained talus and along ridges and rock wall steps. For example, boulder tips and ridge edges were often wrongly classified as vegetation. These errors had to be corrected manually.
This manual correction step was accomplished in a 3D point cloud editor provided by the LIS software package. In addition to a correction of ground points erroneously classified as vegetation, two additional classes were established: Points representing fixed anthropogenic constructions (like building, fences, guard rails, summit crosses, etc.) were differentiated as one class, whereas moveable anthropogenic objects (such as cars, snow cats and humans) represented another class. Points representing objects floating on water surfaces or the surface of frozen lakes were removed from the point clouds. For all classes, the official ASPRS code scheme was used.
The work flow proved feasible for the huge amount of data to be processed. Total processing time for the automatic part was about 180 hours for all georeferenced TLS data sets on a capable computer. Manual correction was time consuming but by far not as extensive and intricate as with ALS data (cf. below), mainly due to the fact that less vegetated areas are present on the TLS scanned areas.

5.4.4.3 ALS point clouds

The processing of the ALS data followed roughly the same approach as the one taken with the global referenced TLS data described above. Notable differences will be outlined here in the following: Steps performed by the Vienna working group included fully automatic strip adjustment using a specific and elaborate variant of ICP (Kager, 2004, Glira et al., 2015b) and georeferencing using four spatially well distributed mountain hut roofs as ground truth. In general, this resulted in a point precision of flat surfaces of about 4–10 cm (oral communication Philipp Glira, March 2015). A thorough presentation of the methodology featuring the same data as used here is provided by Glira et al. (2015a). ALS data provided by the TIWAG were also georeferenced by the Vienna sub-project. A strip adjustment, however, could not be completed for the 2006 data, as the data were not available in strips but only in tiles.
The data provided by the Vienna working group had also been radiometrically calibrated (Briese et al., 2008), i.e. a reflectance attribute value was available for each ALS point (except the flights from 2006 and 2008). This calibration was conducted in three steps by first determining the reflectance for each point, a subsequent compensation of all flight strips that minimized reflectance differences in the overlapping areas of the strips and a minimization of reflectance difference between flight strips and radiometric control surfaces. The reflectance information was very helpful in the manual correction of the ALS classification result (cf. below). The same or similar LIS tools were used to prepare the data

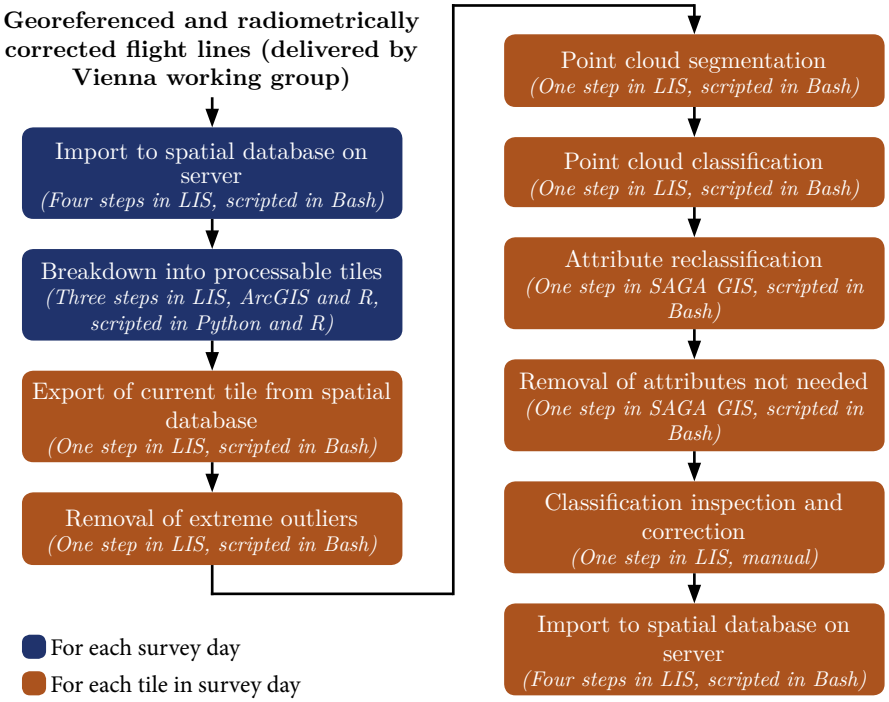

Figure 5.4.8: Simplified work flow followed for (ALS) LiDAR point cloud classification.

for import and the import itself. The difference to the processing of TLS points was that the steps were performed using command scripts in R, Python and bash as the data volume was much higher and manual work in the GUI would have taken too long. Also the ALS points had to be imported multiple times during the project period as successively higher quality points were provided by the Vienna working group.
The main difference to the TLS data when it comes to processing was the number of points and spatial extent occupied by the ALS data. With up to 645 million data points per flight day, all points of the cloud could not be processed at once. Each ALS point cloud was therefore subdivided into square tiles with edge lengths depending on point density. Tile generation was accomplished using the bounding boxes of the respective ALS flights and automated using tools from LIS, ArcGIS (both scripted in Python) and R. As a result, defined tiles contained a maximum of 36.5 million points, which could fit in memory and be processed on reasonably fast PCs. The same tools were used for further processing. Tool calibration, however, was different to account for the, in general, lower point density of ALS point clouds.
For outlier removal, for example, a 25 point neighborhood, much higher distance to mean thresholds and cutoff percentages for both negative and positive outliers (10 m and one percent for negative, 50 m and one percent for positive outliers) were selected to protect isolated but valuable points in steep rock walls.
A main difference to the TLS processing work flow was, that no point cloud thinning was performed with ALS data as its point density is comparatively low and, therefore, no ALS data is redundant.
The segmentation by planes algorithm was also parametrized differently than for TLS data processing: A k-nearest neighborhood of 50 points with a maximum distance threshold of 1 m, a minimum percentage of points used for plane fitting of 80 constitute this difference for the plane fitting subroutine. Region growing was allowed to search within a distance of 1.5 m, while a minimum segment size of 20 points, a maximum normal vector angle difference of 30°and a maximum segment offset of 0.6 m were the parameters fed to the algorithm.
For the TIN densification algorithm, a cutoff cell size of 0.5 m, a maximum TIN facet angle of 30° and a maximum distance to the facet from the previous iteration of 0.4 m were chosen. Segments classified as ground were required to contain at least 100 points. All other parameters were kept at the same values as used during TLS classification. The total processing time for the roughly 3.3 billion ALS measurement points was about 2200 hours for the automatic part and about 500 single man working hours for the manual correction step.
An example for the classification result is depicted in figure 5.4.9. The upper image shows the ALS measurement points colored following the z coordinate, the lower one is colored using the classification attribute generated using the work flow described above. The fact that even objects of small extent (such as crash barrier) were classified shows the quality of the classification. The work flow described above resulted in a successful classification of trees and shrubs as vegetation. Points representing areas covered by very low vegetation, such as alpine meadows or even heath or low alpine rose (cf. figure 5.4.10), were not classified for four reasons. First, alpine roses and heath have very dense crowns close to the ground. This results in elevation differences of DEMs of different time steps being very small and generally below a calculated level of detection. Second, with heath and alpine rose vegetation constituting such dense crowns,

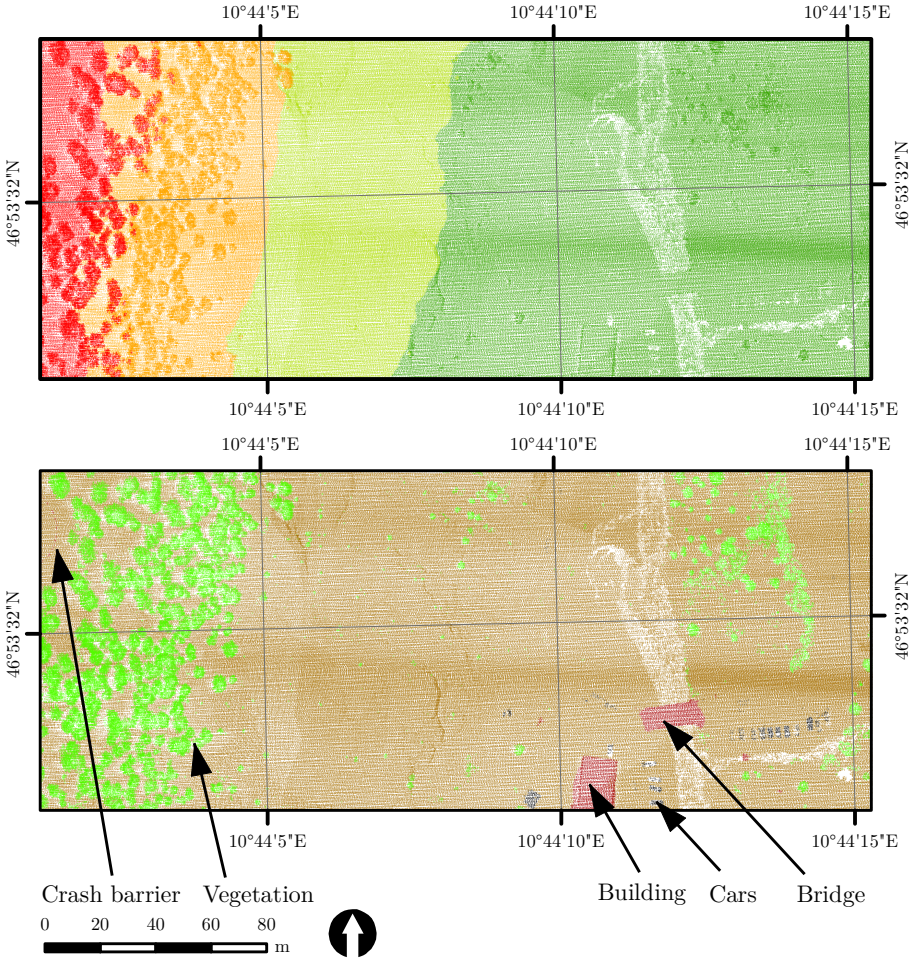

Figure 5.4.9: The ALS representation (July 18, 2014) of the Fernergries area, before and after classification. An oblique view of the same area can be found in appendix one.

the z variability in a local neighborhood becomes very small. This implies that a classification could only be possible using color information. As not all parts of the vegetation display a strong green color, this approach would result in unsatisfactory results. Third, the areas vegetated by heath and alpine roses are generally geomorphologically inactive. Fourth, and most importantly, the plant's surface more or less represents the ground and a removal of alpine meadows and low heath vegetation areas would generate huge holes in the elevation model. The missing surface representation would have to be interpolated. It is virtually certain that the interpolated surface would be much more incorrect

Figure 5.4.10: Heath and alpine rose zone at circa 2170 m h.a.e. above the Fernergries floodplain (background).

than the surface with heath and alpine rose vegetation. This is also the main reason why the removal of such points is usually not undertaken (cf. Carrivick et al., 2013, Hilger et al., 2015a). The same holds true for surfaces covered by grass, moss or lichen.

5.4.4.4 Photogrammetric point clouds

So far, SfM-derived point clouds have not been processed regarding classification of ground points. The classification of all circa 340 Mio. Sfm points would have required a lot of additional work that was not justified given the spatially heterogeneous quality of the point clouds. If a subset of a SfM point cloud showed uncertainties low enough to allow it to be used (as for figure 6.2.2), a work flow ensuring the removal of outliers and vegetation was performed on that subset. This processing was similar to the one used for LiDAR points, but as the quality of the reconstructed vegetated areas was generally more unsatisfying anyway, it was less complex and performed in the GUI of SAGA GIS and LIS.

5.4.5 Data quality on the point level

As LiDAR point measurements are at the heart of the methods used for the quantification of sediment transport in the study area, the quality of these measurements and their derivatives has to be addressed. The quality of each measurement is constituted by both the accuracy and the precision of the measurement (e.g. Holloway, 2003, Milan et al., 2007, Abellán et al., 2014). While, in general, the accuracy of a measurement cannot be determined, it is often only

the precision of a measurement that is used as an indicator of data quality.[1]In some cases, measurements taken with a different measurement device are used to get an estimation of data accuracy (e.g. Hofle et al., 2009, Prokop and Panholzer, 2009, Chassereau et al., 2011).
Often, errors given in the literature are reported as being unrealistically low. Although some studies working with topographic point clouds do not give an estimate of measurement error at all or do not specify how the error was quantified or what (data type) it relates to (as in e.g. Carrivick et al., 2013, Staines et al., 2015), a thorough assessment of errors is indispensable if the results should be regarded as valid. Several factors are associated with errors in topographic data already on the point level.
For LiDAR data, these include intrinsic range errors such as errors arising from the device components or extrinsic range errors as influenced by atmospheric effects, target reflectivity and structure or survey distance. Errors specifically associated with TLS measurements can result from unstable device setup, while positioning errors, attitude error or time offsets are ALS specific, for example. A discussion of all these factors is beyond the scope of this thesis. More information can be found in the respective literature (e.g. Baltsavias, 1999, Beraldin et al., 2010). While all techniques used to obtain point cloud data are associated with specific sources for errors, it is also the transformation of point clouds from one CRS to another that can introduce errors, independent from the sensor originally used to capture the data (Baltsavias, 1999).
No discussion of technical errors associated with dGPS measurements will be undertaken here. The reader is referred to Monteiro et al. (2005). Error in total station data can result from mis-calibrations of the device, lax handling by the operators (both at the device and as a result of unbalancing the reflector rod) or from errors made during the survey of anchorage points during the dGPS campaign.
Errors associated with SfM point data can result from various factors. In the case of historical images (as used in this study), the scanning resolution of the analogue images, their condition (scratches, fox marks, mold spots) and the scale and contrast can all influence the quality of the resulting point cloud. While the latter two can usually not be influenced, all images were checked for scratches, etc. and these areas were excluded from surface reconstruction. The accuracy and spatial distribution of GCP point coordinates is another factor that can be influenced by the user. Corresponding measures were taken by the author (cf. subsection 5.4.2.2).

All errors than can occur on the point level were tried to be kept at a minimum by careful data acquisition and processing. As these errors are propagated into DEMs (cf. below), error assessment was not undertaken before DEMs had been calculated from topographic point data (cf. below).

[1]Especially in the context of topographic point measurements, some geomorphic scientific studies do not distinguish between these concepts and use "accuracy" in the sense of "precision", thereby mixing up these important concepts.

5.5 DTM generation and differencing

Several methods or data structures can be used for the measurement of surface changes using point cloud data. The most commonly used methods in the scientific literature are: (a) point clouds can be compared directly, (b) TINs can be compared directly, (c) A TIN can be compared to a point cloud and (d) Two grids derived from the point cloud can be compared. On the one hand, methods a–c have the distinct advantage that no data is discarded. On the other hand, these methods are very sensitive to point density and position, especially in steep and rough terrain. Data structures of point clouds and TINs require a huge amount of random-access memory (RAM) and processing power for analysis. With more than four billion measurement points generated during the PROSA project, these facts by themselves prohibited a construction of the sediment budget of the study area on the point level and method (d) was chosen for all analysis steps for this thesis.
As a result, all point cloud data was ultimately binned into grids to construct digital terrain and digital surface models[1]. Depending on the cell size used, the data amount is reduced to a size manageable by a standard PC, even for representations of the whole study area.

5.5.1 DTM generation

All DEMs that were used in this study were generated directly from point clouds to avoid interpolation errors and to use as much data as possible for the calculation of DEM cell values. As a result, no grid data sets were resampled from others. There are innumerable methods that can be used for an interpolation of grid cell values from measurement points. The right choice is not easy and is highly dependent on study area, data source and terrain morphology (Bell, 2012).
The most important and/or most often used methods in studies concerning geomorphology and point clouds are: (a) The value of the measurement point closest to the cell center is used as the grid cell value (b) The (trimmed) mean value of measurement points in a certain distance from the cell center is used as the grid cell value, and (c) The value at the cell center coordinates of a 2D regression plane through the measurement points in a certain distance from the cell center is used as the grid cell value. All of these methods have been used at some point during the generation of DEMs for this study. They have different suitability and advantages and disadvantages, depending on the purpose of the resulting DEM. These will be discussed in the following.
With DEMs being a rasterized (sampled) representation of a random field, it is self-evident that using the z-value of the measurement point located closest

[1] In using the term "digital elevation model" (DEM) as a hyperonym for both digital elevation models representing only ground ("digital terrain models" (DTMs)), and those representing ground, vegetation and buildings ("digital surface models" (DSMs), I follow Peckham and Jordan (2007)

to the grid cell center is an obvious choice for cell value assignment. In areas of low point density, however, measurement points might be placed far apart in two different scans. This will lead to greatly differing z-values interpolated for the corresponding DEM cells even though no geomorphic change has occurred. In comparison, to other interpolation methods though, sharp slope breaks and other terrain features are well represented in DEMs obtained using this methodology. For this reason, this gridding method was applied for the construction of all DEMs used for mapping and modeling purposes in this study.

One great problem of using the mean of the points' z-values for DEM cell value assignment (method b) is that it can be skewed by one or more extreme values (outliers). Where the point density is low, the value interpolated for the DEM cell can therefore be highly dependent on one outlier. With laser scanning measurement devices, the placement of measurement points cannot be controlled and it is therefore well possible that the vertical distribution of points within the same defined area differs from scan to scan even though no geomorphic change has occurred between the acquisition dates. This problem is especially pronounced in areas of high slope inclination and surface roughness (high surface roughness has already been identified as a source of measurement uncertainties using the more traditional methodology of profile blocks by Becht (1995b)), where disparities in the spatial (x,y) point distribution can easily lead to differences in z-values even if no geomorphic change has occurred (Wheaton, 2008). This, in turn, leads to increased levels of uncertainty[2] to be assumed for these grids if repeat measurements are used for uncertainty estimation (cf. below) and, consequently, to increased levels of detection. The method is feasible, however, when the point density is very high and the scanned surface is relatively flat (relatively to the scan angle). This method was used by sub-project one to calculate DTMs of difference (cf. below) for rock fall quantification, the rates derived from which were used in this study.

As proposed by Glira et al. (2014), these problems can be avoided by performing a multivariate least-squares regression fit to the data using the x and y-coordinates as predictor variables for the z-coordinate, thereby minimizing the vertical distances of the k nearest neighbor points (in (x,y)-space) to the cell center within a specified radius around the center of the DEM cell. The resulting model is then used to calculate the DEM cell value using the x- and y-coordinates of the DEM cell center. The effect of outliers can be further be reduced by applying robust fitting, thereby reducing their effect. In addition, this approach has the advantage that the resulting z-value is not as much dependent on the (x,y)-distribution of measurement points in areas of high slope inclination. Furthermore, allowing to search for eight neighbors at a greater distance from the cell center, a specified maximum search radius around the center of the DEM cell facilitates the interpolation of grid cell values in areas of low point density, while points located very close to the cell center are used for fitting in areas of high point density. Last but not least, the residuals of the best fit plane can be used as an uncertainty estimate for each cell in the DEM, thereby enabling the calculation of spatial distributed levels of detection (see section 5.5.3). The principle of this fitting method is illustrated in figure

[2]The terms "uncertainty" and "error" are used interchangeably in this study. Technically, "an error is not the same as an uncertainty but a metric for accuracy and can only be calculated if the true value is known" (Wheaton, 2008). As most geomorphological studies spuriously also use the term "error", this differentiation is also not honored very strictly in this study.

5.5.1. For the reasons given above, robust moving plane fitting was used for the

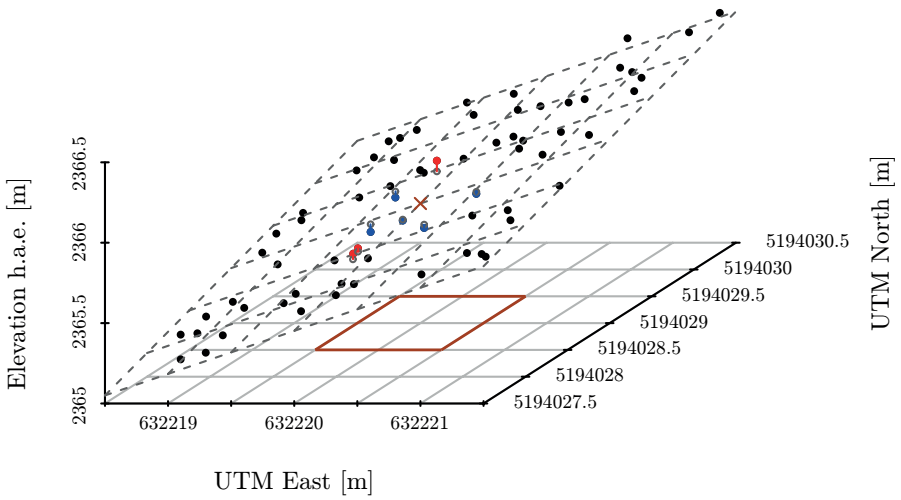

Figure 5.5.1: Principle of moving plane DTM interpolation. A z value is to be calculated for the dark red cell. All black points are located within a distance of 1.5 times the cell size (1 m in this example). The colored points are the eight points located closest to the cell center and are the ones used for robust plane fitting.

construction of all DTMs used for volume calculation in this study.
In addition to the methods mentioned here, interpolation techniques like inverse distance weighting (IDW), radial basic functions (RBF, like thin plate splines or splines with tension) or different kriging procedures have been used for DTM interpolation. These were not discussed as inverse distance has significant shortcomings in situations with low point density and steep terrain while kriging, although probably giving the best DTM results, requires to much user supervision and calculation resources to be of practical interest with the amount of data handled in this study. The main limiting factors with RBF are also the high amount of required computation time and user control in addition to potential difficulties in DTM analysis (Mitas and Mitasova, 2005, (as cited in Bell 2012)).

5.5.2 Data quality on the grid level

With the popularization of LiDAR and dGPS measurements, error assessment of the digital surfaces derived from point measurements (and especially DEMs) has become a subject of discussion in the geomorphological scientific commu-

nity (Lane et al., 2003, Wheaton, 2008). The error should be assessed for each specific pair of point surveys being used to construct DEMs as point density and roughness varies spatially and temporally. As a result, a DEM of difference (DoD) should always be associated with a specific error value or even a spatial representation of errors in the scene. Unfortunately, this is not always the case in the literature and an error derived from on specific survey combination is transferred to other DoDs (as in Carrivick et al., 2013).
As point cloud data is associated with certain errors (cf. section 5.4.5), it is clear that these errors are also propagated into the DTMs and, therefore, also into the elevation difference grids and sediment balances calculated from them. Likewise, all data sets generated from a DEM (such as derived land surface parameters like slope or aspect grids) will be affected by errors present in the DEM (Wechsler, 2006, Bell, 2012). As a rasterization of point data involves an additional discretization step, this constitutes an additional potential source of error (cf. section 5.5.1).
It is therefore necessary and an important goal in every scientific study to estimate uncertainty in DTMs. Independent of the approach used to account for uncertainty in DTMs, the process can be divided into three steps (Wheaton, 2008): a) Quantifying the surface representation uncertainty (cf. below), b) propagating these uncertainty into the difference model (cf. subsection 5.5.3.1) and c) assessing the significance of propagated uncertainty (cf. subsection 5.5.3.2). Assuming that horizontal components are negligible, the digital elevation model uncertainty resulting from these errors can be denoted as $\delta(z)$ as in (Wheaton, 2008):

$$Z_{\text{Actual}} = Z_{DEM} \pm \delta(z) \tag{5.5.1}$$

where Z_{Actual} is the true value of elevation, Z_{DEM} is the elevation value given in the DEM. As Z_{Actual} is not known (in fact, $\delta(z)$ can be seen the DEM equivalent of measurement accuracy on the point level as discussed in section 5.4.5), it is necessary to approximate $\delta(z)$.
There are various ways of approximating $\delta(z)$, the most often used being the utilization of repeat measurements (cf. subsection 5.5.2.1) and stable areas between data acquisition dates (cf. subsection 5.5.2.2). In both of these approaches, precision is substituted for accuracy and it is assumed that $\delta(z)$ is spatially uniform. Other approaches acknowledge the fact that sub-cell size roughness in combination with low point density is a major source in DEM uncertainty and actually spatially variable. Such approaches typically use a roughness related measure for surface representation uncertainty approximation (cf. subsection 5.5.2.3). Which of the methods is most suitable is, among others, dependent on the registration/georeferencing quality and point density of the data and the relative stability of the area represented by the point clouds. All of these three methods were used at some point during data evaluation in this study and will therefore be introduced below. Other possibilities to assess the quality of any interpolated surface is to calculate the RMSE (cf. subsection 5.4.2.2), error budgets, bootstrap experiments (cf. Wheaton, 2008) or the use of Q-Q plots (cf. Bell, 2012).

5.5.2.1 Repeat surveys

One of the most used approaches to assess the uncertainty in a DTM is to conduct a repeat survey of the same surface under unchanged conditions right before or after the acquisition of the point cloud used for differencing and to look at the variation between these surveys. The two resulting DTMs are then set off against each other. These differences represent white noise and follow a standard normal distribution. The surface representation uncertainty can therefore be estimated (σ_{DTM}) as the standard deviation of that distribution:

$$\sigma_{DTM} = stdv(Z_{\text{DoDrep}}) \tag{5.5.2}$$

where Z_{DoDrep} are the cell values of the DoD calculated from the measurement and repeat measurement. Figure 5.5.2 shows a DoD calculated from a TLS scan obtained at scan position five and a scan acquired under unchanged conditions on the same date. The spatial distribution of Z_{DoDrep} indicates that the eleva-

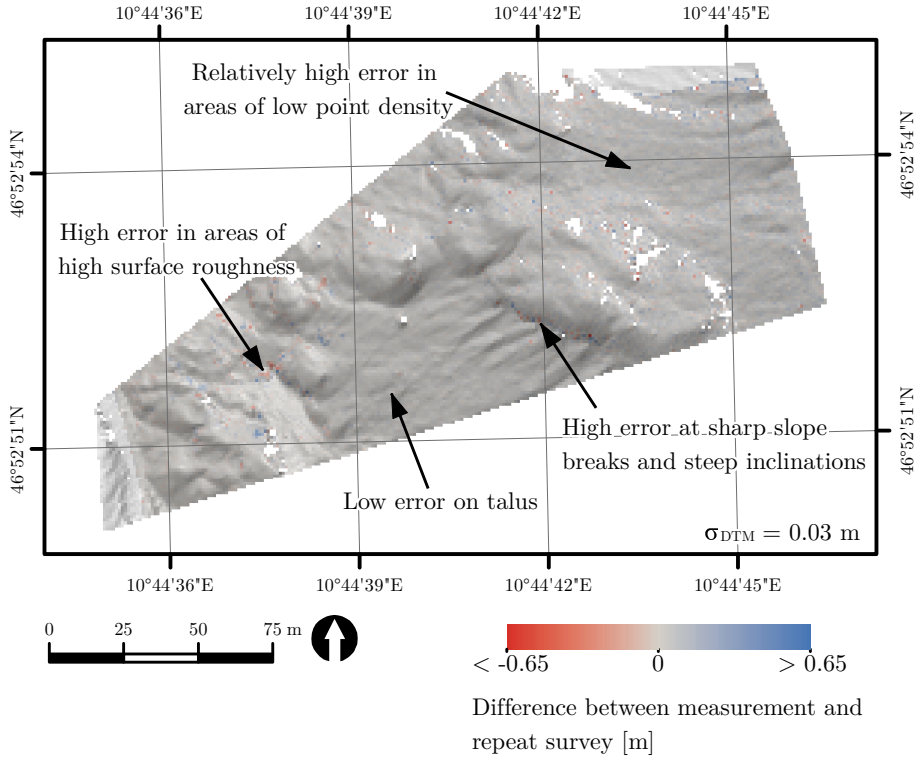

Figure 5.5.2: Spatial distribution of digital surface representation uncertainty. Scans obtained on September 23rd, 2014 at TLS scan position five. Following equation 5.5.2, σ_{DTM} is about 0.03 m. It is evident that the approximated surface uncertainty is highest in areas of high surface roughness and slope inclinations (cf. discussion above).

tion uncertainty is spatially organized. Calculating σ_{DTM}, however summarizes this uncertainty into a single value. This is a crucial weakness as surfaces that could have been budgeted with respect to a lower error might be penalized too

strongly. Nevertheless, this approach has been used widely in geomorphological budgeting (e.g. Lane et al., 2003, Wheaton, 2008, Haas et al., 2012a, Umstädter, 2015, Neugirg et al., 2016b) and was also used in the calculation of DoDs or volumes in some of the other PROSA sub-projects, which were used as input for this thesis.

5.5.2.2 Stable areas

Where no repeat measurement from a single time slice is available, the above addressed approach is approximated by identifying areas that have not changed during the time between the acquisition times of the two point clouds used for budgeting. The error of each DEM is then estimated from the error of the DoD in the stable area by solving equation 5.5.3 for σ^2_{DTM1} and σ^2_{DTM2}, thus leading to identical values of these two quantities. It is important that the used stable areas are of similar complexity and roughness for the assessed error to be representative for the error associated with a single DTM (as in Carrivick et al., 2013). Often, studies assess errors on unnaturally plain surfaces, such as roads or house roofs (e.g. Anderson and Pitlick, 2014). As a result, the assessed DEM error is very small but it is questionable if this error should later be used for a calculation of a LoD applied to natural surfaces in the remainder of the study area. As the resulting error is not spatially distributed, the same drawbacks as with repeat measurement approach are usually in effect. This approach has also widely been used in geomorphological budgeting (Carrivick et al., 2013, Anderson and Pitlick, 2014). It was used by the author in cases when no repeat measurement was available and when it was known that the georeferencing quality of the data was not very good. Virtually all of these cases included a point cloud obtained via SfM from historical images (see subsection 5.4.2.2).

5.5.2.3 2D regression residuals

As the point density and roughness of point cloud data varies, the quality of the digital surface in a DTM is heterogeneous (as clearly visible in figure 5.5.2). Most of the techniques applied for DTM uncertainty approximation are collapsing the spatial distributed elevation uncertainty of DTM down to a single metric (Wheaton, 2008). Also both methods for an assessment of DTM errors presented above yield only one summarizing uncertainty estimate for one DTM which is then to be applied to every cell in the DTM in the same way (cf. below).
This implies an overestimation of uncertainty in areas of favorable data acquisition conditions (such as areas with a steep laser beam incidence angle and areas sampled closely) and an underestimation in areas that are represented rather badly by a DTM (e.g. areas sampled with low point density, areas with a high roughness) (Wheaton, 2008). Experience shows that this often implies a detection of net erosion (even in closed system) as many geomorphological processes tend to erode locally (which yields in a bulky deep scar easily identified as significant elevation changes in the elevation difference model (see below for a further explanation of this term) but spread the corresponding deposits over a larger area (leading to depositional heights below the overall level of detection). It is therefore desirable to balance surfaces with low point density and high roughness with a higher overall level of detection and vice versa.

Several techniques on how to quantify DEM uncertainty in a spatially variable way have been proposed. These include fuzzy inference systems and Bayesian updating of surface change probability and a combination of the two (Wheaton, 2008, Wheaton et al., 2010). Some studies have identified regions of discrete uncertainty classes based on surface wetness (e.g. Lane et al., 2003, Westaway et al., 2003). However, it is also suggested by Wheaton (2008), that there is stronger spatial structure in elevation uncertainty that is related to the already mentioned factors like point density and surface roughness. As a result, elevation uncertainty grids were consistently calculated using the residuals of local multivariate 2D regression in this study to reflect roughness and point density, resulting not in classes of uncertainty but in a continuum of uncertainty values. Glira et al. (2014) has proposed to incorporate information on point density and surface roughness into the estimation of data quality/DTM uncertainty. The technique using local multivariate regression for DTM construction can be used to estimate the quality of surface representation by the DTM by using the standard deviation of regression residuals as a measure of roughness and, therefore, elevation uncertainty in every single DTM cell separately (see figure 5.7.9, middle row, for examples of a corresponding map of elevation uncertainty).

5.5.3 Calculation of elevation difference models

Sediment movement that has occurred between two survey dates can be easily revealed by the calculation of an elevation difference models, often called DEMs of difference (DoDs), that is by a cell by cell subtraction of the older DEM from the newer one.
As the DoD does only show cell changes, an interpretation of these changes regarding the process responsible for them has to be undertaken by the geomorphologist afterwards using expert knowledge and/or a geomorphological map. Otherwise, the resulting budget gives no information on the processes that have been active (as in Carrivick et al., 2013).

5.5.3.1 Uncertainty propagation

ropagated error in DoD, "simple LoD" [m] As every DTM incorporates a certain amount of elevation uncertainty (see section 5.5.2), also the difference values in a DoD will be associated with corresponding errors. It is therefore necessary to respect the errors inherent in both DTMs used for DoD calculations (σ_{DTM1} and σ_{DTM2}). Once these errors have been estimated using one of the methods discussed in section 5.5.2, they can be propagated using simple Gaussian error propagation (Taylor, 1997, Kirchner, 2001, Wheaton, 2008):

$$\sigma_{\text{simple}} = \sqrt{\sigma_{DTM1}^2 + \sigma_{DTM2}^2} \tag{5.5.3}$$

where σ_{DTM1} and σ_{DTM2} are the approximated uncertainties of the two DTMs used for DoD calculation and σ_{simple} is the estimated uncertainty inherent in the DoD[3]. As evident from formula 5.5.3, the single value σ_{DTMs} as estimated using repeat surveys are used as input and only a single metric collapsing the

[3]The propagated uncertainty is sometimes also called "simple level of detection" or "simple LoD", a notion that will also be used in the following.

spatially variable uncertainties results from this approach. The same holds true if stable area statistics are used for σ_{simple} calculation (cf. subsection 5.5.2.2). The usage of a single metric for σ_{simple} has been the standard approach in most geomorphological studies (e.g. Brasington et al., 2000, Wheaton, 2008, Bennett et al., 2012).
As discussed above, it is desirable to use different levels of detection at different locations as DTM uncertainty is dependent on local factors such as point density, surface roughness, etc. This requires the calculation of σ_{simple} for each DoD cell (Wheaton, 2008):

$$\sigma_{\text{simple}_i} = \sqrt{\sigma^2_{DTM1i} + \sigma^2_{DTM2i}} \tag{5.5.4}$$

Here i is the index representing the ith cell in the two input DTM and the resulting σ_{simple} grid. As this requires spatially distributed σ_{DTM} values, only the technique presented in subsection 5.5.2.3 can be used for elevation uncertainty approximation. [4] The error in the DoD can also be propagated into the calculated volumes following Lane et al. (2003):

$$\sigma_v = d^2 \cdot \sqrt{n} \cdot \sigma_{\text{simple}} \tag{5.5.5}$$

where d is the cell size in the DoD, n the number of cells in the DoD and σ_v the error in volume calculation.

5.5.3.2 Significance assessment of difference values in DoDs

After the uncertainty of values in a DoD has been estimated it is possible to relate measured elevation difference to the uncertainty present in the DoD. That is, it is possible to assess the significance of elevation differences and, in doing so, determine the overall level of detection below which all measured surface changed are regarded as error and that is actually applied to the DoD to exclude differences representing presumable measurement errors (Taylor, 1997, Lane et al., 2003, Westaway et al., 2003, Wheaton, 2008).
Referring back to equations 5.5.3 and 5.5.4, these provide a basis for conducting a significance test of calculated differences between the two DTMs. The assessment of elevation difference significance involves a simple two-tailed t-test with a null hypothesis formulated that any calculated difference between DTM cell values is a measurement error. As a result, and relating each elevation difference in the DoD to the simple level of detection, a t-statistic can be calculated for

[4] In using formulas 5.5.3 and 5.5.4, it is assumed that the elevation values in the two DTMs are independent from each other. This is not the case, but formula 5.5.3 is used in virtually all geomorphic studies concerned with topographic data differencing. A mathematically more correct modification of this formula has been proposed to account for this correlation. This correction involves a penalty factor introducing a correlation measure into formula 5.5.3 (Taylor, 1997, Kirchner, 2001). However, it is almost never used in geomorphological studies (see Fuller et al., 2003, for an exception) as it leads to an increase in σ_{simple} and there seems to be a trend in evaluating the quality of scientific results in the light of a (desirably low) level of σ_{simple} ("simple LoD") or σ_{sig} ("overall LoD", see below for an explanation) even though a higher value would be mathematically more correct. Consequently, there seems to be a scientific lock-in in the established methodology in the geomorphological community and no tools are readily available to facilitate the processing of large amounts of data in reasonable time while incorporating this factor. As a result, a correction of the correlation bias was not undertaken in this study and the more simple error model without this correction was adopted.

each cell:

$$tval_i = \frac{z_{DTM2_i} - z_{DTM1_i}}{\sigma_{simple}} \tag{5.5.6}$$

where z_{DTM1_i} and z_{DTM2_i} are the elevation values in the ith cell of DTM1 and 2, respectively. This equation is valid for the case of a spatially homogenous propagated uncertainty but can be altered correspondingly to include σ_{simple_i} instead of σ_{simple} for the case of a spatially variable propagated uncertainty (Wheaton, 2008). This is the equation used on almost all change detection analysis in this study. The t-scores calculated for each cell can then be related to one pertaining to a user chosen confidence level. Whereas Bennett et al. (2012) have used 68 % confidence use a confidence level of 95 %. Virtually all scientific geomorphological studies performing uncertainty propagation do not present t-scores but an overall level of detection σ_{sig} denoting a limit below which the absolute DoD values are considered as errors. This overall level of detection can easily be calculated from the t-value associated with the chosen significance level and σ_{simple}:

$$\sigma_{sig} = tval_{crit} \cdot \sigma_{simple} \tag{5.5.7}$$

where $tval_{crit}$ is the t-value pertaining to the chosen confidence level for a two-tailed test (1.96 for a confidence level of 95 %). This level was also applied throughout this study. Only cells with significant elevation changes were included in balancing calculations.

Calculation of all DoDs in this study was accomplished using respective tools written in C++ for SAGA GIS. For calculations with spatially not distributed DTM errors, the Cut & Fill tool written by Heckmann (2013a) was used. For DoD calculation using spatially distributed overall levels of detection, this tool was modified by the author (Hilger and Heckmann, 2014). Both tools do not only calculate a unthresholded DoD, but also provide a DoD showing only the significant surface changes, a grid of calculated t-values and a result table giving the cut and fill volumes corresponding to both the raw and thresholded DoD (see figure 5.7.9 for an example).

Independent from the measurement technology used to obtain DTMs and their respective quality, it is also the survey frequency that has an impact on the sediment balances obtained by DTM subtraction. A DoD will show sediment movement both due to sediment fluxes from one area to another and fluxes of material entering or leaving the DoD extent at the sides. In addition, a DoD will always reflect the sum of changes (with positive and negative changes possibly balancing each other) within the period between two measurements. It is therefore only possible to quantify single events if point clouds are acquired directly before and after the event. Carrivick et al. (2013) have reported an increasing volume (and therefore rates of sediment movement) with decreasing duration between surveys. This also implies that a bias of higher measured volumes exists for time periods within the summer months in comparison of the time period from the last survey of a year to the first survey of the following year, i.e. surveys to establish a winter budget. If seasonal variations in geomorphological activity are to be assessed, this implication should be taken into consideration. However, the author is not aware of a publication having addressed this issue quantitatively. In addition, survey frequency is not only impacting the volumes calculated from DoDs, but also influence possible scientific interpretations that

are made from them. In a laboratory setting, Lindsay and Ashmore (2002, cited in (Wheaton, 2008)), for example, have shown that coarse survey frequencies not only can mask geomorphological change occurring between acquisition dates but also tend to produce conservative estimates of total change.
Another factor influencing the volumetric result of DTM differencing is the cell size of the DTMs. It is evident, that lower cell sizes enable a more detailed representation of the real world surface. On the one hand, the usage of spatially poorly resolved DTMs leads to relatively high levels of detection, thereby causing correspondingly large part of the overall balance or budget to be discarded (Wheaton, 2008). On the other hand, the number of DTM cells with an insufficient number of measurement points increases with decreasing DTM cell sizes, thereby causing the DTM to contain holes. In this study, the maximum resolution for study area wide DEMs was also limited by computational resources. As a result, a spatial resolution of 0.8 or 1.0 m was chosen for almost all DTMs.

5.6 Mapping

In addition to point cloud and remote sensing data of various origin, several mapping efforts were undertaken to generate data for further analysis.

5.6.1 Geomorphological-geological map

The construction of a sediment budget requires knowledge of the position and extent of the different landsystem units (cf. 2.1 and 2.2). Geomorphological maps are therefore absolutely essential for enterprises of sediment budgeting and are often prepared as a data basis in corresponding studies (e.g. Beylich et al., 2011). As a result, an essential step was obtain a detailed, large-scale geomorphological map of the study area.
It is important to distinguish morphological (which is concerned to record changes in slope character using profiles) from geomorphological mapping, which aims at an identification, interpretation and representation of landforms by using information on their form (morphology) and their genesis (Hubbard and Glasser, 2005, cited in Knight et al. 2011). Detailed information on all aspects of geomorphological mapping can be found in Smith et al. (2011).
A simple and small-scale geomorphological map of the area was compiled by Gerhold (1967). As it used point signatures, was not digitally available, of too small scale and did include only some glaciomorphological and periglacial landforms, it was of no value for the current study. A geomorphological map of the $62\,km^2$ study area had to be constructed from scratch.
Traditionally, geomorphological maps have been constructed based on extensive field (pre-)mapping and aerial photographs at the scale of about 1:10000 (Knight, 2011). During the last two decades, the authors of many papers presenting geomorphological maps have compiled them using numerical data of different sorts and GIS software to produce these maps, not only for mapping purposes, but also for data analysis to support the actual mapping process

(Knight et al., 2011). In recent years, data availability and quality and GIS techniques have been developed so far that some maps are produced purely automatically. Although there is an extensive and fascinating body on automated landform classification based on DEMs (e.g. Prima, Oky, Dicky, Ardiansyah et al., 2006, Iwahashi and Pike, 2007, Seijmonsbergen et al., 2011), such an automated approach was seen as not feasible for the completion of the geomorphological map in this study as classification results are in general of much lower quality than maps delineated manually by the geomorphological expert. Although Knight et al. (2011) states that the construction of a geomorphological map should evaluate additional supplementary information on lithostratigraphy, radiometric dating, soils, ecology and archeology, the only information apart from multitemporal remote sensing products (cf. below) that was available for the extent of the study area was on geology. However, Knight et al. (2011) concede that all these supplementary data are not necessary in most studies as these are targeted for a specific purpose. This was the case in the study presented here. As a result, the following steps were taken to produce a geomorphological map of the study area at a scale of about 1:3000.

In traditional (geo)morphological maps, units and features are depicted with symbols based on the ones proposed by Savigear (1965) and Cooke and Doornkamp (1993) for morphological mapping, which are largely line symbols to depict different grades of changes in slope. However, there are no clear rules for a classification of these changes. In addition, geomorphological mapping requires a more extensive set of mapping symbology. Such a set has been presented by Kneisel (1998) and is based on work by Fischer (1984), Leser et al. (1975), Leser (1977), Leser and Stäblein (1978), Leser and Schaub (1987), Stäblein (1979, 1990). However, it also makes use mainly of line and point signatures to represent landforms which do not lend themselves easily to statistical analysis and are not suitable as input for modeling purposes (see 6.1.1.1.2 for an example) but only for usage in the field. Hence, it was chosen to map landforms/storages using the representation as polygons in addition to the usage of the symbols proposed by Kneisel (1998). As a result, there are, two versions of the geomorphological map of the Upper Kauner Valley: A traditional one using point signatures for landforms, and a second one using polygons.

While Knight et al. (2011) discuss the difficulty of mapping mass movements because they create features too small to be resolved in DTMs, the availability of multitemporal, high density LiDAR data for the whole study area allowed for exactly this. The classes to be mapped were initially selected following the geomorphological maps published on http://gidimap.giub.uni-bonn.de, the mapping done by (Otto, 2006) and discussions in Kneisel (1998). The classes were adjusted to the study area and the purpose of producing a sediment budget valid for recent time scales.

After the bedrock units had been fully mapped, it was subdivided according to the information available in the geological map created by Vehling (cf. figure 3.2.1), yielding a combined geomorphological-geological map. This is contrary to what is recommended by Kneisel (1998), but as the map was to be used as a modeling basis and not as a companion in the field, the combination was necessary (cf. 6.1.1.1.2). It was also refrained to include signatures for different grain sizes in the map. The geological-geotechnical map prepared by Vehling (2016) contains this information and it could be combined with the data prepared in GIS at any time (as done in Vehling et al. (2013a)). Kneisel (1998)

also sets aside point signatures for permafrost and dead-ice. These were also not included in the geomorphological map as an original permafrost map had been prepared (cf. 5.6.3) and the distribution of dead-ice is still currently investigated by Schlobies (2016). Eventually, the unit classes shown in table 5.6.1 were represented in the geomorphological-geological map.
It has been reported that perennial snow patches in channels or other depressions can accumulate sediment bodies of relatively low life span (Lamoureux et al., 2006). Perennial snow patches have been mapped by the author, but as they play a minimal role in the sediment budget of the Upper Kauner Valley, the resulting storage landforms, if present at all, were not included in the map.
Map units were delineated based on the outline of morphological features, usually as defined by the basal enclosing of the landform by convex and concave breaks of slope. The main data basis of this mapping were the prepared orthophotos (cf. 5.4.2.1), multitemporal DEMs and derivatives of these DEMs. The map was mainly prepared on the basis of the orthophotos from 2003 and 2009 as the volume from 2010 shows snow cover in many portions of the study area and neither the imagery from 2003 or 2009 covered the study area completely. Except the mentioned volumes, only the 1953 orthophotos were used in mapping as they proved helpful in distinguishing moraines of different age classes (i.e. pre-LIA vs. post-LIA). Different land surface parameter grids were calculated from 1 m DEMs to enhance the visibility of the general morphology and geomorphological features: Slope (Zevenbergen and Thorne, 1987), Topographic Openness Index in a 25 m and 100 m neighborhood (Yokoyama et al., 2002, Prima, Oky, Dicky, Ardiansyah et al., 2006, Anders et al., 2009), neighborhood percentiles in radii of 4, 7, 15 and 40 m and a hill shade. While every other LSP was also used on its own, the Topographic Openness Index grids were combined with the slope grid to form a composite RGB image which proved very useful in enhancing the visualization of bedrock vs. non-bedrock boundaries. All LSP grids were calculated using tools in SAGA GIS. Furthermore, a grid of LiDAR surface reflectance was prepared. It facilitated the mapping process mainly by helping to distinguish wet and dry areas.
While landforms and process areas were mapped as polygons, important linear features (such as steps of various heights, ridges and arêtes, the outline of gorges, etc.) were mapped as linear features. Point features were used for the mapping of additional landscape features, such as striations. For this more traditional mapping, the symbols proposed by Kneisel (1998) were used.
The lion's share of the landforms was mapped scrupulously by hand in ArcGIS, a process which resulted in about 9000 polygons that were successively dissolved to about 5100. An outline of the glacier surfaces was obtained by sub-project four and was modified to fit the larger scale of the geomorphological map. The bulk unit "bedrock" was largely not delineated by the author but was supplied by Vehling of sub-project two. As it did not differentiate between rock wall segments (a distinction necessary, as all spatially connected rock walls in the study area would have formed a single one, independent of aspect), a segmentation of this unit was accomplished automatically. To accomplish this, a 1 m DTM of the bedrock areas was used to calculate aspects for each cell before it was reclassified to contain classes representative of the eight cardinal and intercardinal aspect directions. To extract rock wall sections on a scale corresponding to the geomorphological map, a majority filter with a radius of 5 m was applied several times and iteratively until the desired resolution had been achieved. The fin-

	Category, Subsystem	Unit classes in map	Examples, comments
Other	Anthropogenic	"Anthropogenically altered surfaces"	roads (gravel or tar), ski tracks, buildings, etc.
	Bedrock	"Bedrock: Amphibolite", "Bedrock: Alternating amphibolite-paragneiss", "Bedrock: Augen gneiss", "Bedrock: Mostly Biotite-plagioclase-gneiss","Bedrock: Biotite-plagioclase-gneiss", "Bedrock: Flaky Biotite-gneiss", "Bedrock: Granitic orthogneiss", "Bedrock: Mica shist", "Bedrock: Granitic porphyry", "Bedrock: Basalt-Diabase dike", "Bedrock: Quarzite"	largely provided by sub-project two
	Glacier	"Glacier ice"	
Loose sediment	Fluvial	"competent channel", "braided channels with bars", "gravel bars", "reworked glaciofluvial and fluvial sediment by slope channel", "moraine partly covered with glaciofluvial deposits" (all within the floodplain) and "old fluvial storage landforms" (i.e. above the floodplain), "fluvial transport zones on slopes"	floodplains mapped by the author, differentiation into subclasses by sub-project three
	Glacial	"Moraine not spec., formed before AD 1855", "lateral or terminal moraine formed before AD 1855", "lateral or terminal moraines formed in or after AD 1855", "ground moraine formed before AD 1855", "ground moraine formed in or after AD 1855"	
	Gravitational	"Talus slope", "Talus cone", "Debris flow deposits", "Deposits of rock falls $> 100\,m^3$", "Avalanche sediment deposits"	differentiation of debris vs. talus cone using slope inclination, field checks and surface texture
	Periglacial	"Block slope", "Rock glacier, not specified", "Rock glacier, active", "Rock glacier, inactive", "Rock glacier, relictic"	mapped by the author, differentiation of rock glaciers into activity statuses by sub-project two
	Other	"Standing water body", "lacustrine sediments", "slope wash areas", "not specified"	Generally of low overall coverage

Table 5.6.1: Units mapped in the polygon-based geomorphological map.

ished segmentation was then vectorized and combined with the remainder of the geomorphological map. These steps resulted in a polygon count increase of the geomorphological map to about 18000. An unification with the geological map (Vehling, 2016) yielded a final count of about 22000 polygon units making up the geomorphological-geological map of the Upper Kauner Valley. Initially, the

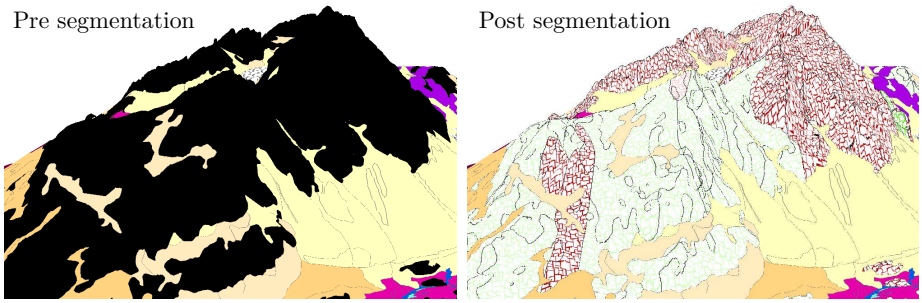

Figure 5.6.1: Representation of the Krummgampenspitzen in the geomorphological-geotechnical map before and after the segmentation using aspect and geology. The relief in the shown area is about 600 m. Please see the map in appendix two for a legend.

map only contained a class of the current floodplain. A further differentiation (see table 5.6.1 for the resulting classes) was completed by Karolin Dubberke from sub-project three. This led to a polygon count increase of a about 200. A differentiation of the rock glaciers according to their activity status was completed using information obtained from sub-project one (see section 5.7.1.5.2). Material grain size and other information was collected during field visits and via terrestrial photographs to settle disputed map units (see Betz (2016) for an example). After each mapping product combination mentioned above, the resulting shapefile was checked for consistency and, if necessary, corrected. This seven step procedure was automated using ESRI's ArcPy package for Python and comprised an identification and correction of mapping gaps, sliver polygons and index inconsistencies of the shapefile. A very small detail of the map, centered southeast of the Riffl rock glacier, shall exemplify the finished map (appendix two).
It is evident, that every mapping process is liable to a certain degree of subjectivity. Despite the high effort undertaken in the construction of the geomorphological-geological map of the Upper Kauner Valley, this also holds true for this one. The high number of polygons and long time needed to finished the map make it very likely that some mapping lapses have occurred. However, errors have been found and corrected since the map has been finished and the resulting map is probably still the most detailed geomorphological map constructed for a high mountain meso-scale catchment up to date.

5.6.2 Land cover map

Most sediment transporting slope processes are influenced by the (non-) existence of stabilizing vegetation within their process areas (e.g. Gegg, 2010). A

simple land cover map giving information on the location of vegetation of different heights is a valuable data basis for process occurrence analysis. Such a map had been an important data input for fluvial slope erosion modeling before (Haas, 2008). As it had been planned to use the same modeling approach as Haas (2008) for fluvial slope erosion regionalization (see 5.7.3.2, a corresponding land cover map was prepared.
A land cover map in a scale of circa 1:800 was to be prepared for the study area. Following Gegg (2010), land cover was classified and mapped into five classes: "no vegetation", "patchy alpine grassland/pioneer vegetation", "alpine grassland", "bushes/krummholz" and "trees". While the former four of these classes were mapped by hand, the trees that were mapped using an automatic procedure using information from the ALS survey data of 2012: The number of returns of a given pulse attribute of LiDAR measurement points was rasterized using the maximum scheme. Every grid cell with a value of greater than three was then reclassified to reveal the locations of trees in the study area (resulting in circa 48000 polygons). A detail of the resulting classification is shown in figure 5.6.2. Due to the large size of the study area, the desired large scale of the map and the spatially highly variable vegetation cover (disregarding the trees, over 46000 separate polygons have been mapped by the author and student assistants as of July 2016), the land cover map could not be finished so far (about seven percent of the area have not been mapped yet). The current state of the land cover map is shown in chapter 3.7 (figure 3.7.1).

5.6.3 Permafrost map

Mapping of landforms and processes was facilitated by information on the spatial distribution of permafrost. In addition to permafrost modeling undertaken in sub-project one (Dusik, 2013), two different permafrost modeling efforts were completed by the author. Both were based on a family of rule-based models developed since 1975 (Imhof, 1996, Haeberli, 1996b)[1]. The models make use of deterministic rules for the assignment of three classes, "permafrost probable", "permafrost possible" and "no permafrost", based on the intersection of elevation and aspect classes.
The newest iteration of the PERMAKART model family (Schrott et al., 2012) was used. This model is much more differentiated than the early PERMAKART models (Hölzle, 1994, Haeberli, 1996a, Imhof, 1996), as it distinguishes between rock slopes and slopes covered by sediment, accounts for foot slopes and respects eight aspect classes. The elevation step for rules is 100 m (cf. figure five in Schrott et al. (2012)). Another advantage of this model is that it had been calibrated in the Eastern Central Alps very recently and should yield satisfying results in the Upper Kauner Valley (personal communication Lothar Schrott, 2014). In addition, the model gives permafrost probabilities (not in a statistical sense, mathematically, it is more like an index) from zero to one instead of the three crude classes mentioned above. After further inquiries with the authors of Schrott et al. (2012) and a correction of the formula given in that paper, the model could be implemented using a combination of tools from R and SAGA GIS. Figure 5.6.3 shows a spatial subset of the permafrost modeling results in

[1] The corresponding GIS software implementations of these models are known as "PERMAKART" (Keller, 1992) or "PERM" (Imhof, 1996).

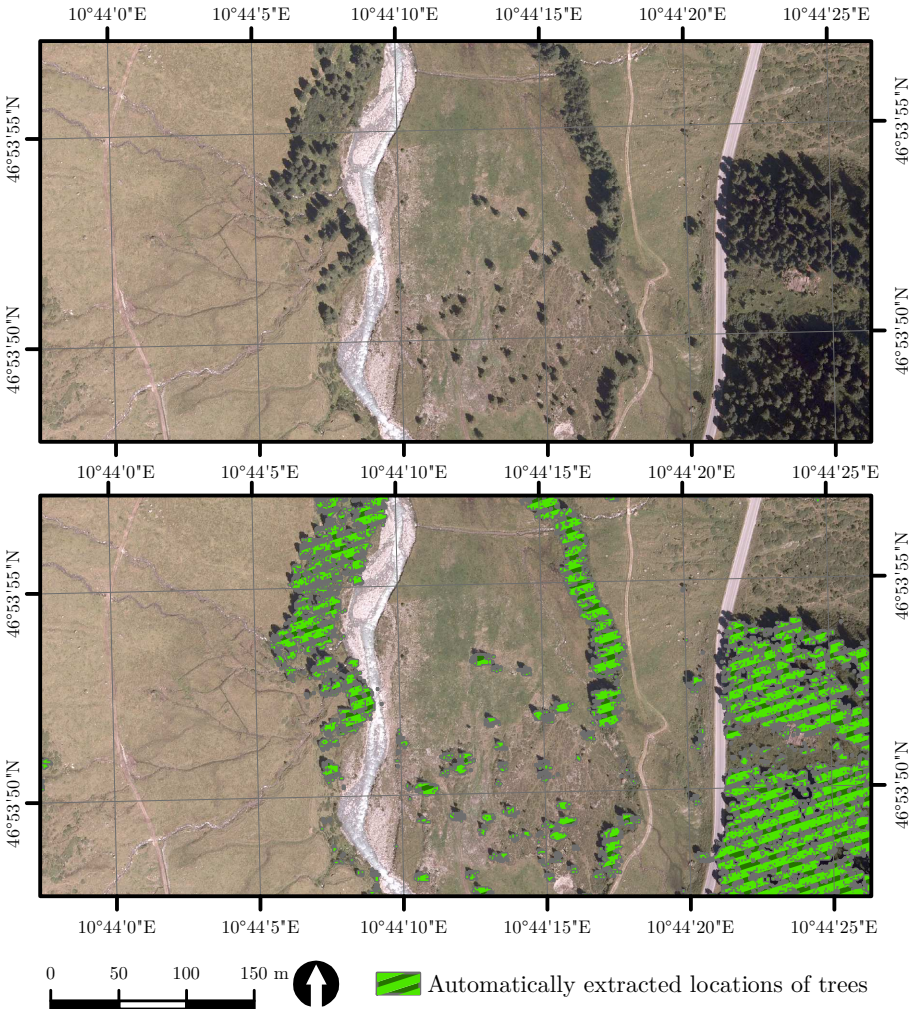

Figure 5.6.2: Trees between Gepatsch alp and Gepatsch mountain hut mapped automatically using the automatic procedure based on the number of returns of a given LiDAR pulse (bottom). An orthophoto from 2010 is shown as a comparison (top). It is evident that the automatic mapping procedure worked very well.

the Upper Kauner Valley. As a rule of thumb, permafrost can be found above circa 2500 m a.s.l. in northerly exposed slopes and above circa 3000 m a.s.l. in southerly exposed slopes (see Schrott et al., 2012). According to Krainer (2010, cited in Betz 2016), permafrost can be found above an elevation of circa 2500–2700 m a.s.l. in the Upper Kauner Valley. As can be seen, the model results correspond well with this expert knowledge.
It has often been reported that the fronts of active rock glaciers indicate the lower limit of discontinuous permafrost. This can be confirmed for the Upper Kauner Valley: Fronts of active rock glaciers are located very close to the modeled lower boundary of discontinuous permafrost in the Riffl Valley, the Ochsen

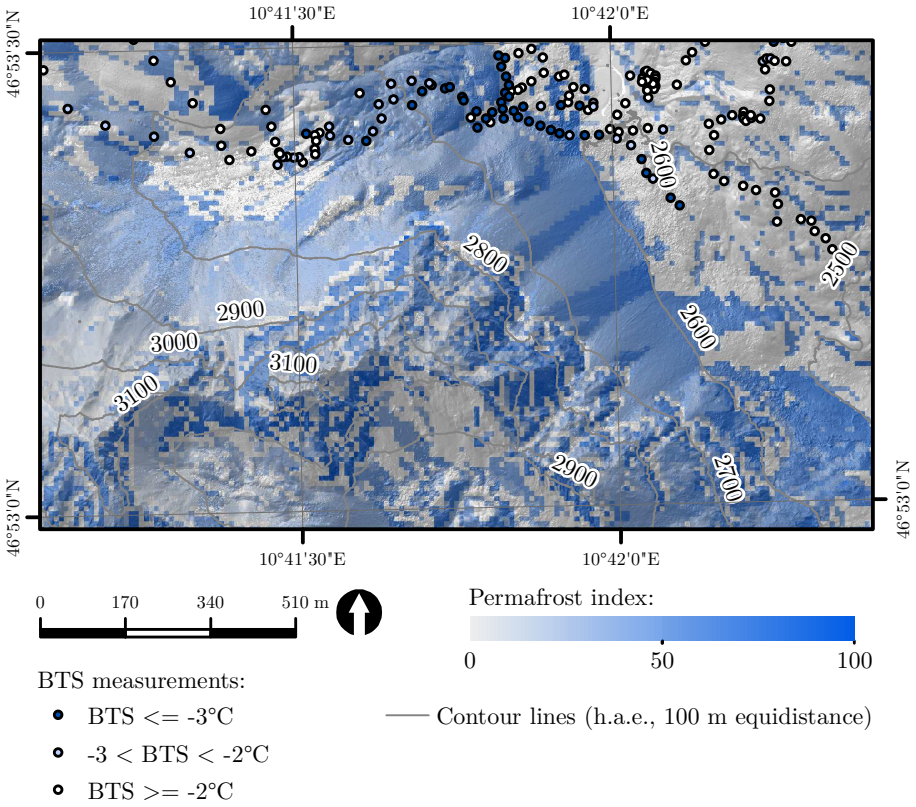

Figure 5.6.3: Result of spatial permafrost modeling. A subset of the BTS measurements obtained by sub-project one is shown as reference.

cirque, the Kühgrube and the Krummgampen Valley. An exception is the large rock glacier in the Ölgrube cirque, whose tongue reaches well below the modeled lower boundary of discontinuous permafrost. This very large rock glacier, however, has a source that contains an exceptionally large amount of sediment and the permafrost index obtained by the model is very high in the rock glacier's root zone. These factors might explain why the Ölgrube rock glacier front was capable of reaching these areas.
Geophysical measurements were conducted by Dusik and Leopold (University of Western Australia) at several locations in the study area in September 2012. These measurements confirm the permafrost modeling result (all Electric Resistivity Tomography (ERT) measurements are conform to the measurement results).
While Schrott et al. (2012) do not describe in detail how their validation of the data was conducted, a validation was undertaken by classifying both the BTS data obtained and the probabilities obtained via the model. BTS temperature was classified into the classes shown in figure eleven of Schrott et al. (2012), while the permafrost index was classified into three equidistant classes (cf. table 5.6.2). Classifying the data as indicated in the table and comparing the modeled data with the data obtained by BTS measurements, it becomes evi-

Model result (index)	**BTS class**	**Interpretation**
100–66	BTS $\leq -3\,^{\circ}\mathrm{C}$	permafrost probable
66–33	$-3\,^{\circ}\mathrm{C} <$ BTS $< -2\,^{\circ}\mathrm{C}$	permafrost possible
33–0	BTS $\geq -2\,^{\circ}\mathrm{C}$	no permafrost

Table 5.6.2: Classes used for the permafrost index and BTS measurements for validation.

dent that approximately 63 % of the locations were classified correctly (Schrott et al. (2012) obtained a value of 46 % in the area where the model was calibrated). Cases in which modeling results and BTS indicate permafrost, but not in the same category, reach a share of circa 8 %. A correct indication that permafrost is at least be possible is made in circa 72 % of all cases. This is regarded as a success, given that Schrott et al. (2012) obtained a value of 69 %. The Kappa statistic (calculated as

$$\frac{\sum_{i=1}^{r} x_{ii}}{n_{BTS}} - \frac{\sum_{i=1}^{j} x_i \cdot \sum_{i=1}^{k} x_i}{n_{BTS}} \cdot \left(1 - \frac{\sum_{i=1}^{j} x_i \cdot \sum_{i=1}^{k} x_i}{n_{BTS}} \right)^{-1} \tag{5.6.1}$$

where r is the number of rows (and columns) in the confusion matrix, j the number of rows, k the number of columns and n_{BTS} is the total number of BTS observations made) is c. 0.24. The result of the validation is summarized in table 5.6.3. The values for overall and permafrost indication accuracy are en-

		Predicted			
		Permafrost probable	Permafrost possible	No permafrost	
Ground truth	Permafrost probable	0	0	0	**0**
	Permafrost possible	38	39	50	**127**
	No permafrost	43	31	240	**314**
		81	**70**	**290**	**441**

Table 5.6.3: Confusion matrix for the permafrost modeling in the Upper Kauner Valley. The error of commission* for "permafrost probable" is 100 % (See discussion below.), while the error of omission** is circa 0 %. For "permafrost possible", these errors are 44.2 % and 69.3 %. For "no permafrost", the values are 17.2 % and 23.5 %.
*Representing pixels in the permafrost map that do not belong to the ground truth class but were classified as such.
**Representing pixels in the permafrost map that belong to the ground truth class but were assigned to another class by the model/classifier.

couraging as they are in the range or even better than what has been found by

Schrott et al. (2012) in the area where the model was calibrated. The errors of commission and omission are less encouraging, however. It is immediately evident from the confusion matrix that no proper validation of the class "permafrost probable" could be undertaken. This is due to the low variation in geofactors covered by the BTS data. A proper validation should use ground truth data covering all geofactor combinations (elevation and aspect). The BTS measurements, however, are almost all from comparatively low altitudes and are not very variable in aspect. The BTS data displaying very low temperatures, were almost all obtained in areas of high surface roughness, a geofactor the PERMAKART model does not account for, and not at high elevations of northerly aspects. Also, most measurements were made in flat areas. This explains the high error of commission (actually it is not an error, but no BTS values were available for altitudes and aspects where the model predicts that class). Other reasons, less related to methodology, for the mismatches between BTS data and modeling results include the following (Schrott et al., 2012): i) The model was calculated on a 10 m raster. BTS measurements, however, are based on point measurements and permafrost is known to be spatially highly variable, ii) BTS measurement error could have occurred due to water or ice layer within the snow cover, iii) It is possible that the snow cover did not isolate the ground well enough, thereby reducing the validity of BTS measurements and iv) reduction of validity of BTS measurements because of special local effects (e.g. Balch ventilation as a result of blocky subsurface, cf. above).

5.7 Methods specific to the quantification and regionalization of different geomorphic processes

Before the different processes are going to be looked at in greater detail, several problems and/or basic assumptions must be stated:

- It must be emphasized that using the research design that was chosen for this study, a differentiation of erosion and transport rates is not possible most of the time. In all cases except rock fall, the re-mobilization of sediment will therefore be regarded as erosion.

- A recurring problem is the fact that many different processes act on the same slopes (see Becht (1995b) for a more detailed discussion of this subject). It has already been stated that many studies aiming at quantifying sediment transfer on hill slopes using remote sensing technology do not differentiate between these processes. This differentiation has been attempted in this study wherever possible and the topic will be discussed where required. However, a certain degree of error stemming from the coalescene of different processes cannot be ruled out.

As the different processes active within the catchment are operating at different time scales, velocities and transport sediment over different (vertical) distances, the specification of moved masses per year for process comparison is not constructive. A rock glacier, if compared with a debris flow, for example, transfers sediment at a much lower velocity but often not over a great vertical distance. In contrast, rock glaciers transfer a much bigger mass of sediment. In order to make the different processes comparable, all mass transfers will at one point (if possible) be compared in terms of potential energy destroyed during sediment movement. As a result, processes will be balanced in Joule per year (J yr^{-1}) in addition to more common units as tons or t km^{-2} yr^{-1}, for example.

5.7.1 Mass wasting processes

5.7.1.1 Rock fall

5.7.1.1.1 Debris fall

The methodology presented here is based on the study published by myself and others in Heckmann et al. (2016), but includes a set of improvements. It is especially these improvements and additional analysis that will be in focus here. Two different general strategies were tested to investigate the catchment-wide small-scale rock fall sediment budget of the study area: The first (henceforth "strategy one") is a slight improvement of the work flow presented in Heckmann et al. (2016) and constitutes a new framework for estimating sediment transfer rates by debris fall on the scale of a meso-scale catchment. While it is possible to

achieve complete coverage of large to very large events through geomorphological mapping (cf. 5.7.1.1.2) and volume estimation (Krautblatter et al., 2012), the quantification of debris fall for a whole catchment has always relied on only a few measurements acquired on a test plot scale.
The study presented here has tried to improve this methodology: rock fall was measured using rock fall collectors and TLS at 20 different locations. Given the position and extent of a rock fall collector or the scanned area, rock wall retreat or production rates could be calculated by relating the measured volume or mass of rock fall debris to the sediment contributing area on the rock wall determined. Three different scenarios were used in SCA calculation to investigate result sensitivity to SCA calculation for rock fall collectors.
For the construction of the catchment-wide rock fall sediment budget, however, the obtained rates of rock fall production were regionalized to all rock walls in the study area. Instead of assigning one of the measured discrete values to different subarea of the study area (as traditionally done), a statistical theoretical distribution was fitted to the data and values were assigned to each pixel in a rock fall starting area map obtained using a spatial susceptibility model by drawing from this distribution. A much simplified flow chart of the work flow used in strategy I is depicted in figure 5.7.1.
The second overall strategy (henceforth "strategy two") applied to obtain a study area-wide rock fall sediment budget made use of a spatial distribution of six distinct classes of a newly developed rock mass stability index as suggested by Vehling (2016). As the index had proven to be strongly correlating with rock fall production rates, a regionalization of rates was possible. Only rock fall collector net measurements were used to assign rates to the different rock mass stability index classes. It was this regionalization result that was used by the author for the construction of the final sediment budget.

The focus of purely geomorphological studies on rock fall is mainly on rock wall production rates of different scales or the spatiotemporal variability of these rates (e.g. Coe and Harp, 2007, Chiessi et al., 2010, Sass, 2005a, Krautblatter and Moser, 2009). For a construction of the sediment budget, however, also the sediment pathways are needed. The methodology for the identification of rock fall particle transfer paths was the same for both strategies of determining the spatial distribution of rock fall production rates in the study area. Numerical models simulating the descend of rock fall particles from their detachment zones to their deposition areas were used for an identification of rock fall sediment pathways between zones of different scales in the study area. Becht (1995b), Wichmann et al. (2009) and Heckmann and Schwanghart (2013) pioneered the use of such models for the spatial analysis of sediment cascades. However, quantification of these sediment cascades was not undertaken at that time (see chapter 2.2). In the present study, the values obtained by measurements were combined with the identified sediment pathways. Heckmann et al. (2016) is, to my knowledge, the first assigning masses to modeled debris fall trajectories. For the evaluation of sediment delivery to different (types of) landforms, the modeled trajectories were later combined with the geomorphological-geological map and represented in form of a directed graph. By aggregating these trajectories using the geomorphological map (section 5.6.1) it was possible to quantify rock fall sediment fluxes not only on the scale of individual DTM pixels, but also on the scale of individual landforms and landform types (up-scaling, cf. Blöschl and Sivapalan, 1995).

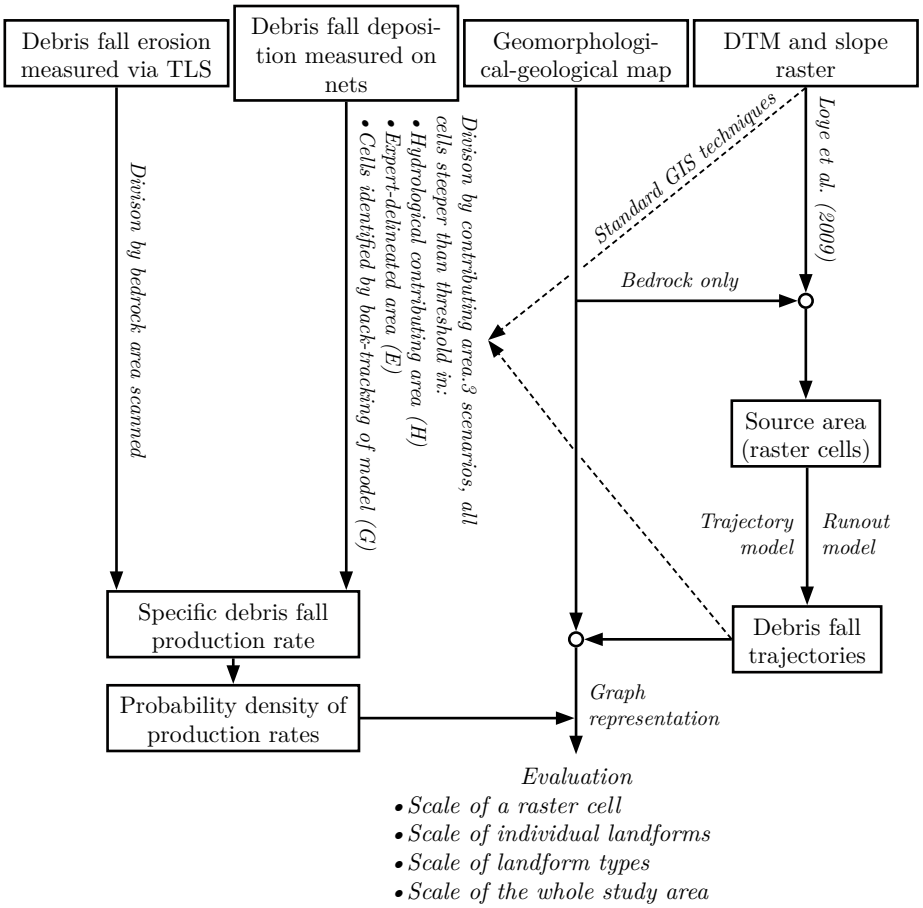

Figure 5.7.1: Simplified work flow for debris fall quantification for the whole study area in strategy one.

Slope threshold identification for debris fall starting zone identification

It is very common to use a slope threshold and a bedrock mask for rock fall starting zone identification (e.g. Toppe, 1987, Guzzetti et al., 2003). The same slope threshold was applied in both overall strategies and all three scenarios of strategy I (cf. below for these scenarios).

However, some studies have assumed all mapped bedrock areas as potential starting zones (e.g. Heinimann et al., 1998, Meißl, 1998, cited in Wichmann 2006). Anyhow, if thresholds are used, these are often determined quite arbitrarily. For example, Guzzetti et al. (2003) assumes a threshold of 60° in Yosemite Valley (California, USA) based on the location of previous rock falls. Also van Dijke and van Westen (1990) use this value, while Dorren and Seijmonsbergen (2003) and Wichmann (2006) use 40° (based on assumption and the spatial distribution of talus landforms in the study areas). Grunder and Kienholz (1986) and Toppe (1987) propose a value of 30° (cited in (Wichmann,

2006)): Obviously, there is a wide range of thresholds applied in the literature. Although the differences in the used thresholds might be legitimated by different geologies and geotechnical properties in the respective study areas, the interplay of these factors are too complex to be used in the determination of a slope threshold (Wichmann, 2006). As a result, it was also only the slope that was used to identify rock fall starting zones (independent of whether strategy one or two was used to assign production values to these zones) in this study. The threshold, however, was not defined based on assumptions, but was investigated empirically using two different empirical approaches: Both approaches are based on empirical probability density estimations, created from a spatially high-resolution DTM (1 m) in order to represent high slope inclinations as well as possible (Wilson and Gallant, 2000):
The first approach made use of probability density estimations of the slope values for two different debris fall process area sub-zones. A slope raster of the whole study area was truncated to areas with bedrock and talus cones/sheets. Subsequently, a density estimation of these slope values was completed and the point of intersection of both density curves was used as a representative slope threshold. This procedure yielded a threshold of 43.61° (cf. figure 5.7.2, left).
The second approach involved the methodology proposed by Loye et al. (2009): The empirical slope probability density was decomposed into different normal distributions, each theoretically representing a large-scale morphological landscape unit. In contrast to Heckmann et al. (2016), only three classes were used to represent plains, (hill) slopes and cliffs (rock walls). As this approach is only suited for areas without significant glaciation and anthropogenic alternations, the respective surfaces were excluded from the analysis. Decomposition of the probability density was accomplished using tools from the R package mixtools (Young et al., 2009), which estimates parameters of the mixed model using an expectation maximization technique (Meng and Rubin, 1993). This approach yielded a slope threshold of 47.57° (cf. figure 5.7.2, right). Both approaches were completed using a combination of tools from ArcMap, SAGA GIS and R. Eventually, the higher threshold was chosen for usage as a debris fall start zone identification threshold. This decision can be justified by several reasons: The slope inclination probability density estimation for the bedrock surface slope values makes direct use of the slope values on roche moutonnées, quite many of which can be found in the study area. It can be assumed that these flat bedrock surfaces cause the density curve for bedrock to shift to the left. The found slope threshold of 47.57° is similar to the value identified by Heckmann and Schwanghart (2013) in another Central Alpine high-mountain valley (45°), but smaller than the values found by other authors using the density curve decomposition technique (49 and 53° (Loye et al., 2009, , in the Helvetic Alps and Préalpes Médianes) and 49–54° (Jaboyedoff and Labiouse, 2011)). In order to be used as debris fall start cells in the numerical model (Wichmann, 2006, , cf. below), the cells steeper than the threshold were truncated with a bedrock mask and the resulting raster was resampled to a spatial resolution of 5 m using the majority scheme. The described procedure identifies 173808 cells or circa 7 % of the planimetric study area as debris fall source area.

Strategy one: Debris fall quantification
In strategy one, actual measurements of debris fall deposition within the study area were used to quantify the contribution of rock fall of that scale to the sed-

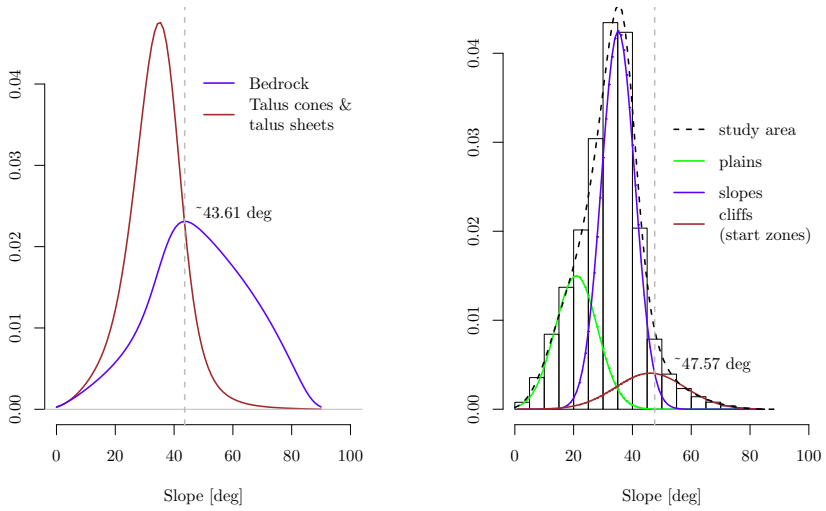

Figure 5.7.2: The two slope thresholds derived using the two methodologies described above: rock fall accumulation body/bedrock distributions (left) and after Loye et al. (2009).

iment budget.

Quite some studies have quantified debris fall and a variety of methods have been applied to quantify debris fall in high mountain areas. The most important of these are: (a) Lichenometry (e.g. André, 1997), (b) volume estimation of rock fall accumulation landforms via geophysical methods or bedrock base interpolation (e.g. Hinchliffe and Ballantyne, 1999, Hoffmann and Schrott, 2002, Curry and Morris, 2004, Moore et al., 2009, Siewert et al., 2012), (c) indirect measurements using cosmogenic nuclides (e.g. O'Farrell et al., 2009), (d) painted rock surfaces (e.g. Matsuoka and Murton, 2008), (e) rock fall collectors (such as nets set on rock fall accumulation landforms) to measure rock fall deposition masses directly (e.g. Becht, 1995b, Keller and Moser, 2002, Sass, 2005a, Krautblatter and Moser, 2009), (f) measurement of volumes using multitemporal terrestrial LiDAR surveys (e.g. Rosser et al., 2005, Mikos et al., 2005, Haas et al., 2009, Abellán et al., 2010, 2011) and (g) indirect measurement with terrestrial photogrammetric methods (e.g. Rabatel et al., 2007). The mentioned methods imply two different time scales. While methods (d–g) are applicable to determine historic to recent debris fall rates, i.e. operate at the present timescale, methods (a-c) yield rock fall rates valid for much longer time periods, most often the Holocene. Such values should not be used to estimate current rock wall erosion rates (Becht, 1995b). As this study is concerned with recent process rates, data generated from the methods (e) and (f) were applied.

Due to the extensive field work required, inaccessibility, exposure to natural hazards and the great effort in digital terrain analysis required to achieve reliable values, a direct measurement could only be undertaken for a selected and rather small subset of rock walls in a meso-scale catchment as the Upper Kauner Valley.

Measurements via rock fall collectors

Data from rock fall collectors was supplied by sub-project two of the PROSA-project. Seven nets had been installed (see also Vehling et al., 2013b, 2015). In addition, 13 sites with undisturbed flat surfaces that serve as natural rock fall traps were identified and used as natural collector "nets". The nets (mesh size 2 mm) were installed at the contact of the rock wall and the talus surface. They were fixed to the rock wall using iron rods (Keller and Moser, 2002, Vehling et al., 2015). To prevent particles from leaving the nets down slope, 60 cm high steel fences or simple batters from sediment were erected at the nets' lower ends. As the monitored rock walls were, at maximum, only a few tens of meters high, Vehling et al. (2015) is confident that no particles could gain enough kinetic energy to jump over these barriers. Nevertheless, additional nets were installed downslope the barriers (cf. Becht, 1995b). In doing so, it could be shown that the mass of the particles material reaching these areas was much lower than one percent of the annual sum. Steel barriers were also installed to prevent particles entering the nets from the sides. As a result, the measured masses represent only debris fall stemming from the monitored rock wall section (Vehling et al., 2015, Heckmann et al., 2016). The material was collected from the nets and measured mechanically in the field. Rounded rock fragments, rock pieces with striations or rock pieces of different geological quality than the monitored rock wall were sorted out by hand before weighting in order to measure only primary rock fall (Krautblatter and Dikau, 2007, Krautblatter et al., 2012, Vehling et al., 2015). Depending on the time when the collector net was installed, the measurement time ranged between 353 and 1068 days. A detailed description of the nets, including location, elevation, aspect, geology and measurement period for each of the rock fall collectors can be found in Vehling (2016, p. 186f.).

To convert the masses obtained from the rock fall collectors (in kg yr^{-1}, cf. above) to rock fall production rates (kg m^{-2} yr^{-1}), the rock wall surface area contributing to the rock fall collectors, needs to be determined. A wide range of methods to determine this area can be found in the literature. As the size of this area has a definitive impact on the resulting rock fall production rates, different methods were applied to do so. This enables a better comparison to other rates from the literature and gives an impression on the errors associated with each SCA derivation method. Therefore, the sediment contributing areas of the rock fall collectors were defined and determined in the three following ways: i) Real surface area of bedrock cells steeper than a slope threshold within the hydrological contributing area of the rock fall collector (henceforth referred to as scenario "H"), ii) Real surface area of bedrock cells steeper than a slope threshold within an area delineated by an expert (scenario "E") and iii) Real surface area of bedrock cells steeper than a slope threshold and delivering to the net as identified by back-tracing of the trajectories modeled (scenario "G"). The determination of these areas, independent of the scenario, makes use of 1 m ALS DTMs for each of the AOIs around the rock fall collectors (summer 2012, constructed manually using the point values closest to the cell centers, please see 5.4.1.2, 5.4.4 and 5.5.1 for more information) and spatially corresponding sub-sections of the geomorphological-geological map (cf. 5.6.1), modified to contain codes for each net and rasterized to the same spatial resolution as the DTM. For application in the numerical model (as used in scenario S-I-G, cf. below), the DTMs were resampled to a spatial resolution of 5 m using the nearest neighbor

approach. An analogous data basis was used for the regionalization to the whole study area.
For the first scenario ("S-I-H"), the hydrological catchment of each debris fall collector was identified using a eleven step procedure involving standard GIS techniques (e.g. Freeman, 1991, Wang and Liu, 2006). In doing so, the border line of the rock wall and the net was taken as a target. Later, a bedrock mask and the slope threshold were applied to the found hydrological catchment of the nets. The usage of a modified hydrological catchment of a debris fall collector or a rock fall depositional landform to identify debris fall source area is quite common in the literature (e.g. Menéndez Duarte and Marquínez, 2002), but it is well known that it tends to overestimate the sediment contributing area (Frattini et al., 2008). As a result, the values calculated using these method will be used as a reference to facilitate a comparison with the debris fall production values found in the literature. The analysis was conducted on a 1 m DTM and the found cells were then resampled to a spatial resolution of 5 m using the majority scheme. The resampling step was necessary for comparative reasons as the rock fall simulation models is running on a 5 m DTM.
For the second scenario ("S-I-E"), the rock wall areas probably contributing to the net were delineated by sub-project two (based on field experience, mapping and the orthophotos generated by the author) and provided as raster data sets. These were then further prepared by the author using standard GIS techniques before the bedrock mask and slope threshold could be applied. The found cells were then resampled to a spatial resolution of 5 m to enable comparison with scenario "G".
The third scenario ("S-I-G") made use of the numerical rock fall trajectory model and the representation of these trajectories as a graph. Debris fall was modeled on the 5 m DTM from all start cells in the wider vicinity of each net using the same parameter settings as for the regionalization step (see table 5.7.2). To model the effect of the steel fences and other barriers erected at the downslope boundary of each net, the values of the respective cells in the DTM were increased. Then for each rock fall collector, all trajectories stopping on its spatial representation (polygon) were selected and the pertaining source cells were identified using the graph representation of the trajectories. This was accomplished with tools from R and its igraph package. A similar approach was used by Frattini et al. (2008) to identify the "physically feasible" source areas of active and dormant rock fall deposits. This allocation was based on a GIS overlay of modeled trajectories and a map of the rock fall deposits. As all start cells used in the model had been selected using the bedrock mask and the slope threshold, a subsequent application of these was not necessary. Figure 5.7.3 shows the principle used in finding the sediment contributing area using the model. Debris fall is modeled with the calibrated numerical model from all bedrock cells steeper than the determined threshold (brown). All trajectories that terminate on a cell covered by the net (green) are traced back to their start cells. These start cells are then classified as sediment contributing.
Independent of the scenario used for the identification of SCA cells, the sediment contributing area was then calculated by summing the real surface area (Jenness, 2004) of the identified cells. For scenario "G", the area was additionally weighted by the number of trajectories having stopped on the net. Figure 5.7.4 on page 115 shows the cells identified as SCA for three different collector nets. Given the masses collected from and the sediment contributing areas calculated

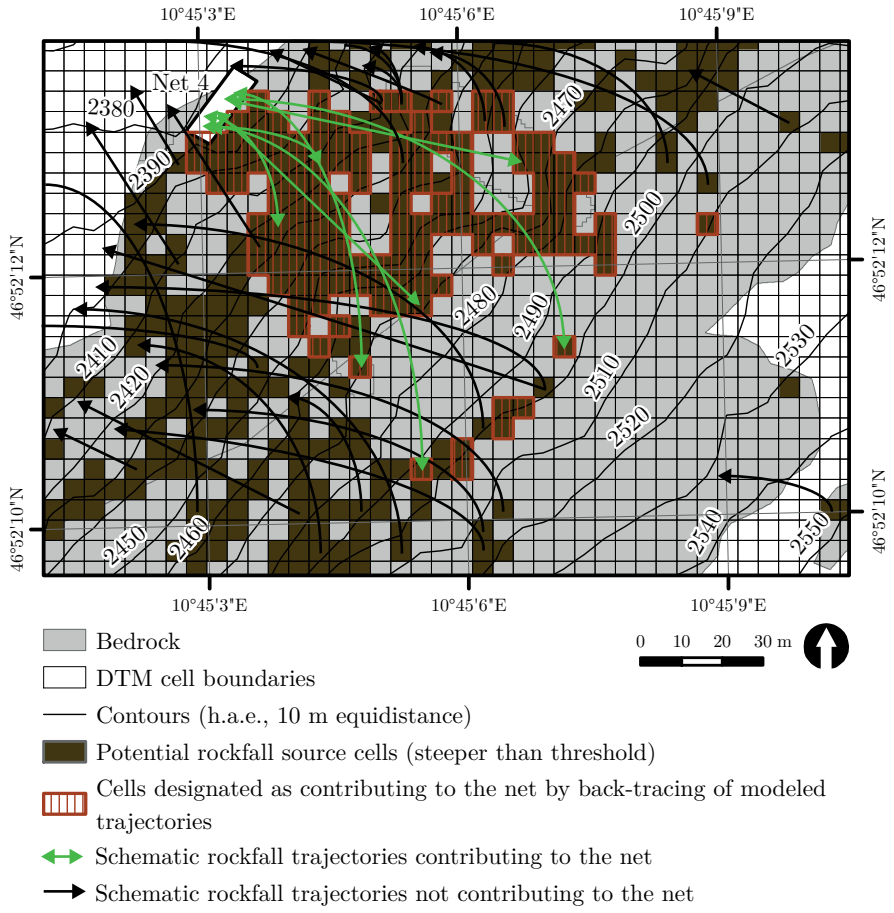

Figure 5.7.3: Principle of finding the sediment contributing area for a rock fall collector using the model in scenario S-I-G.

for each rock fall collector, a rate of annual debris fall production [kg m^{-2} yr^{-1}] could be calculated by dividing the measured masses by the sediment contributing area. Data data basis of rock fall rates was further enriched using measurements obtained via TLS.

Measurements via TLS
Over 40 finished DoDs showing significant surface changes and corresponding DTMs of rock walls were obtained from sub-project one. These had been generated using data from the TLS measurement sites 8, 9, 10, 11, 15 19, 20 and 21, representing rock walls of differing geology, aspects, and elevations (see table in the appendix three). Work in sub-project one included a rotation of the point clouds to facilitate rock fall detection using grids as digital surface representation, a clipping of the area to the bedrock surfaces, manual outlier removal, gridding and differencing of the DTMs. DoDs were generated using a spatially distributed overall LoD. After DoD calculation, remaining noise was removed by applying a grid based majority filter. The obtained DoDs and

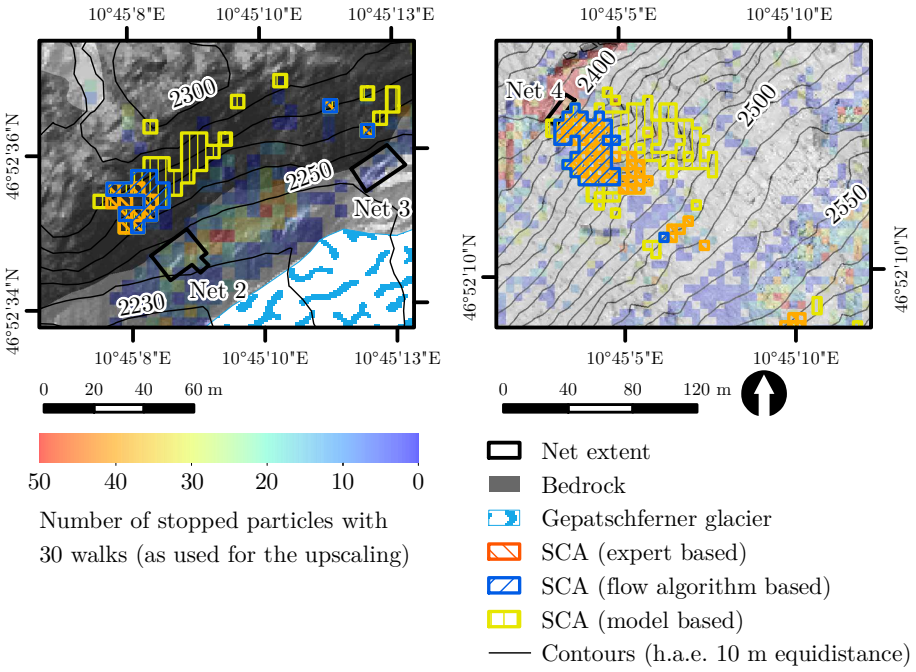

Figure 5.7.4: Sediment contributing areas as determined with three different scenarios, exemplified for three debris fall collector nets. The SCA for net four is not shown completely as it is very large. A second, large section can be found above 2550 m h.a.e, the lowest areas of which can be seen in the lower right corner.

DTMs were subsequently used by the author to calculate the true surface area of the scanned rock walls, the volume mobilized on these rock walls, erosion and rock fall production rates. The rock fall production rates gained by LiDAR were then combined with the data obtained using rock fall collector nets for a regionalization of the rates.

Strategy two: Debris fall quantification
While the debris fall production rates used in strategy one were obtained by actual measurements on test sites via rock fall collector nets and TLS, the rates used for a regionalization of rates in strategy two was based on a expert-based mapping of a rock mass stability index developed by Vehling (2016) which was correlated with material transfer rates. The non-linear correlation between the newly developed index and erosion rates at the rock fall collectors has proven to be very strong ($r^2 = 0.92$). The index was mapped by Vehling for the whole study area, which made it possible to deterministically regionalize (cf. (Becht, 1995b)) rock wall retreat rates to the whole catchment using the six classes of distinct erosion rates as depicted in table 5.7.1 on the next page (Vehling, 2016).

Debris fall process area modeling
In order to estimate the contribution of debris fall to the overall sediment bud-

Geotechnical rock class	**Rock mass stability index**	**Representative rock fall collectors**	**Sediment transport rate [t km^{-2} yr^{-1}]**
Intact rock mass	> 75	4 (rn),7 (rn)	40
Largely intact rock mass*	75–60	6 (rn),2a (rn), 5 (rn), 10 (nn)	200
Largely intact squared-bedded rock mass		10 (nn)	550
Partially fragmented rock mass	60–45	1 (rn), 9 (nn), 2b (rn), 7 (nn), 13 (nn)	1700
Largely fragmented paragneiss	45–30	12 (nn), 14 (nn), 3 (rn), 5 (nn)	7500
Entirely fragmented rock mass*	< 30	2 (nn), 4(nn), 6(nn)	32000

Table 5.7.1: Ground stability index classes and corresponding rock fall collectors used to determine representative sediment transfer rates for each class (after Vehling (2016)). These rates were used in S-II for a regionalization of debris fall.
(rn): real net, (nn): natural "net" (cf. above)
* all lithologies

get, it is necessary to localize the process area of debris fall on the scale of the whole study area. This can be achieved using numerical trajectory models. Such trajectory models had been used to delineate hazard zones (e.g. Dorren and Seijmonsbergen, 2003, Guzzetti et al., 2003, Michoud et al., 2012) or identify and map sediment cascades (e.g. Wichmann, 2006, Wichmann et al., 2009, Heckmann and Schwanghart, 2013). In this study, such a model was applied for two reasons: First, to back-trace modeled trajectories for a identification and calculation of debris fall collector sediment contributing areas and sediment production rates (cf. scenario "G" above). Second, to delineate debris fall process areas, to identify GPUs (sensu Wichmann et al. (2009)) and to be able to transfer sediment production rates downslope on the scale of each trajectory. Both applications make use of the trajectories being stored in form of edges of a directed graph, connecting every debris fall source and the respective deposition area. This can be used to visualize and analyze sediment movement by debris fall on the scale of each pixel, landform or the whole study area.
The process model used to delineate process pathways is not the focus of this paper. As a result, its basic functionality and parameters are only briefly touched upon here. More and detailed information can be found in Gamma (2000), Becht et al. (2005), Wichmann and Becht (2006), Wichmann (2006). The model had been extended by Heckmann to store the modeled trajectories, which allows to track sediment movement from start to deposition cells (Heckmann and Schwanghart, 2013). In the naming and symbols used for the different model parameters, I am following Wichmann (2006) whenever possible. The model can be divided into two sub-models, one for identifying the process path and one for the process runout length.
The process path model implements a modified random walk algorithm pre-

sented by Gamma (2000, originally for debris flows). This algorithm is controlled by three parameters and Monte Carlo methodology is usually used to delineate the whole process area of rock fall (independent of volume). In this study, 30 walks were simulated from each start cell.
In order to determine the runout length and stopping position of each particle, a one-parameter friction model is coupled with the process path model. The numerical model calculates the velocity of the particle based on the velocity of the particle on the previous cell, the slope inclination and length of the current cell-to-cell segment and a friction parameter (μ_{rfm}). Free fall is modeled as long as the slope on the current segment is above a user-defined threshold (β_{ff}). As soon as the slope inclination drops below this threshold, an impact is assumed, the energy of the particle is reduced by a user-defined percentage and the one parameter friction model is used. As soon as the velocity reaches zero, the particle is modeled as deposited. See table 5.7.2 for the parameter settings for both process path and runout length models used in this study. All parameters

Susceptibility model:	slope $> 47.57°$
Process path model:	
Slope threshold (β_{thres})	45°
Dispersion exponent (a)	6
Persistence factor (ρ)	5
Runout length model:	
Free fall threshold (β_{ff})	50
Energy reduction upon impact	75 %
Friction coefficient (μ_{rfm})	0.6–0.7
Number of random walks	30

Table 5.7.2: Parameters for the rock fall susceptibility, process path and runout length models used in this study.

were calibrated in different, carefully selected, test sites in the study area. The parameters were chosen so that the modeled depositional areas matched the extent of obviously active depositional areas on talus cones and sheets. Activity was assessed using deposit color and the absence of vegetation. As a result, the friction parameter for the runout length model (μ_{rfm}) was drawn from a uniform distribution of values $0.6 \leq \mu_{rfm} \leq 0.7$.
A validation of the selected values was undertaken at a rock wall where a huge combined rock slide/rock fall has successively deposited several tens of thousands tons of material as a huge talus cone: For validation purposes, a 1 m DoD (representing a time period of July to September 2012) was calculated from ALS data (cf. figure 5.7.5, left). Then, the process area was reproduced on the 5 m DTM using the raster cells within the conspicuous rock fall scar as starting cells (cf. figure 5.7.5, right) with the same parameters used for the modeling of debris fall in the whole study area. Figure 5.7.5 shows that the chosen parameter values lead to the process area being reproduced very well. The numerical model results in two rasters, one containing the modeled maximum particle velocity and one the number of particle stops. In addition, a list with an entry for each modeled trajectory is produced.

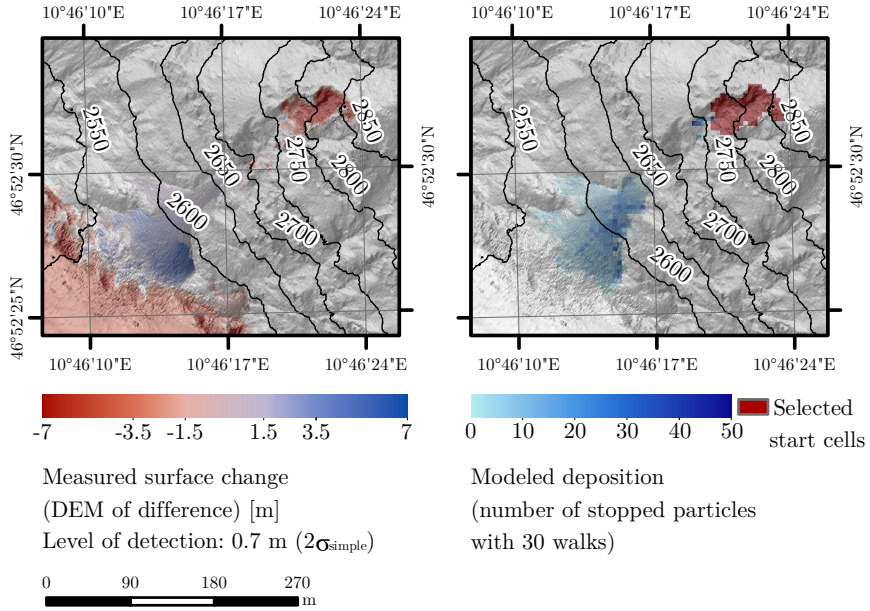

Figure 5.7.5: Qualitative validation of the rock fall model, using surface changes measured from ALS-derived DTMs (left) and modeled deposition area (right). The area of negative surface change in the southwestern corner of the left map is part of the Gepatsch Glacier tongue and ablation can clearly be seen for the time period (July to September 2012).

Assigning rates to modeled trajectories

For each trajectory, this list contained the identifiers of both start and stop cells, a code of representing landform units in the geomorphological-geological map and a weight accounting for the random walk approach: If all 30 modeled trajectories from one source cell have different stopping/deposition cells, the weight of each trajectory will be 30^{-1}. Trajectories with the same start and stop cell combination will be aggregated later and then have a weight with an integer multiple of 30^{-1}.

Containing start and stop cell identifiers, the trajectory list can be used as an edgelist to construct a directed graph. Storing the sediment pathways in form of a directed graph makes it not only possible to manage the high amount of data but a whole lot of concepts and techniques from graph theory can be used to analyze the debris fall pathways on the scale of the whole 62 km^2 catchment. In creating a graph from this edgelist, all information in the list is stored as node or edge attributes and can be used for analysis. Node attributes are landform codes (providing information: e.g. if a particle has stopped on a glacier) and node coordinates. Depending on the scale the analysis is undertaken in, these coordinates pertain either to DTM cell centers or the centers of polygons representing the center of landforms in the geomorphological-geological map. Additional and informative attributes can be calculated using techniques based on graph theory. These attributes can, for example, give information about the relative coupling status of a landform, i.e. whether it is a sink for debris fall

or from how many (different) rock wall sections a landform receives its input. This makes it possible to classify each landform according to their functions in the debris fall section of the sediment cascade: A landform can be classified as either a pure sediment source (trajectory only leaving the unit, e.g. a rock wall), a unit functioning as temporary sediment storage (trajectories entering the unit from above and leaving it downslope, e.g. a rock wall section below another rock wall section), or a sink (only trajectories entering the unit, e.g. a rock wall or a talus cone) (Heckmann and Schwanghart, 2013). The edge attribute, on the other hand, represented the mass flux [kg yr^{-1}] transported along the edge, and therefore from a certain rock wall section to a certain landform (class). In strategy one, the sediment flux rates [kg m^{-2} yr^{-1}] were assigned to each cell-to-cell trajectory by randomly sampling from a Weibull distribution fitted to measurement rates (cf. below). Then, the sampled value was multiplied with the weight of the trajectory (to account for the random walk approach in the numerical model) and the real surface area of the source cell to arrive at mass flux values for each trajectory [kg yr^{-1}].
With the nodes of a graph representing raster cells and edges mass flux between these cells, trajectories with the same start and end cells can be aggregated. Analogously, where trajectories connect different cells but the same start rock wall section (polygon in the geomorphological-geological map) and the same target landform unit, these can be aggregated to calculate the sediment flux between landforms or, on the scale of the whole catchment between whole landform types (e.g. all sediment flux from rock walls to the fluvial system). Thus, on the landform scale, the resulting graph represents a network of landforms, with rock wall sections or all bedrock surfaces in general connected to debris fall deposition landforms by debris fall sediment pathways. On the catchment scale, it directly represents the debris fall part of the sediment budget.
The network model can also be used in the opposite direction: By back-tracing all trajectories leading to a certain deposit unit, the sediment contributing area of that unit can be determined (this was made use of in scenario "G" in calculating the SCA of the debris fall collectors in this study). Graph construction and analysis of debris fall pathways was accomplished using the igraph package for R (R Development Core Team, 2012, Csardi, 2014).
The regionalization work flow followed in strategy two was essentially the same as in strategy one, with the important difference that production rates were not sampled from a distribution based on empirical rock fall net or TLS measurements and SCA modeling using three different techniques, but were deterministically taken from a map prepared by sub-project two. Rock fall trajectory and runout modeling, analysis of sediment pathways and so forth, however, were the same as the ones used in strategy one.

Strategy I: Distribution fitting to debris fall rates
Even though rock fall measurements were available from 16 sites in the study area (from collectors and TLS), these did not reflect the wide range of different geofactors controlling rock fall production in the 62 km^2 catchment completely. It was therefore not possible to use direct measurements from each relevant rock wall class to use in a rule-based or deterministic regionalization of rates. In order to be able to use the measurement values obtained by sub-projects one and two, a distribution was fitted to all available data to be used in production rate assignment to each bedrock cell steeper than the slope threshold in the study area.

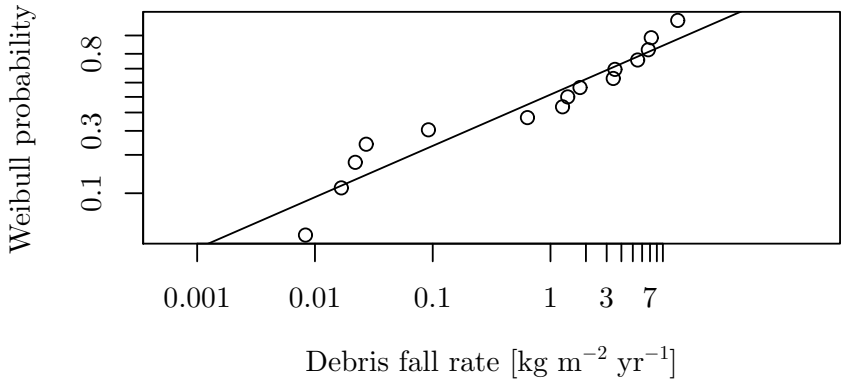

Figure 5.7.6: Weibull plot for the data from strategy one, scenario G

Independent of the type of slope failure in general or rock fall under study and given the general geomorphic understanding of the process, it is clear that small magnitudes occur more often then high ones. This is confirmed by many published scientific studies (Bennett et al., 2012, Lari et al., 2014, Heckmann et al., 2016). In the case of debris fall, the size (and consequently also rate) distribution is mainly controlled by the distribution of joints in the bedrock and the effective depth of temperature gradients within rock wall surfaces (Hales and Roering, 2007). A theoretical distribution needs to be chosen that is suitable to model these characteristics. Quite some studies (e.g. Heckmann et al., 2016) have used the log-normal distribution to describe the distribution of rock fall volumes or production rates. There is, however, no reasonable indication why the logarithm of the rock fall production rates should be normally distributed. With rock fall over one year occurring in a number of discrete events and both, high magnitudes of single events and yearly sums following a strongly right skewed distribution, it is especially three distributions that lend itself for potential fitting: i) Pareto distribution, ii) Gumbel distribution and iii) Weibull distribution (Günther Wirsching, personal communication, May 2016). In using these discrete distributions, the yearly debris fall production rates is conceptualized as the sum of a large number of homogeneously sized debris fall events, which is scientifically more correct than choosing any theoretical distribution capable of modeling a right-skewed empirical distribution (Günther Wirsching, personal communication, May 2016). Several tests were conducted to determine whether the assumption of rock fall production values following any of these distributions could be hold. In addition, the data was also tested for a log-normal distribution.
A Shapiro-Wilk test for the log-transformed data has shown that the data is in fact not log-normally distributed ($p = 0.03$ for values obtained via scenario G, only the test results for this scenario are reported here. The data from the other strategies led to similar results). All tests and data exploration was completed

using both ready-made and self-written methods in R. Fitting was achieved using methods from the MASS package (Venables and Ripley, 2002). In order to assess whether the data could be fit by a two-parameter Weibull distribution, a Weibull plot can be used (Günther Wirsching, personal communication, May 2016). Figure 5.7.6 shows the Weibull plot for the data calculated using strategy one/scenario G. With the points approximating a straight line, a Weibull distribution can be assumed. Additionally, a χ^2 goodness of fit test was conducted to test the empirical data against the fitted Weibull distribution. A p-value > 0.15 indicates that a Weibull distribution can in fact model the distribution of the debris fall production rates calculated from the measurement data of sub-projects one and two satisfactorily. The parameters of the respective fitted Weibull distributions are given for each scenario in table 5.7.3.

Method of SCA derivation	Shape	Scale	Expected value
S-I-H	0.64 ± 0.13	1.83 ± 0.75	2.56
S-I-E	0.60 ± 0.12	2.32 ± 1.02	3.52
S-I-G	0.54 ± 0.12	1.90 ± 0.95	3.3

Table 5.7.3: Fitted parameters and expected values [kg m^{-2} yr^{-1}] of the Weibull probability density functions of debris fall production rates, depending on SCA delineation method.

Despite using TLS and rock fall collector measurements, 16 rock fall production values were available. An extensive literature review was conducted to open up supplementary data on rock fall rates determined in similar environmental settings and under usage of similar quantification methods for purposes of comparison (see 6.1.1.1.1). The table in appendix four shows the values found. The fitted distribution, exemplified for strategy one/G, is presented in figure 5.7.7 on the following page.

Regionalization in strategy two
As strategy two relied on a deterministic regionalization approach, material transport rates were easily assigned to the rock mass stability classes (Vehling, 2016). Figure 5.7.8 on page 123 shows a spatial subset of the resulting regionalization result.

5.7.1.1.2 Block fall, Cliff fall and Bergsturz

As the identification and quantification of rock fall of higher magnitudes was accomplished in sub-project two, the reader is referred to Vehling (2016): Vehling has mapped about 166 rock falls of magnitudes between 100 and 1×10^6 m^3 using the historical orthophotos (see subsection 5.4.2.1) and ALS data. More information an results are given in subsection 6.1.1.2.

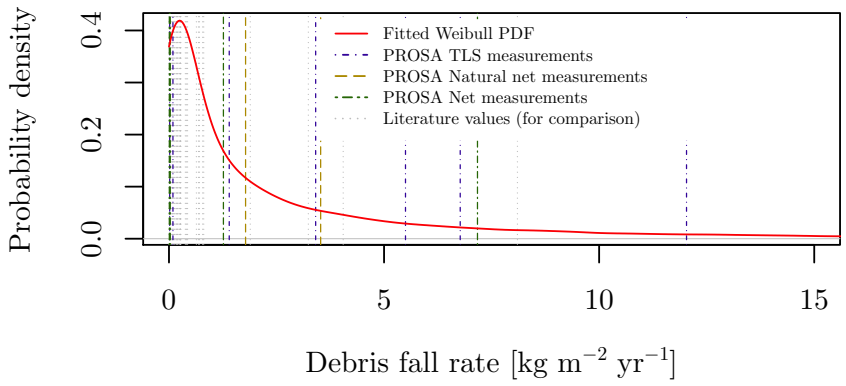

Figure 5.7.7: Kernel density estimation and Weibull probability function fitted to rates based on measurements in PROSA and calculated with strategy one and scenario G.

5.7.1.2 Debris flows

5.7.1.2.1 Volume measurement

The goal being to arrive at a database of all detectable debris flows having occurred in the study area from 1953 on, different types of data had to be valued. Where two temporal volumes of 3D-data were available (post 2006), volumes could be measured directly from it (henceforward strategy "A"). Where 3D-data was available only for the post-event time step, a pre-event surface was reconstructed to facilitate measurements (strategy "B"). Where no 3D-data was available for any of the two time steps (1990 and before), the volume was calculated using a fitted deposition area-volume relationship (strategy "C").
In total, a number of thirteen different time periods between fourteen volumes of orthophotos, some 60 TLS scans from seven different TLS scan positions and up to 14 time steps and seven ALS surveys of varying extents had to be evaluated (see below for details). As the data stemmed from dozens of different time steps, three different data sources and debris flows were to be identified all over the 62 km^2 study area, a semi-automated work flow was developed. This included the production of dozens of DoDs from the different ALS and TLS scan combinations using a spatially distributed σ_{simple}, a propagation of these errors, a identification of debris flows on DoDs and orthophotos, a calculation of their volume and potential energy transformed and, at the same time, keeping track of respective meta-data such as time period, location and data source (combination). This work flow was implemented using a variety of tools in LIS, SAGA GIS and ESRI ArcMap. DoD were generated with spatially distributed error (see subsection 5.5.2.3 and section 5.5.3.2). The automated work flow parts were scripted in R (using methods from the rsaga (Brenning and Bangs, 2016) and rgdal (Bivand et al., 2016) packages) and Python enabling a precise reproduction and future enlargement of the debris flow inventory. Given the

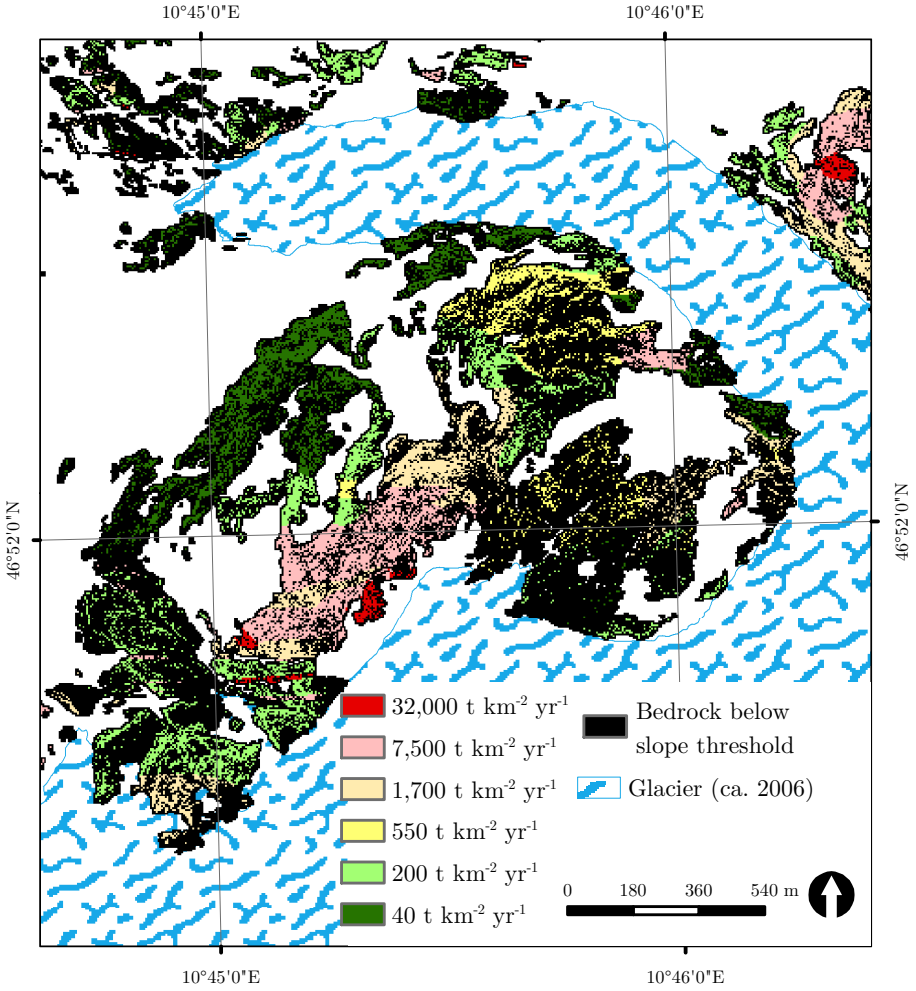

Figure 5.7.8: Bedrock production rates as mapped by Vehling (2016) around the tongue of the Gepatsch Glacier. This spatial distribution was used to regionalize debris fall in strategy two.

high number of data sources, processing steps and used tools, only a summarized work flow will be presented in the following for each of the three strategies.

Direct measurement from point cloud data

As the whole extent of the study area was surveyed by ALS several times since 2012, it was possible to measure sediment transport by debris flows directly from point cloud data all over the study area for this time period. ALS to ALS comparison was feasible at all locations not surveyed by TLS (see figure 5.4.2 and the table in appendix three), in cases where no TLS scans were acquired at TLS monitoring sites between two ALS surveys or when debris flows were visible on TLS scans, but the point density was lower than on ALS scans (at lateral TLS scan margins).

To locate these debris flows, DTMs with a spatial resolution of 0.8 m were con-

structed and DoDs were calculated for all subsequent ALS time step pairs and the process areas of all debris flows were mapped. Taking the debris flow shown in figure 5.7.9 as an example, depending on the roughness of the surface (see subsubsection 5.5.2.3), spatially distributed propagated errors (σ_{simple}) for the single cells on a DoD ranged between circa 0.01 and 0.34 m (mean 0.08 m resulting in overall LoDs between 0.02 and 0.66 m with a mean of circa 0.16 m) within the process areas of debris flows[1]. The mapped accumulation bodies were then clipped from the DoD and the following attributes of the debris flow were stored in the debris flow inventory: Time period start and end dates, ALS survey IDs, volume, planimetric area of deposition body, elevation for both start and depositions zone centroids and their elevation difference. Figure 5.7.9 shows debris flow nr. 86 as an example.

Several TLS scan positions had been set up at locations that had been identified as debris flow prone. About 60 TLS scans had been acquired from these locations in the course of the project and each location was also surveyed by ALS two times (on average, all seven ALS survey data sets were checked for overlap with the areas scanned at the seven TLS monitoring sites) during the course of the project. The TLS scans had been georeferenced to the global coordinate system to facilitate an offset against ALS data (see section 5.4.3 and subsection 5.4.4.2). Now, these data sets were sorted temporally to determine successive LiDAR surveys (ALS or TLS) and differences were calculated for each of the successive time periods. Table 5.7.4 shows the scans offset against each other for TLS monitoring position six. This resulted in a total of 80 scans (ALS and TLS) having been evaluated for debris flow quantification at the TLS monitoring areas. As with debris flows quantified with ALS-ALS differences, the point data from each TLS monitoring site were gridded to the same 0.8 m grid system using local plane fitting as a gridding method to produce DTMs for each time step. As a result, spatially distributed LoDs could be used to quantify debris flows from these data sets. ALS-TLS propagated cell errors (σ_{simple}) on the debris flow accumulation bodies typically ranged between 0.04 and 0.24 m. Later, individual debris flow process areas were mapped manually from the calculated differences to obtain values for each individual debris flow. As some of the areas scanned from different monitoring positions overlapped, it was paid attention that individual debris flows were not recorded multiple times. Then all necessary debris flow attributes (as mentioned above) were calculated and stored in the debris flow inventory. In some cases, differencing of ALS and TLS data has revealed that TLS data was not georeferenced satisfactorily. As a result, some DoDs, especially from TLS scan position 16, had to be neglected for debris flow quantification.

Using the methodology described above, it was possible to quantify all debris flows that have not reached the fluvial system. Where a debris flow had reached the fluvial system (as indicated by the track on the DoD), a direct budget was

[1] As already indicated above, for strategy A alone, over 70 DoDs with spatially distributed propagated uncertainties were generated for a quantification of all debris flows in the study area. Strategy B involved an additional 71 DoDs. Many studies and papers using topographic data for balancing report the propagated uncertainties for their DoDs. Most of them, however, use a spatially uniform uncertainty and present DoDs from only a few time steps and locations. As the LoDs are spatially distributed and dozens of DoDs were generated for the quantification of debris flows in this study, a representative range of LoDs used for a quantification of a single debris flow instead of tens of mean values for the different DoDs is presented here. This range can be considered as representative for all DoDs calculated.

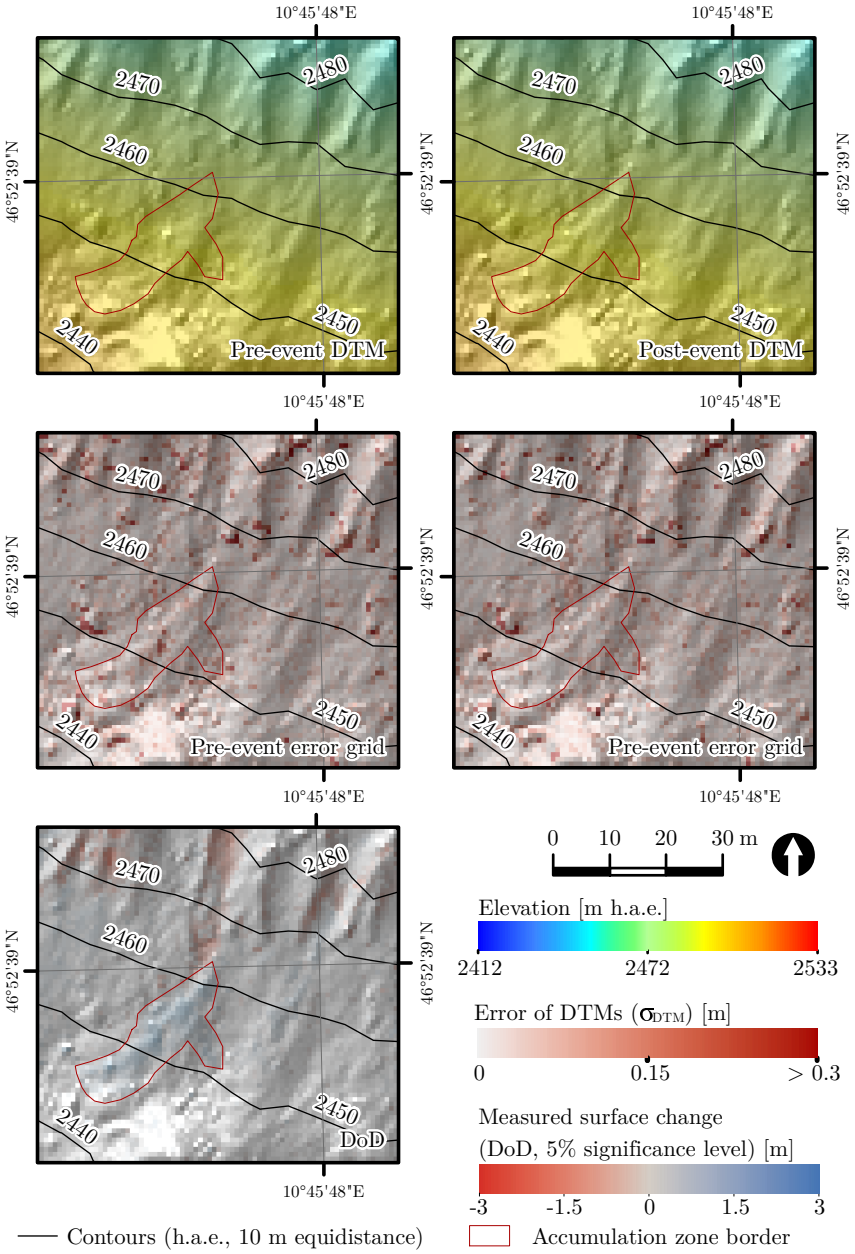

Figure 5.7.9: Accumulation zone of debris flow nr. 86, quantified using data from the ALS surveys July 18, 2014 and September 28, 2012. It occurred on the true right lateral moraine of Gepatsch Glacier above the present glacier tongue (outside any area monitored by TLS) but has not reached the glacier ice. A volume of about 117 m^3, which corresponds to a mass of 258 t, has been deposited on a planimetric area of circa 276 m^2. The sediment was deposited circa 26.5 m below the erosional zone. As a result, the debris flow has transformed an energy of circa 6.7×10^7 J.

Data source	Scan number	Date
TLS	1	2010-07-13
TLS	2	2011-09-24
ALS	3	2012-07-04
TLS	4	2012-08-24
TLS	5	2012-09-20
ALS	6	2012-09-28
ALS	7	2012-10-25
TLS	8	2013-07-01
TLS	9	2014-07-08
ALS	10	2014-07-18
TLS	11	2014-09-23
TLS	12	2014-10-20
TLS	13	2015-07-10
TLS	14	2015-09-22

Table 5.7.4: LiDAR data available for the area surveyed at TLS scan position six. Each scan was offset against the scan with the next higher scan number to identify debris flows.

calculated for the whole process area of the debris flow (i.e. including erosion, transport and deposition zones) to obtain the volume of the debris flow that has left the subsystem.

Measurement with a reconstructed pre-event surface
As point cloud data was only available from 2006 on, the constructed orthophotos (cf. subsection 5.4.2.1) were studied and all visible debris flows having occurred since the acquisition of the previous orthophoto volume were mapped with an analogous zonation as used for the ones measured using point cloud data. The resulting shapefiles were then split and sorted according to zonation and time period. Then, all data from later time steps (orthophoto or ALS, TLS) were checked for a later debris flow. If none was found, an ALS-derived 80 cm DTM was constructed for the area around the mapped deposition zone of the debris flow using the moving planes scheme. The mapped deposition zone was then cut from the DTM and the pre-debris flow surface was interpolated from the remainder of the DTM values. This was accomplished using spline interpolation while using a 0.1 tension parameter to obtain a reconstructed surface as objective as possible. This surface was then subtracted from the original DTM to obtain a DoD displaying the material accumulated by the debris flow. All relevant attributes of the debris flow were stored to the inventory. Figure 5.7.10 shows an example.

Estimating debris flow magnitudes using a fitted area-volume relationship
Where no 3D or 2.5D data is available for the application of the geomorphological method, an empirical relationship between projected debris flow deposition area and volume can be used to estimate volumes from areas. This approach had to be undertaken in balancing debris flows that occurred before 2006, that is, the date of the first high quality point cloud (cf. 5.4.2).

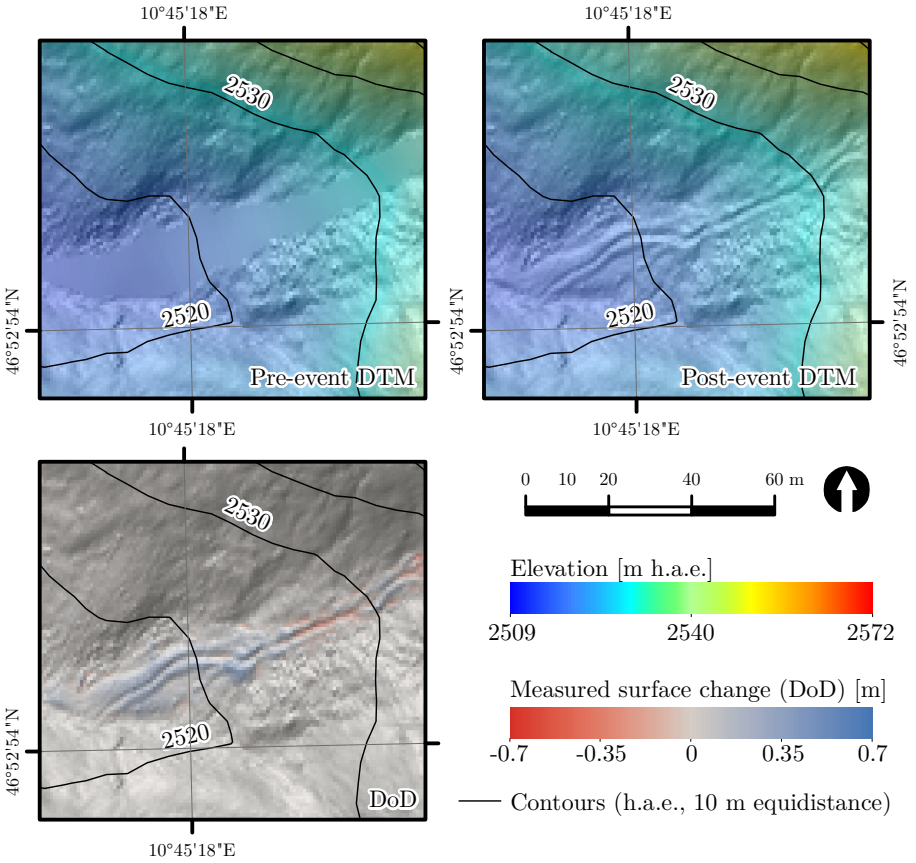

Figure 5.7.10: Quantification of a debris flow using a reconstructed pre-debris flow surface. The pre-debris flow surface is constructed by clipping the mapped debris flow accumulation area from a recent DTM and interpolating the resulting data gap (top left). This DTM is then subtracted from the current state DTM (top right) to give the DoD (bottom left).

The estimation of volumes or associated erosion rates from either depositional or erosional areas is very common in geomorphological and sediment budget studies and has proved a valuable tool for balancing of historical slope failures of various types (e.g. Malamud et al., 2004, Larsen et al., 2010, Bennett et al., 2012). Many studies that have applied this methodology have found the relationship between area (A_{sf}) and volume (V_{sf}) to follow a simple positive power-law with exponent $\gamma > 0$ as in equation 5.7.1 (Simonett, 1967, (as cited in Bennett et al. 2012)).

$$V_{sf} = \alpha_\nu \cdot A_{sf}^{\gamma} \tag{5.7.1}$$

Although Larsen et al. (2010) have found different values of γ for different types of landslides, the fact that similar values of γ have been found in studies balancing the same type of slope failure from many different climatological and geological settings (cf. table 6.1.5) allows the conclusion that the relationship is controlled by geometrical factors rather than physiographic ones (Guzzetti

et al., 2009, as cited in Bennett et al. 2012). As a result, many studies have used values of γ found in other studies to convert areas to volumes and further to erosion rates (Hovius et al., 2000, Lavé and Burbank, 2004, Gabet, 2007, (as cited in Bennett et al. 2012)). The slight variation in γ values found by the different authors is probably due to inconsistent volume and area measurement procedures, but Larsen's findings underline the necessity to keep inventories as homogenous as possible when it comes to different subtypes (Bennett et al., 2012). That is, it is preferable to parametrize this relationship using data that is as valid as possible. As a result, only debris flows quantified directly from ALS or TLS data differencing (strategy A) was used, which implied a data set size used for fitting of 62. To fit the power law to the volume-area data, the data were logarithmically transformed before a robust linear regression using least squares fitting was performed. Guzzetti et al. (2009), cited in Bennett et al. (2012) have shown that the parameter γ is not very sensitive to the exact fitting method used but suggested that robust linear regression is preferable as this reduces the effect of outliers. The associated regression model is

$$\log_{10}(V_{sf}) = \beta_0 + \beta_1 \cdot \log_{10}(A_{sf}) + \epsilon \tag{5.7.2}$$

where β_0 is the regression intercept, β_1 the slope and ϵ the random error.
As the usage of least squares linear regression of log-transformed variables to fit power laws introduces bias (due to the expected value of ϵ only being zero in log-log space but not in non-log space) into values estimated using this relationship, a bias correction was necessary. This was accomplished using a factor correction during the back transformation of β_0 to α_ν following Newman (1993) as the residuals of the linear regression in log-log space were not necessarily normally distributed ($p = 0.16$ in Shaprio-Wilk test, a p-value of at least 0.2 is recommended by Günther Wirsching (personal communication, May 2016). Fitting of power law-relationships has been criticized, probably because a bias correction is often not performed. An alternative to linear fitting in log-log space would have been non-linear regression or quantile regression (Blöthe and Korup, 2013, Spencer and Morrison, 2014, Morrison and Spencer, 2014). Xiao et al. (2011), however, have shown that linear regression in log-log space generally does not a priori yield results worse than the alternative methods.

5.7.1.2.2 Magnitude-frequency relationship

An extensive body of scientific studies have observed that the frequency distribution of slope failures (independent of the type, including debris flows) follows a power-law with negative exponent above a certain magnitude (e.g. Hovius et al., 1997, Hungr et al., 1999, Stark and Hovius, 2001, Dussauge-Peisser et al., 2002, Guzzetti et al., 2002, Hergarten, 2002, Malamud et al., 2004, Stark and Guzzetti, 2009, Lim et al., 2010, Bennett et al., 2012). Below this magnitude, frequency declines as well, a phenomenon called the "rollover" of the probability density function that describes the frequency distribution. The origin of the rollover is debated in the scientific literature. While some studies attribute the lower frequency of small magnitudes to a deficient representation of small events in the inventories, others attribute the hybrid nature of the PDFs to the inclusion of different slope failure subtypes in the same inventories. The general shape of the magnitude-frequency distribution seems to hold true for slope failures of various geology and climate. Of course, a variability in power-law

exponent values can be observed. Reasons for this include, among others, differences in material strength and statistical noise (Bennett et al., 2012, and the works cited therein). The PDF of a negative-power law takes the general form:

$$p(x) = C \cdot x^{-\beta} \tag{5.7.3}$$

where x is the volume of the debris flow, C is a normalization constant and β is the scaling exponent of the tail of the distribution. As $p(x)$ diverges when $x \to 0$, there must be a lower bound, $x_{\min}$, to the power law behavior. This lower bound is contained in the normalization constant, C (Bennett et al., 2012). The corresponding cumulative distribution function (CDF) is obtained by integration of equation 5.7.3:

$$P(x) = \left(\frac{x}{x_{\min}}\right)^{\eta} \tag{5.7.4}$$

where $\eta = \beta - 1$ is the slope of the CDF and $P(x)$ the probability of a randomly picked volume or area exceeding x. It is recommended that the CDF be used to obtain an estimate for the power law exponent as the value estimated from linear regression on the logarithmically transformed magnitudes and PDF is biased (Bennett et al., 2012).The magnitude-frequency distribution of the debris flows in the study area were fitted only to the 62 debris flows quantified using strategy A. Fitting was performed using methods from R's poweRlaw package (Gillespie, 2014).
As only the tail of the magnitude-frequency distribution can be modeled using a power-law model, it was tried to model the whole distribution using a Weibull model. This, in turn, is justified with the data points lying on a more or less straight line in the Weibull plot. The resulting distribution could then be used to estimate the occurrence probabilities of different debris flow magnitudes in the study area.

5.7.1.3 Shallow soil slips

In order to determine the intensity of shallow soil slip scar modification since 1953, Betz (2016) has mapped shallow soil slip scars on orthophotos of four different time steps and then compared their number and areas from time step to time step. Betz has found that between 2003 and 2010 no new shallow soil slips have occurred and no new shallow soil slips have been mapped on the ALS-derived DTMs by her. It is unclear whether actually no new scars could be found on the DTMs or whether Betz has not undertaken this. As no new scars formed between 2003 and 2010, it is assumed by the author that activity was also low from 2010 to 2014. A quick search for new shallow soil slip scars on a 1 m DoD of the proglacial areas of Gepatsch and Weißsee Glaciers (Fall 2012 to July 2014) has not yielded any new scars. It must therefore be stated that probably no sediment transfer by shallow soil slips has occurred in the Upper Kauner Valley during the time of the PROSA project. To get an idea of past intensities, the sediment moved by shallow soils slips between 1970/71 and 2003 was estimated. Betz reports the occurrence of seven shallow soil slips in the study area during this time period, which relates to an increase in the total area covered by shallow soil slip scars of roughly[2] 800 m^2. Assuming an average

[2]Betz (2016) gives a value for the total increase of areas covered by shallow soil slip scars. It is therefore unclear which share of the 800 m^2 are to be attributed to the enlargement of scars that had already existed in 1970/71.

thickness of the moved sediment/soil body of 0.15 m (based on field observations by the author and photographs in Betz (2016)) and using a density of the moved material of 2.1 t m^{-3} (Betz, 2016), the sediment mass moved by shallow soil slips was estimated.

5.7.1.4 Rock slides and Deep-seated Gravitational Slope Deformations

As the identification and quantification rock slides and DGSDs was accomplished in sub-project two, the reader is again referred to Vehling (2016). Vehling has located a number of large mass movement complexes moving very large volumes (> 10 000 m^3) at very slow velocities all over the study area. They cover about 3 km^2 (circa 5 %) of the planimetric study area.

5.7.1.5 Creeping Permafrost

5.7.1.5.1 Talus creep

If the release mass of creep processes to the fluvial system is to be computed, it is necessary to both determine creep velocity values and average sediment thicknesses affected by this movement (Dietrich and Dunne, 1978). Measurement of creep processes could have been accomplished by distance measurement of steel rods installed on the landforms (cf. Beylich, 2000). This process, however, was not considered important enough by Eichstätt working group to be specifically measured. As a result, we use measurements found in the literature for an estimation of correspondent sediment movement in the Upper Kauner Valley. Beylich (2000) finds a strong (r = 0.85) although not significant linear regression between talus cone slope (as sine) S and transport rate by creep R (m yr^{-1}) as reproduced in equation 5.7.5.

$$R = 32.88 \cdot \sin(\alpha) - 19.18 \tag{5.7.5}$$

This equation was applied to all talus cones and sheets mapped by the author in the study area to arrive at a spatial distribution of debris movement on these landforms by frost creep. Only non-vegetated talus cones as indicated on the prepared vegetation map (cf. 5.6.2) were used. Figure 5.7.11 shows a spatial example of the modeling results. When estimating the mass transfer by frost creep, the same assumption as in Beylich (2000) were made, i.e. a 20 cm debris layer being affected by frost creep. As density of the material a value of 2 g cm^{-3} was presumed, following Sass and Wollny (2001) and Krautblatter et al. (2012). Due to the generally broad valley bottoms, only very few locations exist in the study area where steep and unvegetated talus landforms border directly to the main fluvial system. These locations were found by intersecting creep rate grid with a one meter buffer of the main fluvial system (i.e. the current floodplain as mapped in the geomorphological, geotechnical map). All talus creep pixels located within this buffer were used to estimate the yearly supply of sediment to the main fluvial system based on the modeled creep rate and the estimated thickness of the moving debris layer.

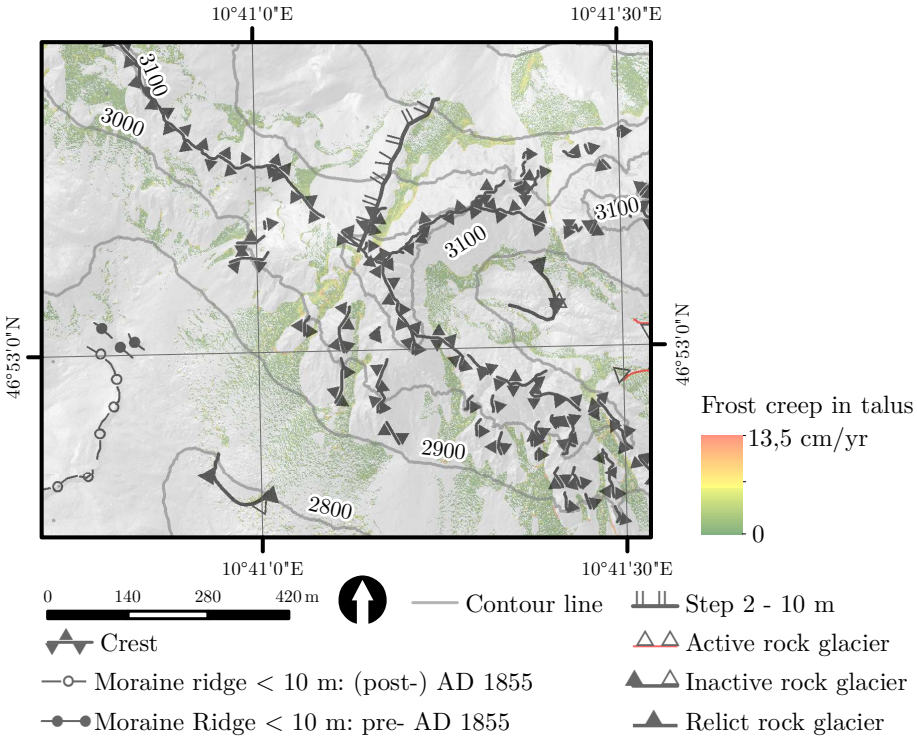

Figure 5.7.11: Creep rates after equation 5.7.5 in the Krummgampenspitzen area

5.7.1.5.2 Rock glaciers

For a quantification of the sediment transfer managed by rock glaciers in the study area, information on geometry and flow velocity of all active rock glaciers in the study area is necessary. In total, 76 locations that show signs of present or past creeping and a superficial aggregation of coarse debris have been mapped by the author. Some of these landforms, however, might represent push moraines, that is, transitional landforms between glacial moraines and rock glaciers (Dusik et al., 2015). 17 of these debris bodies show signs of recent movement and were therefore classified as active by sub-project one, 15 were classified as inactive and 27 as relict as they seem to be totally devoid of ice and presumably date back to the early Holocene (see Neugirg (2013) for definitions of the three activity classes). The remainder of 17 bodies have either not moved far enough to exhibit the characteristic tongue-shape morphology of rock glaciers or were not classified by sub-project one. It must be noted that the number of rock glaciers reported here is much larger than the number of rock glaciers listed in the rock glacier inventory of the Tyrolean Alps (Krainer and Ribis, 2012) for the study area. The main reason for this is that the mentioned work incorporates length and size thresholds in their definition. As the work presented here is more concerned with process areas, a length and width threshold was not used to constrain areas of permafrost creep of sediment bodies characterized by large grain sizes.

Horizontal displacement measurement and sediment transfer estimation

For an estimation of sediment transfer by rock glaciers, both sediment mass and displacement speed had to be determined. Measurements of vertical and horizontal displacements for 17 rock glaciers in the study area have been made by Neugirg (2013). Sediment mass was estimated based on rock glacier extent mapping, thickness estimation and sediment percentage estimates taken from the literature (Neugirg, 2013). Horizontal rock glacier displacement speed was estimated by both mapping of rock glacier front advance mapping on the multi-volume orthophotos and automated feature tracking on ALS-based DTMs of 2006 and 2012.

Mean annual displacement rates for the time from 2006 to 2012 were estimated using a SAGA GIS implementation of the image correlation IMCORR (image correlation) software (Scambos et al., 1992, Fahnestock et al., 1992). The feature tracking analysis was conducted using DTM-derived hill shade grids for each rock glacier (Kaufmann and Ladstädter, 2003, Gärtner-Roer, 2012).

Volume and mass estimation

To this date, no standardized methodology is available for a reliable estimation of rock glacier masses. Main reasons include the unknown topography at the base of the rock glacier and the unknown share of sediment in the rock glacier volume. Some information can be gathered by geophysical methods or by drilling. As these techniques are very expensive and time consuming, they could not be applied to determine the thickness of the 17 active rock glaciers in the study area and a transfer of results from one rock glacier to another is not possible. If they had been, a considerable amount of uncertainty would have remained in the sediment transfer estimation anyway, as often not all vertical sections of the rock glacier bodies are actually moving. In addition, it has been shown by Wagner (1992, cited by Neugirg 2013) that geophysical methods can easily yield wrong thickness estimates. As a result, rock glacier thicknesses were estimated as being identical to the height of rock glacier fronts. These were obtained by mapping based on orthophotos and an ALS-based DTM (Neugirg, 2013). Given the thickness estimation is reasonable, the sediment mass held by rock glaciers can be easily obtained by multiplying it with the rock glacier's base area.

As a result, rock glacier extent mapping (conducted by the author and (Neugirg, 2013)) included: i) A multi-temporal mapping of the fronts of the active rock glaciers, ii) A mapping of the base area of these rock glaciers. As the orthophotos did not cover the whole study area in all temporal volumes (cf. table 5.4.3), not all rock glaciers could be mapped on each of the the seven temporal volumes used. All rock glaciers could be mapped on the volumes of 1953 and 2010, however.

The calculated volume was then converted to masses assuming a sediment proportion of 40 % and a density of the sediment of $2.69\,\mathrm{t\,m^{-3}}$ (following Hausmann et al. (2012, cited in Neugirg 2013) and Gärtner-Roer (2012)). These masses were then combined with data on flow velocities to obtain sediment transfer rates of all 17 active rock glaciers in the study area.

Vertical changes
Vertical changes on rock glaciers were quantified by offsetting ALS-based data from 2006 and 2012. Significant DoDs were created using the stable area approach for σ_{simple} calculation.

5.7.2 Avalanches

A quantification of the sediment transport by avalanches in the Upper Kauner Valley was accomplished after Becht (1995b) and Heckmann (2006b), i.e. by mapping all sediment transporting avalanches in the field using different sediment cover classes, taking samples for these cover classes in the field, determining dry weight and using total areas of mapped avalanches to extrapolate transported masses for each mapped avalanche. Due to safety concerns, not all parts of the catchment could be mapped each spring. As a result, the amount of sediment transported by avalanches all over the study area was estimated via up-scaling. The outlines of field work and data processing steps are presented in the following.

5.7.2.1 Quantification

Field and laboratory work as well as mass calculations for the study area were completed in large parts by two master students supervised and instructed by myself and Jana-Marie Dusik (of sub-project one) in the years of 2014 and 2015. Their work constitutes a very important basis of what is presented here in summary. Their unpublished master theses (Näher, 2013, Rumohr, 2015) give more information on sediment transporting avalanche quantification and mapping in the Upper Kauner Valley and are referred to wherever appropriate.
Field work for avalanche sediment transport quantification was conducted during the snow melt period as this is the main time during the year when relevant avalanches occur (Gardner, 1983b). Wet snow slab avalanches could be watched early in May, while wet loose snow avalanches would trigger shortly later (see also Baggi and Schweizer (2009) and Näher (2013)).
Field work was largely completed during late May and early June in the years of 2013 and 2014. As the triggering for sediment transporting avalanches is mainly controlled by rising temperatures and, even more important, rainfall (Baggi and Schweizer, 2009, Conway et al., 2009, Eckerstorfer and Christiansen, 2012) and the study area stretches of over almost 2000 vertical meters, several on-site visits were necessary each year to map and sample avalanches at different elevations. In winter 2013/2014, for example, these monitoring visits stretched over a time period of five months. Field planning was made difficult by the fact that neither avalanche triggering time nor the spatial distribution of sediment transporting avalanches was dependent on aspect, a finding is partly in contrast to experiences reported in the literature (Jomelli and Bertran, 2001, Näher, 2013, Rumohr, 2015).
Mapping and sampling was undertaken as soon as all sediment was to be found on top of pure snow on avalanche accumulation bodies but before the avalanche accumulation bodies showed signs of significant lateral melting, which would cause material to slide off onto bare ground where it is indistinguishable from other sediment. It cannot be ruled out that some sediment had been lost to

quantification this way, but the resulting error should be is small. Hence, sediment could be collected from the top of the avalanches for mass quantification. The reason why avalanche sediment concentrates on top of pure snow on virtually all avalanches in late winter is not well explored (for more information on the morphology of STA deposits, see André (1990b), Bell et al. (1990), Jomelli and Bertran (2001), Freppaz et al. (2010, cited in Rumohr 2015)). One possible explanation is the theory by Heckmann (2006b), which attributes this circumstance to sediment transporting avalanches being deposited on top of snow accumulations of surface layer avalanches having been released earlier in winter. A second theory states that the mobilized sediment is deposited delayed in comparison to avalanche snow and therefore deposited on top (Becht, 1995b).

5.7.2.2 Mapping

Avalanches were either mapped onto laminated orthophotos in the field and later transferred into the GIS (2012/2013) or directly into the GIS from digital photos obtained in the field (2013/2014). Mapping was accomplished in a scale of about 1:2500. Following André (1990b), Jomelli and Bertran (2001), Sass et al. (2010) six sediment cover classes were chosen for sediment mapping on avalanche bodies. Except of a self-contained class representing bare snow free of any sediment cover (class zero), five equidistant classes representing a sediment cover of $0\% < x_{sc} \leq 20\%$ (class one) to $80\% < x_{sc} \leq 100\%$ (class five) were defined for mapping. After the outline of the total process area of an avalanche

Figure 5.7.12: Sediment cover classes one (far left) to five (far right) as used for avalanche sediment cover mapping.

had been mapped, homogenous areas in regard to these sediment cover classes were delineated. Figure 5.7.13 exemplifies a resulting map for two large sediment transporting avalanches recurring every year on the western moraine above the Fernergries and gives an impression on how mapping results looked like.

5.7.2.3 Sampling and laboratory work

As snow melt does not change the total mass but only concentrates the material on top of the snow body (cf. above and Jomelli and Bertran (2001)), it could simply be scratched from the avalanche surface. Thickness of the sediment layer varied from zero to up to 70 mm (Näher, 2013). Sampling areas were 0.25 m^2 most of the time (cf. areas delineated by metering rulers in figure 5.7.12). Sampling areas were placed randomly within the sediment covered part of an avalanche deposit by throwing the metering rule blindfolded from uphill onto the surface. All sediment found within a sampling area was collected and taken to the lab for drying and weighting. Boulders and cobbles (> 64 mm) were weighted in the field using a digital scale to reduce transport effort from sampling sites difficult to access. In total, 20 sampling sites were evaluated in

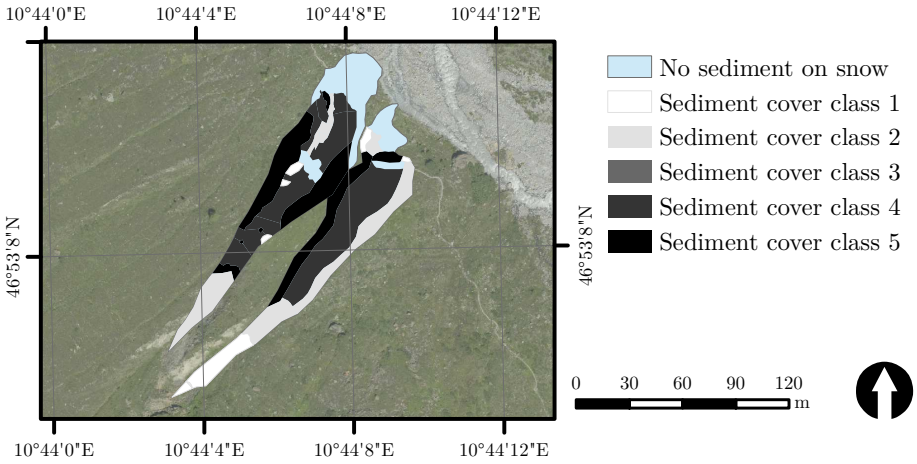

Figure 5.7.13: Sediment cover classes mapped on the two large Fernergries avalanches in spring 2014.

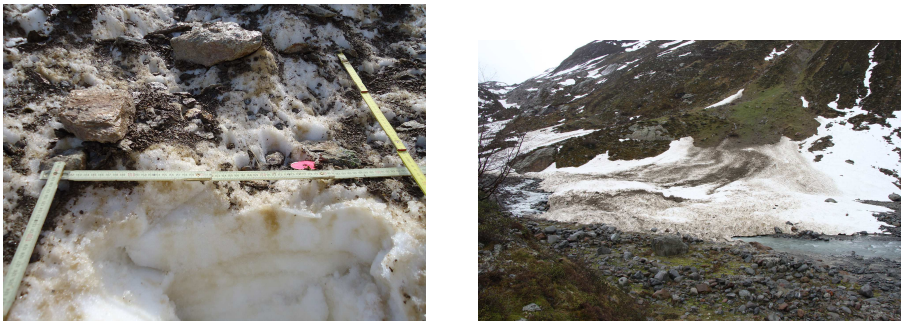

(a) (b)

Figure 5.7.14: (a) Sediment transported by an avalanche on top of melting snow in the accumulation zone (left), (b) The large avalanche mapped in figure 5.7.13. It is obvious that it has deposited sediment on the braidplain (right, see below).

Winter	**Number of avalanches sampled**	**Number of sampling plots**	**Number of STAs mapped**	**Percentage of study area mapped**
2012/2013	7	20	c. 60*	51.09
2013/2014	5	40	53	59.25

Table 5.7.5: Summary of avalanche mapping efforts from 2013 and 2014.
*Based on figure 42 in Näher (2013).

2013 and 40 sampling sites in 2014 (cf. table 5.7.5).
Samples collected in the field were taken into the laboratory and dried at 105 °C before the weight of the material on each sampling plot was calculated by adding the weights of the boulders and cobbles found on the respective plots to obtain

Sediment cover class	Average weight [kg m^{-2}]
One	0.065
Two	0.513
Three	3.232
Four	6.563
Five	32.076

Table 5.7.6: Average weight contained on one square meter of each sediment cover class in winter 2012/2013 (Näher, 2013).

the total mass for each sampling plot. These masses were then grossed up to obtain values for one square meter. Samples taken from the same sediment cover class were then averaged to obtain a mean sediment mass for each sediment cover class (table 5.7.6). During winter 2013/2014, the masses obtained from the additional 40 sampling sizes were added to the data base and masses were calculated from average values obtained from all 60 sampling plots. The average weight of the different classes in table 5.7.6 is circa $8.49\,\mathrm{kg\,m^{-1}}$. Although the values are not directly comparable, this value is of a similar magnitude as the $5.26\,\mathrm{kg\,m^{-2}}$ reported by Becht (1995b) as the average sediment weight on four STAs quantified in the Kesselbach Valley in spring 1992. Becht (1995b) has attributed the fact that a greater mass of sediment can be found on avalanches of the Pitz Valley (Central Alps) in comparison to the Kesselbach Valley (Northern Calcareous Alps) to the higher amount of unconsolidated glacial sediment present in this area. The same reason can be offered for the Upper Kauner Valley.

5.7.3 Fluvial hill slope sediment transport

5.7.3.1 Measurements

Fluvial hill slope erosion was to be quantified at positions in the small channels draining the hill slopes. Both material from the surrounding linear slopes and sediment eroded from the channel beds and sides is transported in these channels. They collect sediment and pass it on to the main channels. This often happens episodically during extreme rainfall events in summer (Becht, 1995b). This fact shows, that the coupling of hill slope channels and the main fluvial system is not permanent.
Measurement and extrapolation to the whole catchment (cf. 5.7.3.2) was accomplished based on the work flow presented by Becht (1995b) and Haas (2008), Haas et al. (2011b).[3]
Measurements had to be taken in different environments regarding degrees of vegetation cover in the hydrological catchment of a location in a channel, slope inclinations, material the channel is incised in, etc. This diversity was tried to achieve by combining multitemporal data from TLS measurements and subsequent modeling and data from sediment traps placed into the channels.

[3]Data evaluation was conducted by two MSc theses in sub-project one. Methodology and measurement results are therefore only summarized here. For more information on the measurement in the channels see Riehl (2015) and Messerschmidt (15.06.2016).

It was not possible to maintain fluvial sediment traps on the steep unvegetated LIA lateral moraines of the study area. Two sediment traps had been placed in these areas (cf. below). One of them had been destroyed by a debris flow shortly afterwards, while the other was over-filled with sediment on a regular basis (personal communication Jana-Marie Dusik, August 17th, 2016). This is why the TLS scans acquired of these hill slopes were used to quantify fluvial sediment transport at these locations. This strategy implies DoD calculation and a subsequent downslope accumulation of the determined elevation differences to an user-defined point in the channel. These channel points can therefore be regarded as "virtual" sediment traps (Neugirg et al., 2015, 2016a).
Such measurements and modeling efforts have been undertaken by Messerschmidt (15.06.2016), evaluating both ALS and TLS data. His work has revealed the same registration and georeferencing errors that had also been noticed by the author during the evaluation of the same TLS scans for debris flow quantification (cf. subsubsection 5.7.1.2.1). As the surface changes caused by fluvial hill slope erosion are typically even smaller than the ones caused by debris flows, Messerschmidt's elaborate efforts had to fail. Testing different grid cell sizes, he could show that, in general, the point density of both TLS and ALS scans was too low for a reliable measurement of fluvial sediment transport on 1855 lateral moraines in the study area. This rendered the data from "real" sediment traps even more important.
Maintaining such sediment traps with a high spatial and temporal resolution in a high-mountain area is a challenging task. As the number of sediment traps installed in the study area was rather small (cf. below), data collected in previous research by the Eichstätt working group from other alpine valleys was considered as additional input for an estimation of study area wide fluvial channel hill slope sediment transport. This data basis is reported in short in the following.
Data from six sediment traps which operated from 1990 to 1992 were available for this study from work by Becht (1995b). Further analysis and processing of the samples and data gained from these traps was in general the same as for the measurement results from the Upper Kauner Valley (see below).
Eleven sediment traps had been installed by sub-project one in August 2014 (first eight) and June 2015 (all others) in the Upper Kauner Valley. Large plastic tubs (with a volume of 90 l) were placed into small hill slope channels at selected places all over the study area (cf. figure 5.7.15) at elevations of circa 1961–2490 m h.a.e. These places were carefully chosen to represent the distribution of various geofactors in the study area. These included, most importantly, time since deglaciation, vegetation cover in the tubs' catchments and slope inclination. Hydrological catchments of the sediment traps varied from 1350 to 220 125 m^2 and covered an elevation zone between 1961 and 2718 m h.a.e. Other factors were accessibility and a relatively low expected discharge to prevent tub overflow by sediment.
Installation sites were chosen in a way that all flow from the hill slope channel traveled through the tubs. The inlets of the tubs were fixed locally with pond liners (Becht, 1995b). The reduction of flow velocity in the tubs leads to a trapping of most solid load. The effectiveness of these traps, i.e. the proportion of transported sediment trapped to all sediment transported through the tub is highly dependent on discharge (Bezinge et al., 1989). While it can be expected that virtually all of the bedload is trapped, it is probable that some of the suspended load is escaping during high discharge events. It is for this rea-

son why the values found should be treated as minimum values. This approach

(a) (b)

Figure 5.7.15: Sediment traps placed in channels draining the hill slopes.

to quantify hill slope channel sediment transport has been used successfully in many studies (e.g. Young, 1960, Becht, 1995b, Rey, 2003). The sediment traps were generally emptied about once in two to three weeks (oral communication Jana-Marie Dusik) during the snow-free times of the year from May to October (for more information on emptying intervals, problems occurred and the specific data on each trap for each emptying (at least for the time period from August 2014 to August 2015), see Riehl (2015)). During each visit, all sediment was removed from the traps and later weighed after drying in the laboratory.

5.7.3.2 Regionalization

A simple statistical model was used to extrapolate the measurements from the sediment traps to the whole catchment (Haas, 2008, Haas et al., 2011b). A simplified flow chart of the steps taken is depicted in figure 5.7.16. As the required input data had not been provided by sub-project one, results from Riehl (2015) are reported here. The weaknesses of this approach will be discussed and an alternative of determining the sediment transfer via fluvial hill slope erosion to the main fluvial system will be presented later on. In a first step, the slope area probably delivering material to each sediment trap, i.e. the sediment contributing area (SCA) was delineated using a rule-based model based on DTM analysis and mapping. It is evident, that not all surfaces within the hydrological contributing area of a given point also deliver sediment to that point. The fluvial SCA of a given point in the landscape has been defined as the sum of all locations within the hydrological catchment of that point that can (i) produce and maintain discharge and ii) are coupled to that point (Haas et al., 2011b). The methodology to delineate these locations is based on work by Heinimann et al. (1998) for a identification of areas inclining to the channel system and is implemented in a largely raster-based work flow as described in the following.
The hydrological contributing area was found using standard GIS techniques. A 5 m-DTM was derived directly from classified ALS point data from fall 2012. A 5 m spatial resolution was chosen for the grid for several reasons. First, the methodology has been developed for grids of that resolution (cf. Haas et al., 2011b). Second, several authors have advocated to use 5 m grids in raster-based

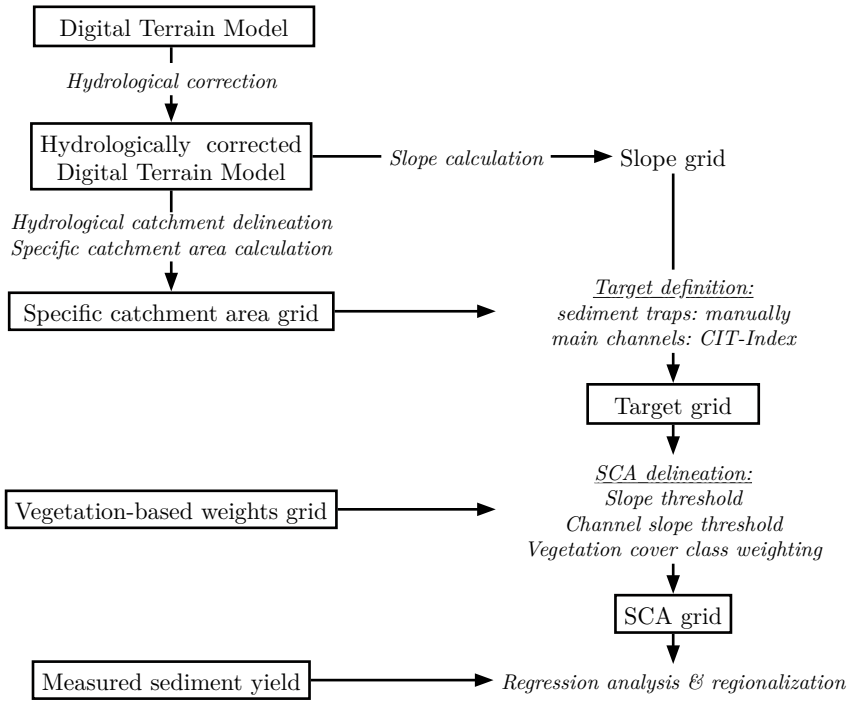

Figure 5.7.16: Schematic work flow for regionalization of fluvial hill slope channel sediment transport.

process modeling, arguing that they represent a compromise between not enough and too much topographic information (Kienzle, 2004, Wichmann and Becht, 2005, Heckmann and Schwanghart, 2013). The chosen resolution was also used for all products derived from the DTM to maintain data integrity as different raster cell sizes can have significant impact on calculated land surface parameters such as slope or the CIT-Index (cf. below). The same spatial resolution and DTM base were used to determine the SCAs for both each single sediment trap and the main channel system (e.g. Garbrecht and Martz, 1999, Wechsler, 2007). DTM gaps were closed and the hydrological contributing area, slope and specific catchment area grids were derived using a chain of standard algorithms (O'Callaghan and Mark, 1984, Zevenbergen and Thorne, 1987, Freeman, 1991, Cadell, 2002, Erskine et al., 2006, Wang and Liu, 2006).
Also the main channel network and the channel heads were derived using well known standard algorithms (Montgomery and Dietrich, 1989, Montgomery and Foufoula-Georgiou, 1993) as these have proven to provide reliable results, both in the Northern Calcareous (Haas, 2008, Haas et al., 2011b) and the Central Alps (Thiel, 2013). The approach used for channel head identification is based on the CIT-Index, calculated as

$$CIT = A_s \cdot \tan^2(\alpha) \tag{5.7.6}$$

where A_s is the specific catchment area of a raster cell and α the slope inclination. As this index combines both specific catchment area as a measure of

available water and inclination, it is a good index of potential erosional power. A cutoff threshold can then be used to localize cells probably pertaining to an active channel network.
A further narrowing of raster cells being part of the SCA is achieved using both lower thresholds for hill slope and channel inclination and an upper threshold for distance to hill slope channels. These are hard criteria deciding on whether a cell is included in the SCA or not. In addition, weights based on vegetation cover can be introduced as soft criteria determining the factor with which a certain cell is included. This has been proposed to account for the different erosion inhibiting influences of different vegetation within the hydrological contributing areas (Haas et al., 2011b, Riehl, 2015):
Only steep cells are thought to be laterally coupled to the hill slope channel. As a result, a threshold was applied to all cells within the hydrological catchment of the target cells, but not the cells representing targets themselves. The threshold value was determined by correlating the SCAs resulting from different thresholds for sediment traps with the measured annual sediment yield in g yr^{-1}. The threshold yielding the best correlation was then used (cf. Haas et al. (2011b)). A threshold for hill slope inclination of 32° was found to yield the strongest correlation between the resulting SCA and measured sediment yield, but was lowered to 25° based on expert knowledge (Riehl, 2015). This value is similar of what has been chosen by other authors using this model (Haas (2008), Haas et al. (2011b): 20°, Thiel (2013): 30°, Heckmann and Schwanghart (2013): 30-33°).
A lower threshold for channel slope inclination was applied to identify reaches of hill slope channels too shallow to allow sediment transport and therefore disconnecting, i.e. longitudinally decoupling the up-slope reaches. Methodologically, it was identified analogously to the hill slope inclination threshold. Results have shown that this parameter has only a low impact on resulting SCA sizes. Consequently, coefficients of determination for the correlation between SCA and measured sediment yield varied only slightly. These results comply with the findings in other studies (Heckmann and Schwanghart, 2013, Riehl, 2015). Eventually, a threshold of 3.5° was chosen for longitudinal hill slope channel coupling in this study. Also this value is comparable to what has been used in other studies (Haas (2008), Haas et al. (2011b): 3.5°, Church (2010): 4°, Thiel (2013): 3.8°, Heckmann and Schwanghart (2013): 2°) (Riehl, 2015).
In former studies (Haas, 2008, Haas et al., 2011b), an upper distance to channel threshold was used to identify non-channel cells probably contributing to a hill slope channel. More recent work has shown, however, that this parameter has no influence on the modeled SCA (Heckmann, oral communication). Therefore, it was not accounted for (Riehl, 2015).
As fluvial sediment transport on hill slope is highly dependent on the vegetation present (Rey, 2003), it was taken into account by weighting each non-bedrock and non-glacier cell in the SCA according to the vegetation class identified on the vegetation cover map in analogy to Haas (2008), Haas et al. (2011a), Riehl (2015). The values of weights used in these studies, however, lack scientific justification and were determined subjectively without any measurement basis or controlled procedure (Heckmann, oral communication). As a result, weights could be chosen similarly to model parameters just to enhance the model fit. As this is unsatisfactory and as the selection of (arbitrarily determined) weights has a great impact on the overall result, vegetation should not have been used

as a variable in Riehl (2015). However, weights were used and as no other data on fluvial hill slope channel erosion in the Upper Kauner Valley accounting for the spatial heterogeneity of the process in the study area is available weights used in this and different studies are summarized in table 5.7.7.

Vegetation cover class	**Assigned weight**	**Source**
Not mapped	0.5	Riehl (2015)
Glacier	0.1	Thiel (2013), Riehl (2015)
Bedrock	0	Riehl (2015)
Unvegetated	1.0	Haas (2008), Riehl (2015)
Patchy alpine grassland/ pioneer vegetation	0.9	N/A*
Alpine grassland	0.2	Haas (2008), Riehl (2015)
Bushes/Krummholz	0.2	Haas (2008), Riehl (2015)
Trees	0.2	Haas (2008), Riehl (2015)

Table 5.7.7: Weights assigned to different vegetation cover classes for SCA modeling.
*The value used by Riehl (2015) is not reported in his thesis.

A regression model (power law, i.e. simple linear regression in log-log space[4]) between SCA and measured sediment transport was established. As not enough measurements were available from the Kauner Valley, measurements from the Horlach Valley obtained over a period of three years by Becht (1995b) were used as supplementary data for model parametrization. Although this data stems from a different valley, this procedure is justified by five reasons: i) Only a few sediment traps are available in the relatively large study area and a separation of the data into training and validation subsets is unacceptable, ii) Sediment trap data from the Upper Kauner Valley is only available for a short time period (August 2014 to August 2015); The model, however, implies the usage of mean yearly sediment yield data. The short measurement period is therefore problematic as data representing one year only is unlikely to conform to the long term mean (cf. Becht, 1995b); iii) Haas et al. (2011b) have shown that the model can be transferred to different catchments as long as its characteristics are similar to the one it has been parametrized in. The Horlach Valley shows in general widely similar characteristics to the Upper Kauner Valley when it comes to climate, elevation, glacial history, vegetation and geology (cf. Becht, 1995b, Thiel, 2013, Riehl, 2015) and iv) first exploratory work by Huber seems to indicate that the model form does not change over a wide range of spatial scales (personal communication Heckmann and Huber, May 2016) and it is assumed that data from different sized (sub-)catchments can be mixed. v) The measurement data from the Upper Kauner Valley could be used as validation data for the model parametrized in the Horlach Valley. This parametrized model was later be used to estimate yearly sediment yield from the catchments of each cell in the DTM of the whole study area by establishing the SCAs of all hillslope channels reaching the main fluvial system (at the locations of confluence) and calculating a corresponding sediment transport rate. Pertaining results are re-

[4]As has been discussed and performed in subsubsection 5.7.1.2.1, this would require a bias-correction. This correction, however, has not been completed by Riehl (2015), weakening the validity of his results.

ported in section 6.4.2.
As it was clear from the beginning that the usage of data from another valley for a parametrization of the SCA model for the study area was a suboptimal solution of estimating the fluvial hill slope contribution to the main channels, a second, very different approach was followed that involved an ALS-based budgeting of the areas thought to be the hot spots of delivery (see below). Both approaches have advantages and disadvantages. As a consequence, two estimates for fluvial hill slope contribution to the main channels were obtained.

Fluvial hill slope sediment delivery estimation via ALS differencing
As no sufficient sediment transport/SCA data have been provided by sub-project one, the fluvial hillslope SCA modeling had to be based on data from the Horlach Valley and Riehl's approach was sub-optimal, a second strategy was adopted to get an estimate for the amount of sediment that is delivered by of fluvial hill slope transport to the main fluvial system: ALS data from two time steps as far apart as possible of the true right lateral moraine of Gepatsch Glacier were set off against each other to determine a total balance irrespective of the acting processes. This balance was then combined with the results concerning the mass transferred to the main fluvial system by debris flows at this location (see table 6.1.4) to obtain an estimate of the non-debris flow sediment mass delivered to the Fagge river in this time period.
The ALS data used dates from July 4, 2012 and July 18, 2014 (representing the longest period of observation for which classified LiDAR data of high density in the channel heads was available). The grid size chosen was 0.7 m, the lowest one possible without causing data gaps and enabling the usage of a spatially distributed overall LoD (which had a mean of circa 0.08 m). Results are reported in section 6.4.3.

6 Results and discussion: Sediment production and transport by geomorphic processes

After having introduced the various methodological strategies to obtain estimates of sediment transfer of all relevant geomorphic processes, the results of these efforts will be presented in the following.

6.1 Mass wasting processes

6.1.1 Rock fall

6.1.1.1 Debris fall

6.1.1.1.1 Measurements

Debris fall rates estimated from collector measurements
During data analysis, it became clear that only the data from eight rock fall collectors could be used for a regionalization of the debris fall rates. The data from the other measurement locations were not used for varying reasons: The debris fall rate calculated from data of collector three (a real net), were extraordinarily high. There are three reasons for this and why it was excluded from further analysis: First of all, the net is located below a very active gulch in the rock wall, not representative of a production rate but of the channeling of debris. Second, and most importantly, a debris flow had buried the net almost completely in late summer of 2012 and it was not possible to excavate the net afterwards. Since then, debris fall particles have been collected directly from the debris fall deposition surface (Lucas Vehling, oral communication) and it cannot be excluded that only particles having been deposited by debris fall since the debris flow occurrence have been included in the total mass provided by sub-project two. Third, the SCA identified for net three is very small: Only two (scenario S-I-H and S-I-E) or six (S-I-G) DTM cells were delineated.
rock fall collectors seven to twelve were no installed nets, but surfaces of fluvial sediments located below steep but only a few meters high rock walls of a small gorge directly downstream the Gepatsch Glacier snout. Due to the spatial extent of the rock walls at debris fall collectors seven to nine being smaller than the spatial resolution of the DTM, it was not possible to delineate SCAs for

these locations. In addition, nets ten to twelve were also located nearby and the inclusion of nets seven to nine would have led to an overrepresentation of rates typical for this specific locality in the final budget. Also rock fall collector location twelve (a natural surface) was located within this former channel bed of the Fagge river within the proglacial area. It was possible to delineate SCAs for these surfaces. These, however, were very small, and in case of scenario S-I-G, definitely too small. The small graph-based SCA resulted in outrageous erosion and production rates, which is why this measurement location was excluded from further analysis in strategy S-I-G.

The calculated rock slope erosion rates (cf. table 6.1.1) vary between 0.003 and 4.5 $\mathrm{mm\,yr^{-1}}$ over all three scenarios with most values ranging from 0.003 to 1.2 $\mathrm{mm\,yr^{-1}}$. In general, with the exceptions of a few scenarios in collectors ten to twelve (cf. discussion below), they are consistent with rates reported from other alpine regions although most of them have been made in areas of different geology, glacial history and climate (please see the table in appendix four for a list of umpteen comparative values in [$\mathrm{kg\ m^{-2}\ yr^{-1}}$] as they cannot all be discussed here.). Also using rock fall collector traps, Sass (2005a,b), for example, has calculated values 0.03 to 0.7 $\mathrm{mm\,yr^{-1}}$ in a limestone region, while Södermann (1980) reports 0.07–0.18 $\mathrm{mm\,yr^{-1}}$ from northern Finland. Krautblatter et al. (2012) reported 0.29 $\mathrm{mm\,yr^{-1}}$ for the Rein Valley using a very much different strategy for SCA calculation.

Generally, it is not straightforward to compare the values given in this study with values in other studies, as the methodology used to delineate the SCA is often not reported (a fact also Vehling (2016) complains about) in sufficient detail and/or different slope thresholds for start area identification are used. Also Becht (1995b) has stated that reported rock wall retreat rates are fluctuating over several orders magnitudes and Vehling (2016) reports that the rates calculated from his SCA calculations and rock fall collector data ranges over four orders of magnitude.

Nevertheless, it is conspicuous that the values calculated from rock fall collectors ten to twelve are in general higher than the ones measured at the remaining ones, with the values from scenario S-I-E and S-I-G being especially high. These values are much higher than the ones reported in many studies, although Francou (1988, cited in Coultard and Francou 1989) also reports a rock wall retreat rate of 3 $\mathrm{mm\,yr^{-1}}$ after seven years of measurement for the leucocrate granite north face of Roc du Noir du Combeynot, France.

Possible reasons include the following. First, most rock fall erosion rates reported in the literature are not specifically measured within a proglacial area. Recent relief from additional load by glacier ice and proximity to the glacier tongue after deglaciation can lead to increased rock fall rates resulting from heightened rates of frost shattering and the formation of clefts. All three measurement locations with increased rates are located within the proglacial area and only two hundred meters downstream the glacier tongue. Second, however, rock fall collector two is located even closer to the glacier tongue and displays much lower rates. As the gorge in which these rock fall collector surfaces are located was flown through by the Fagge river before August 2012, it is possible that the rock walls are shattered by bedload transport and freeze-thaw processes of spray from the river within the gorge. The third possible explanation for increased rates in rock fall collector nets ten to twelve is of methodological nature. It has already been mentioned that a DTM-based delineation of

SCAs of the collection surfaces is difficult within the gorge due to the small spatial extent of the rock walls in all directions. It is possible, that the SCAs are being underestimated in such cases. Vehling (2016), who used a different methodology for SCA derivation at these nets, also comes up with similarly high rates and gives a variety of plausible geotechnical reasons for these high values. Looking at only the data used for further analysis, the variability of the

rock fall collector		**S-I-H**	**S-I-E**	**S-I-G**	**nr days**
1 (rn)	SCA [m^2]	869.73	555.87	922.57	1068
	DPR [kg m^{-2} yr^{-1}]	0.68	1.06	0.63	
	ER [mm yr^{-1}]	0.25	0.39	0.24	
2 (rn)	SCA [m^2]	549.57	423.41	701.96	1068
	DPR [kg m^{-2} yr^{-1}]	1.62	2.10	1.26	
	ER [mm yr^{-1}]	0.60	0.78	0.47	
4 (rn)	SCA [m^2]	2348.6	5779.8	5401.51	707
	DPR [kg m^{-2} yr^{-1}]	0.06	0.03	0.03	
	ER [mm yr^{-1}]	0.02	0.01	0.01	
5 (rn)	SCA [m^2]	427.28	427.28	1763.98	1079
	DPR [kg m^{-2} yr^{-1}]	0.09	0.09	0.02	
	ER [mm yr^{-1}]	0.03	0.03	0.01	
6 (rn)	SCA [m^2]	536.87	630.97	1186.85	1051
	DPR [kg m^{-2} yr^{-1}]	0.02	0.02	0.01	
	ER [mm yr^{-1}]	0.01	0.01	0.003	
10 (nn)	SCA [m^2]	160.58	38.44	65.17	353
	DPR [kg m^{-2} yr^{-1}]	2.91	12.15	7.17	
	ER [mm yr^{-1}]	1.08	4.50	2.66	
11 (nn)	SCA [m^2]	1942.92	960.64	642.45	353
	DPR [kg m^{-2} yr^{-1}]	1.17	2.36	3.52	
	ER [mm yr^{-1}]	0.43	0.87	1.30	
12 (nn)	SCA [m^2]	631.36	366.94	(74.45)	353
	DPR [kg m^{-2} yr^{-1}]	1.82	3.14	not used	
	ER [mm yr^{-1}]	0.68	1.16	(5.73)	

Table 6.1.1: Overview of debris fall collector sediment contributing areas (SCA), calculated debris fall production rates (DPR) and calculated erosion rates (ER) as resulting from three different methods to delineate SCA. "rn" indicates a real net , "nn" represents natural surfaces used as a baseline for debris fall particle collection as used by sub-project two. All values are rounded to the second decimal place.

measurement/calculation results for an individual collector is relatively high for some of the collectors. This variability between the SCA derivation scenarios is highest with net ten, where the lowest calculated erosion rate represents 24 % of the highest one. These observations underline the sensitivity of debris fall rates to the method used to determine the rock wall area contributing to the net and the statement made above that rates from different studies are only comparable to a limited degree. The contributing areas determined using strategy S-I-G are in general smaller than the ones derived using the other two SCA delineation

techniques. Naturally, this also leads to lower calculated erosion and debris fall production rates. This fact is certainly due to the model's capability to simulate both abrupt trajectory changes and the crossing of small watersheds (as typical for rock fall particles) (cf. Wichmann, 2006, Frattini et al., 2008). As a result, a higher number of DTM cells is identified as contributing to the rock fall collector (see also figure 5.7.4).
The fact, that the data from rock fall collectors ten to twelve do not follow this rule can be explained by the extremely short horizontal distance and steep angle between debris fall source and deposition areas: The particles simulated by the model travel only over a very small number of DTM cells. As a result, a high total lateral dispersion of particles is not simulated and only a few potential SCA cells are available before the SCA cells are identified using graph-based tools. In combination with the high masses measured at these locations (as discussed above), this results in the very high rates. Also net four represents an exception from the rule that rates calculated from S-I-G are lower than the ones calculated using the other strategies. Rounded to the second significant digit, rates for S-I-E and S-I-G are identical. This can be explained by the fact that the number of cells identified as potential SCA by the expert is very high (Heckmann et al., 2016): The bedrock at this location is petrographically heterogeneous: coarse grained orthogneiss can be found in the lower section of the rock wall, while orthogneiss is predominant in the higher one. Both sections are separated by a talus sheet located within the rock wall (cf. figure 5.7.4, between 2500 and 2550 m h.a.e.). Since also orthogneiss particles were found within the net, the expert has included the upper section in his delineation, while it was not identified using the flow algorithm (which is certainly the least suitable method for debris fall trajectory modeling anyway). In strategy S-I-G, the debris fall model and graph-based methods, however, are successful in identifying the source locations in the upper orthogneiss zone.
The quality and the temporal distribution of debris fall during the year suggest that most of the material found in the rock fall collectors represents primary debris fall and not sediment mobilized from rock ledges within the rock walls during intense thunderstorms (cf. Krautblatter and Moser, 2009). It is therefore questionable of this finding is representative of a long-term average (that is a time period including such thunderstorm events). If not, the resulting rates should be regarded as minimum rates.

Debris fall rates estimated from TLS measurements
Data from eight TLS monitoring stations was evaluated. Table 6.1.2 shows the results.

TLS scan position	period start	period end	nr days	mm yr^{-1}
08	2011-09-25	2012-07-16	295	0
08	2012-07-16	2012-08-25	40	0.39
08	2012-08-25	2013-07-01	310	0.58
08	2013-07-01	2013-09-04	65	0
08	2013-09-04	2014-07-17	316	0

Continued on next page

Table 6.1.2 – continued from previous page

TLS scan position	period start	period end	nr days	mm yr^{-1}
08	2014-07-17	2014-09-25	70	0
08	2014-09-25	2015-07-11	289	0
08	**2011-09-25**	**2015-07-11**	**1385**	**0.65**
Real surface area of reference bedrock surface: 8565.61 m^2 rock fall production rate from first to last time slice: 1.78 kg m^{-2} yr^{-1}				
09	2011-09-25	2012-08-24	334	0.21
09	2012-08-24	2013-07-02	312	1.18
09	2013-07-02	2014-07-17	380	2.09
09	2014-07-17	2014-09-23	68	63.89
09	2014-09-23	2015-07-29	309	0.01
09	2015-07-29	2015-09-22	55	1.34
09	**2011-09-25**	**2015-09-22**	**1458**	**1.26**
Real surface area of reference bedrock surface: 4271.47 m^2 rock fall production rate from first to last time slice: 3.41 kg m^{-2} yr^{-1}				
10	2011-09-25	2012-08-23	333	0.08
10	2012-08-23	2013-07-01	312	0.48
10	2013-07-01	2013-09-04	65	2.58
10	2013-09-04	2013-05-28	-99	0.23
10	2013-05-28	2014-07-08	406	0.09
10	2014-07-08	2014-09-23	77	0.36
10	2014-09-23	2015-07-29	309	0.09
10	**2011-09-25**	**2015-07-29**	**1403**	**0.03**
Real surface area of reference bedrock surface: 72 258.63 m^2 rock fall production rate from first to last time slice: 0.09 kg m^{-2} yr^{-1}				
11	2011-07-14	2012-08-27	410	0.02
11	2012-08-27	2013-09-06	375	0.10
11	2013-09-06	2014-07-19	316	0.02
11	2014-07-19	2014-09-25	68	1.84
11	2014-09-25	2015-07-11	289	0.003
11	**2011-07-14**	**2015-07-11**	**1458**	**0.006**
Real surface area of reference bedrock surface: 409 242.5 m^2 rock fall production rate from first to last time slice: 0.016 kg m^{-2} yr^{-1}				
15	2012-08-21	2013-07-03	316	0.57
15	2013-07-03	2014-07-18	380	0.43
15	2014-07-18	2014-10-21	95	48.5
15	2014-10-21	2015-07-30	282	0.66
15	**2012-08-21**	**2015-07-30**	**1073**	**0.52**
Real surface area of reference bedrock surface: 4526.87 m^2 rock fall production rate from first to last time slice: 1.4 kg m^{-2} yr^{-1}				

Continued on next page

Table 6.1.2 – continued from previous page

TLS scan position	period start	period end	nr days	mm yr^{-1}
19	2012-08-22	2013-09-05	379	0.49
19	2013-09-05	2014-09-24	384	4.65
19	2014-09-24	2015-07-28	307	0.006
19	**2012-08-22**	**2015-07-28**	**1070**	**2.03**
Real surface area of reference bedrock surface: 30 269.18 m^2 rock fall production rate from first to last time slice: 5.49 kg m^{-2} yr^{-1}				
20	**2014-09-24**	**2015-07-28**	**307**	**2.5**
Real surface area of reference bedrock surface: 16 234.61 m^2 rock fall production rate from first to last time slice: 6.77 kg m^{-2} yr^{-1}				
21	2012-08-22	2013-09-05	379	3.12
21	2013-09-05	2014-09-24	384	0.64
21	2014-09-24	2015-07-28	307	0.34
21	**2012-08-22**	**2015-07-28**	**1070**	**4.45**
Real surface area of reference bedrock surface: 98 343.38 m^2 rock fall production rate from first to last time slice: 12.03 kg m^{-2} yr^{-1}				

Table 6.1.2: Rock wall retreat rates calculated from the TS-based DoDs provided by sub-project one.

Table 6.1.2 shows discrepancies between short-term and long-term rates obtained via corresponding TLS measurements. This is a well know problem and shows the weakness of TLS for measurement of debris fall on such spatial scales (cf. below). As a result, only the values obtained by evaluating the longest possible time period was used as accumulated change (over time) is easier detectable via TLS (personal communication Florian Haas, July 2016). The obtained values are in the same range as the ones published by other authors using different methodology (see appendix four and Vehling (2016, p. 39)) and the ones obtained using rock fall collector nets.

Rates obtained from rock fall collectors vs.rates from TLS
Three of the rock walls TLS scanning positions (11, 15 and 29) were located at rock walls that had also been monitored via rock fall collector nets. Scan position 11 surveyed a large rock wall below which two rock fall nets (nr. four and seven, (Vehling, 2016)) were located. The rate of 0.006 mm yr^{-1} obtained via TLS is much lower than the rates obtained by Vehling at the two nets (0.0154 and 0.0133 mm yr^1). At scan position 29, a rate of 0.036 mm yr^{-1} was measured via rock fall collector, while TLS yielded a value of 0.52 mm yr^{-1}. Possible reasons for these discrepancies (exemplified here for scan position 29) are manifold: First, net and TLS monitoring times are not congruent. TLS scans were never obtained on days on which rock fall collector nets were emptied. Second, TLS scan positions had not been set up specifically for a comparison of TLS and rock

fall collector measurements, but to monitor a comparatively large rock wall sections (to enlarge the data basis). The rates obtained via TLS measurements could therefore also represent larger events having occurred outside of the rock fall collector SCA or incorporate rock wall sections that are less active. This is, by the way, is the main reason why rates obtained via TLS showing discrepancies to measurements at the rock fall collector nets should not be dismissed from the evaluation (personal communication Florian Haas, August 2016). Third, it is also worth mentioning that no rock fall collector nets had been installed by Vehling below very active rock walls as it was feared that they would be destroyed (Vehling, 2016). The TLS measurements cover rock wall sections of all activity states, a fact that might explain some of the higher values obtained via TLS measurements (in comparison to all rock fall collector net measurements in general). These measurements are also important to render the data base more representative of the rock fall processes in the whole catchment and are another reason why TLS measurements were used for distribution fitting. Fourth, a direct comparison of rock fall rates obtained by rock fall collectors and via TLS is only valid if the geological, geotechnical and geometrical properties of the larger rock wall section scanned via TLS is the same as the SCA of the respective net. This is never the case. Fifth, another, less relevant problem is constituted by the fact that mass determinations by Vehling were accomplished after rounded material (i.e. moraine material deposited on ledges of the rock wall) had been sorted out. This cannot be done using indirect measurements via TLS and was also not desirable as secondary rock fall is also of interest (cf. above). A sixth reason possibly explaining discrepancies between TLS and rock fall collector measurements relates to the particles sizes measured on the nets: Given that most rock fall particles (50 % on average, based on Fig. 134 in Vehling (2016)) collected in nets are of sizes smaller than 10 cm, it is evident that a detection using TLS measurements allowing a maximal spatial DTM resolution of 50 cm is difficult.

Nevertheless, rates obtained by Vehling at rock fall collector net one were directly compared by the author to rates obtained via TLS at the same site (scan positions 29 and 29b). To accomplish this, and to eliminate the second possible reason for rate discrepancies above, the DTM of the rock wall was clipped to the rock fall collector net SCA as determined and used by Vehling. Results still showed significant discrepancies (with the TLS rates being much larger than the ones obtained via rock fall collectors), the reasons of which (in addition to possible ones already discussed) were identified as the strike and dip of the rock wall foliation: It strikes perpendicular to the general laser beam direction and dips away from the rock wall surface. This causes a large number of artifacts in the resulting DTMs, rendering the TLS measurements not very suitable for rock fall quantification at this location. Another problem is caused by the fact that the rock walls monitored via TLS are seldomly steeper than 60° (Vehling, 2016), causing the laser beam incidence angle being rather flat, which causes uncertainties in point measurements.

The author believes that there can be no better ground truth than direct measurement of particles actually collected in a net if the net extends far enough from the rock wall. TLS measurements of rock fall are indirect measurements incorporating only a representation of the rock wall, the calculation of an overall LoD and moving window filtering of the resulting significant DoD. All these processing steps are a potential source of error. These errors can be controlled

if very small distances between the TLS device and the rock wall is chosen, resulting in only very small rock wall sections being monitored. This in turn, results in rates being not very representative for the whole rock wall. This opinion is shared by most authors quantifying rock fall of magnitudes $< 10\,m^3$ (e.g. Krautblatter et al., 2012, Vehling, 2016) and is also the main reason why measurements via TLS have quantified rock fall of larger magnitudes (e.g. Abellán et al., 2006, 2010, Haas et al., 2012b). However, it is also possible that the rates obtained via rock fall collector nets are underestimating the real debris fall production when particles falling on snow travel over the extent during the winter or early spring.

6.1.1.1.2 Regionalization

Total mass mobilized - Strategy one

In using strategy one, the total catchment wide sediment mobilization by debris fall [t yr^{-1}] can be calculated using the susceptibility model, the true surface areas of the identified source cells and the fitted probability density function (Figure 5.7.7). Dependent on the scenario used, a total mass of circa 20 034 t yr^{-1} (S-I-H, circa 323 t km^{-2} yr^{-1}), circa 27 562 t yr^{-1} (S-I-E, circa 445 t km^{-2} yr^{-1}) and circa 25 803 t yr^{-1} (S-I-G, circa 416 t km^{-2} yr^{-1}) is estimated.[1]. Using the modeled trajectories of the rock fall particles and the recorded elevations of the starting and deposition grid cells, the total geomorphic work accomplished by debris fall in the study area was estimated at c. 829 W (S-I-H; 13.37 W km^{-2}), 1141 W (S-I-E; 18.41 W km^{-2}) and 1069 W (S-I-G; 17.24 W km^{-2}), which corresponds to a transformed energy of circa 26.2 GJ yr^{-1}, 37.7 GJ yr^{-1} and 36 GJ yr^{-1}.

Total mass mobilized - Strategy two

Using strategy two, a rate of 28 738 t yr^{-1} (circa 463 t yr^{-1} km^{-2}) was estimated. The geomorphic work performed is estimated at circa 1565 W (circa 25.3 W km^{-2};the energy transformed is 49.4 GJ yr^{-1}). The difference of Watts performed to what has been estimated using strategy one is easily explained by the fact that many rather high and steep rock walls in the study area (e.g. the west facing rock walls between Großer Nörderberg and Nörderschartl) had been assigned a low rock mass stability index by Vehling (2016), which resulted in higher masses negotiating high relief.

Vehling (2016) uses two different calculation scenarios (one using the same classes as in strategy two, one using the nonlinear regression function between rock mass stability index and debris fall production rates) to obtain values for the total mass of sediment transfer rate by debris fall in the study area. His first scenario gives an estimate of circa 36 400 t yr^{-1}, while the second one yields an estimate of about 46 934 t yr^{-1}. It is evident that Vehling's estimates are generally much higher than the ones obtained in this study. The reason for this is that Vehling uses a slope threshold of 40°, while a threshold of 47.57° has been used by the author. Sensitivity analysis (see below) indicates that a similar total mass as estimated by Vehling would have been resulted using strategy one/G if the same threshold as used by Vehling had been adopted for this study.

Studies having estimated the mass of sediment mobilized by debris fall on the catchment scale are rare, especially in areas that are comparable to the study

[1] The values in [t km^{-2} yr^{-1}] refer to the planimetric study area of 62 km^2

area in terms of glacial history, geology and geotechnical variables. Actually, this holds true for all processes. In addition, comparisons are hampered by different methods of regionalization, SCA delineation, etc. (see above). Krautblatter et al. (2012) have estimated a total mass of mobilized sediment by debris fall of 180.2 ± 81.65 t km^{-2} yr^{-1} (calculated from values given in [t day^{-1}] in the paper) for the Rein Valley in the Northern Calcareous Alps (circa 17.3 km^2). The power performed by debris fall of 83 W km^2 given in Krautblatter et al. (2012) is about three times of the highest one for the Upper Kauner Valley in this thesis. This reflects the comparatively high concentration of very high and steep rock walls in the Rein Valley. On the scale of a cirque (study area circa 1.64 km^2), Sanders et al. (2013) estimated the mass of sediment mobilized by debris fall at circa 1000 t km^{-2} yr^{-1} (circa 152.4–4847.5 t km^{-2} yr^{-1}).
Also, few studies have quantified the sediment flux from surrounding areas to a glacier, thereby enabling a comparison of non-glacial sediment input to the glacial system from outside to the export of sediment from the glacier. O'Farrell et al. (2009) report that the sediment input to the glacier studied by them accounts for about 50 % of the flux in the proglacial stream. No value is given for rock fall alone and they estimate rock fall erosion using only eight cosmogenic nuclide sampling points for a 600 km^2 catchment, which is hardly comparable to the methodology used in the PROSA project. A estimating of debris fall delivery to the glaciers of the Upper Kauner Valley will be presented below.

Sensitivity analysis - strategy one
The sensitivity of the total sediment mass mobilized to the slope threshold used to narrow down the amount of source cells and the stochastic nature of drawing from the Weibull distribution was investigated by a 100fold repetition of sampling from the distribution, using thresholds between 42° and 52° for an identification of source areas (figure 6.1.1). Depending on the slope threshold, between 119186 (52°) and 251117 (42°) bedrock cells (i.e. 2.98 km^2 and 6.28 km^2 or 4.8 % and 10.13 % of the planimetric study area) are identified as start cells. The resulting total mass of mobilized sediment varies between circa 18 863 t yr^{-1} (52°) and circa 34 913 t yr^{-1} (42°, both scenario G). The dependency of both the size of the rock fall source area and the total mass of mobilized sediment on the slope threshold is linear with a decrease of circa 0.49 km^2 and 1626 t yr^{-1} per degree of increasing slope threshold. The variability stemming from the sampling of the Weibull probability distribution function is comparatively small: For scenario G and the slope threshold of 47.57°, the values range between circa 25790 and 26 370 t yr^{-1}. The difference of 580 t yr^{-1} represents about 2.2 % of the total budget.
In addition, the effect of DTM spatial resolution on the overall mass of mobilized sediment was investigated. This was accomplished by comparing the total mass resulting from using source cells on the 5 m DTM (as used in this study) to the mass resulting from using the 1 m cells corresponding to these 5 m cells. An aggregation of the 1 m cells to a 5 m resolution using the majority scheme can lead to two effects: First, an underestimation of the rock fall source area is possible, as a 1 m grid can represent higher slope inclinations than one with a 5 m spatial resolution (Wilson and Gallant, 2000). Second, an over- or underestimation can occur when the amount of 1 m cells steeper or flatter than the slope threshold within a 5 m cell is close to 50 %. Tests have shown that the overall amount of mobilized sediment derived from the 5 m DTM is only 75 %

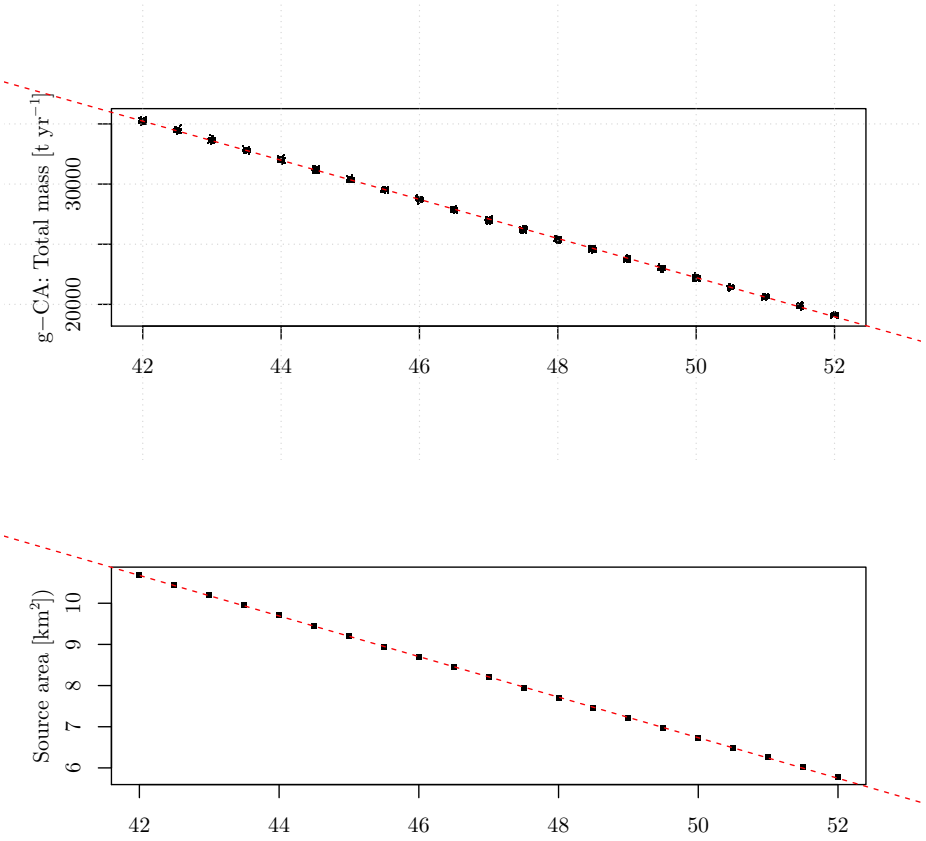

Figure 6.1.1: Results of the sensitivity analysis of the area declared as rock fall source (top) and rock fall production [t yr^{-1}] rate on the catchment scale (bottom) using scenario G of strategy one.

of the total mass obtained using the 1 m DTM.
It can be stated, that the total mass is most sensitive to the choice of the slope threshold. Lan et al. (2010), for example have found that 50 % of rock fall occur on slopes with an inclination below 40° and that 16 % of all rock fall activity is located on rock slopes with inclination below 30°. It is evident that loose particles cannot stay in place on slopes steeper than 40° as the slope inclination of un-vegetated talus landforms usually does not exceed 36° (e.g. Gardner, 1983a).

Magnitude and spatial distribution of deposition
Figure 6.1.2 shows both the spatial distributions of erosion from each cell/node per year (which was calculated using graph-theory based methods as the out-strength of each cell/graph node) and the deposition on each cell/node per year (which was calculated analogously as the in-strength of each cell/graph node). The spatial distribution of erosion is controlled by the spatial distribution of bedrock cells steeper than the slope threshold and their real surface area. The spatial distribution of deposition rates range from 0.00047 to 11.06 mm yr^{-1}

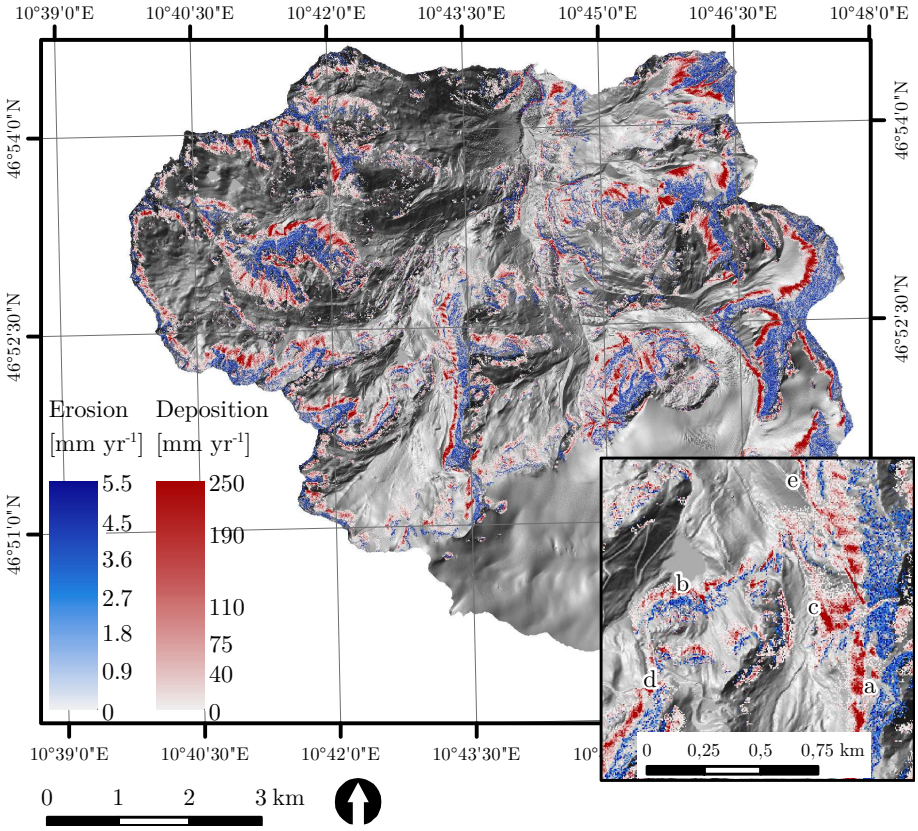

Figure 6.1.2: Raster maps of debris fall erosion and deposition (both in [mm yr^{-1}], assuming a bulk density of the deposition material of $2\,t\,m^{-3}$ (based on measurements by sub-project two) in the study area. For the explanation of the small letters in the inset map refer to the text.

(0.01 and 0.99 quantiles) and they seem to be Weibull distributed (KS test with n = 1500, p = 0.47, expected value circa $1.04\,mm\,yr^{-1}$). This is in accordance with debris fall deposition reported from other sites in the literature, the mean of which is $1.05\,mm\,yr^{-1}$ (Gardner, 1983a, Luckman, 1988, Curry and Morris, 2004, Krautblatter et al., 2012, , cited in Heckmann et al. 2016). Becht (1995b) has reported a mean of $0.39\,kg\,m^{-2}\,yr^{-1}$ with a standard deviation of $0.53\,kg\,m^{-2}\,yr^{-1}$ for 17 nets located in the Horlach Valley. Using a density of $2.7\,t\,m^{-3}$ for a quick reference, this corresponds to circa $0.14\,mm\,yr^{-1}$ and $0.2\,mm\,yr^{-1}$. One reason for the difference could be that the percentage of nets under the influence of recent glaciation is much higher in the Upper Kauner Valley than in the Horlach Valley. As Becht (1995b) does not give a theoretical distribution followed by his data, quantiles cannot be calculated to compare his results more correctly to the ones obtained in this study. For the Höllen Valley in the NCA, Becht reports values of 1–$2\,kg\,m^{-2}\,yr^{-1}$, which corresponds to roughly 0.35–$0.71\,mm\,yr^{-1}$ using a density of $2.8\,t\,m^{-3}$ (Becht, 1995b).
The reproducibility of deposition rates calculated from the measurements by sub-project two and the range of rates obtained by modeling is encouraging

concerning the validity of the modeling methodology: If the parametrization of the numerical trajectory model had been decidedly wrong, the resulting lateral dispersion or excessive concentration of trajectories would have led to modeled deposition rates much lower or higher than the ones calculated from the measured masses and net extents. The spatial distribution of modeled debris fall deposition is heterogeneous (see inset map in figure 6.1.2). First of all, it is mainly the rock wall topography (esp. couloirs) that control the formation of either talus sheets or cones. The modeling results also show that many particles stop at the apices of talus cones (letter a in inset map) and that deposition rates decrease with increasing distance from the rock wall. The fact that most particles are deposited close to the rock wall is a well known fact and is also confirmed by observations in the study area and has been empirically investigated by both Krautblatter et al. (2012) and Vehling (2016). In general, the lion's share of the particles is deposited within 100 m of the rock walls. It is understood that these findings only hold true for rock falls of small magnitude. Bigger particles have a greater potential of achieving high travel distances (e.g. Azzoni and Freitas, 1995, Haas et al., 2012b, Bourrier et al., 2013).
The obtained map of debris fall deposition also shows that many steep rock walls are located close to glaciers and that deposition is modeled on top of the glaciers or in the randkluft. It is very likely that this material will become englacial or supraglacial morainic material and will therefore contribute to the budget of the proglacial zone. The locations marked by letters b and c in the inset map of figure 6.1.2 show that particles reach both lakes and floodplain of the main fluvial system. In the latter case, this shows the rare case where debris fall contributes more or less directly to the sediment budget. It is also evident from the map of debris fall deposition rates that some landforms act as effective barriers decoupling the rock walls from fluvial system. In many cases, these are broad ground moraine surfaces or lateral moraines (letter e). Finally, it is also evident from the modeling result, that at least some sections of the toll road traverse the process area of rock fall, for example just below the highest point of the toll road (letter d).
Figure 6.1.3 shows the area around the small cirque on the left side of the main Fagge river valley. Here, the nodes of the debris fall sediment transport network were aggregated (using tools from graph theory and R's igraph package) using the polygon ID of the geomorphological-geological map (see 5.6.1). This enables a quantification of the debris fall sediment flux from each rock wall section (defined by homogenous geology and aspect) to each landform. As a result, the lines connecting the centroids of each rock wall section with the centroids of all landforms (they deliver rock fall particles to) are colored accordingly [kg yr^{-1}]. The western part of the map section shows that the small rock glacier in the cirque receives material from many different rock wall sections, but mainly from the rock walls located to its south, while the granitic gneiss rock walls located in the west are not steep enough to be included in the debris fall source areas. This result is also supported by evidence from recent orthophotos showing the debris fall accumulation landforms to the west vegetated by alpine meadow while the south-western part of the rock glacier is covered by the red debris stemming from biotite-plagioclase gneiss rock walls to the south. The visualization of the debris fall sediment transport as a network also shows that talus sheets and talus cones receive input from multiple sections of the rock wall located above. In contrast, a rock wall section distributes sediment to several different accu-

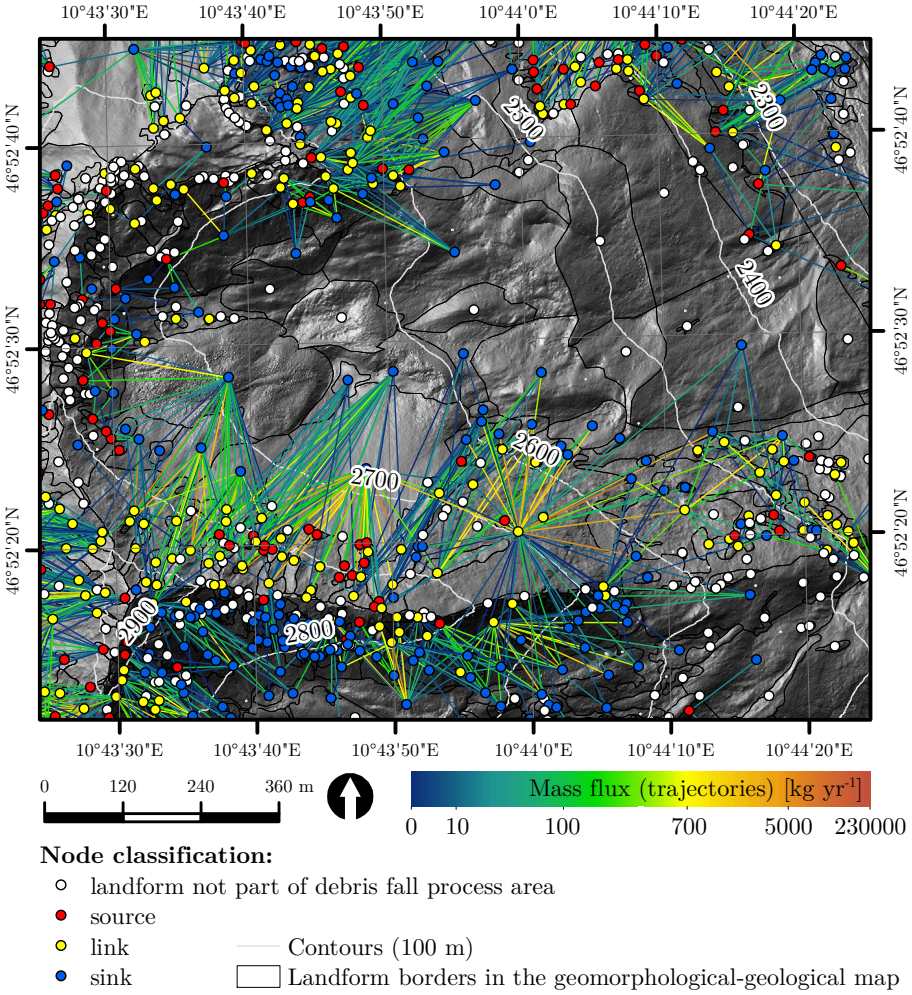

Figure 6.1.3: Detail of the debris fall sediment transport network showing the coupling of rock wall sections with individual landforms. Nodes are placed at the centroid coordinates of each polygon and colored according to their classification as either sediment source, link or sink.

mulation landforms. Such an analysis is not possible with conventional spatial representations of debris fall accumulation bodies as they do not contain information on the location of sediment sources. The graph approach makes it possible to determine the sediment contributing areas of any landform.
The numerical model the trajectories are identified with is superior to conventional methods used to determine the SCA of a landform (such as flow algorithms). Some edges with low sediment fluxes crossing low local watersheds are visible in figure 6.1.3. The reason for this is a mismatch between the (at least in part) manually drawn landform borders and their representation in the DTM. This error could be eliminated by using digitizing tools capable of respecting morphometric data. An overall summary of the results is shown in table 6.1.3 for two different levels of aggregation: i) The classes represented in the geomorphological-geotechnical map (columns one to three) and ii) Groups of landforms, based on the affiliated overall process regimes.

Landform target class	**Mass [t yr^{-1}]**	**Percentage**	**Category**	**Sum mass for category [t yr^{-1}]**	**Percentage**
Bedrock	1569.37	6.08	Bedrock	1569.37	6.08
Talus sheets	4397.87	17.04	Gravitational	9662.48	37.45
Talus cones	4052.83	15.70			
Debris cones	1211.78	4.70			
Block slope	610.88	2.37	Periglacial	1724.25	6.68
Rock glacier, not spec.	87.12	0.33			
Rock glacier, active	569.46	2.21			
Rock glacier, inactive	161.53	0.63			
Rock glacier, relictic	295.26	1.14			
Glacier	6779.22	26.27	Glacier	6779.22	26.27
Gravitational glacial	601.07	2.33	Glacial	4669.00	18.10
Moraine, not spec., pre-1855	258.29	1.01			
Terminal/lateral moraine, pre-1855	331.03	1.29			
Ground moraine, pre-1855	218.85	0.85			
Terminal/lateral moraine, post-1855	1078.48	4.18			
Ground moraine, post-1855	2181.28	8.45			
Active, competent channel	396.46	1.54	Fluvial	669.34	2.60
Gravel bars, shallow braided channels and fluvial reworked sediments	57.13	0.22			
Old fluvial storage	215.75	0.84			
Anthropogenic	178.84	0.69	Anthropogenic	178.84	0.69

Table continued on next page

Table 6.1.3 – continued from previous page

Landform target class	Mass [t yr^{-1}]	Percentage	Category	Sum mass for category [t yr^{-1}]	Percentage
Lakes, not spec., etc.	550.55	2.13	Other	550.55	2.13
Total	25803.05	100	Total	25803.05	100

Table 6.1.3: The contribution of low-magnitude rock fall to the sediment budget, unraveled to show sediment delivery to different target landforms or process domains present in the study area in scenario strategy one/G.

Looking at the results in table 6.1.3, it becomes clear that most sediment mobilized by rock fall of small magnitude is deposited on the typical accumulation landforms, bedrock (indicating a substantial deposition in less steep zones of the rock walls) and glaciers. Less than 2 % of the debris reaches the floodplain in this first step of the sediment cascade. This reflects the broad valley bottoms and chambered topographic structure of the Upper Kauner Valley. In addition, debris fall pathways are quite often blocked by both late-glacial and LIA lateral moraines: It is noteworthy that the younger LIA lateral moraines block about 4.18 % or material transported by small magnitude rock fall, while the moraines from the Egesen and Daun stadials receive only about 1.29 %. A similar proportion can be observed for the ground moraine surfaces. On the scale of the whole catchment, rock glaciers seem to receive comparatively low amounts of sediment as input. This is surprising as rock fall is often seen as being the main sediment supply in rock glacier formation. In the Upper Kauner Valley, however, multiple rock glaciers seem to have evolved at least partly from moraine deposits. One example is the Riffl Valley rock glacier (Dusik et al., 2015) and also the large Ölgruben rock glacier has its current root zone in glacial deposits. At least the latter rock glacier is so large that it can never have formed in just a few hundred years and it is obvious that current debris fall input might very well be much different to debris fall conditions in the earlier phases of rock glacier formation. Another reason for rock glaciers receiving surprisingly small amount of debris fall input is that the root zones of rock glaciers, which are often talus sheets or cones, had been consistently mapped as talus landforms and not as rock glaciers. In addition, the rock fall model was calibrated to represent debris fall and not the subsequent transition zones of talus into rock glaciers. This implies an end point of modeled trajectories on the taluses, which is the correct way. The amount of debris fall stopping on block slopes is also rather small. This is consistent with the theory and definition by Otto (2006). He defines block slopes as rock slope areas with straight and not steep vertical profiles and lacking steep bedrock outcrops that could serve as rock fall source areas.

While the active, competent channel and the current floodplain receives circa 1.76 % of all debris fall directly in strategy one/G (see table 6.1.3), it is only about 0.656 % (circa 188.5 $\mathrm{t\,yr^{-1}}$) using strategy strategy two. This difference is the result of the spatial distribution of debris fall rates based on rock mass stability. Rock masses along the current floodplains and channels seem to be relatively stable, an assessment that is confirmed by observations of the author (e.g. roche moutonnée in the proglacial area of the Gepatsch Glacier). Glaciers receive about 52.3 % of all debris fall occurring in the study area, a result of the high rock walls and fragmented rock in their vicinity. Also this value is a notable increase from the circa 26.27 % found with strategy one and underlines the importance of spatially distributed rock fall production rates based on geotechnical assessments. As the values obtained strategy two are considered more valid, it is these values that will be reported in the sediment budget (figure 7.1.4).

Comprehensive discussion of the approach

In the course of this chapter, it has been indicated several times that the methodology used to measure and regionalize debris fall rates is very heterogenous in the body of scientific literature, which impedes a comparison of rates in the

context of geofactors present in the different areas studied. Krautblatter et al. (2012), for example, also use rock fall collectors to measure masses, but calculate daily debris fall deposition rates based on the specific length of the contact line of accumulation landforms and the rock walls and the distance from that contact line. In order to upscale from measurement at the rock fall collectors to the scale of the whole catchment, they use the state of the vegetation cover as a proxy for three different rock fall intensity classes. However, they do not incorporate different sizes and morphology of the contributing rock walls which assumes a great homogeneity in the rock walls all over the study area. The approach presented here as strategy one and in Heckmann et al. (2016), however, has the disadvantage that it relies on a simple (although fitted to empirical data) relationship between real rock wall surface area and rock fall production rates, without incorporating information on the spatial distribution of geology or geotechnical properties. This has already been identified as the main shortcoming of this approach in Heckmann et al. (2016) and observations and mapping results by sub-project two have supported this view.

It was for this reason that strategy two had been additionally adopted. It is believed by the author that this gives more reliable results than strategy one, although it does help to close the probable knowledge gap concerning boulder falls (cf. 6.1.1.2) and does not incorporate TLS measurements (as does strategy one). This judgement is based on the fact that the debris fall rates in strategy two were spatially distributed, are based on a very strong correlation between a meaningful rock mass stability index and debris fall production rate.

Of course, it is desirable to combine the study area wide expert based mapping by Vehling (2016) and the measurements using nets and TLS. Such a combination, however, was beyond the scope of the PROSA project. An even more sophisticated approach should include local morpho-climatic conditions at potential debris fall start zones, for example, frost cracking potential. Time since deglaciation is also a factor that should be looked at more closely. A relationship between these factors and debris fall production rates should be established using actual empirical (measurement) data, which means that a refinement of the regionalization approach would also require a much more diverse and much higher number of measurement locations by the sub-projects actually conducting the measurements. Given the large size of the PROSA study area, its glacial history and the diverse lithological and geological-geotechnical properties within it, it becomes evident that such a refinement could only be conducted reliably in a smaller and more homogenous catchment. Independent of the additional factors that could be incorporated in the regionalization approach, an implementation into the proposed framework would be possible as debris fall start cells need only be grouped accordingly (Heckmann et al., 2016) as undertaken in strategy strategy two.

The rock fall model is not capable to deliver any information on the transport of sediment after it has been deposited on a (storage) landform (cf. discussion on rock glacier input above). This also includes, for example, a re-mobilization of rock fall material by debris flows or by a fluvial undercutting of the storage landforms. This is why these other processes have been treated in the following sections of this thesis.

In contrast to what had been published in Heckmann et al. (2016), the overall result using strategy one is quite different. This can be ascribed to several reasons. First, a measurement period of about three years was now available for

distribution fitting, while only measurements from two years had been available back then. Therefore, the yearly average values should be more representative now. A broader measurement base in the study area allowed for fitting a different distribution to measurements from the study area only without the use of supportive literature values. However, even more measurements would be desirable to improve the representativeness of the data base (see Becht, 1995b, for a similar conclusion). Another main difference to what had been published in Heckmann et al. (2016) is the usage of a second strategy with spatially distributed rock fall erosion rates as provided by Vehling (2016).

6.1.1.2 Block fall, Cliff fall and Bergsturz

Block and cliff fall

108 of rock fall events of a magnitude greater than $100\,m^3$ could be quantified by Vehling using the ALS data from September 2006 and September 2012 to arrive at a total sediment transfer rate of circa $111\,680\,t\,yr^{-1}$, while alone circa $66\,000\,t\,yr^{-1}$ must be attributed to the highly active rock slide/rock fall complex at the "Schwarze Wand" above the glacier tongue (cf. 6.1.4.1, (Vehling, 2016))[2]. Of the remaining circa $45\,680\,t\,yr^{-1}$, only about $1000\,t\,yr^{-1}$ are probably deposited in the main fluvial system (personal communication Lucas Vehling, 2016), $7640\,t\,yr^{-1}$ do not leave the hill slopes and circa $37\,040\,t\,yr^{-1}$ fall onto glacier ice at locations other then the "Schwarze Wand". Block and cliff falls having occurred since 2006 were quantified by ALS differencing. A quantification of correspondent falls before 2006 was very difficult or not possible as their deposits have already been reworked (Vehling, 2016). It is clear that the values given above must be regarded as minimum values. It is well possible that not all rock falls between 100 and $1000\,m^3$ were detected, as indicated by a rollover identified by Vehling (2016) in the magnitude-frequency distribution of rock falls $> 100\,m^3$. Further analyzes by him estimate that, for example, probably only half of the rock falls of magnitudes 100–$200\,m^3$ could be identified and quantified.

The problem that rock falls of such magnitudes can only be insufficiently detected and quantified becomes even more pronounced when it comes to boulder falls. Due to their small magnitudes, they are hard to detect on ALS-ALS DoDs, especially because the intensities of other geomorphic processes leads to a fast reworking of the resulting deposits. According to Vehling (2016), a knowledge gap exists for these magnitudes concerning the sediment budget. While no individual boulder falls could be quantified using either rock fall collector nets or ALS-ALS DoDs, they have been accounted for by using TLS measurements of large rock wall areas in addition to rock fall collector nets (cf. subsubsection 6.1.1.1.1 for a short correspondent discussion, where this circumstance was mentioned as a possible explanation of relatively high debris fall production rates obtained by TLS measurements) in debris fall quantification. This implies that the rates and masses reported for total debris fall sediment transport in the study area probably contain some signal of boulder falls. Boulder falls also probably occur at a very high frequency at the "Schwarze Wand" rock wall (Vehling, 2016), the total production of which was quantified as reported above

[2] Also debris and boulder falls are actually being released from the "Schwarze Wand" rock slide complex. As the size distribution of all rock falls being released at that location is unknown, the total mass is reported here.

independently of the magnitudes of the single rock falls.
Bennett et al. (2012) report that 99 % of the total volume eroded in the Illgraben catchment, Switzerland, is mobilized by "rockslides and rock falls" of high magnitude and low frequency and report erosion rates of $0.39 \pm 0.03\,\mathrm{m\,yr^{-1}}$ for the studied slopes. The values found in this study are significantly lower, a fact that can be explained by the weak rock and heavy jointing parallel to rock face surface in the catchment studied by Bennett et al. (2012).
The results of Vehling also reveal that large magnitudes (within the range from 100 to $1 \times 10^6\,\mathrm{m^3}$) are unproportionally rare (see Vehling (2016, p. 223 and p. 239) for a table of absolute frequencies of six size classes within that range). According to him, this is caused by the geotechnical structure of gneisses present in the study area. These contain up to four dense joint face systems, causing smaller rock bodies to fail before a bigger single event can occur.
The occurrence of rock fall above $100\,\mathrm{m^3}$ in the Upper Kauner Valley follows a distinct spatial pattern Vehling (2016): The bulk of events has taken place in the upper regions of the study area, in or close to the proglacial areas (cf. 7.2, please see Vehling (2016, p. 217) for a map). Vehling also reports that many of these starting zones are located in areas of (degrading) permafrost. It is conspicuous that also a great part of rock falls over $100\,\mathrm{m^3}$ fall onto the glaciers of the study area, the reason of which is the high degree of fragmentation of the rock masses in these areas (Vehling, 2016). This suggests that at least a part of the sediment mobilized by large magnitude rock fall has a comparatively high potential of reaching the proglacial system fast.
About 80 % of block and cliff fall came from paragneiss rock walls (15 events per $\mathrm{km^2}$ of planar rock wall area). Orthogneiss rock walls were less productive (8 events), with amphibolite taking the middle rank (13 events). There is a dominance of N, NO and W aspects in rock walls having produced events $>$ $100\,\mathrm{m^3}$. This has been ascribed to the foliation of rocks in the study area and the proportionally large share of these aspects in rock walls that are affected by permafrost degradation (Vehling, 2016).

Bergsturz
Vehling (2016) has also identified a bergsturz event (circa $1 \times 10^6\,\mathrm{m^3}$) in the Riffl Valley, a sub-basin of the Upper Kauner Valley. It has occurred in amphibolite and detached from the NE side of the Krummgampenspitzen (please see Vehling (2016, p.226) for a very knowledgeable treatise of this event). With an estimated age of circa 11 500 yr, a material density of $3.1\,\mathrm{t\,m^{-3}}$, this would imply a transport rate of circa $130\,\mathrm{t\,yr^{-1}}$ (Vehling, 2016). Virtually all of the fine particle size content of the deposit has been transported away since the bergsturz event at the end of the Egesen (Vehling, 2016). Due to the immense difference in the duration of the time reference period, this event was not used in the construction of a recent sediment budget of the study area.

6.1.2 Debris flows

It has been supposed and reported that debris flows are mainly triggered in areas of degrading permafrost as the permafrost table at depth can act as an aquiclude and cause the growing active layer to fail (Lewkowicz and Harris, 2005, Sattler et al. 2011). Such active-layer detachment failures, however, have been

rarely observed on Alpine talus, as they are very well drained (see Zimmermann and Haeberli, 1992, cited in Sattler et al. 2011). A visual intersection of the permafrost modeling result (section 5.6.3) and the mapped debris flow starting zones in the Upper Kauner Valley does not encourage the hypothesis of increased debris flow activity in areas of degrading permafrost: Debris flows have occurred in areas way outside the modeled distribution of permafrost just as in zones where permafrost is possible or probable. This result, however, is not surprising (although contradicting conceptual models in various studies), as permafrost in loose material may respond to climate forcing over a period of several decades to centuries and many more factors in addition to degrading permafrost are responsible for debris flow formation, all of which are spatially and temporally highly variable (such as rainfall, debris availability/replenishing of sediment stores in the starting zones, etc.) (Haeberli, 1992, Sattler et al., 2011). The reported faster replenishing of debris storages due to accelerated permafrost creep (Hölzle et al., 1998, cited in Sattler et al. 2011) is believed to not to be of relevance in many cases. Also Sattler et al. (2011) have not found a connection between debris flow activity since 1983 and permafrost degradation in the Schnals Valley, Italy, only seven kilometers south of the PROSA study area.
No debris flows deposits could be detected below the treeline. This might be either due to the fact that vegetation roots in general provide cohesion and make for good water permeability, which prevents buildup of high pore pressures in the sediments. Tree roots probably even anchor the sediment to the underlying bedrock (cf. Dietrich and Dunne, 1978). The by far greatest amount of debris flows has been located on the true right lateral moraine of Gepatsch glacier, with some other hot spots on the talus cones of the eastern cirques of the study area.

6.1.2.1 Volume measurements

Debris flows were quantified using three different quantification methods, depending on the data (and its quality) available and the debris flow activity history at the different locations (cf. 5.7.1.2.1). Figure 6.1.4 shows the deposition areas of debris flows near scan position three, differentiated to show the strategies used. Strategy “A” has been broken up to show which debris flows were quantified using data covering a TLS monitoring site and which were quantified in other areas.

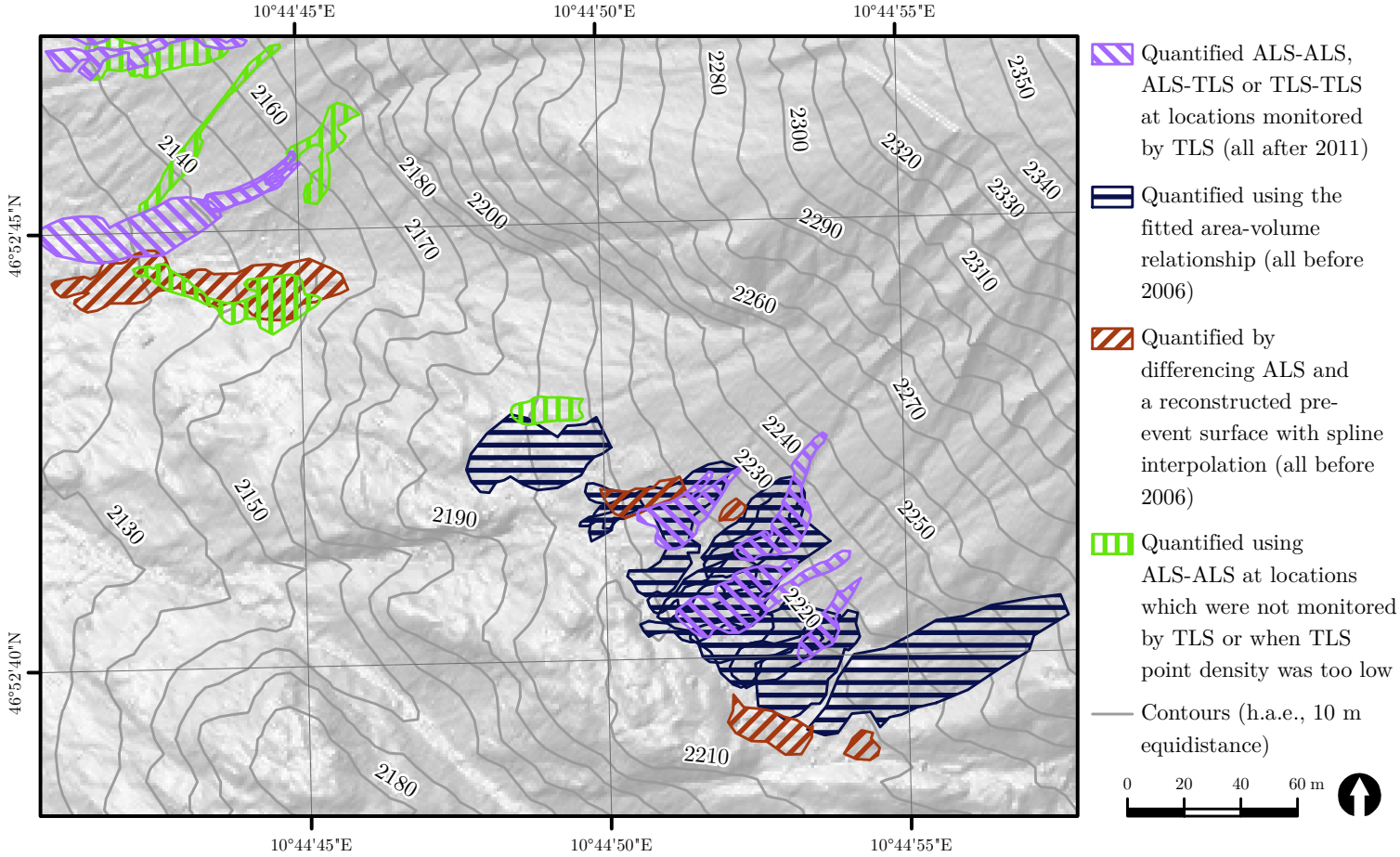

Figure 6.1.4: The area around TLS scan position three, showing the outlines of the depositional areas having been quantified using one of the three strategies discussed above.

The deposits of 62 debris flows having occurred since 2006 could be detected on ALS-ALS, ALS-TLS and TLS-TLS DoDs (strategy "A") using a spatially distributed overall LoD. As this data was the most reliable, it was used for estimating the deposition area-volume relationship (see below). The volumes and deposition areas of these debris flows is presented in figure 6.1.5 together with the fitted relationship in log-log space. Becht (1995b) reported that debris flow

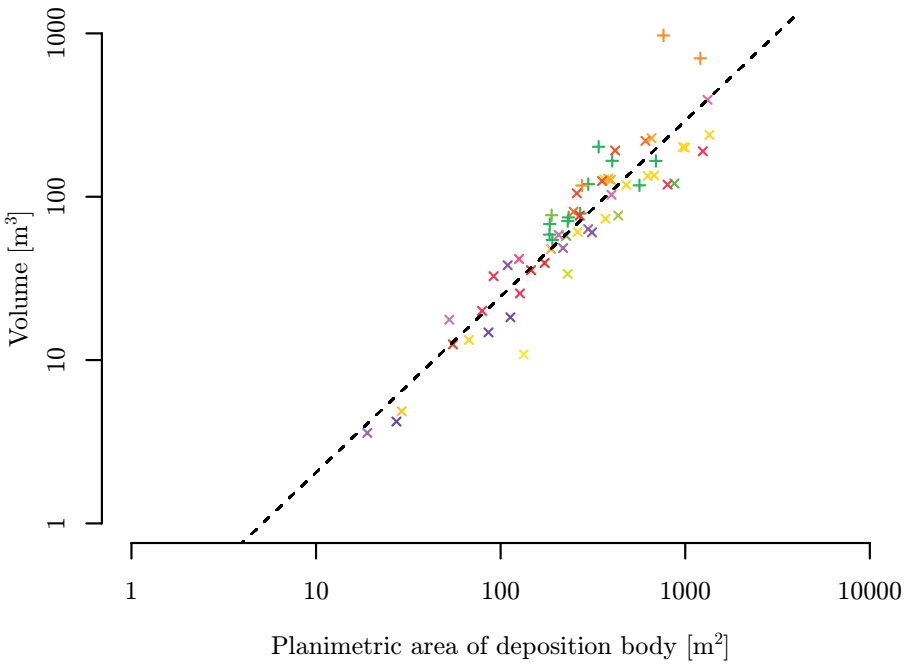

Figure 6.1.5: Subset of the debris flow inventory (n = 62) that was quantified by differencing LiDAR data of different time steps (strategy "A"). The dashed black line shows the power law fitted the data and used in strategy "C" to estimate debris flow volumes.

accumulation bodies mapped by him largely displayed a thickness of 0.3–1.0 m. This also holds true for most of the debris flows quantified in this study.
Sediment masses transported into the fluvial system were calculated by budgeting the whole process area of the debris flow as the corresponding accumulation bodies cannot be measured on the DoD. What can be done in such situations

is offsetting cells showing erosion and accumulation on the hill slope, as done in Haas et al. (2012a). This approach has the disadvantage that the obtained slope budget incorporates sediment transport not only by debris flows, but also by fluvial sediment transport, that is, a differentiation of different processes is not possible. It is more than evident that during weather conditions that can lead to debris flow initiation (heavy rain, snow melt) also fluvial erosion is present. As a result, it was tried to exclude areas of fluvial erosion from quantification. This was achieved by mapping the debris flow process area on the DoDs before an offsetting of erosion and deposition cells was undertaken. Figure 6.1.6 shows the significant difference grid for such a spatial subset of the hill slope/specific debris flow. Table 6.1.4 gives an overview of all debris flow events from 2006 to

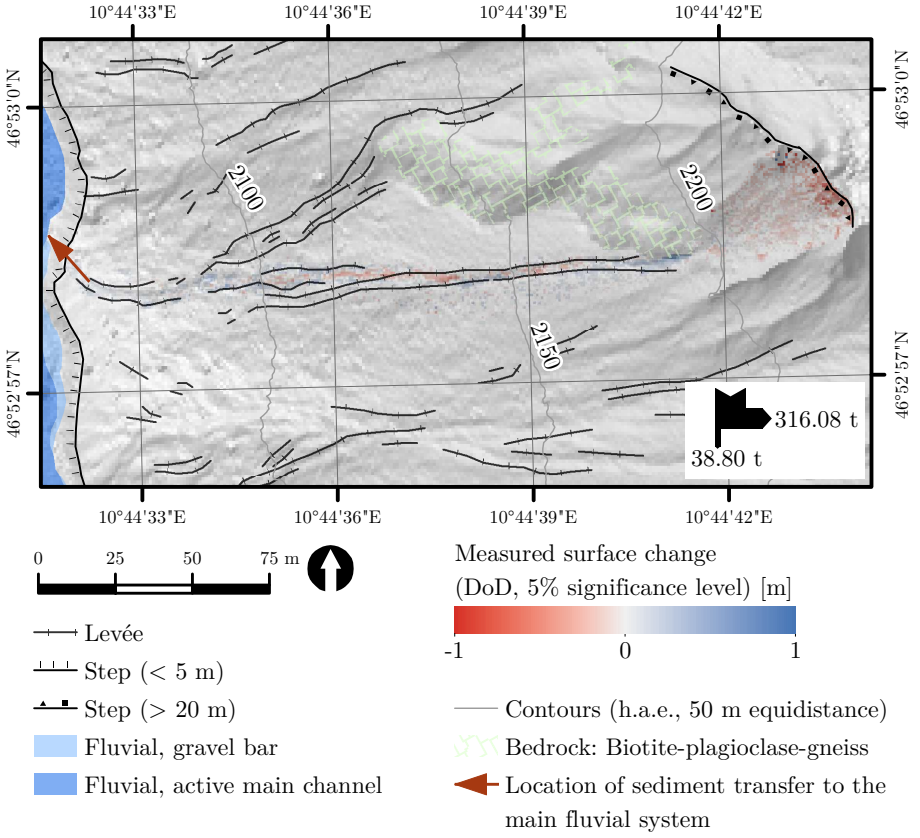

Figure 6.1.6: Example for a debris flow that has reached the main fluvial system since 2006. This debris flow occurred between July 1st, 2013 and August 7th, 2014. It has transferred almost 39 t to the Fagge river, while just over 316 t were deposited on the hillslope, mainly in form of levées.

2015 during which one or more debris flows reached the main fluvial system of the Upper Kauner Valley.

In total, 71 debris flows having occurred since 1953 have been quantified using a reconstructed pre-event surface. The single volumes are shown in figure 6.1.7. The figure also reveals that this strategy tends to underestimate debris

Source	Period	Mtfs [t]
TLS-TLS (TLSSp 04)	August 25th, 2010 - September 24th, 2011	178.65
TLS-ALS (TLSSp 04)	September 28th, 2012 - July 1st, 2013	146.74
TLS-TLS (TLSSp 06)	July 1st, 2013 - August 7th, 2014	38.8
TLS-ALS (TLSSp 04)	July 18th, 2014 - September 23rd, 2014	N/A
TLS-TLS (TLSSp 05)	October 20th, 2014 - July 20th, 2015	91.57
Sum		$>$ 455.76

Table 6.1.4: Mass transferred to the main fluvial system (Mtfs) during debris flow events since 2006, detected and quantified using all TLS and ALS data available. If multiple debris flows had reached the floodplain during the same event, they are summarized into a single event. The event in late Summer 2014 has clearly reached the main fluvial system, but quantification was not possible because TLS georeferencing quality was too bad (TLSSp = TLS-scan position).

flow volumes in comparison to the fitted linear relationship (indicated by the line of circles). As this relationship is both very strong and highly significant (cf. below), this is regarded to be the case. As a consequence, all debris flows that initially have been quantified using a reconstructed pre-event surface, were later quantified using the fitted depositional area-volume relationship. A better calibration of the spline tension threshold could improve the results obtained using strategy "B". This, however, would require both a separate treatment of each debris flow accumulation body and measurements of sediment thicknesses in the field (via extensive drillings on a small scale, see also Becht (1995b)).

The linear relationship fitted to the depositional area/LiDAR volume data has proven to be both highly significant (p-value $< 2.2e-16$) and strong ($R^2 = 0.85$). Initially, 66 debris flows had been quantified using this relationship. The number later rose to 137, when strategy "B" was abandoned. Figure 6.1.7 shows the 66 debris flows quantified using the linear relationship as circle symbols. Table 6.1.5 shows several studies that have fitted power-law correlations between area and volume for different types of slope failures and in different areas of the world. The value of $\gamma = 1.08$ found for debris flows in the Upper Kauner Valley catchment fits well into the values reported elsewhere.

After the volumes of all 199 debris flows not having reached the main fluvial system had been completed, masses were calculated using a density of $2.2\,\mathrm{t\,m^{-3}}$ (which was measured by sub-project two on debris flow deposition areas. The value is slightly higher than the $2.0\,\mathrm{t\,m^{-3}}$ used by Becht (1995b) in the Horlach Valley). As the elevations of debris flow start and deposition zones had been registered (cf. above), it was possible to calculate the elevation negotiated by each debris flow and the potential energy transformed by each debris flow.
In total, 204 debris flows have been quantified. A presentation of the single volumes, deposition body areas, masses, elevation difference negotiated, used overall LoDs, etc. is therefore beyond the scope of this thesis. Single debris flow volumes ranged from circa 0.54 to 2200 t (median: 124 t, planimetric deposition

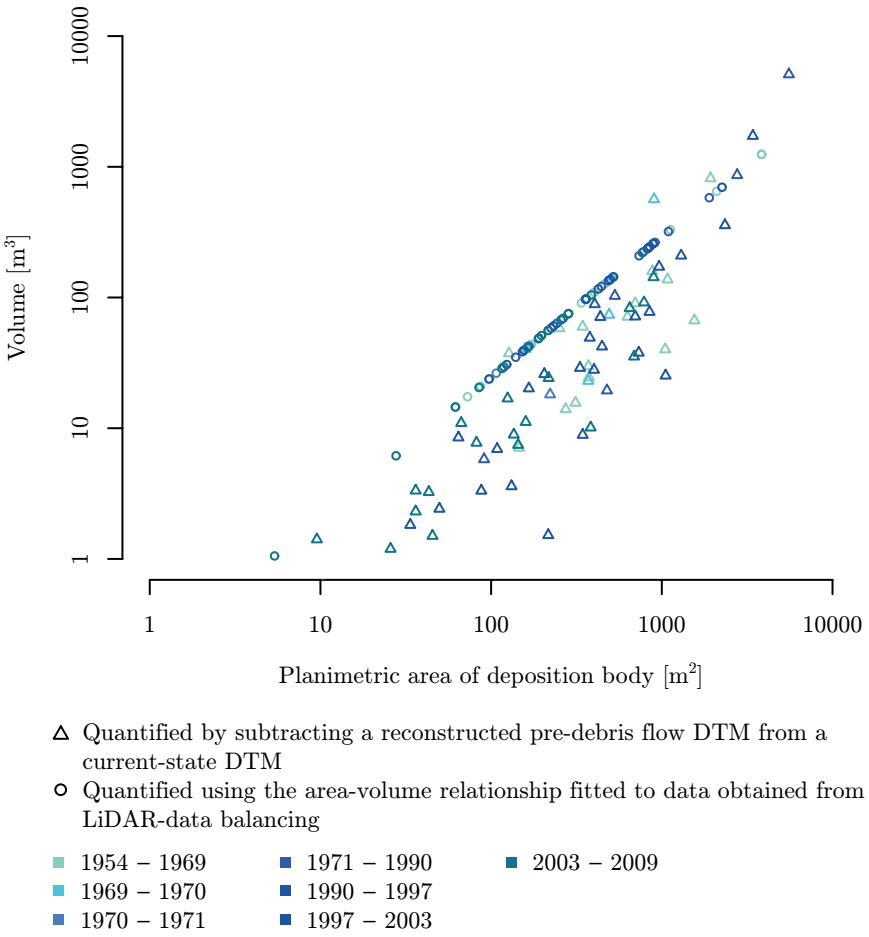

Figure 6.1.7: Subset of the debris flow inventory (n = 137) in which the debris flows were either quantified using strategy B (triangles) or C (circles).

body areas ranged from circa 3 to 5550 m^2, median: 284 m^2). These values fit well into what has been published by Becht (1995b) concerning the Horlach Valley, where total debris flow volumes (summed for different monitoring sites) are in the same range of magnitudes.

Between AD 1953 and 2015, debris flows have moved at least 43 680 t of sediment and transformed an energy of circa 41.4 GJ. The former value corresponds to a rate of circa 704 t yr^{-1} or circa 0.67 GJ yr^{-1}. If only the time period from 2006 to 2015 is taken (that is the time period in which all debris flows were quantified using LiDAR data), the total mass of sediment moved is circa 16 107 t or

Study	Type of slope failure	Location	Fitted function
Guzzetti et al. (2009)		World	$\gamma = 1.45$
Larsen et al. (2010)	Shallow, soil-based landslides	New Zealand	$\gamma = 1.1 - 1.3$
Larsen et al. (2010)	Landslides involving bedrock	New Zealand	$\gamma = 1.3 - 1.6$
Bennett et al. (2012)	Slope failures in general	Illgraben, Switzerland	$\gamma = 1.1$
This study	Upper Kauner Valley, Austria		$\gamma = 1.08$

Table 6.1.5: Power-laws fitted to represent area-volume relationships of slope failures. See Larsen et al. (2010) for more comparative values for γ.

circa $1790\,\mathrm{t\,yr^{-1}}$, which corresponds to a transformed energy of $0.61\,\mathrm{GJ\,yr^{-1}}$[3]. Although it is possible that the frequency of debris flows has been increasing due to global change (and the resulting high amount of sediment having been exposed in the proglacial areas), it is unlikely that the discrepancy of $1000\,\mathrm{t\,yr^{-1}}$ is due to a change in debris flow frequencies. It is much more likely that the usage of study area wide LiDAR data made it possible to detect virtually all debris flows, while this was not possible using the historical orthophotos (cf. discussion below). The same argumentation holds true if the time period of 2012–2014 is used (the time period for which the rates of all other processes could be calculated, see chapter 7.1). With the onset of TLS measurements in 2012, probably all debris flows in the study were detected, causing the yearly rate to increase to circa $4300\,\mathrm{t\,yr^{-1}}$. Only a very small percentage of all debris flows reach any part of the main fluvial system. This result fits well into the finding by Becht (1995b) who states that most debris flows do not reach the main fluvial system. Since 2006, a minimum of 455 t of sediment have entered the fluvial system by means of debris flows (see table 6.1.4). It must be stressed that all values presented here are minimum values as debris flows that have entered a randkluft or the deposits of which had been covered by snow during aerial image acquisition time could not be quantified.

It is evident that the total mass determined is highly dependent on the area-volume relationship used to quantify debris flows that cannot be traced on two LiDAR-derived DTMs. This dependence was explored by ordinary bootstrapping (and assigning equal weights to each of the 62 debris flows used to parametrize the model, 3000 bootstrap replicates) the relationship reported above (Canty and Ripley, 2016). This revealed a standard error of roughly 3600 t ($58\,\mathrm{t\,yr^{-1}}$), or circa 8 % of the total sediment transfer estimated for the time period AD 1953 to 2015.

Again, suitable values for comparison are hard to find in the literature as these values are referring to a specific time period and location. Becht (1995b) reports

[3]The fact that this $\mathrm{GJ\,yr^{-1}}$ value is similar to the one valid for the total time period of 62 years reflects the circumstance that the debris flows mapped on the historical orthophotos were relatively few but rather large and traveling over great (vertical) distances.

a total accumulation by debris flows of 38 400 t during an extreme precipitation event in Horlach Valley. This shows the importance of extreme events for geomorphic processes in high-mountain areas. A debris flow event in the Rein Valley, Germany, was estimated at yielding 12 000 t (using the channel elevation as reference for the deposit, this corresponds to a work done of circa 18.83 GJ), with about 7000 t leaving the slope subsystem and entering an active channel.
In total, debris flows in the study area since 1953 are accountable for an erosion rate (in relation to the 62 km^2 of the study area) of 0.01 $mm\,yr^{-1}$ (using a density of 2.7 $t\,m^{-3}$ and the reference time period 2006 to 2015). The erosional activity of the average debris flow in the data set (circa 214 tons) is equal to 0.8 % of the basin wide mean annual small-scale rock fall debris production. With about four debris flows occurring every year (rounded from the average AD 1954–2014), it is evident that, rock fall accumulation landforms like talus cones or slopes are generally still building up (even when disregarding the fact that most debris flows in the study area occur on lateral moraines and not on talus). This fits well into findings in other glacial valleys in the Central Alps (Becht, 1995b).

During data processing for volume determination with TLS data, it became evident that some of the TLS data was insufficiently registered or georeferenced. It was therefore not used for debris flow quantification. Similar problems with the same data had been encountered by Messerschmidt (15.06.2016).
Especially the TLS scans obtained with an angular resolution of 0.05° are of too low point density in the upper parts of the slopes monitored for debris flow quantification. Where this was not a problem in the quantification of debris flow that had not reached the main fluvial system (as the deposition bodies were used for quantification), some errors might have been introduced in the estimation of net balances for debris flows that have reached it (see table 6.1.4 for the estimated vales). One TLS scan showing a debris flow having reached the main fluvial system had to be excluded from the quantification efforts for these reasons. This is why the overall sediment mass estimated to have reached the main fluvial system should be seen as an absolute minimum value.
One common problem with all historical inventories of slope failures, independent of size and type, is coalescene of single failures inherent in the data. As the time windows used in this study are rather wide (up to 16 years for the historical orthophotos), it cannot be ruled out that the depositional body in the database represents the volume resp. mass mobilized by two or even more debris flows. In theory, it might have been possible to separate distinct debris flows using dating techniques on the levees (Beylich et al., 2011). As this would have required additional extensive field work and expensive outsourcing of dating, the additional expenses were not justified.
Deposition bodies were used, because a area-volume relationship could be fitted using this data and erosional volumes in the highly active lateral moraines represent both debris flow and fluvial slope erosion. This, of course, makes a direct measurement of masses entering the fluvial system difficult as no direct budgeting of the slope as a unit is possible (as done in Haas et al., 2012a). Experience has shown, however, that even with debris flows not reaching the channel, the budget of the slope is highly unbalanced. This is most likely due to fluvial erosion modifying the slope to a significant degree in addition to debris flows (see section 6.4.3). No data on fluvial hill slope erosion in the same

temporal resolution as debris flow data was available for the sites where debris flows contribute sediment to the fluvial system. This is because sub-project one had not finished the respective LiDAR data evaluation and sediment traps had been destroyed repeatedly, were not emptied that often and had been installed much later than the commencing of TLS measurement.

6.1.2.2 Magnitude-frequency relationship

The estimated $x_{\min}$ is circa $135\,\mathrm{m}^3$, that is, a negative continuous power-law can be assumed to describe the data above a magnitude of that value. The estimated scaling parameter is circa 2.55. Figure 6.1.8 shows the cumulative distribution function and the fitted power-law for the debris flow data of strategy A. To get an idea about the uncertainty in the parameter estimates, a bootstrapping procedure (3000 simulations) calculating Kolmogorov-Smirnoff statistics for different parameter estimates was used (Gillespie, 2014). Thus, the standard deviation of the $x_{\min}$ estimate is circa $48\,\mathrm{m}^3$, while the standard deviation of the scaling parameter estimate (standard error) is circa 1.3. A visual inspection of bootstrapping results shows that the estimated values for $x_{\min}$ and the scaling parameter are highly dependent on a rather small subset of debris flows quantified and that a higher number than 62 is desirable to estimate the parameters of the magnitude-frequency distribution more reliably.
Figure 6.1.8 reveals, for example, that about 50 % of debris flows in the Upper Kauner Valley since 2006 had a volume below c. $100\,\mathrm{m}^3$, while only about 5 % had volumes above circa $400\,\mathrm{m}^3$.
As only the tail of the distribution can be modeled with a power-law, the whole PDF was additionally modeled using a Weibull distribution. The modeling result is depicted in figure 6.1.9. Looking at figure 6.1.9, it can immediately be told that most debris flows in the Upper Kauner Valley are of comparatively low magnitude. Using this distribution, the following statements about the magnitude and frequencies in the study area can be made (given that the inventory of 199 debris flows is valid): About 66.5 % of all debris flows occurring in the study area have a volume $< 100\,\mathrm{m}^3$, while debris flows of 100–$200\,\mathrm{m}^3$ occur with a probability of circa 19.3 %. Debris flows with volumes between 200 and $500\,\mathrm{m}^3$ are more rare (approximately 12.7 % probability), while debris flows with a magnitude of 500 to $1000\,\mathrm{m}^3$ are truly extreme events (probability of just below 1.5 %). Debris flows $> 1000\,\mathrm{m}^3$, can occur. The probability of such an event, however, is dwindling small (less then a tenth of percent).
The uncertainty in the parameters of the Weibull distribution was again investigated using ordinary bootstrapping (cf. above). The standard error for the shape parameter (0.83) is 0.05, while the standard error for the scale parameter (8988.46) is 806.9. Please note that these parameters are valid for volumes transformed for Weibull distribution fitting (volume $\cdot 0.01^{-1}$) and can therefore not be related directly to volumes.

In constructing this debris flow inventory, a traditional approach was followed (Dietrich et al., 1982). That is, no specification of debris flow site conditions was used to form several classes of debris flows. This is the strategy followed by virtually all studies on magnitude-frequency relationships of mass wasting processes of all kinds. Per definition, the resulting magnitude-frequency distribution is therefore assumed to apply for all areas within the Upper Kauner

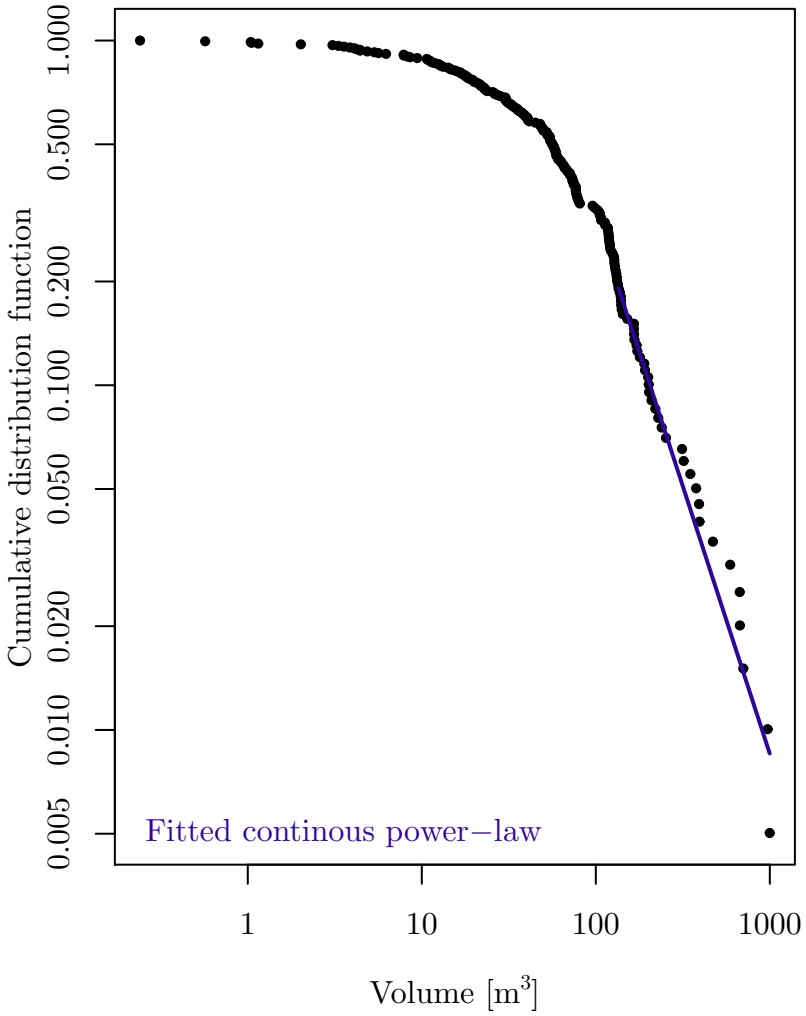

Figure 6.1.8: Empirical cumulative distribution function of debris flows quantified using LiDAR data and fitted continuous power-law (blue line).

Valley. While other studies have fitted the relationship to other mass wasting processes such as rock fall or classical landslides, this study provides the only parametrization of the model to a pure slope-type debris flow inventory, thereby enlarging the knowledge base on magnitude-frequency relationship parametrization differences between different types of mass movements. While probably most other inventories suffer from small events being underrepresented, the use of spatially and temporally highly resolved data in this study enables also to

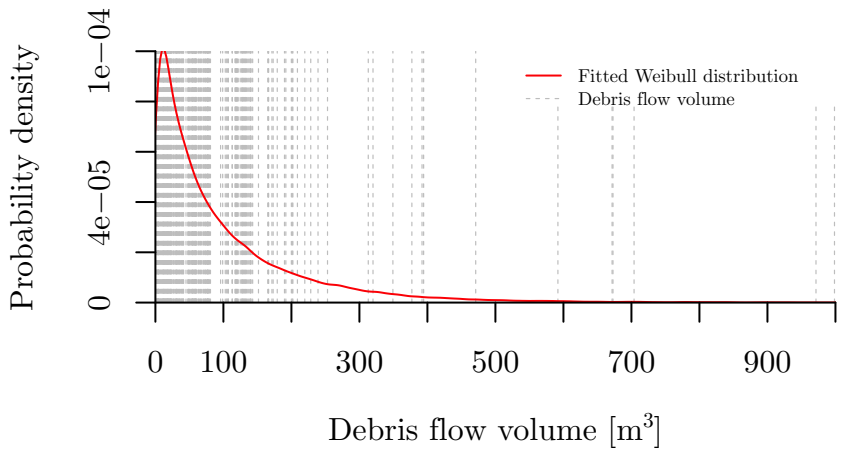

Figure 6.1.9: Fitted Weibull distribution to represent the magnitude-frequency relationship of debris flows in the study area.

capture small debris flows. This might also explain the comparatively small rollover (as visible in figure 6.1.9; Bennett et al. (2012) has found the rollover at circa 50 m^3) of circa 20 m^3, even though some small events were probably still hidden by coalescene (cf. Bennett et al., 2012). Tables summarizing the results of different studies on the magnitude-frequency relationship of different slope failures can be found in Bennett et al. (2012) and van Den Eeckhaut et al. (2007). Some comparative values for β are given in table 6.1.6

Author	Type of slope failure	Location; Geological setting	Scaling exponent
Malamud et al. (2004)	rock fall	Various; Various	$\beta = 1.07$
Guzzetti et al. (2002)	rock fall	Central Italy; Granitic cliffs	$\beta = 1.1$
Dussauge-Peisser et al. (2002)	rock fall	Near Grenoble, French Alps; Calcareous cliffs	$\beta = 1.41$
Hungr et al. (1999)	rock fall	British Columbia; Massive felsic rock	$\beta = 1.43$
Dussauge-Peisser et al. (2002)	rock fall	Arly gorges, French Alps; Metamorphic and sedimentary rocks	$\beta = 1.45$
Dussauge-Peisser et al. (2002)	rock fall	Yosemite Valley, USA; Granitic cliffs	$\beta = 1.46$
Dussauge-Peisser et al. (2002)	rock fall	Various; Undifferentiated rock cliffs	$\beta = 1.52$
Hungr et al. (1999)	rock fall	British Columbia; Jointed metamorphic rock	$\beta = 1.65$
Bennett et al. (2012)	Mixed	Illgraben, Swiss Alps; Quartzitic rock and sediment	$\beta = 1.65$
Gardner (1970a)	rock fall	N/A; Calcareous and quartzitic rock	$\beta = 1.72$
Bennett et al. (2012)	Mixed	Illgraben, Swiss Alps; Quartzitic rock and sediment	$\beta = 1.76$
Lim et al. (2010)	rock fall	North Yorkshire, England; Sandstone and mudstone capped in glacial till	$\beta = 1.8$
Malamud et al. (2004)	Landslide	various; various	$\beta = 1.93$
Stark and Guzzetti (2009)	Landslide	N/A; Sandstones, marls, limestones	$\beta = 2$
Stark and Hovius (2001, cited in Bennett et al. 2012)	Landslide	New Zealand; N/A	$\beta = 2.11$
Stark and Guzzetti (2009)	Landslide	N/A; Clay and silt and clastic sediments	$\beta = 2.19$
Malamud et al. (2004)	Landslide	N/A; Weakly cemented clastic sediment	$\beta = 2.4$
Malamud et al. (2004)	Landslides	N/A; Clay and silt and clastic sediments	$\beta = 2.4$
Malamud et al. (2004)	Landslide	N/A; Soil, siltstone, volcanic rocks, phyllite and schist	$\beta = 2.4$
Stark (2001)*	Landslide	Taiwan; N/A	$\beta = 2.48$
This study	Debris flows	Upper Kauner Valley; Mainly glacial till, talus	$\beta = 2.55$

Table 6.1.6: Selection of studies that have determined magnitude-frequency relationships and scaling exponents found therein. A list with more details is provided by Bennett et al. (2012). See van Steijn (1996) for comparative qualitative results.

* The corresponding bibliography entry in Bennett et al. (2012) is missing. The value cannot be found in Stark and Hovius (2001).

It is evident from the literature, that larger scaling exponents are found in studies that investigate slope failures in either soil mantled slopes or weak bedrock. Both characteristics lead to comparatively small slope failures. Mass movements in strong bedrock, contrariwise, lead to lower exponents because they tend to mobilize more material (Bennett et al., 2012). The finding of $\beta = 2.55$ for debris flow events, which initiate in areas of low slope strength, i.e. low cohesion and friction angle, supports the hypothesis that debris tends to generate comparatively small mass movements. This result also supports the findings and interpretations of Bennett et al. (2012). She gives scaling exponents from 1.07 to circa 1.8 for rock fall or slope failures in strong bedrock and higher values (up to 2.48) for mass movements (mainly landslides and soil slip) in weaker material and flows with a higher water content. The slightly higher value for debris flows fits therefore very well into the values published and compiled by others.

6.1.3 Shallow soil slips

In total, 194 shallow soil slip scars have been mapped by Betz (2016), based on the orthophoto of 2010.[4] Most of these (i.e. 81 %) are concentrated in three delimited areas in the Wannet, Münchner Cirque and Riffl Valley areas of the Upper Kauner Valley and over 50 % of scars are located on lateral or terminal moraines deposited before AD 1855. Only a few shallow soil slip scars could be found below the treeline by Betz (2016), probably for the same reasons why no debris flows have been detected there (cf. 6.1.2). All scars are located at elevations between 2149 and 2978 m h.a.e. (average 2623 m h.a.e.). In AD 1953, only 174 shallow soil slip scars were mapped and Betz (2016) states a continuous increase of shallow soil slip scars after this date.
Also the area occupied by shallow soil slip scars has increased from 2.92 ha to 3.07 ha between 1953 to 2010. The average size of the scars has decreased between 1953 and 1970/71 by 15 m^2, but has increased again from 2003 to 2010 (the average over the whole period is circa 160 m^2). A temporal breakdown of the development can be found in Betz (2016). It must be noted that the secondary enlargement of scar area is most likely due to fluvial processes operating on the scar (e.g. undercutting of the upper margin by piping processes). Strictly speaking, the area increase should be assigned and reported to/under fluvial hill slope processes. However, it is reported and discussed here for reasons of coherence.

The greatest increase in the number of shallow soil slip scars can be found in the Fernergries and Münchner Kar, where the number of scars has risen from 41 to 51 resp. 13 to 20. Most of the other areas where shallow soil slip scars could be identified have been relatively stable over the whole time period. An exception is the big scar in the Riffl Valley (which has also been surveyed via TLS at scan position 13), which has greatly increased in size since 1953. The Fernergries area has displayed the greatest intensity: The total scar area has increased strongly from 1953 to 2010, while almost half of the scars that had existed in 1953 has decreased. This implies that the area of the new scars is bigger than the one of the ones that have disappeared due to vegetation growth. Shallow

[4] The results presented in the following (except the rough quantification of the sediment mass moved by the shallow soil slip) are extensively based on Betz (2016).

soil slips have also occurred below the Ölgrube and the Kühgrube since 1953, but the greatest activity can definitely be stated for the Fernergries area (Betz, 2016). This fact is probably due to the high importance of sediment transporting avalanches in the Fernergries area (see chapter 6.3), hereby keeping shallow soil slip scars free of vegetation and also probably contributing directly to their enlargement and formation. It is conspicuous that shallow soil slips seem to be concentrated on hill slopes of southern and south-western aspects, which could be due to the fact that vegetation necessary for shallow soil slip formation can be found predominantly on such slopes (Betz, 2016).
It would be expected that the locations prone to shallow soil slips are characterized by subsurface water concentrations, as created by the subsurface bedrock configuration. Dietrich and Dunne (1978) and Dietrich et al. (1982) argue that bedrock depressions both lead to comparatively thick soil and sediment pockets and an increased subsurface water flow causing these areas to fail. Such soil bodies located in a convergent topographic position could be observed at several locations in the study area, especially along road cuts. Also Betz (2016) reports these topographic configurations as being probably advantageous for shallow soil slip occurrence in the PROSA study area. The comparatively high number of new shallow soils slips (since 1953) in the Fernergries, however, is probably due to two other factors: i) The area had been covered by ice until comparatively recently (c. 1860) and it is possible that the resulting relative instability of the sediments has fostered shallow soil slip susceptibility (this also explains the high number of scars visible in 1953, although some of them have been stabilized by vegetation in the meantime) and ii) some of the soil slip scars mapped by Betz (2016) are located in the starting and transport zones of the large Fernergries avalanche recurring almost every winter (figure 5.7.13 actually shows some of them in the starting zones of the avalanche(s)). It is therefore possible that a few of the scars mapped by Betz (2016) were not formed by a shallow soil slip (alone) but were modified by avalanche activity.
The majority of the scientific literature reports an increase of shallow soil slips in the Alps in the context of global warming and the abandonment of mountain pastures (which implies that erosion counter measures are being neglected) (e.g. Konz et al., 2010, Wiegand and Geitner, 2013, cited in Betz 2016). A continuous increase in both the number of shallow soil slip scars (in total by 13 %) and the area covered by them (by 5 %) could also be determined for the Upper Kauner Valley. The increase, however, is much lower than reported for other alpine areas (Betz, 2016). The PROSA study area has some characteristics that make it stand out in comparison to these other areas: i) It is located at a much higher elevation than the study areas of other research concerned with shallow soil slips in the Alps and ii) grazing has been of comparatively low importance in the Upper Kauner Valley in the 20th century. Especially the second factor might explain the deviation of the results obtained for the Upper Kauner Valley from the ones in other areas of the Alps. Similar conclusions were drawn by Becht (1995b) who identified a decrease of the number of shallow soil slip scars in the Kesselbach Valley of circa 21 % from 1952 to 1990. Only few new shallow soil slips have occurred since AD 1953. This implies that no magnitude-frequency relationships for this process can be estimated (cf. Dietrich and Dunne, 1978).
Based in the simple estimation approach presented in subsection 5.7.1.3, about $7.6\,\mathrm{t\,yr^{-1}}$ of sediment have been moved between 1970/71 and 2003 by shallow soil slip formation. As the average elevation negotiated by each of the seven

shallow soil slips and their individual sizes are not known, it is not possible to calculate the geomorphic work accomplished by them. It can be estimated as being around $44 \times 10^{-5}\,\mathrm{GJ\,yr^{-1}}$ (based on the average values of the mapped scars). As no new shallow soil slips could be detected after 2003, however, the geomorphic activity of shallow soil slips in the Upper Kauner Valley seems to have (temporarily) ceased.

6.1.4 Rock slides and Deep-seated Gravitational Slope Deformations

6.1.4.1 Rock slides

In total, six more or less slowly moving rock slides have been identified by Vehling (2016). While most of them are fossile or inactive (see Vehling (2016, p. 129) for a location map), it is the rock slide "Schwarze Wand" that must be particularly noted.
This rock slide is by far the most active rock slide in the study area, a fact that is a consequence of a combination of favorable geotechnical, geological and geomorphological factors. The moving body is mainly made up of strongly foliated paragneiss and has displayed high activity since circa 2010. Its movement has been monitored by sub-projects two and three using a combination of TLS and ALS data (Baewert et al., 2014) via IMCORR feature tracking and an increase in activity since 2012 has been stated Vehling (2016). While average movement rates are in the range of dm, surface deformation velocities of more than $1\,\mathrm{m\,yr^{-1}}$ have been measured lately. The rock slide mass has been showing signs of disintegration, which is why a scenario of a single massive failure is regarded as unlikely (Vehling, 2016). In the study area, rock slides like the "Schwarze Wand" do not contribute any sediment to the main channels but rather prepare material for other processes as rock falls or debris flows (Kellerer-Pirklbauer et al. 2010 and personal communication Vehling, June 2016): While the toe of the rock slide complex has not moved much, its activity has led to a great degree of fragmentation of its body causing it to be an major source of debris and boulder fall summing up to a value about two times of the debris and block fall amount occurring in the remainder of the study area together (cf. 6.1.1.1.2). Given a estimated total mass of circa $1\,100\,000\,\mathrm{m^3}$, a material mobilization rate of $371\,000\,\mathrm{t\,yr^{-1}}$ is estimated[5] ($42\,200\,\mathrm{t\,yr^{-1}}$, if only the more active sub-body is taken into account) by Vehling (2016). Combining velocity, mass and slope inclination values, a geomorphic work accomplished by the "Schwarze Wand" rock slide complex (the rock fall originating from the complex excluded) of $9\,\mathrm{GJ\,yr^{-1}}$ for a reference period of 2006 to 2014 has been estimated. Between 2012 and 2015, the geomorphic work accomplished by the slide is circa $18.4\,\mathrm{GJ\,yr^{-1}}$ (Vehling, 2016).
A similar, but much larger combined rock-ice slide at the Weißseespitze has gotten scientific attention already in the late 1990s (Heißel and Weber, 2000).

[5]These rates are reported as material transport rates by Vehling (2016). The formulas given and used by him for the calculation of these rates, however, do not incorporate a cross section of the rock slide body and make no sense to the author. It is unclear what these values represent. Sediment transfer rates of rock slides and deep-seated gravitational slope deformations will therefore not be included in the sediment budget.

In summer 1997, a circa 5 000 000 m^3 rockslide was moving at up to 1.2 m day^{-1} and endangered the skiing area in the Upper Kauner Valley. In the following years, the slide's activity has decreased significantly and is generally regarded as inactive. As it is located in the heavily glaciated NW face of the Weißseespitze, a quantification of its current activity status is difficult (Vehling, 2016).
While the Weißseespitze rock slide is a slide incorporating both rock and ice masses, the complex at the Nörderscharte is a classical rock slide. It also shares many characteristics with the "Schwarze Wand" rock slide. Its movement velocity, however, could not be determined. A geomorphic work of circa 0.08 GJ yr^{-1} is estimated for this rock slide (Vehling, 2016). Also the other rock slides in the study area are either fossil, inactive or moving at too low velocities to be measured.

6.1.4.2 Deep-seated Gravitational Slope Deformations

Vehling (2016) has identified two DGSDs in the Upper Kauner Valley. They are located at the "Vorderer Nörderberg" (a very large complex with a relatively active sub-section developed in the lateral LIA moraine at the true left hill slope in the Fernergries area) and the "Vordere Kühgrube". While the latter one is rather small (circa 160 000 m^3) and shows no distinct activity (geomorphic work is circa 0.004 GJ yr^{-1}), it is the currently active sub-section of the former one that is of interest concerning sediment transport processes in the Upper Kauner Valley: A comparatively large number of shallow soil slips (cf. subsection 6.1.3) have developed on its surface. These, in turn provide a large amount of material to the large Fernergries avalanche(s) that are capable of transferring sediment to the main fluvial system (see 6.3). This shows that also GDSDs (just like rock slides) are of great importance in preparing material for secondarily acting processes. According to Vehling, about 15 % of the material originally affected by the Fernergries DGSD has been eroded by avalanches, debris flows and fluvial hill slope erosion since its activation (which is dated into the second half of the 20th century by Vehling (2016)). About 300 000 m^3 remain and move at velocities of about 5 mm yr^{-1}, accounting for a geomorphic work of circa 0.016 GJ yr^{-1}. Activity shows a seasonal pattern, with the highest movement rates being achieved in spring (Vehling, 2016).
The sediment transfer by the other four rockslides and DGSDs could not be quantified. Vehling (2016) estimates the the geomorphic work accomplished by them at being smaller than 0.01 GJ yr^{-1} each.

6.2 Creeping Permafrost

6.2.1 Talus creep

Due to the high number of large and steep talus landforms located high above the vegetation zone, the sediment transfer by creep processes on talus is estimated at circa 1597.5 t yr^{-1} using the methods described in subsubsection 5.7.1.5.1. Only 0.49 t yr^{-1} of that total mass (0.03 %), however, are estimated to be transferred to the main fluvial system. It must be kept in mind that creeping processes can only occur if enough water is present in the subsurface. This is mainly conditioned by the grain size distribution of the material. There can be no presumption that this is the case on all surfaces used to model creeping processes in the Upper Kauner Valley. The presented values should therefore be regarded as maximum values.
It is obvious that the estimation of sediment transfer by creep processes could be significantly improved. Own measurements of creep rates and of the thickness of the sediment layer affected by creep could yield much more reliable results. It is possible that the thickness of the debris layer moved by talus creep is 50 % of what has been used here. Roughly, this would also cause the sediment transfer rate to halve. A map of the spatial distribution of the sediment layer thicknesses could yield a much better spatial representation of creep rates. Such a map could be constructed from a slope to sediment/soil thickness regression and mapping as in Dietrich and Dunne (1978). Measurement of talus creep, however, would be a challenging task. One possibility would be the application of denudation gauges (iron rods) (Rapp, 1957, Becht, 1995b). However, they cannot be used to establish sediment balances and the installment and maintenance would cause a disturbance of the creeping system on the talus (Becht, 1995b).
Only talus creep on non-vegetated surfaces has been roughly estimated using the relationship described in equation 5.7.5. During several field visits, bound solifluction was observed at a few locations in the study area, most impressively on the largest talus cone in the lower Riffl Valley (cf. figure 6.2.1). It is therefore

Figure 6.2.1: Solifluction lobe in the Riffl Valley. Jana-Marie Dusik for scale.

evident that solifluction transfers sediment in the Upper Kauner Valley. As it is of minor importance for the overall sediment budget, no measurement have been taken.

6.2.2 Rock glaciers

Rock glacier mapping resulted in an inventory of 17 active rock glaciers in the study area, four of which are multipart-rock glaciers. All active rock glaciers in the study area cover about 1.25 km^2, i.e. circa 2 % of the study area. Active rock glacier sizes are very variable, with the rock glacier located in the Ölgrube covering 0.25 km^2 alone. Also front heights are highly variable (mean: 29.5 m, standard deviation: 21.2 m) (Neugirg, 2013). The average sediment volume of rock glaciers calculated for the Upper Kauner Valley (disregarding different densities of the ice and sediment). is circa 0.97×10^6 m^3. Barsch (1996) (cited in Neugirg 2013) gives an estimate of an average volume of 0.66×10^6 m^3. This difference can easily be explained by the fact that both the Riffl Valley and especially the Ölgrube rock glaciers are exceptionally large.

Horizontal and vertical displacement - Results
Mapping of the rock glacier fronts has revealed advances of up to 35 m or 0.61 $m\,yr^{-1}$ between 1953 and 2010 (at the southern lobe of the Ölgrube rock glacier). Also the rock glacier front in the Krummgampen Valley already discussed above has moved about 26 m during the 57 years before 2010 (circa 0.46 $m\,yr^{-1}$). Most other rock glacier fronts in the study area, however, have displayed advances of much lower magnitude (maximum at circa 0.3 $m\,yr^{-1}$), while for eight of the 17 rock glaciers no displacement could be determined at all (Neugirg, 2013).
The feature tracking analysis on the rock glacier surfaces between 2006 and 2012 revealed geomorphologically meaningful displacement vectors and average yearly surface velocities in the decimeter range for 14 of the 17 rock glaciers (Neugirg, 2013). The yearly average values roughly confirm the result obtained by manual front advance mapping. Surface velocities on the rock glacier surfaces are spatially highly variable, with every rock glacier also showing horizontal surface displacement speeds in the meter range. This variability is the reason why an average value was calculated from the velocity values obtained by feature tracking to be used in sediment transfer estimation. These average values are reported in table 6.2.1. An alternative for the automatic feature tracking using the IMCORR algorithm would have been a manual identification of blocks and mapping on orthophotos. As a large number of blocks would have been necessary to be able to calculate representative mean surface velocity values for each rock glacier, the automatic procedure had been adopted. Tests by Neugirg (2013) have shown that values obtained by manual feature tracking tend to be slightly higher than the ones obtained by IMCORR.
Except for four individuals, all rock glaciers display a mean negative vertical displacement (mean of all cells on the rock glacier surface), i.e. have subsided between 2006 and 2012. The areas showing subsidence are highly variable between rock glaciers and between different areas of a single rock glacier when it comes to the amount of negative vertical displacement. Values between rock glaciers range between -0.9 and -9.39 m. All rock glaciers also show zones of

Rock glacier ID	Mean yearly horizontal displacement and standard deviation[m yr^{-1}]	Rock glacier ID	Mean yearly horizontal displacement and standard deviation [m yr^{-1}]
1	0.35 (0.75)	10	0.14 (0.77)
2	0.41 (2.14)	11	N/A (N/A)
3	0.24 (1.08)	12	0.11 (0.26)
4	N/A (N/A)	13	0.14 (0.62)
5	0.20 (0.92)	14	0.17 (0.74)
6	0.20 (0.58)	15	N/A (N/A)
7	0.33 (0.91)	16	0.19 (0.8)
8	0.19 (1.09)	17	0.12 (0.27)
9	0.10 (0.25)		

Table 6.2.1: .
Mean surface velocities (2006–2012) and corresponding standard deviations for the seventeen active rock glaciers in the study area (numbered clockwise as in figure 9 of Neugirg (2013)) as determined by IMCORR feature tracking by Neugirg (2013).

uplift (usually of two to three meters), almost exclusively caused by the downslope movement of compression ridges close to the fronts (cf. discussion below). The subsidence on almost all rock glaciers probably indicates a melting of the internal permafrost and could lead to a climatic deactivation of the rock glaciers in the study area. This interpretation is supported by the fact that surface velocities increase strongly near the rock glacier fronts. The subsidence in the central parts of the rock glaciers could be indicative of thinning by extension, which could lead to a dynamic deactivation of the rock glaciers. A thorough discussion of the spatial patterns of uplift and subsidence and statistics on the vertical change values of each individual rock glacier and their optional single lobes can be found in Neugirg (2013).
Also both the Ölgrube and Riffl Valley rock glaciers have experienced a vertical lifting of their front areas, while surface changes on the remainder of their bodies are lower and more variable (see Dusik (2013) for a (lobe-) differentiated report of the vertical surface changes on these two rock glaciers).
Avian et al. (2009) observed a consequent lifting of the rock glacier surface in the Hinteres Langtal cirque between 2000 and 2008. As the area monitored by these authors represents the lower part of the rock glacier and a decreasing rate of surface lifting during the last three years of their observation period was conspicuous, their results are very similar to the findings in PROSA at the Riffl Valley rock glacier. Both rock glaciers seem to have experienced accelerated movement in recent years, causing a sediment compression at the fronts and subsequent lifting. This acceleration has repeatedly been ascribed to higher temperatures due to global warming.
The rock glacier in the Krummgampen Valley is no exception to the general trend. According to Neugirg (2013), its surface has subsided by circa 0.22 m

between 2006 and 2012. As the quality of the historical SfM data was comparatively good in the region of this rock glacier, it was possible to compare this value with information obtained from a DoD of DTMs from September 8th, 1953 and October 25th, 2012 (cf. figure 6.2.2). While the root zone of the rock

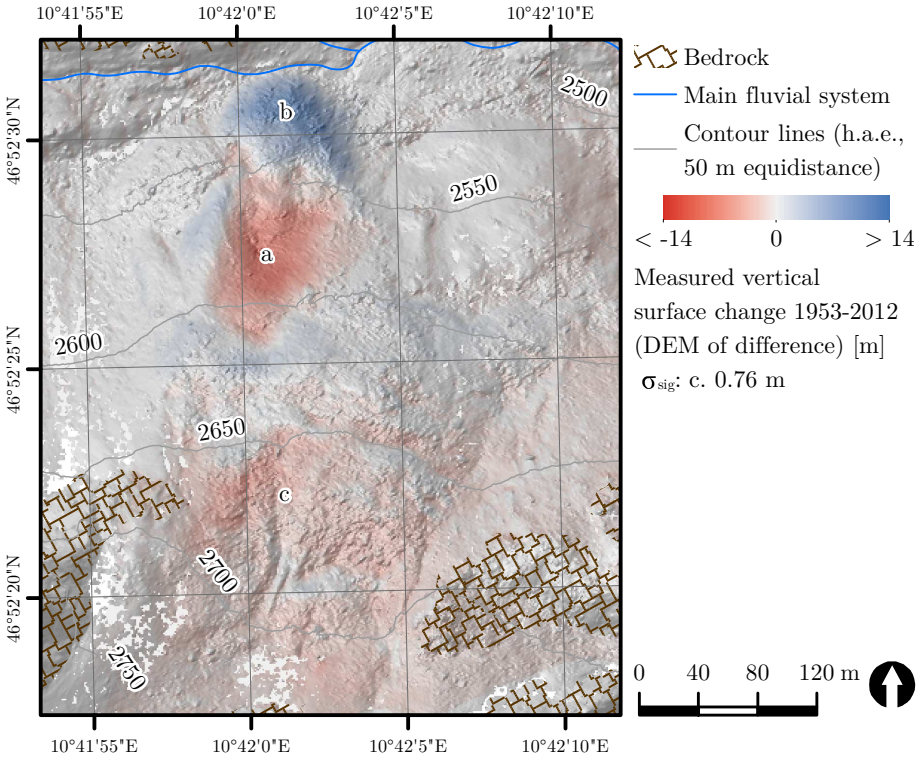

Figure 6.2.2: Vertical changes and front movement of the rock glacier close to the channel in the Krummgampen Valley (ID 8) between 1953 and 2012.

glacier (c) has not subsided much, but only shows signs of horizontal movement (alternating ridges of positive and negative surface changes), it is the front of the rock glacier that has moved about 60 m horizontally (from (a) to (b)). It can clearly be seen that no sediment has been supplied from the root zone to replace the massive amount of material that has moved downslope. This has caused the middle part of the rock glacier to be up to 14 m (a) lower in 2012 than in 1953, while the true right lateral side of the Krummgampen Valley bottom (b) has been run over by a rock glacier body up to 17 m thick, 75 m wide and 60 m long. A quick estimation of the moved mass results in circa 37 700 t (cf. below for sediment percentage and density values). The fact that the moved sediment has not been replaced from the rootzone (which has caused massive rock glacier body extension) is typical for many rock glaciers in the Alps under warmer climate conditions (cf. above). Something that attracts attention is that the rock glacier west (the front is visible between the 2500 and 2550 m contour labels) of the one under discussion seems not have moved at all during the last 60 years while the common root zone (c) seems to have moved by the same amount in its eastern and western parts.

Sediment transfer - Results

Haeberli (1985) has estimated that rock glaciers can be held accountable for 20 % of all sediment transfer in the Alps, while Giardino and Vick (1987, cited in Neugirg 2013) report that about 40–60 % of all sediment transport is accomplished by rock glaciers. Corresponding estimates for periglacial areas in the Swiss Alps are 15–20 % (Barsch et al., 1979, Burger et al., 1999, cited in Neugirg 2013). Today's regional studies, however, estimate the share of rock glacier sediment transport as being as high as 60 %. This transfer, however, is predominantly of internal nature. Only few attempts have been made to quantify the sediment transfer of rock glaciers (Gärtner-Roer, 2012). Most studies content themselves with a determination of flow velocities, probably because the estimation of the mass is so difficult (cf. below).

Seventeen rock glaciers were identified for sediment transfer analysis in the Upper Kauner Valley. Estimation of the masses yielded values between 0.25 and 22.63 Mt, assuming a sediment content of 40 % (Gärtner-Roer, 2012). In summary, a total mass of 52.92 Mt is currently bound within rock glacier bodies in the Upper Kauner Valley. These move, on average (total area), with a speed of $0.17\,\mathrm{m\,yr^{-1}}$ at the surface. Using the measured annual average horizontal displacement rates at the surface, length and width of each rock glaciers body and, again, assuming a sediment content of 40 % and a density of $2.69\,\mathrm{t\,m^{-3}}$ (Hausmann et al., 2012), the total sediment transfer of all 17 rock glaciers in the study area was estimated at circa $21\,497\,\mathrm{t\,yr^{-1}}$.

It must be emphasized that the obtained sediment transfer rate should be regarded as an absolute maximum value. The main reason for this assessment is the fact that rock glacier body thicknesses were estimated using the heights of rock glacier fronts. Rock glacier frontal heights are often higher than the average height of the whole rock glacier bodies as a result of compression effects (Gärtner-Roer, 2012). Many rock glaciers have experienced an influx of a large amount of material due to increased rock glacier velocities as a result of global warming in the 20th century. This has caused even an increased compression and uplift in the frontal rock glacier areas and has also been observed in the study area (Neugirg, 2013).

As in Gärtner-Roer (2012), no information on the internal deformation of rock glaciers was accounted for in this study. It is unlikely that the whole rock glacier mass moves at the speed measured at the surface. Instead, it is expected that flow velocity values decrease with increasing depth in the rock glacier body. The surface velocity represents the cumulative deformation of the whole landform. Information from borehole deformation measurements shows that while some rock glaciers move as one block, only the upper layers move in others (Arenson et al., 2002, cited in Gärtner-Roer 2012). It is very probable that sediment transfer rates are therefore much lower than the ones obtained. However, up to now, there is no reliable method to account for eventual shear horizons in rock glacier bodies in sediment transfer rate calculations (personal communication, Rudolf Sailer, August 22nd, 2016). It is therefore evident that sediment transfer rates given in Gärtner-Roer (2012) and also in this study are absolute maximum values and could be much lower in reality.

In addition, it is known that the velocity of rock glaciers increases from the root zone to the front and from the sides to the center (Berger, 2002, cited in Dusik 2013). While Gärtner-Roer (2012) has used median surface velocity values to

describe the flow velocity of a rock glacier, Neugirg (2013) has used mean velocity values. Given that the mean is more sensitive to extreme values than the median, a more robust result could have been acquired by using the median instead of the mean values.

None but one rock glacier in the Upper Kauner Valley is close enough to the main fluvial system to immediately deliver material to it. It is possible that some of the rock glaciers deliver suspended sediment via the streams emerging from them (as reported from other locations). This, however, is sediment transport by fluvial processes. In addition, no measurements of fluvial suspended sediment transport at rock glaciers snouts have been made by sub-project three. In cases where particles of bed load size are falling into these channels, a transport is very unlikely as the flow velocity and depth of these streams is generally very low (Neugirg, 2013, and own observations). This decoupling function is typical for rock glaciers as they are usually located at positions far above the main fluvial system and the torrents draining them are usually too small to transport any (coarse) provided by the rock glaciers (Wahrhaftig and Cox, 1959, Barsch, 1996, Gärtner-Roer, 2012).
The rock glacier's front in Krummgampen Valley is located right at the lateral side of the channel draining the valley. Historical imagery from 1997 shows coarse sediment from the rock glacier having advanced into the channel with the river flowing through and under the blocks of the rock glacier. It is impossible, however, to estimate the amount of sediment mobilized. It is probable that the sediment was not moved very far from this locations as the channel slope is very low at this location. Guesses are that less than 300 kg of sediment were moved into the main fluvial system at this location.

6.3 Avalanches

The mapping of STAs has revealed that while in winter 2012/2013, STAs were occurring also on south and west facing hill slopes, no STAs could be mapped on south facing slopes in the following winter. Figure 6.3.1 shows the spatial distribution of mapped STAs for winter 2013/2014. Reasons for this include the low amount of snowfall in winter 2013/2014 in combination with relatively warm phases (temperatures above zero) in both January and February, causing the snow on these slopes to melt early and gradually. Mapping results have shown that, most avalanches in the Upper Kauner Valley do not transport sediment to localities where material can be re-mobilized by other processes (cf. below for one exception). The total masses moved by sediment transporting avalanches, however, is not to be scoffed at. In general, the variability in the sediment transported by different avalanches in one winter is very high. This had also been reported by Becht (1995b), who attributes this to differences in soil, vegetation and land use. Similar conclusions can be made for the Upper Kauner Valley. It is conspicuous, however, that transport rates are much higher in areas where shallow soil slip scars are located (especially in the Fernergries area). This confirms the results obtained by Becht (1995b).

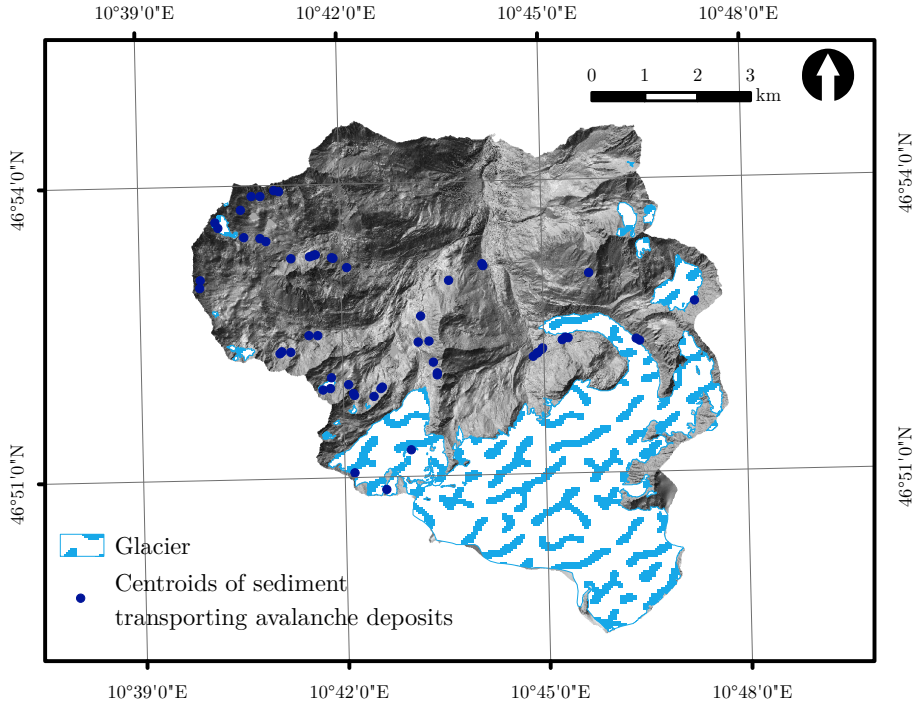

Figure 6.3.1: Locations of mapped sediment transporting avalanches in winter 2013/2014.

The sediment masses transported by single avalanches alone can be very impressive: The 2012/2013 avalanche on the north slope of Vorderer Nörderberg has transported about 41 t of sediment and the two avalanches in the Fernergries (see figure 5.7.13) have transported more than 62 t. In general, the values for sediment transport by single avalanches fit well into the finding by Becht (1995b) who quantified single STAs ranging from 18.4 t for four STAs and 750 t for one enormous single STA from Kesselbach Valley in 1992. Beylich (2000) reports a sediment transport of 30 m^3 by two ground avalanches in Erdalen, Norway.

If the data obtained on the measurement plots is regionalized to all STAs mapped in the two different winters, a total mass of sediment moved by avalanches of circa 276 t on about 31.67 km^2 can be stated for the winter 2012/2013. This corresponds to circa 8.71 t km^{-2} (Näher, 2013) or an denudation rate of approximately 0.003 mm yr^{-1} (using a density of the transported material of 2.7 t m^{-3}) if the total planimetric study area is taken as a reference. For the winter 2013/2014, a total mass of 597 t can be related to a mapped area of circa 36.12 km^2 (Rumohr, 2015), which corresponds to circa 16.52 t km^{-2} yr^{-1} or 0.006 mm yr^{-1}.

Taking the results from the winters of 2012/2013 and 2013/2014, an average 12.61 t km^{-2} yr^{-1} was moved by avalanches in the study area. Given that avalanches are occurring in the parts of the study area that have not been mapped in the two winters at the same spatial density and intensity, an average total sediment mass moved every winter by sediment transporting avalanches of

782.1 t yr^{-1} is estimated.
Again, a comparison with other studies is difficult, as the exact reference area the published erosion rates are referring to and used sediment densities are often not reported (Heckmann, 2006b, Näher, 2013). Becht (1995b), however, gives a value range of 0.01–0.02 mm yr^{-1} for Horlach- and Zwieselbach Valleys and 0.017–0.05 mm yr^{-1} for the Pitz Valley (all Central Alps). This corresponds to circa 28–56 t km^{-2} yr-1 and 47.6–140 t km^{-2} yr-1 (density 2.8 t m^{-3}). These values are higher than the ones found for the Upper Kauner Valley, but the values of 5.9 t km^{-2} and 0.002 mm yr^{-1} found by Beylich (2000) (cited in Rumohr (2015)) are lower (see table 6.3.1). For the reasons mentioned above, the values should be taken with a grain of salt if compared directly. In addition to the problem regarding unknown densities and reference areas in many publications, most values refer to differently long time periods, which further complicates direct comparison.
In winter 2012/2013, a mean deposition value of 2.5 kg m^{-2} or 0.5 mm was found (Näher, 2013), while in winter 2013/2014, a value of 10.5 kg m^{-2} or 2.3 mm was determined. Also, the accumulation mass values obtained from the work in the Kauner Valley are comparable to rates found in the literature. The found rate of 2.5 kg m^{-2} (2012/2013) is in the same range as the 0.4–7.5 kg m^{-2} given by Becht (1995b), 0.004–12.7 kg m^{-2} by Heckmann (2006b) and 0.8–55.4 kg m^{-2} by Eckerstorfer et al. (2012).
As with debris flows (cf. 6.1.2), sediment transport by avalanches seems to be most potent within the proglacial area of the Gepatsch Glacier, a fact that is very likely attributable to the loose sediment stores available on the steep moraines from AD 1855. It is conspicuous that the start and transport zones of STAs are often associated with channels or gullies eroded into the hill slopes. Work on other hill slope processes (debris flows and fluvial transport) has shown that these processes often share the same process areas: The lateral moraines in the Fagge river valley, for example, are shaped by all three processes: fluvial transport, debris flows and avalanches. It seems that also debris flow tracks are a significant sediment source for avalanches. Most avalanches do not transport sediment to localities where material can be re-mobilized by other processes (cf. below for one exception). Of this amount, only a very small portion enters the fluvial system as most avalanches act on the hill slopes of tributary valleys with broad valley bottoms (such as the Riffl Valley or Krumgampen Valley).
It could be observed in only one case that an avalanche has reached the fluvial system directly, that is in the case of a avalanche originating from the true left lateral moraine in the Fernergries area. Fluvial sediment has also been moved from the braidplain onto the avalanche deposit by the impact of this avalanche in winter 2012/2013. This could be proven by Näher (2013) by means of particle size and rounding analysis. The mass, however, is i) very probably negligible and ii) unknown, which is why it was not accounted for in calculation of the overall sediment budget. This avalanche, however, has moved quite an amount of sediment from the 1855 lateral moraine (and parts of the hillslope above) into the fluvial system. Visual interpolation of the outline and sediment cover classes over the gap created by the Fagge river (see figure 6.3.2 on page 187) trough the avalanche deposit yields an area of about 4200 m^2 of the main fluvial system covered by avalanche snow directly after the event. Using an average value of sediment cover from the avalanche snow sampled around the gap created by the Fagge river and melting (as indicated by deposits on gravel bars and

Author, year	**Study area**	**Mass eroded [t km^{-2}]**	**Erosion rate [mm yr^{-1}]**
Rapp (1960)	Kärkevagge (Sweden)	1.4	0.01
Ackroyd (1986)	Torlesse Range (New Zealand)	N/A	0.17
		N/A	0.08 (schist)
André (1990a)	Kongsfjord, Svalbard (Norway)	N/A	0.007 (gneiss)
		N/A	0.08 (schist)
Becht (1995b)	Kesselbach Valley (Austria)	N/A	0.008–0.011 (bedrock)
Becht (1995b)	Pitz Valley (Austria)	47.6–150	N/A
Becht (1995b)	Horlach- and Zwieselbach valleys (Austria)	28–56	0.01–0.02
Beylich (2000)	Aust Valley (Norway)	5.9	0.002
Kohl et al. (2001)	Sölk Valley (Austria)	2500 (Triggering area)	N/A
Heckmann (2006a)	Lahnenwiesgraben & Rein Valley (Germany)	56	0.026
Sass et al. (2010)	Arnspitze (Austria)	126	0.048 (bedrock) 0.07 (loose material)
Ceaglio et al. (2012)	Aosta Valley (Italy)	N/A	0.97–1.24
Moore et al. (2013)	Matter Valley (Switzerland)	N/A	0.01–0.05
This study*	Upper Kauner Valley (Austria)	12.61	0.004

Table 6.3.1: Erosion rates for sediment transporting avalanches published in other studies.
* Mean of the results from (Näher, 2013) and (Rumohr, 2015).

snow remaining on the other side of the river) it is estimated that a sediment mass of circa 1.37 t was delivered by the avalanche to the fluvial system in the winter of 2012/2013. This avalanche has not reached the main fluvial system in winter 2013/2014 (see figure 5.7.13) and the recurrence interval of this event is unknown. It is therefore estimated that the transfer of sediment to the main fluvial system in the Upper Kauner Valley is circa 0.69 t yr^{-1}.

Some weaknesses of the used methods have to be discussed. The problem of

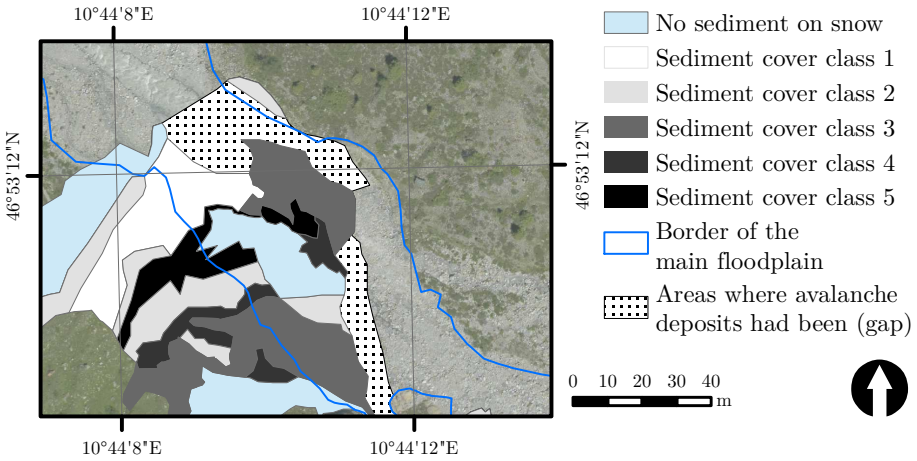

Figure 6.3.2: Map of the avalanche having reached the floodplain in winter 2012/2013.

finding the right time to map the whole, original extent of a sediment-bearing avalanche deposit has been addressed before. This can be confirmed by own observations during field work in the Fernergries (Näher, 2013). This is why the calculated erosion rates should be regarded as minimum values. Another factor to be mentioned is the occurrence of coalescing events in a similar way as has been discussed in the chapter on debris flows 6.1.2. This would especially complicate magnitude-frequency analyzes, but may not be a too significant factor here. Where sediment from two sediment bearing avalanches unifies on a sampled and mapped deposit, it would be assigned a very high sediment class. If the same class is then mapped on other avalanche deposits, it is not of interest if it stems from one or multiple events but the total mass. If the sediment cover is comparable, so would be the masses. It could be observed multiple times that surfaces appearing very dark from afar had only a very thin cover of small-size particles (Näher, 2013). With the framework used in this study, such surfaces would have been assigned to sediment cover class five, which results in a overestimation of the sediment mass transported by avalanches. It is also desirable to further enlarge the database to investigate the variability of avalanche sediment transport in the Upper Kauner Valley to be able to specify reliable confidence intervals for sediment cover classes.
Only data from two winters could be used for mapping and sampling. Considering the very high temporal variability of avalanches in general and occurring in the study area (Luckman, 1977, Näher, 2013), this is a very short time to assess the contribution of avalanches reliably. Based on an interview of a local avalanche expert, Näher (2013) reports that the winter of 2012/2013 had been a "normal" avalanching winter, i.e. "normal" in comparison to historic winters. Changing climate, however, has a severe impact on the number of avalanches in the Upper Kauner Valley and the two winters before 2012/2013 were seen as under average when it comes to avalanches (Näher, 2013). The winter 2013/2014 fits more into this trend, as less sediment transporting avalanches than in 2012/2013 could be mapped. While the total amount of snow fall at

the Weißsee station in the 2012/2013 winter had summed up to circa 943 cm in 2012/2013, only circa 431 cm were recorded in the following winter (Rumohr, 2015). Also the mean winter temperature of the winter 2013/2014 are well above the long term average. The avalanche warning service of Tyrol has classed the winter 2013/2014 as the second warmest in the valleys and the third warmest in the mountain areas in recorded history (Arbeitsgemeinschaft österreichischer Lawinenwarndienste, 2014, cited in Rumohr 2015). This fact of low total snow fall in winter 2013/2014 is also likely to explain that less STAs acting on moraines were recorded in winter 2013/2014, although the total number of avalanches mapped by Näher (2013) is not known (cf. table 5.7.5). The steep moraines on which full-depth avalanches had gone off in winter 2012/2013 are generally located at comparatively low elevations (below circa 2200 m h.a.e.) in the Fagge river valley below the Gepatsch Glacier snout. A snow pack thickness of only 169 cm has been recorded at the Gepatschalm weather station in winter 2013/2014 and also photographs taken in the field in early February 2014 by Rumohr show no heavy snow packs in the area. A comparison of the snow data of the two winters to historical data is difficult, as snow height data for the study area is only available since 2009. It is conspicuous, however, that although less or at least a comparable number of STAs occurred in winter 2013/2014, the total erosion caused by these processes was about double of what has been recorded in winter 2012/2013. This shows that the number of STAs and also the thickness of the snow pack cannot be related to the amount of erosion caused by STAs.

6.4 Fluvial slope processes

6.4.1 Measurements

Detailed information on the exact values measured in sediment trap tubs can be found in Riehl (2015). They range from circa 295 to 172 600 kg km^{-1} for the time period from August 2014 to August 2015. Riehl's results emphasize that sediment yield is highly variable both temporally over the measurement period and spatially, i.e. over the different hill slope channels sampled. Reasons for this variability are manifold and include plausible explanatory factors like vegetation cover or slope (the variance of which was actually taken as a tub placement criterion) and differently strong influence of the tub catchments by anthropogenic activities. For absolute values and qualitative information on the particle size distributions characterizing the sediment collected in the traps see Riehl (2015). It is conspicuous that traps in the Upper Kauner Valley show a higher sediment yields than the ones in the Lahnenwiesgraben catchment. One possible reason includes the higher amount of unconsolidated and unvegetated glacial sediment in the Kauner valley. Still, it must be stated that the values measured in the tub are minimum values as not all small size particles transported in suspension are probably being deposited in the tubs during high flow events (Becht, 1995b). In using the measurements obtained by Riehl (2015), several factors reducing their value need to be addressed:

The temporal measurement resolution was much higher in summer than in winter. In fact, tubs cannot be emptied during winter as they are covered with snow. It is very unlikely that hill slope channels do transport a substantial amount of sediment during the winter months, but as at least some of these sediment traps were located in the process areas of avalanches transport some material could have been transported into the tubs by avalanches or other processes (e.g. gliding on snow). Nevertheless, a closer look at Riehl's measurement data indeed reveals a lower sediment yield during winter than during summer. Two sediment traps, however, actually display heightened sediment transport during winter. These locations are influenced by avalanche sediment transport or are highly influenced by a road crossing their catchments and, therefore, collect a large amount of grit during snow melt. Given the short total measurement time in the study area, interacting effects with other, episodically active processes might have influenced the measured amount of transported sediment significantly. Riehl (2015) reports that at least one sediment trap was located within the potential process area of debris flows and that one trap had been destroyed by a debris flow. It is suspected that fluvial hill slope sediment transport is increased after a debris flow has destroyed a formerly relatively stable fluvial channel structure (Becht, 1995b, Haas et al., 2004). In long measurement campaigns, this effect would be leveled out and contribute to a reasonable degree to the measured fluvial sediment transport in sediment traps. In a short measurement period, such an event could lead to measured sediment transport being overestimated significantly, especially when the number of other sediment traps not affected by such an event is comparatively low (as with the sediment traps in the Upper Kauner Valley).
Several authors have emphasized the great importance of extreme events for fluvial hill slope sediment transport (e.g. Becht et al., 2005). During some extreme events, the sediment traps were filled to the top with sediment (oral communication Dusik, May 6th, 2016). This rendered the data from these traps and the respective time period useless and no quantification of fluvial hill slope sediment transport during these important events was possible. This emphasizes the importance of the virtual sediment traps set in LiDAR DoDs (the data of which has not been provided by sub-project one). One way to alleviate this problem could be the usage of multiple tubs installed consecutively (Rey, 2003).

6.4.2 Regionalization

Discussion of chosen modeling parameters
Modeling results are highly dependent on the threshold values chosen for CIT-Index cutoff, hill slope inclination, channel inclination and distance to channel. Therefore, the used values need to be discussed. Values for these thresholds as used in other studies are given in table 6.4.1
The CIT-Index is a purely topographic index, i.e. it does not incorporate other factors important for channel formation such as geology, soil permeability or vegetation. As these factors are different from catchment to catchment, cutoff values for channel classification have to be determined for each catchment separately (Montgomery and Foufoula-Georgiou, 1993, Thiel, 2013, Riehl, 2015). CIT thresholds found for other catchments are given in table 6.4.1. This also implies, that problems arise when channel networks of large catchments are to

Study	**CIT threshold**	**hill slope inclination threshold [°]**	**channel inclination threshold [°]**	**Location**
Montgomery and Foufoula-Georgiou (1993)	2000	-	-	South Fork Smith River Valley
Haas (2008)	100	20	3.5	Lahnenwiesgraben & Rein Valley
Thiel (2013)	485	30	3.8	Lahnenwiesgraben
	2937	-	-	Zwieselbach Valley
Heckmann and Schwanghart (2013)	-	30–33	2	Zwieselbach Valley
Riehl (2015)	60	25	3.5	Upper Kauner Valley
	700	32	3.5	Horlach Valley

Table 6.4.1: CIT threshold values found in other studies.

be identified as it cannot be expected that the factors mentioned above are constant over space. Corresponding problems also occurred when finding a CIT threshold for channel derivation in the Upper Kauner Valley. The threshold yields a very good channel representation in some parts of the catchment and worse ones in others (see also Riehl, 2015), a fact already observed by Haas (2008), Haas et al. (2011b). In general, model based channel network derivation is more difficult in recently deglaciated areas than elsewhere as the location of channels is not only determined by topography but also by subsurface processes such as macropore flow, flow in shattered bedrock or piping processes (Hastings and Kampf, 2014, cited in Riehl 2015). Shortcomings of the derived channel network in some parts of the study area are probably to be attributed to such factors. The chosen threshold, however, yielded good representations at the sediment trap locations.

As the values found for the CIT-Index are derived from the DEM, it is also the DEM quality that influences the overall result. Riehl (2015) has used a DSM for his modeling efforts. The use of a DTM is likely to improve the quality of modeling results. This had not yet been available when Riehl had completed his work.

The applied model is rather simple using only some factors influencing sediment transport in hill slope channel, all derived from a DTM. Other factors of relevance that were not accounted for include different geotechnical characteristics of the material within the SCA, as these influence water permeability or control mobilization of sediment (see also Hattanji and Onda, 2004, Hastings

and Kampf, 2014, for a related discussion). Some channels are active only intermittently during large rain storm events or during snow melt. As sediment particle size distributions are not a factor accounted for in the used methodology, it is likely that the channel density modeled is to high in comparison to reality. As mean yearly sediment transfer rates are used for modeling, this might not have a great influence on the final total sediment budget, but the SCA as modeled using the DTM-derived LSPs should be taken with a grain of salt. Similar considerations could be of importance when it comes to different subsurface drainage systems of areas of different geology/lithology (cf. Hattanji and Onda, 2004).

Modeling results
SCA derivation for the Horlach Valley revealed values ranging from 7875 to 86 300 m^2 for the different sediment traps.
The SCAs determined for the different sediment traps in the Upper Kauner Valley range from 900 to circa 80 700 m^2. SCA modeling for the whole catchment showed that about 18.37 km^2 (circa 29.6 %) of the study area are identified as sediment contributing areas of hill slope channels (Riehl, 2015). These areas, are not always connected to the main fluvial system, which is a mainly a consequence of the chosen channel inclination threshold. In flat areas, the SCA is limited to the immediate vicinity of the main fluvial system channels. This is in accordance with expert-based assessment. This longitudinal decoupling is mainly caused by anthropogenic surface modifications, rock glacier surfaces collecting all sediment from up-valley and fluvial terraces at the lateral side of the broad valley bottoms (Riehl, 2015).
The model describing the relationship between SCA and mean yearly sediment yield parametrized using data from the Horlach Valley is given in equation 6.4.1. The coefficient of determination of 0.92 and a p-value of < 0.001 indicate a strong and significant relationship between SCA and mean yearly sediment yield.

$$log(M_{\text{sca}}) = -4.65 + 1.76 \cdot log(A_{sc}) \tag{6.4.1}$$

with A_{sc} representing the SCA and M_{sca} standing for the mean yearly sediment yield. Discussing the relationship fitted to the Horlach Valley data, it has to be kept in mind that a time period of 14 years had passed between the collection of sediment trap data (1990–1992) and the LiDAR survey (2006) the DEM of the valley resulted in (which was used as a basis for SCA derivation). Given the high intensities of sediment transfer processes in high-mountain areas, it is very unlikely that the topography of the hydrological catchments of the sediment traps had not changed during this time period. This inconsistency could easily lead to sediment trap data not pertaining to the derived SCAs any more. In fact, corresponding topographical changes in the catchment of one sediment trap in the Horlach Valley (forest road construction) could be observed during a field visit by Riehl (Riehl, 2015). It is therefore surprising that the correlation is as strong as reported above.

Although it was clear from the beginning that tub measurement data from one year is unlikely to be of much use in the SCA model, a model was also parametrized using only the measurement data from the eleven sediment traps in the Upper Kauner Valley. A R^2 of 0.06 and a p-value of 0.29 speak for them-

selves, however.
Equation 6.4.1 was used to estimate the sediment yield on each raster cell on the DTM representing the study area and the sediment contributed to the main fluvial system by the hill slope channels. This estimate is circa $2.5\,\mathrm{t\,yr^{-1}}$. The validation conducted by Riehl (2015) revealed that the correlation between modeled and measured sediment yield at the eleven sediment traps in the Upper Kauner Valley is weak ($R^2 = 0.33$). This validation even leads to an optimistic assessment as no sediment traps had been installed in the highly active lateral moraines of the true right AD 1855 lateral moraine of the Gepatsch Glacier and quantification efforts using "virtual sediment traps" were of not successful (Messerschmidt, 15.06.2016, cf. above).
The spatial distribution of relative high and low sediment transfer in hill slope channels is represented quite well (as no sediment trap data is used for the modeling of the spatial distribution), the absolute transfer values, however, are modeled too low (Riehl, 2015). Riehl's (2015) results are in contrast to findings by Haas (2008), who observed a good transferability of a model from one study area to another. It is not to be expected that a model parametrized in one study area should perform well in another one, especially if the number of used sediment traps is as low as in (Riehl, 2015) and the heterogeneity concerning influencing geofactors is as high as in the studied valleys. The possibility of model parameter transfer has been investigated only very few times before. Therefore, it is too early to draw any final conclusions. Problems concerning transferability had already been observed in Sass et al. (2012). One possible reason for the bad transferability of model parameters from the Horlach to the Upper Kauner Valley is the differently sized sediment contributing areas of the sediment traps in the different catchments. All sediment traps in the Horlach Valley had SCAs bigger than circa $8000\,\mathrm{m^2}$, while many traps in the Upper Kauner Valley have SCAs lower than this. This may lead to a bad modeling result for the sediment yield of contributing areas of sediment traps in the Upper Kauner Valley and contradicts initial findings by Huber. In addition, it is evident that the different areas investigated in the mentioned studies have different characteristics of fluvial sediment transport (e.g. transport limited vs. material limited as the percentage of proglacial areas is different or a different drainage density, causing the parametrization of the model to be not well comparable). Another possible, but less important reason is the certainly inferior quality of the Horlach Valley DEM to the Upper Kauner Valley DEM. It is possible that the Horlach Valley DEM represents the topography less accurately than the DTM of the Upper Kauner Valley. This might have led to methodological inconsistencies in the SCA modeling.
In summary, results show that hill slope channels deliver relatively little sediment to the main channels, the main reason being probably the low discharge of these channels during the sampling period. It cannot be ruled out that (temporary) deposition of fluvial sediment is also occurring in the channels of the hill slopes below the sediment traps and that not all sediment measured will reach the main fluvial system right away. Given the steepness of these hill slope channels, however, the duration of this temporary storage should be comparatively short. This has already been discussed by Becht (1995b) for his study areas and largely also holds true for the Upper Kauner Valley catchment.
The work flow followed by Riehl (2015) leaves room for improvement, independent from the insufficient data basis that has been used (cf. above): No bias

correction during back-transforming sediment yield data has been performed and glaciated areas were not excluded from the model in Riehl (2015). "Glacier" should have been used as a separate target to quantify the fluvial hill slope sediment input to glacial system. Riehl's work flow has allowed water to flow on the glacier surface, therefore directly contributing sediment to the main fluvial system. This does not conform to reality, where respective flows enter the Randkluft and contribute sediment to either subglacial streams or build up (then) subglacial sediment storages.

6.4.3 Estimation of fluvial hill slope sediment yield via ALS differencing

The alternative strategy followed by the author to obtain a more reliable result of fluvial hill slope sediment contribution to the main fluvial system yielded very different results to the ones obtained by Riehl (2015) even though only the probable hotspots in the study area were accounted for (see the end of subsection 5.7.3.2 for the chosen method). Figure 6.4.1 shows the resulting thresholded DoD. Its net balance indicates that about $836\,m^3$ or $1837\,t$ (using a density of $2.2\,t\,m^{-3}$ as measured by sub-project two for this material) have been moved from the lateral moraine to the main fluvial system. This value, however, is undifferentiated, when it comes to which processes have transported the material: The studied lateral moraine is the only location in the study area where debris flows have directly reached the main fluvial system since 2006. More than $190\,t$ of material have been routed to the Fagge river during this time period. A look at the DoD not used for debris flow quantification due to insufficient TLS point cloud reference quality shows that debris flows reached the Fagge river via three gullies in the lateral moraine. This is interpreted as a major event. The event between August 25th, 2010 and September 24th, 2011 has transferred $178\,t$ to the main fluvial system (a value which certainly also includes fluvial erosion). During this event it was also three debris flows having reached the Fagge river (at almost the same locations). The sediment transfer to the main fluvial system in late summer 2014 is therefore estimated as being of a similar magnitude. These considerations lead to a sediment mass of circa $1400\,t$ moved to the Fagge river by processes other than debris flows.
Given that sediment transporting avalanches are not of great importance on the moraine (not much snow accumulates in the steep channel heads of the lateral moraine), it is estimated that the ratio of sediment transported by debris flows vs. fluvial hill slope processes from the true right lateral AD 1855 moraine of the Gepatsch Glacier to the Fagge river is circa 3.7^{-1}. Neugirg et al. (2016c) reports that fluvial hill slope processes erode more material than debris flows. Although the landform he is monitoring is made up of more fine-grained material, this supports the assessment that fluvial hill slope erosion transfers about double as much sediment to the main fluvial system than debris flows in the Upper Kauner Valley. A greater importance of fluvial sediment transport than transport by debris flows on steep moraine material is also reckoned by Neugirg in the Lainbach Valley (personal communication Neugirg, September 13th, 2016). Becht (1995b) also reports that fluvial processes are of great importance for erosion of moraine material.

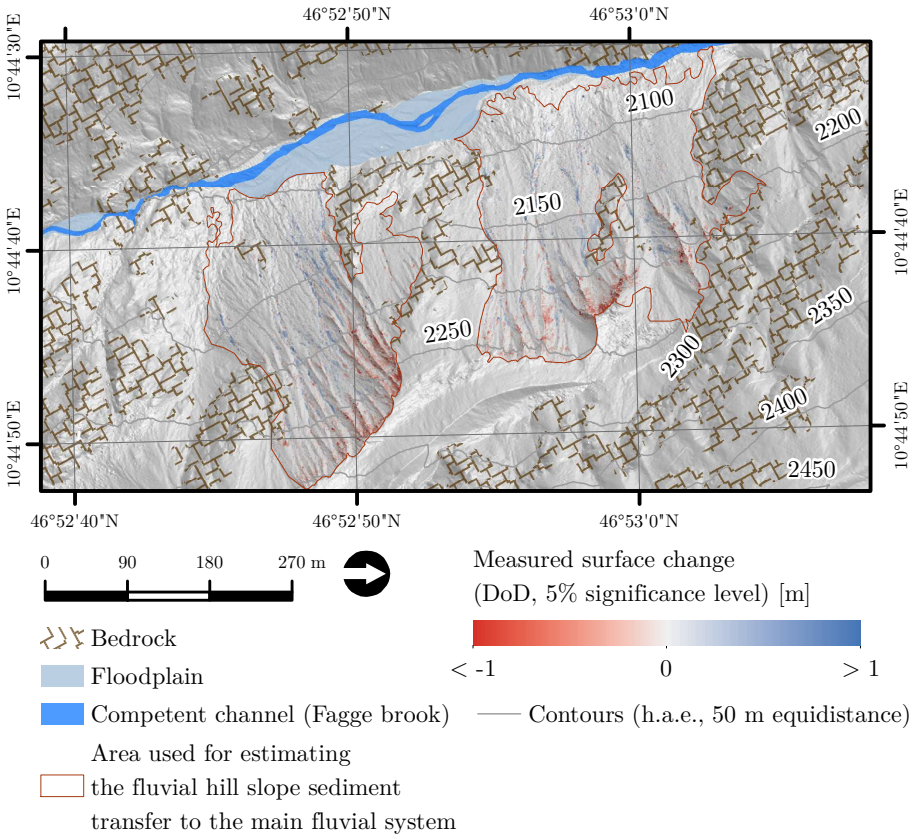

Figure 6.4.1: Erosion and accumulation on the true right lateral moraine of Gepatsch Glacier. Calculated from ALS data dating from July 4, 2012 and July 18, 2014.

As the net balance of the lateral moraine was determined using DTM differencing with error propagation and accumulation bodies by fluvial transport are typically spread out and of low height, it is well possible that some deposition that has occurred on the lower parts of the lateral moraine was not accounted for and that the true amount of sediment having reached the Fagge river by fluvial transport is lower and the debris flow/fluvial transport ratio is higher. Estimating the fluvial hill slope contribution to the main fluvial system at only one location in the study area is probably underestimating the total value. It is likely that the true right 1855 lateral moraine of the Weißsee Glacier, for example, is coupled to the upper reaches of the Riffler river. As this river passes below significant depositional areas downstream, it is improbable that much of this sediment reaches the Fagge river in the Fernergries area (personal communication Becht, July 2016). Another case is a steep slope of unvegetated moraine material at the true left lateral moraine of Gepatsch Glacier, where it is well possible that sediment is transported to the upper reaches of the Fagge river. The slope, however, is very small in comparison to the one balanced via ALS. Nevertheless, the value reported above should therefore be regarded as a minimum value.

As has been shown by the sediment trap measurements at other, more vegetated hill slopes in the study area, sediment transport occurs in these areas. Transport rates, however, are relatively low (mean of all sediment trap tub data: $5.82\,\mathrm{t\,km^{-2}\,yr^{-1}}$) in relation to the sediment transport on the vegetation free lateral moraines ($5830\,\mathrm{t\,km^{-2}\,yr^{-1}}$, using the red bordered area in figure 6.4.1 as a reference). These findings are supported by results by Becht (1995b), who has shown that fluvial transport on non-vegetated moraine material is 1000 times higher than on other surfaces, and that fluvial hill slope transport in other areas is almost negligible. He also reports that fluvial erosion is about 90 % lower in vegetated moraines than on unvegetated ones in the Pitz Valley. It is for these reasons that the value obtained on the AD 1855 Gepatsch Glacier lateral moraine can be see as representative for the sediment delivery to the main fluvial system by fluvial processes in hill slopes in the study area. It is evident that the value obtained from the lateral moraine is about 400 times larger than what has been determined by Riehl (2015) using sediment trap data and SCA modeling. As discussed above, no measurements from the steep unvegetated moraine surfaces were included in his calculations (besides other weaknesses of the approach, cf. above). The discrepancy can therefore be seen as a confirmation of the findings by Becht (1995b). As a result, only the value of circa $700\,\mathrm{t\,yr^{-1}}$ as determined via ALS-ALS differencing on a area of $0.12\,\mathrm{km^2}$ will be used for sediment budget construction.

6.4.4 Excursus: Sediment exhaustion model for lateral moraine storages

As can be seen from the results of ALS-ALS differencing (see figure 6.4.1) the true right 1855 lateral moraine is heavily reworked by fluvial hill slope erosion, debris flows and, to a small degree, also avalanches and rock fall. This has caused the sediment body to be dissected by a number of large gullies. It has been shown by Curry et al. (2006), that such gullies reach their maximum sizes within 50 years from deglaciation and stabilize after circa 80 to 140 years, mainly due to the influence of vegetation.
Sediment yield from a catchment or a storage landform rises fast after deglaciation as a lot of unconsolidated sediment becomes available. The reworking of this sediment does not follow a linear model which is the main reason why measurements of sediment exported from alpine catchments cannot simply be transferred to longer time periods (such as the Holocene) (Becht, 1995b). As the reworking of the unconsolidated sediment progresses, sediment transport rates decline and approach a base level (often called the "geological norm", a term very misleading as rates are not primarily controlled by local geology but, as the model actually tries to underline, availability of unconsolidated sediment) representing sediment transport without the influence of glacial sediment reworking. It is this period of increased process rates that has been termed "paraglacial period", i.e. the period within which sediment transporting processes operate at intensities higher than the norm, due to the sediment inheritance of a glaciated period (Mercier, 2008b). These intensities, higher than the "geological norm" are the sediment transport intensities that can be termed "paraglacial intensities".

Since its coinage, the term "paraglacial" has been used inflationary in all kinds of contexts of high mountain geomorphology. Examples include terms like "paraglacial landforms", "paraglacial processes", "paraglacial systems", "paraglacial landscapes", "paraglacial geomorphology" or even excrescences like "neoparaglacial" (Matthews and Shakesby, 2004) or "paraperiglacial processes" (Mercier, 2008a). Concerning these usages, I want to state that they will not be used in this study as they lack a justification. Processes are fluvial, gravitational, glacial, etc. but not paraglacial. Landsystems are constituted by landforms that are not "paraglacial" but also fluvial, gravitational, glacial, etc. as elements and respective fluvial, gravitational, glacial processes as system links (cf. 2.3). The same holds true for landscapes and branches of geomorphology. The only justification for the term "paraglacial" is, in the opinion of the author, to describe process rates or intensities at a level higher than under conditions of no glacial sediment inheritance, and, to a lesser degree, to refer to the period of time in which these intensities are reached and the mathematical model used to estimate the length of this period. This conceptual model has been used either process-specific, or lumping together all sediment transferring processes (Ballantyne, 2002a).
The conceptualization of paraglacial intensities was cast into a simple negative exponential exhaustion model to allow generalized statements on post-glacial sediment transport rates by comparing model parametrization results from different study sites (Embleton-Hamann and Slaymaker, 2012). An early form of the model was applied to landslides by Cruden and Hu (1993) and it was later adapted to the "paraglacial" paradigm by Ballantyne (2002a). Being an exhaustion model, the model allows to estimate either the amount of sediment remaining for erosion at some instant after deglaciation or the time after deglaciation needed until a given portion of sediment has been eroded from the sediment store(s).

$$S_t = S_0 \cdot e^{-\lambda \cdot t} \tag{6.4.2}$$

where t is the time since deglaciation, S_t the portion of sediment available for mobilization at time t, S_0 the amount of sediment available for mobilization at the moment of deglaciation, and λ the rate of storage sediment loss (erosion). This model can only be used for primary glacial sediment stores. It has been parametrized to different distinct processes/landforms to show the different length of the adaption time (= paraglacial period) of different landscape elements, even rock wall adjustment or modification of glacier forelands (see figure 6.4.2 and Ballantyne (2002a)). The comparison of the models shows that adaption time is much longer, for example, for rock slopes than for moraines. As virtually all high mountain areas had been glaciated during the Pleistocene and their current relief, valley cross-section and major landforms are the result of this glaciation. There is probably no catchment in high-alpine areas that has reached "pre-Pleistocene conditions" as adaption times are very long. Therefore all processes acting in high mountain areas now and even in some thousands of years are operating and will be operating at paraglacial intensities. A usage of the exhaustion model (as in figure 6.4.2), however, can enable comparative investigations in such areas.

With the proglacial areas of Gepatsch- and Weißsee Glaciers being the geomorphologically most active areas in the study area, it was also to be expected that the reworking of lateral moraine storages should follow the negative ex-

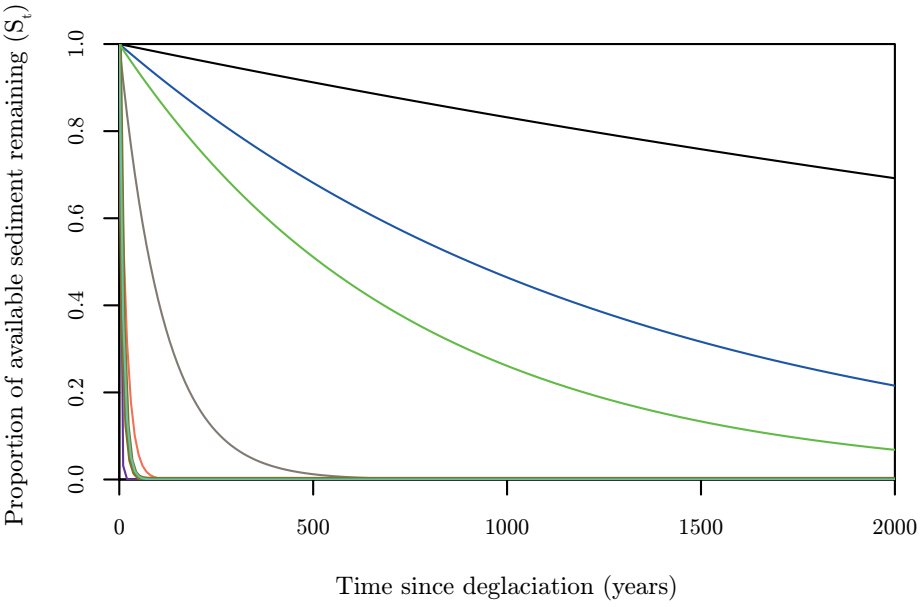

Rock–slope failure: λ = 0.00018 (Cruden and Hu 1993)
Rock–mass deformation: λ = 0.00077 (Hinchliffe and Ballantyne (1999))
Evolution of fines: λ = 0.00268 (Ryder (1971) & Lian and Hickin (1996))
Rock–mass deformation: λ = 0.00883 (Beget (1985) & Bovis (1990))
Gully & debris cone formation:λ = 0.05756 (Ballantyne (1995) & Curry (1999)
Evolution of fines: λ = 0.09868 (Boulton and Dent (1974))
Frost–modification of till: λ = 0.10416 (Matthews et al. (1998))
Moraine stabilization: λ = 0.34539 (Welch (1970) & Sharp (1984))

Figure 6.4.2: Sediment storage exhaustion models of the form of equation 6.4.2 fitted to different single processes or process collectives reworking a landform.

ponential model introduced above. A parametrization of such a model could give insights into the sediment transport on the lateral moraines during the last circa 160 years and therefore enable a more differentiated view on the overall sediment budget as calculated for the years during which the PROSA project maintained its monitoring efforts. To investigate the dependence of the amount of sediment that has been reworked since the time of deglaciation, 20 different historical extents of the Gepatsch Glacier tongue were mapped based on orthophotos and ALS-derived DTMs by the author and sub-project four. Using the outlines of these extents, a representation of the time since deglaciation field was interpolated. Later, all 68 erosion gullies on the Gepatsch right lateral moraine were mapped and the mean time since deglaciation of each gully was calculated before neighboring gullies that had been deglaciated at a similar point in time were grouped into "age groups". As most gullies are located high above the valley floor and the upper areas of them had become ice free while the tongue was still located vertically below these areas, no gully receives a age younger than around 1940. This effect of a glacier tongue loosing thickness but not melting backwards horizontally is also the reason for some older age groups being located higher upstream than younger ones. The location of the

age groups is given in figure 6.4.3, while the mean year of deglaciation of the gullies within the different groups is reported in table 6.4.2. It is evident from

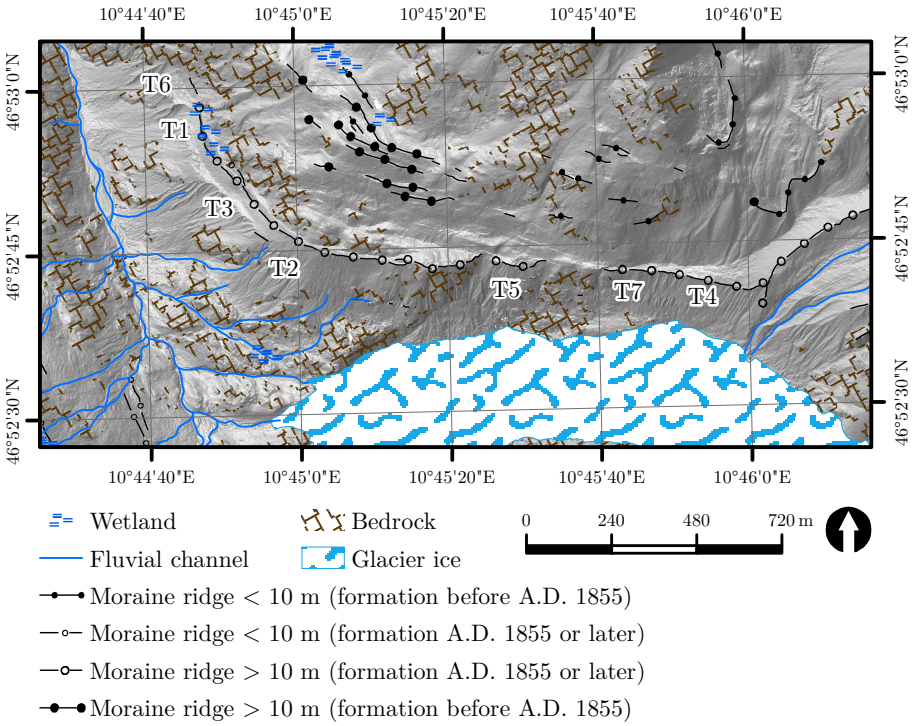

Figure 6.4.3: Location of gully groups of different ages as calculated from the age surface obtained by glacier tongue extent interpolation.

figure 6.4.3, that three of the time since deglaciation gully groups are located above the current glacier tongue. It is therefore likely that the toe of this hill slope is being modified (undercut) on a regular basis, which disturbs the development of gullies following the sediment exhaustion model discussed above. The data set was therefore divided into two groups for the following analysis.
To estimate the amount of sediment that has already been removed from the location of the gully since deglaciation, the extent of every single gully was clipped form a 2012 ALS-derived 1 m DTM and a pre-event surface was reconstructed using spline interpolation before a volume of each gully was determined via DoD calculation (just as in subsubsection 5.7.1.2.1). As the heights of the ridges between gullies were used for this interpolation, the resulting volumes must be regarded as minimum values. In addition to volumes of the 68 gullies, the median inclination of the main flow path in each gully and the planimetric area of each gully were calculated. These three variables, gully volume, median inclination and planimetric area were then related to the time since deglaciation. Curry et al. (2006) found temporally consistent significant correlations between these variables and the four age groups they identified at Fee Glacier. At Gepatsch Glacier, however, the situation was found to be more complicated: There is a significant ($p = 0.03$ in Mann-Whitney-U test) drop in gully planimetric area for gullies deglaciated in 1892 in respect to 1940. This fits the

Age group	Mean year of deglaciation (AD)
T7	1884
T6	1892
T5	1893
T4	1900
T3	1909
T2	1917
T1	1940

Table 6.4.2: Mean years of deglaciation of the different age groups defined on the right lateral moraine of Gepatsch Glacier.

conceptual understanding of gully development as younger gullies should be smaller than older ones. The development of the gullies deglaciated in 1940, however, could be inhibited by underlying bedrock as they are located closed to bedrock outcrops. In addition, the trend of reducing gully planimetric area is not consistent from one age group to the next younger/older one. For example, there is a (not significant, however) increase of gully planimetric area from deglaciation time group 1884 to 1900.
When it comes to median gully floor inclinations, results are more consistent with Curry et al. (2006). Inclinations were found to increase with time since deglaciation in both the gullies above the active glacier tongue ($p = 0.006$ from 1884 to 1900) and downstream of it. The increase for the latter ones, however, is not significant. The relations between gully age groups and cut volume show a similar pattern to what has been found in planimetric gully area, which is not surprising as the variables are expected to correlate.
The fact that the relationship between time since deglaciation and gully variables is less convincing and clear at the Gepatsch Glacier than at the Fee Glacier can be explained by several reasons: First, the lateral moraine studies by Curry et al. (2006) does not show (many) bedrock outcrops or bedrock near the surface. This allows a continuous and undisturbed development of gullies at intensities controlled by slope inclination and the availability of sediment as it is a prerequisite of a successful application of the paraglacial sediment exhaustion model. The proglacial area of the Gepatsch Glacier, however, is much more complex than the one of Fee glacier, with bedrock outcrops inhibiting gully development. Second, the lateral moraine of the Gepatsch Glacier is undercut by the Fagge river from time to time, thereby triggering increased erosion rates in the upslope gullies due to headward erosion. The same problems occurs when the glacier modifies the hill slope downslope the gully groups T4, T4, T7. Third, vegetation development leading to the stabilization of the moraines will proceed differently on slopes located above glacier ice than on slopes downstream of the glacier snout. These results and considerations correspond well with the findings of Harlaar (2015) working on soil formation. Also soil formation does not seem to be primarily controlled by time since deglaciation in the Gepatsch Glacier proglacial area. Reasons given by Harlaar are also, among others, the relative complexity and steepness of the Gepatsch Glacier proglacial area. This shows that the analysis as conducted by Curry et al. (2006) can only be undertaken in optimal conditions for such an analysis, a situation that is not given most of the time in proglacial areas.

As a result, it was difficult to parametrize model 6.4.2 in the forefield of the Gepatsch Glacier. To get a rough estimate of the parameters nevertheless, a large gully that has already become stabilized by vegetation was used to determine the length of the "paraglacial period" in years. Using a value of $S_t = 1\,\%$, λ was estimated. The resulting paraglacial sediment exhaustion model is depicted in figure 6.4.4. The estimated graphical range for the sediment exhaus-

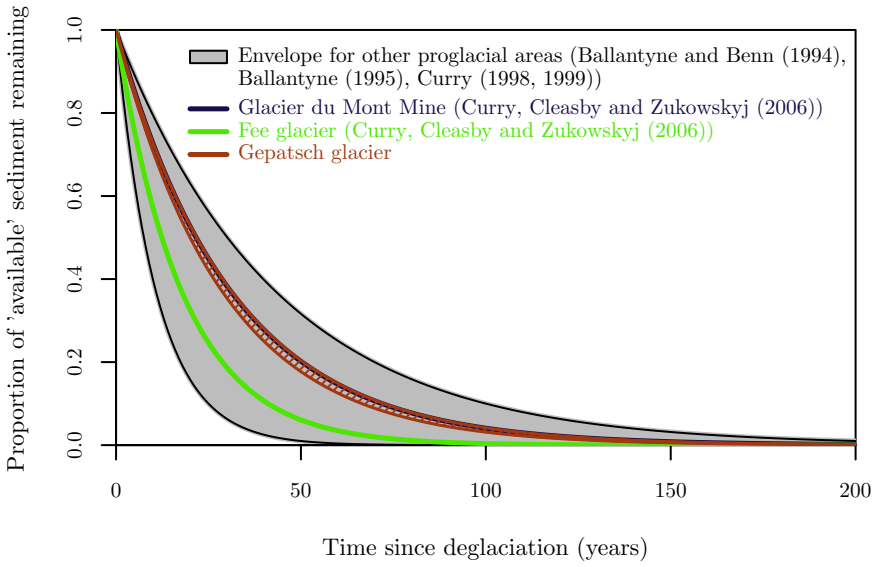

Figure 6.4.4: Different sediment exhaustion models and envelope estimated for the Gepatsch Glacier proglacial area. Figure after Curry et al. (2006).

tion model fits well into what has been reported for the reworking of other later moraine sediment storages (see the figure for references).

7 A process-distributed sediment budget for the Upper Kauner Valley

7.1 The sediment budget

Having quantified and localized all of the relevant (hill slope) processes on the scale of the whole study area of the PROSA project (cf. above), only the sediment transfer and production by glacial processes and sediment transfer rates in the main fluvial system of the Upper Kauner Valley are needed to construct the sediment budget.

Glacial processes
The total sediment budget of the Gepatsch Glacier is not known as it is impossible to measure (everywhere) the erosional work at the glacier basis. Advance has been made by PROSA's sub-project four. The authors have estimated the sediment mass flux and its changes through the glacier tongue using a variety of methods. Their results are published in Stocker-Waldhuber and Kuhn (2016). They estimate the sediment production of the Gepatsch Glacier at 1000 to 100 000 $m^3\,yr^{-1}$, which yields masses of 1700 to 170 000 $t\,yr^{-1}$ using estimated density of the sediment produced at the glacier basis of 1.7 $t\,m^{-3}$ (personal communication Lucas Vehling, 2016).
It has often been reported that the volume of ice within a catchment is directly proportional to the denudation rate of that catchment (e.g. Hicks et al., 1990, Hallet et al., 1996), although exceptions seem to exist (Owens and Slaymaker, 1992, cited in Carrivick et al. 2013). The discussion of increased denudation rates of partially glaciated catchments often neglects the influence of catchment internal factors, such as the role of storage (cf. Harbor and Warburton, 1992, 1993) and connectivity (cf. below). With measurements taken at three different positions downstream of the Gepatsch Glacier snout, some light can be shed on this topic, especially in the context of an extreme event, probably caused by the outburst of a water pocket from the glacier in August 2012.
O'Farrell et al. (2009) have estimated that non-glacial processes account for 80±45% of the sediment yield in one of the two proglacial areas they study (58 % ice-cover), whereas they found a value of $10 \pm 7\%$ in the other one. This shows that the importance of glacial vs. non-glacial processes is probably highly dependent on local factors. Nevertheless, it is stated by O'Farrell that non-glacial processes are probably of similar importance as glacial ones when it comes to their relative importance in sediment budgets of glaciated catchments.
No information is available on the masses deposited as moraines in the forefield to this date. Also, no data is currently available for the other glaciers in the study area, which is why the sediment budget of the Upper Kauner Valley remains incomplete concerning the sediment transfer by glaciers. Only the fluvial

transport at the glacier snout of one of the many glaciers (although it is by far the biggest one) in the study area could be used as a surrogate measure (cf. discussion below). As these values are highly dominated by the glacier water pocket outburst in August 2012, only tentative statements about the relative importance of glacial transport in the PROSA study area will be made.
The differences in relative importance of glaciers identified in the scientific literature in different high mountain areas could be attributed to different rates and styles in glacial recession as this probably highly influences its sediment budget: Fast retreating glaciers release a large area of unconsolidated sediment in a short time, thereby fostering the importance of sub-aerial processes and shifting the relative importance of different processes towards non-glacial ones. How the relative importance of the Upper Kauner Valley's glaciers for the sediment budget will develop in the future is hard to say. While more sediment stores will be cleared from the retreating ice, the export of suspended sediment from below the glacier is highly dependent on the configuration of sub-glacial channels and the possible existence of water pockets that could lead to more extreme events (cf. O'Farrell et al., 2009).

Transport in the main fluvial system
Detailed measurements on the absolute volumes of all forms of fluvial sediment transport in the main stream are needed so that the sediment yield from the other subsystems can be interpreted more accurately (Fenn, 1987, Warburton, 1990). Fluvial sediment transport in the floodplains of high-mountain areas is characterized by steep channel inclinations, a high and turbulent discharge and a strongly altering morphology of the channels. Reasons include the, in general, strong relief and the relatively coarse sediment particles which lead to a high surface roughness at the scales relevant for flow conditions (cf. Wohl, 2000, cited in Dubberke 2014).
Due to increased discharge as a consequence of rapid glacier melt and the high amount of subaerial glacial sediments available in the proglacial area (Krigström, 1962, Morche et al., 2012, cited in Dubberke 2014), sediment transport by the fluvial system in the main channel(s) is of utmost importance in the Upper Kauner Valley. It is fluvial sediment transport in the main channel that ultimately and solely exports sediment from the catchment. The main channels do not only transport sediment from the glacier margins to the basin outlets, but they also integrate all masses finally contributing to the basin sediment export and mobilized by any of the non-glacial sediment transport processes discussed in part 6. As soon as a particle is deposited within the floodplain (either an active, competent channel or on a gravel bar), chances of it being transferred to the basin outlet (in a given time) are much higher than before. However, the main fluvial system[1] does not only transport sediment provided by other processes but actively erodes and deposits sediment from both system internal (e.g. gravel bars) and external storages (e.g. debris cones). This is why, for a full sediment budget, knowledge of the quantities and locations of these erosional and depositional processes in addition to measurement of the overall in- and output of the integrated system are necessary.

[1] I use the term "main fluvial system" in the sense of the fluvial system (with the floodplain) excluding the hill slope channels (which were looked at more closely in 6.4)

For the construction of the sediment budget in the study area, fluvial sediment transfer measurements at two locations are of importance: i) at the glacier snouts and ii) at the basin outlet. Both bed load and suspended load were measured in the river draining from the Gepatsch Glacier snout during the ablation periods of 2012, 2013 and 2014 on an average of circa 96 days per year (during the main discharge period in summer). Average daily transport rates were calculated by the author from this data and are circa $52\,\mathrm{t\,day^{-1}}$ for bed load and circa $173\,\mathrm{t\,day^{-1}}$ for suspended load. Taking a period of 184 days (May to October, pers. communicaton Morche, Oct. 2016) at the period of fluvial transport from the glacier snout (as the subglacial channels are frozen shut during the remainder of the year), a total sediment yield from the fluvial system draining though the glacier snout of circa $41\,400\,\mathrm{t\,yr^{-1}}$ could be estimated.
Often, such vales have been used to determine glacial erosion rates, and, later on, the relative importance of glacial erosion to the sediment transport of a whole catchment (e.g. O'Farrell et al., 2009). O'Farrell et al. (2009) state that this tends to underestimate true glacial erosion rates as it neglects englacially, supraglacially and basally transported debris by the glacier itself. The authors admit that nothing is known about the glacier bed configuration and that temporally increased sediment yield from the glacier is to be attributed to mobilization of subglacial sediment storages but argue that the fact that the "water discharges through a tunnel exiting at ground level suggests that at least near the margin, no overdeepening is present" (O'Farrell et al., 2009, p. 2020). In 2012, also the Fagge river has exited Gepatsch Glacier through a tunnel at ground level. Melting in the following years has revealed a chaotic landscape configuration with alternating whalebacks and sediment storages showing that significant deposition and re-mobilization of material eroded by the glacier is taking place below the glacier. All these considerations also show the conceptual error when using fluvial measurement in the proglacial streams as indicative of sediment transport by glaciers. What is measured here is fluvial transport below the glacier and no glacial transport in any way, which is why no statement on the relative importance of glacial sediment transport can and will be made in this study (cf. above). Only the importance of the transport in the main fluvial system will be addressed.

One of the most important components of a sediment budget is the overall output, that is, the sediment yield of the catchment at its outlet. As the outlet of the study area is located below the bridge across the Fagge river at the upper end of Gepatsch reservoir, it is the amount of sediment transported to the Gepatsch reservoir by the Fagge river that is needed for a complete budget.
At the Fernergries bridge, a location downstream of the confluence of all main channels draining to the basin outlet, discharge was determined by TiWAG almost continuously (on an average of 331 days per year). A rating curve for suspended load was determined by sub-project three, which enabled a calculation of suspended load for the corresponding times. As virtually all water draining through this location stems from glacial streams, a daily transport rate was calculated in analogy to the glacier tongue measurement location. These calculations yielded a transport rate for suspended sediment of $121\,\mathrm{t\,day^{-1}}$ and $22\,267\,\mathrm{t\,yr^{-1}}$, respectively.
Bed load measurements at the Fernergries bridge, however, could not be done as often and continuously as suspended sediment transport, which is why mea-

surements of the topographic change of the Fagge river delta in the Gepatsch reservoir had to be used to obtain an estimate of bed load transport in the Fagge river at the basin outlet (personal communication David Morche). Corresponding TLS surveys of the Fagge river delta were possible because the water level of the reservoir is being lowered by circa 45 m during the winter. The surveys were conducted by the Eichstätt (sub-projects one and five) working groups.
TLS surveys of the sediment fan in the drained Gepatsch reservoir were conducted annually each May from 2012 to 2016. In addition, data from a TLS survey conducted in November 2015 was provided by TiWAG. Only the balances calculated from the TLS data obtained in the years 2012, 2013 (both Eichstätt) and 2015 (TiWAG) are going to be presented here (the data from 2014, 2015 and 2016 obtained by the Eichstätt working group are still to be registered by sub-project one). The topographic changes of the Gepatsch reservoir floor could be surveyed only in the upper third of the lake by TLS between Spring 2012 and Spring 2015. The lake was completely drained in November 2015 but two surveys of the whole lake floor would have been necessary to calculate changes. As can be seen on the digital elevation difference models (figures 7.1.1 to 7.1.3), different extents of the lake floor could be surveyed from year to year. This also implies that the volume presented in table 7.1.1 are representative of different extents of the Fagge river delta. To make the value directly comparable, the extents would have had to be reduced to the joint extent covered by all surveys. The 2012 point cloud was acquired with the LMS-Z420i device and contains much more data gaps than the other survey products (see colored area in figure 7.1.1). This would have excluded large areas from the delta survey for the other time periods. This is why such a clipping was not undertaken for this study.
Using data from only three time steps spanning a period of only three years makes it difficult to obtain reliable mean annual sediment transport rates, especially when an extreme event has occurred during this time period. With an extreme discharge event having occurred in the Fagge river in August 2012 (Baewert and Morche, 2014), a long time mean sediment yield value was estimated by setting off the 2015 TLS data and a DTM constructed from a photogrammetric point cloud constructed from aerial images of September 1st, 1954 (see table 5.4.3 and figure 5.4.3). This model represents the topographic state of the reservoir bed before the construction of the dam and can therefore be used as a long-term baseline.
As the whole subaerial area of the delta exposed every spring is too large to be surveyed using only a single scan position, a total of five scan positions were set up around the delta.[2] Between circa 13 (2012) and 100 (2013) Mio. points were acquired in the TLS surveys. The point clouds were then registered to a common local coordinate system by sub-project one. As some vegetation is present at the lake's banks, these areas were excluded from volume change calculation by using mapped vegetation masks. Areas showing minor deltas of tributary streams at the sides of the area of interest were also masked as only the sediment delivered by the Fagge river was to be quantified. Quantification then was accomplished using a DTM cell size of one meter. The overall level of detection was estimated using the stable area technique (see subsection 5.5.2.2) and volumes were converted to masses using a density of $2\,\mathrm{t\,m^{-3}}$ (as recommended by

[2] Positions 25–28 and 35, positions 42 and 44 are an alternative for position 28 if it is not accessible (cf. appendix three).

David Morche, personal communication July 15th, 2016).
The obtained overall levels of detection and the balances obtained for the investigated time periods 1954-2015, 2012-2013 and 2013-2015 can be found in table 7.1.1. The corresponding significant elevation difference models are presented on the following three pages.

Time period	σ_{sig}	**Volume (unthres.) [$\mathbf{m^3\ yr^{-1}}$]**	**Volume (thres.) [$\mathbf{m^3\ yr^{-1}}$]**	**Mass (unthres.) [t $\mathbf{yr^{-1}}$]**	**Mass (thres.) [t $\mathbf{yr^{-1}}$]**
1954–2015	0.44 m	3223.52	3191.83	6447.04	6383.66
2012–2013	0.12 m	7593.25	2404.27	15186.50	4808.54
2013–2015	0.12 m	23898.70	24418.22	47797.43	48836.43

Table 7.1.1: Results of the sediment yield quantification efforts using point cloud data of the Fagge river delta in the Gepatsch reservoir. All values are rounded to two decimal places. The period 2013–2015 included the summers of 2013, 2014 and 2015 and was therefore regarded as representing three years (see discussion in the text).

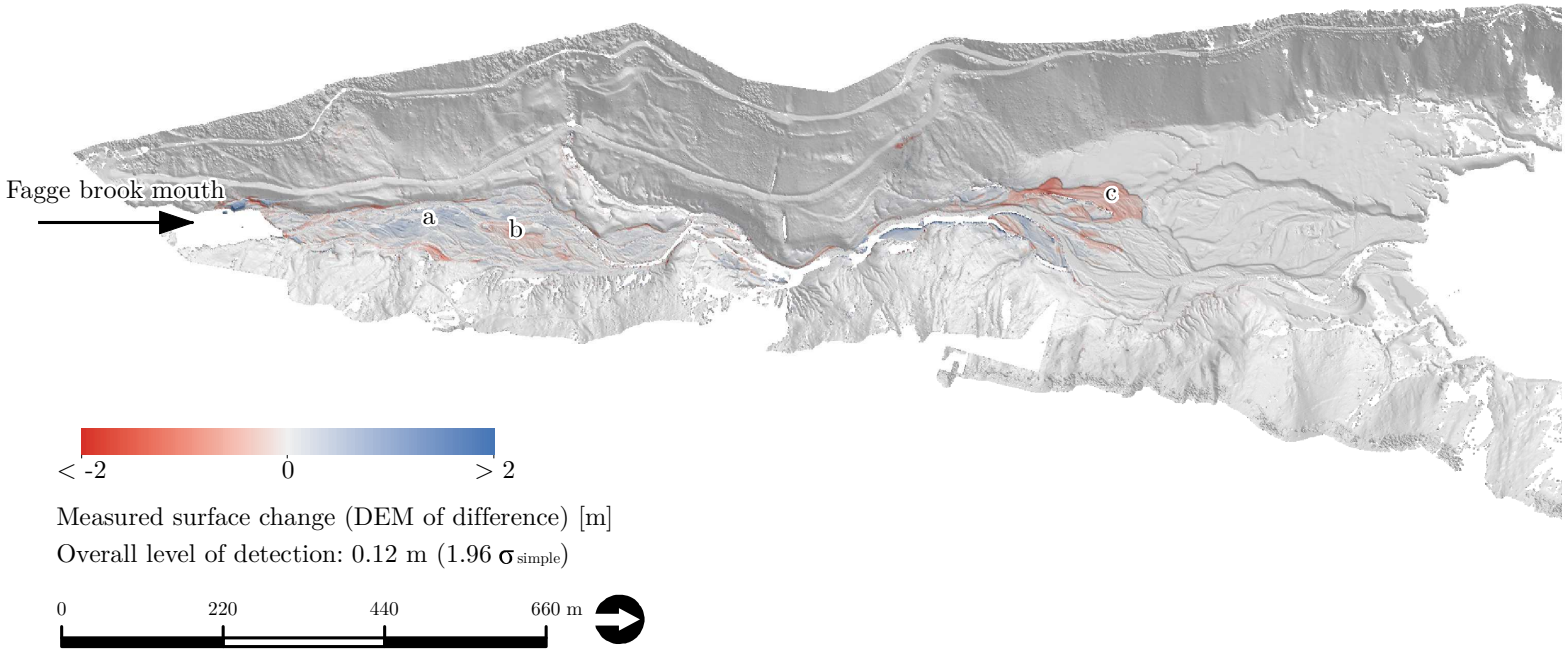

Figure 7.1.1: Significant difference grid for the time period from 2012 to 2013. The hillshade represents the state/extent of data of 2013. The water table in 2012 was located just to the north of letter (c). See the text for a short discussion.

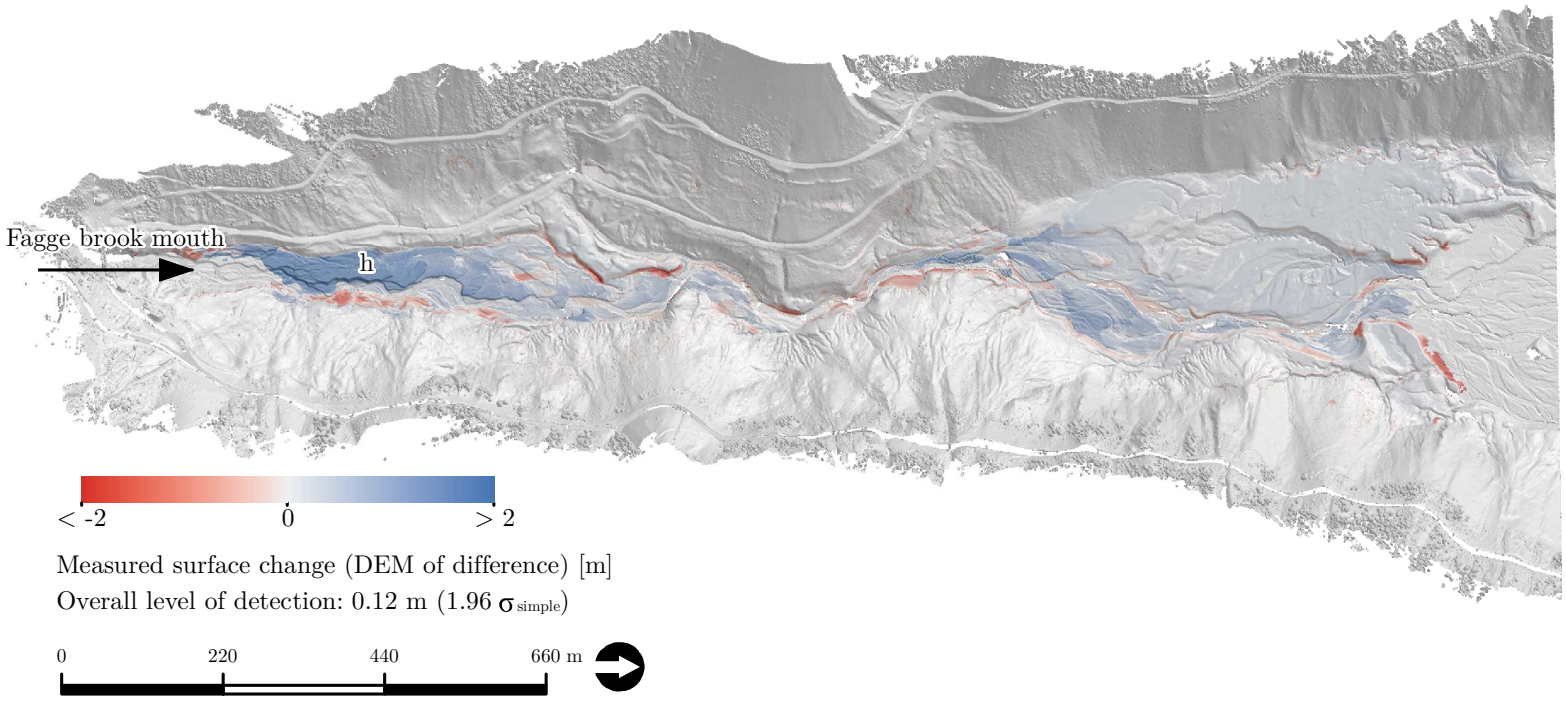

Figure 7.1.2: Significant difference grid for the time period from May 2013 to November 2015. The hillshade represents the state/extent of data of November 2015. See the text for a short discussion.

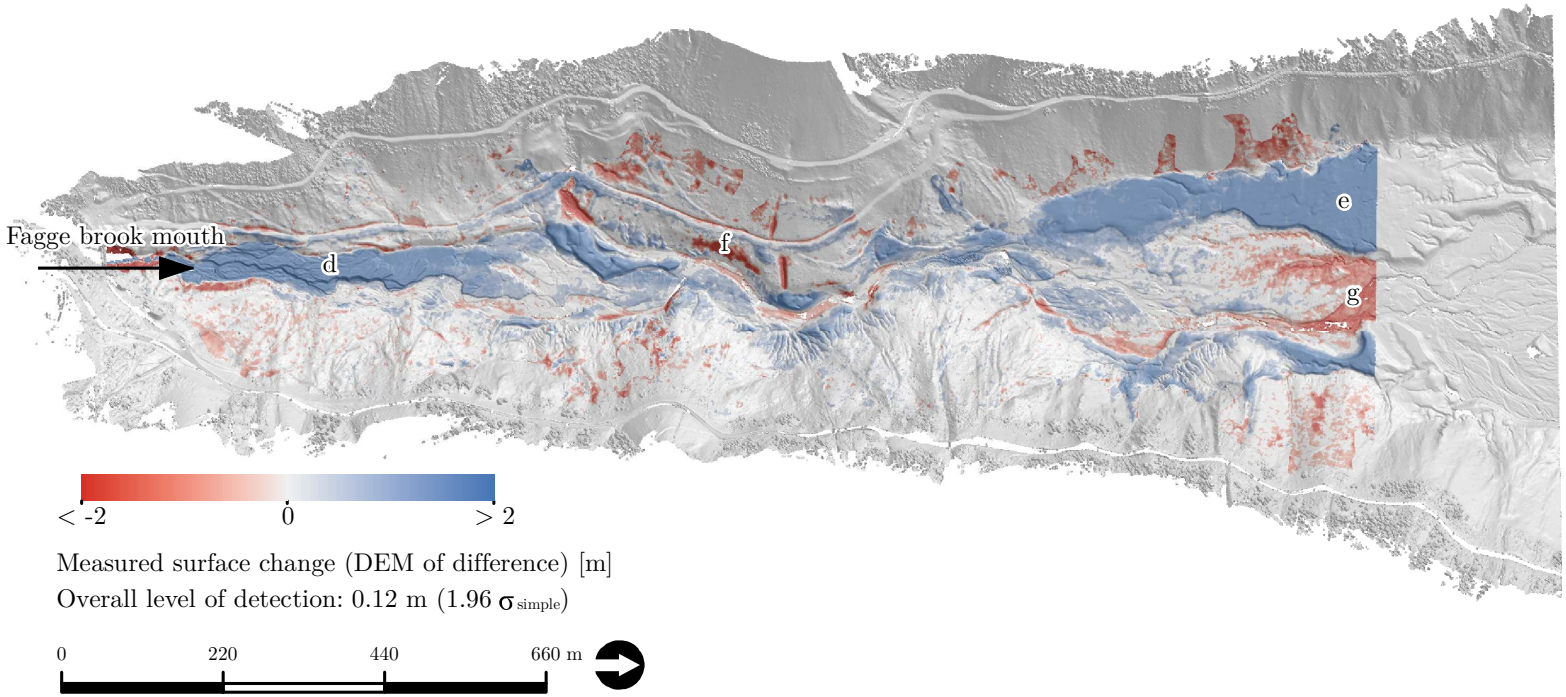

Figure 7.1.3: Significant difference grid for the time period from 1954 to 2015. See the text for a short discussion.

Figure 7.1.1 shows the topographic changes in the delta from 2012 to 2013. Geomorphic change is concentrated to the central and proximal (in relation to the Fagge river mouth) part of the reservoir (letter (a)). These changes are indicative of bed load deposition occurring as soon as the stream reaches the standing water body of the reservoir. This main bed load deposition area is also subject to reworking, probably as soon as it emerges from the water during winter, as the Fagge river undercuts gravel bars, etc (b). This reworking of delta sediments by the river is most evident near the water table of 2012 (c). It is obvious that a large amount of sediment has been eroded from the delta and moved into the water, a fact that makes budgeting difficult (cf. below). A discrete and high accumulation of sediments is well visible at the river mouth. It is well possible that this is sediment piled up by road workers who remove sediment from the delta on a regular basis as road repair material (cf. below). The volume quantification gives a positive balance of just over 4800 t (see table 7.1.1). This value is about 25 % lower than the average value determined for the time period 1954–2015. Due to the rapid enlargement of the proglacial areas upstream in that time period, a higher value was expected by the author. This is where the erosional zone at location (c) (or in other words, the fact that not the whole lake floor could be surveyed), probably shows its adulterating influence. A look at the unthresholded DoD reveals that a large amount of positive values just below σ_{sig}. Some of these cells are certainly representative of errors. Some others, however, show spatial contiguity and could therefore well represent areas of low deposition. The corresponding balance of the unthresholded DoD is 7593 m^3, a value much higher than the long term average. This is probably due to the largely positive errors mentioned above. Looking at the areas that probably represent low depositional areas just below the overall LoD, it is likely that the balance is somewhere close to the long-term average for the period 1954–2015.

The topographic changes for the time period May 2013 to November 2015 is shown in figure 7.1.2. What is immediately evident from the DoD is the huge accumulation body (letter (h), showing accumulation heights of up to circa 6 m) just downstream the Fagge river mouth, which also accounts for the lion's share of the large total positive balance of circa 73 254 m^3 calculated for the 2.5 years/three ablation periods.[3] Also the other surveyed areas show largely positive changes. This calculated balance value of just above 70 000 m^3 now is representative of the reworking of the sediment that had initially been deposited in the gravels beds within the study area during the extreme event of August 26, 2012 as reported by Baewert and Morche (2014). This means that about 77 % of the material stemming from the water pocket outburst and accumulated within the floodplain of the Fagge river was transported out of the catchment in the following three ablation periods. This finding and interpretation is supported by results of sub-project three (David Morche, personal communication August 15th, 2016). The result of this sediment wave reaching the delta after three years is also responsible for the high yearly balance values of circa 24 418 m^3, that is circa 48 836 t yr^{-1} calculated for this period. It can also be expected that the balance of the ablation period 2016 will be higher than the long term

[3] A time period of three years was used for the calculation of the yearly value in table 7.1.1, as this time period includes three ablation periods. The topographic change having occurred in the delta in Winter 2015/16 was regarded as insignificant as sediment transport is mainly limited to the warmer months (personal communication David Morche, July 2016).

average, as still circa 23 % of the material eroded by the 2012 extreme event was present within the study area in November 2015 and will have been reworked to some degree in summer 2016. Of course, another reason for the high amount of sediment having reached the reservoir in that time period could be the general strong melt of Gepatsch Glacier in more recent years and the successive exposure of sediment stores in the upper end of the proglacial area.
It is conspicuous that the thresholded and unthresholded balances for this time period are very similar. This is very probably due to the fact that most topographic changes in this time period are way above the LoD of 0.12 m.
The long term average value was calculated by setting off the photogrammetrically derived point cloud of September 1954 and the TLS point cloud of November 2015. Figure 7.1.3 shows the corresponding elevation difference model. It is evident that the accumulation body stemming from the reworking of the 2012 extreme event is also conspicuous in the 1954–2015 DoD. This implies that this event is also significant for this long time period. A total balance of + c. 194 701 m^3 was determined for that time period. This means that 37.6 % of the material accumulated (and having stayed) in the visible delta since 1954 are to be attributed to the 2012 extreme event. It is evident that quite some sediment must have been reworked and transported to the more northern parts of the lake during that time, but the percentage value is very impressive nevertheless. This result underlines the importance of extreme events for sediment transport in high mountain rivers.
In all difference grids, also internal sediment transport in the storage area was observed. Most of the time, it is not possible to identify the accumulation bodies pertaining to these delta internal sediment movements as the sediment was moved into the part of the lake still covered by water or because it is indistinguishable from the sediment stemming directly from the study area. In the former case, it is possible that the erosional scar causes the net balance to be calculated as too low.
During the extreme discharge event in August 2012 most of the mobilized sediment was deposited in the Fernergries. During this event, about 70 000 m^3 were removed from the upper proglacial area while about 90 000 m^3 were deposited in the lower proglacial area. Therefore, about 20 000 m^3 must have been flushed from the glacier bed (Baewert and Morche, 2014), allowing a glipse at the relative importance of glacial processes for the overall sediment budget.

The methodology and values on fluvial sediment transport in the main channels used to construct the sediment budget will be discussed in more detail in the following. Despite the availability of study-area wide ALS data, all of the measurements acquired by sub-project three have been made within the proglacial zone of the Gepatsch Glacier. Nothing is known about sediment storage changes within the main fluvial subsystem in the Riffler river upstream of the Fernergries bridge. This, however, is not regarded as a great problem, as the large sedimentation areas between the measurement station and the Weißsee glacier prevent much sediment from being transferred to the Fagge river from this part of the catchment (personal communication Becht, July 2016).
22 267 $t\,yr^{-1}$ of suspended sediment transport had been determined at the TiWAG measurement location (Gepatschalm) during the three ablation periods 2012–2014. Assuming that all sediment (including the suspended one) has been deposited in the area surveyed by TLS in the delta and that the reworking of

the sediments mobilized during the extreme event was temporally uniform[4], this implies that the bedload share of the sediment exported from the study area is 11 893 t yr^{-1}, or circa 34.8 %.

The calculated mean annual bedload yield over 25 years of monitoring (1964–1989) from the Fagge river to the delta is estimated at 7192 m^3 yr^{-1} using data from Tschada and Hofer (1990), which yields roughly 10 000 t yr^{-1} using a density of 1.39 t m^{-3} (this value is valid for bedload sediment with components < 64 mm personal communication David Morche, August 25th, 2016)[5]. However, the data given by Tschada and Hofer (1990) and used for this estimation had been obtained by averaging data obtained at the Taschach and Pitz rivers as no sediment transport measurement station is located at the Fagge river.
The same strategy was followed in the estimation of suspended sediment transfer in the Fagge river. As a result, the amount of suspended sediment transport by the Fagge river at its outlet from the study area is estimated (such calculations are necessary as Tschada and Hofer use the total catchment of the Dam site as a reference for their sediment yield data) at 26 598 m^3 yr^{-1} or circa 47 876 t yr^{-1} for the time period 1964 to 1989, assuming a density of purely suspended load deposits of 1.8 t m^{-3}, as used by Tschada and Hofer (1990).
The value of 22 267 t yr^{-1} determined for suspended transport in the time period 2012–2014 is lower than the one obtained using Tschada and Hofer's data but of very similar magnitude. However, the value obtained by the PROSA project should still be a minimum estimate: It is certain that not all suspended sediment had been deposited in the area surveyed by TLS. This can be seen in figure 7.1.3, where large areas of homogenous sedimentation are evident which obviously continue to the north (letter e). This shows that sedimentation has been taking place far from the delta from 1954 to 2015 and there is no reason that this has been different in recent times. The true bedload share in the sediment exported from the study area is therefore probably higher than 34.8 %. As the bedload transport is quantified by offsetting the suspended sediment transport measured in the Fernergries and the TLS measurements, the total mass of bedload must also be higher. The relative coincidence of bedload transport values by Tschada and Hofer (1990) and in this study is encouraging, nevertheless.
The results concerning the share of bedload in the sediment transport of the Fagge river at the outlet fits well into the values reported in the literature: Church (1972, cited in O'Farrell et al. 2009) reports a bedload percentage of 20–80 % in Arctic environments of Baffin Island. 30–60 % are reported by Østrem (1975) and Bogen (1989, cited in O'Farrell et al. 2009) for glacial streams in Norway. A percentage of circa 20 % has reported for the Pitz river by Lauffer and Sommer (1982) in 1982 for the Pitz Valley, which was glaciated to a degree of 60 % at that time (Becht, 1995b). Other authors, however, report bedload

[4]This is not very likely, but as the TLS point cloud from 2014 is yet to be registered, this assumption has to be made. The average mass exported from the catchment during this period was therefore estimated as $(2 \cdot 48836 \text{ t yr}^{-1} + 4808\text{t yr}^{-1}) \cdot 2^{-1}$ (cf. table 7.1.1).

[5]The value was determined by sub-project three by averaging the densities of sediment samples of 17 different distinct size classes ranging from 0.2 to 64 mm (lower class boundary). Naturally, a mixed sample of bedload sized sediment would have been preferred. As the grain size distribution of bed load in the Fagge river is not known (and is also dependent on flow conditions), not representative mixed sample could be used. Initially, the values seems to be low. It must be kept in mind, however, that "pure bedload" sediment contains many large pores.

transport as being in ranges from 4 to 20 % (Emmett, 1975, cited in Dietrich and Dunne 1978) and (Dietrich et al., 1982). The difference in these values is probably due to the different percentages of glaciated terrain present in the different study areas as there is a very strong correlation between suspended load [t km^{-2} yr^{-1}] and percentage of glaciated terrain (Becht, 1995b, Tschada and Hofer, 1990).
The Gepatsch reservoir is not only fed by the Fagge river draining the study area. A series of small tributaries reach the lake from the cirques located above on both sides (e.g. the Bligg torrent, the main channel of the Kaiserberg Valley, etc.), causing the natural catchment of the reservoir being as large as 107 km^2. It is evident that these rivers also transport sediment into the reservoir. With only the upper third of the reservoir floor being surveyed (cf. above), however, it is not very likely that a significant amount of sediment transported by these tributaries was included in the TLS balancing efforts for the Fagge river delta. Where corresponding sediment accumulations could be attributed to one of the side-tributaries, they were masked during the quantification efforts (cf. above). In addition, several rivers and torrents from neighboring valleys had been diverted to the Gepatsch reservoir to reach the planned annual water level. Measures included a diversion of the Pitz, Taschach, Radurschl and Tschey rivers, causing the overall hydrological catchment area of the Gepatsch reservoir to increase to circa 279 km^2 (Wiggenhauser, 2015). The water intakes of these diversions (except the one from the Taschach river) are equipped with Tyrolean weirs (with sediment screen racks and de-silting chambers) (Tschada and Hofer, 1990). This is why it is correctly assumed by Wiggenhauser (2015) that no significant amount of bedload is contributed to the Fagge river delta by these water diversions. Tschada and Hofer (1990), however, report that only bedload is prevented from reaching the reservoir via the diversions. The mouth of the Pitz Valley diversion is located just north of the area that could be surveyed by TLS. It is therefore possible that some, but not very much, of the sediment accumulations surveyed by TLS are from the Pitz Valley diversion and that the TLS measurements yielded values overestimating the sediment export from the study area. The total amount, however, cannot be known.
Another source for potential uncertainty in the mean yearly sediment yield from the study area are extreme events. Work by Dubberke (2014) and observations by the author in the field have shown that the main channel of the Fagge river is spatially unstable on the temporal scale of even months or a few years. Especially important in this context are extreme flood events truncating non-fluvial sediment storages (such as debris fans or talus cones) (Warburton, 1992, Baewert and Morche, 2014). During the 2012 extreme event, a discharge of 47.3 m^3 had a significant impact on the sediment budget of the whole basin is reminiscent of the findings by Warburton at Bas Glacier d'Arolla, where large magnitude, low frequency flood events are the dominant control of sediment transfer in the proglacial zone (Warburton, 1990).

The sediment budget

Bringing together the results for the different processes treated above, a first tentative representation of the Upper Kauner Valley's sediment budget can be presented in figure 7.1.4. The main fluvial system is represented as a thick blue arrow, while the contributions by hill slope processes are indicated by thinner black arrows. Process names are given in small caps, the time periods the values refer to are written in brackets. I am fully aware that the reference periods

should be the same for a valid sediment budget. Most of the (intermediary) results provided by different sub-projects, however did not correspond to the exact same time period. One reason for this is that the ALS data from July 2014 did not cover the whole study area. Rock glacier velocity rates, however, were based on IMCORR feature tracking, which required a representation of all rock glaciers in a ALS DTM. The latest DTM covering the whole study area available (to date), however, dates from fall 2012. Debris fall, on the other hand, could have been balanced using the time period 2012 to 2014 as a reference period. As the results are based on measurements from only a small area of all rock walls in the study area, values measured in 2015 were included to enhance the reliability of measured values. Values next to a circular arrow represent internal sediment transfer (with no sediment delivery to the main channels).
It is typical of sediment budget studies that obtained values are associated with relatively high uncertainties, especially in catchments displaying a high relief and topographical heterogeneity (Sanders et al., 2013). This holds true even more when the studied catchment is comparatively large and processes are studied only for a few years (cf. discussion in part 2). All these unfavorable conditions are met in the Upper Kauner Valley. Nevertheless, a sediment budget has been constructed and will be discussed in the light of the problems mentioned above in the following.
The first fact that is conspicuous from looking at figure 7.1.4 is that the sum of sediment masses delivered to the main fluvial system from hill slope processes (circa $2000\,\mathrm{t\,yr^{-1}}$) is much lower than the sediment exported from the catchment. This is where the already discussed extreme event from August 2012 has left its mark (as it has eroded extreme amounts of sediments from the river banks) and is also indicative of a possibly increased fluvial sediment delivery from below the glacier. However, it is not clear how much of the sediment eroded from the banks and how much sediment could have been mobilized from the glacier bed, just as it is not know which percentages of the sediment pertaining to each of the two sources has been deposited in the main fluvial system. Looking at the export value for the year 2012 (see table 7.1.1), when the sediment wave from the extreme event had not yet reached the basin outlet, the difference to the total sediment mass delivered to the main fluvial system by hill slope processes is lower, but the ratio is still about 2.5^{-1}. This shows that a substantial amount of the sediment must be i) exported from below the glaciers of the study area and/or ii) eroded by the water in the main channels from its banks and/or iii) mobilized from the channel beds in the main fluvial system. Measurements by sub-project three have shown that an enormous amount of sediment is exported from below the snout of Gepatsch Glacier, actually more than is deposited in the Fagge river delta (cf. above). This supports the interpretation that the excess material has been exported from the Gepatsch Glacier and much of it has been eroded from the glacier bed at some point in time or entered subglacial streams more or less directly from the slope surround in the glaciers. The amount of bedload exported from the glacier snout is numbered lower than the mass calculated from the discrepancy between total amount of sediment deposited in the delta and the suspended sediment load obtained in the Fernergries area. Regarding the considerations concerning the share of bedload in the total sediment exported from the catchment made above, the measurements of working group three made at the glacier snout do not fit in: The value for suspended load is too high, while the bedload estimate is too low.

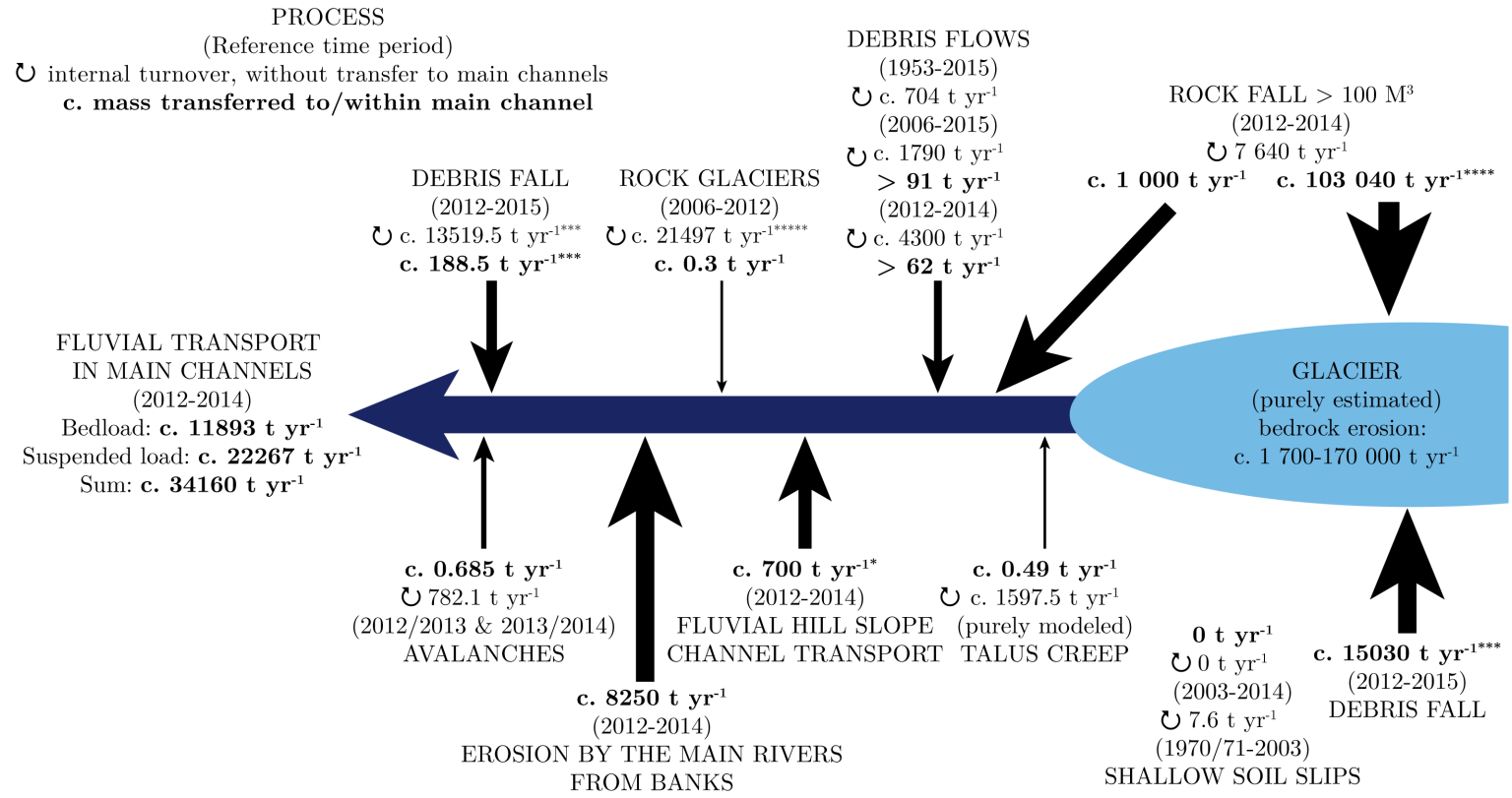

Figure 7.1.4: Upper Kauner Valley's sediment budget for the time period 2012 to 2014 (see discussion in the text).
* Only true right lateral moraine of Gepatsch Glacier.
** Mobilized on unvegetated soil surfaces.
*** Strategy two.
**** Including debris and boulder fall from the "Schwarze Wand".
***** Maximum value (whole body moving at surface velocity).

This discrepancy can be explained in two ways: i) Fluvial sediment transport measurement (especially bedload) at the glacier snout by sub-project three could be less accurate than the estimations based on the TLS measurements in the delta by the Eichstätt working groups and ii) significant erosion and deposition processes were active in the floodplain between the glacier snout and the suspended load measurement station of sub-project three in the Fernergries area. The respective contribution by this process, however, has not been investigated by sub-project three. A quick estimation by the author via differencing ALS data from July 2012 and July 2014 yielded a mass of circa 8250 $\mathrm{t\,yr^{-1}}$ having been mobilized by the main rivers themselves from their banks. It has been observed, however, that much of this sediment has been deposited just downstream of the locations it has been mobilized from and it is not known which portion of this mass has been transported through to the outlet in relation to material of other origins.
Another source of error is the anthropogenic modification of the sediment transport in the Upper Kauner Valley. Anthropogenic sediment transport has been observed multiple times and various locations within the study area or at the Gepatsch reservoir delta: On a regular basis sediment is excavated from the main fluvial system just below the Fernergries bridge, from the delta head at the reservoir (cf. figure 7.1.5) and from the floodplain within the proglacial area of the Weißsee Glacier. It is unclear how much sediment is moved during these

Figure 7.1.5: Sediment removed from the Fagge river delta and stored for further usage in construction (May 12, 2014). Master student Sebastian Wiggenhauser for scale reference.

measures and no information can be obtained from the company in authority (personal communication David Morche). In addition, it is not known where the sediment has been moved to during each excavation activity.

Usually sediment transfer or erosion data is presented in mass-based units such as masses moved annually (t $\mathrm{yr^{-1}}$). As a result, however, it is very difficult to compare processes of, for example high frequency and small magnitude (such as small-scale rock fall) with processes continuously transporting huge amounts of sediment but at a very slow quasi-constant rate (such as rock glaciers or rock slides). As a result, the potential energy transformed has been estimated for the geomorphic processes where possible. The results are given in table 7.1.2 Rock falls of different magnitudes are dominating the sediment transfer on hill slopes in the Upper Kauner Valley, followed by rock glacier transport and de-

Process	t yr^{-1}	GJ yr^{-1}
Block and cliff fall	111680**	44.1 + 90**
Debris fall	28738	49.3*
Rock glaciers	< 21497	N/A
Glacial transport	prob. high	N/A
Main fluvial system	> 8250	N/A
Debris flows	4300	2.47
Creeping permafrost on talus	1597.5	N/A
Avalanches	782	N/A
Fluvial slope processes	> 700	N/A
Bergsturz	130	0.34–0.68***
Shallow soil slips	7.6	N/A
Rockslides	N/A	> 9.08***
DGSDs	N/A	< 0.06***

Table 7.1.2: Comparison of different geomorphic processes investigated by the PROSA project in terms total mass moved and potential energy transformed. Please see figure 7.1.4 for the corresponding reference time periods.
* Strategy two. Using his slope threshold and SCA derivation and height difference estimation (flow algorithm) techniques, Vehling (2016) arrives at a value of circa 17 GJ yr^{-1}. This value is much lower than the one found using strategy two, which was estimated using actual modeled debris fall trajectories.
** Vehling (2016); Including debris and boulder fall from the "Schwarze Wand".
*** Vehling (2016)

bris flows. The relatively high internal (i.e. decoupled from the main fluvial system) transfer by talus creep is explained by the high proportion of talus surfaces in the study area. Avalanches transport a substantial amount of sediment but cannot compete with other processes, while shallow soil slips seem to have ceased activity in recent years. Overall, sediment transfer in the main fluvial system is of greater importance to the total amount of sediment exported from the catchment than all hill slope processes combined, which is mainly the result of transport of sediment flushed from below the snout and mobilization from the banks (esp. during the extreme event).
As can be seen from table 7.1.2, it was only possible to estimate the potential energy transformed for some of the investigated processes. While it could be possible to obtain the respective values for avalanches, rock glaciers and creeping talus creep if more information is obtained from the different subgroups in the future, it is hardly possible to estimate the potential energy transformed for the other processes. Obtaining Joule values for avalanches would require the mapped sediment transporting avalanches of the winter 2012/2013. Unfortunately, the mapping results seem to be lost (personal communication Martin Näher, 2014). A calculation of 3D movement vectors for rock glaciers would enable an estimation of the Joule value for rock glaciers. Appropriate data evaluation had been planned in sub-project one, but has not been completed so far (personal communication Dusik and Haas, 2016).
It is very conspicuous that rock falls of magnitudes > 100 but $< 1 \times 10^6\,m^3$ are much more relevant for sediment transfer in the Upper Kauner Valley than debris (and block) fall. The energy transformed by these high magnitude events is far higher than the one of small magnitude rock falls. In addition to the

higher total mass mobilized, this can also be explained by the higher vertical distances negotiated by the debris (Vehling, 2016). Because of their long recurrence intervals, bergsturz events are of minor importance among rock fall processes in the Kauner Valley. This result is different to what both Krautblatter et al. (2012) and Caine (1986, cited in Vehling 2016) report from their study areas. Krautblatter et al. (2012) state that bergsturz events, followed by debris fall are of greatest importance when it comes to sediment transfer in the Rein Valley, Northern Calcareous Alps. The importance of bergsturz events in the Rein Valley, however, is caused by large joint systems organizing the high and very steep rock walls composed or otherwise compact rock in the Rein Valley. Vehling (2016) concludes that although extreme magnitudes are less effective than smaller ones, it is "extreme locations" that are very important: The "Schwarze Wand" rockslide complex is a source of small magnitude rock fall releasing about two times the total mass of what is mobilized at all other rock walls combined. A dominance of rock fall of small magnitudes is reported by Sanders et al. (2013). As Vehling (2016) correctly states, however, this could be the result of the short measurement/reference period their results refer to.
Studies that have compared the relative importance of different geomorphic processes in high-mountain areas are rare. Södermann (1980) reports from a catchment in northern Finland, slope wash is the most important process with sheet erosion accounting for circa 28-62 $\mathrm{mm\,yr^{-1}}$, values for other processes are either not given or only in cm $\mathrm{yr^{-1}}$. Warburton (1990) has determined a relative importance of different processes for the proglacial zone of the Bas Glacier d'Arolla. As his measurements were only conducted for a short time during the 1987 ablation season, they are not directly comparable to the result obtained in this study, based on a monitoring program spanning several years (no data on avalanche sediment transport is available from Warburton (1990), for example). In general, however, the results seem to complement one another: Warburton has found transport in the channels dominating the sediment transfer in his study area, followed by hillslope processes (including rock fall) and slope wash being of minor importance. Beylich (2000) gives a ranking of many geomorphic processes following their relative importance in terms of total mass transfer (i.e. independent to the respective contribution to the main fluvial system) in Aust Valley, East Iceland, thereby ranking aquatic slope denudation first, followed by geochemical denudation, avalanches, debris and boulder falls, talus creep, debris slides and flows and deflation. This is very different to what has been found in the Upper Kauner Valley. Reasons include, among others, the relatively low relief in Beylich's study area (which relates to the occurrence of comparatively few rock walls), the absence of a glaciers (and corresponding land forms) and rock glaciers. In addition, a much larger percentage of Aust Valley is vegetated.

7.2 Importance of proglacial areas

It has often been reported that geomorphological activity is more intense within the proglacial area than outside (Carrivick et al., 2013).
It has also been shown repeatedly that rock fall is more intense in areas of recently deglaciated areas because debuttressing of the rock walls destabilizes

them (Kellerer-Pirklbauer et al., 2010, McColl et al., 2010, McColl, 2012, Nagelisen et al., 2015). Similar observations have been made in the Upper Kauner Valley:
Rock fall measurements at the rock fall collector nets have revealed that rates within the proglacial area(s) are generally higher than in the remainder of the catchment, a statement that is also supported by the rates obtained by Vehling (2016). He reports that (depending on the scenario used by him for regionalization), rates for debris fall (without the contribution of the "Schwarze Wand") range (using only the bedrock surface areas of the study area as a reference) between 0.72 and 0.92 $\mathrm{mm\,yr^{-1}}$ for the whole catchment. If the non-proglacial area alone is looked at, the rates drops to circa 0.29 $\mathrm{mm\,yr^{-1}}$ (Vehling, 2016). Vehling gives the greater rock mass strength of these areas as a reason.
It is also conspicuous that more than 80 % of the rock fall events larger than 100 $\mathrm{m^3}$ (see subsection 6.1.1.2) since AD 1850 have become detached from rock walls within the proglacial area close to the current or former glacier tongues of Gepatsch and Weißsee Glaciers (Vehling, 2016).
The fact, that about 75 % of all debris flows detected and quantified for the time period from 2006 on occurred within the proglacial areas of either Gepatsch or Weißsee Glaciers underlines the spatial activity focus of this process in areas of recent deglaciation.
Shallow soil slips, however, are an exception to the general rule of higher activity in proglacial areas. Although no new shallow soil slips have occurred in the reference time period 2012–2014, it is notable that most older scars are located outside the 1855 moraine ring. Scars are primarily found on Egesen or Daun lateral moraines or in soil developed on top of talus. The only location with a concentration of shallow soil slip scars within the proglacial areas of the Upper Kauner Valley is in the Fernergries. Their occurrence, however, is likely to be influence by their location on top of the DSGD and the avalanches occurring in this area.
A concentration of rock slides and DGSDs in the proglacial area has been stated by Vehling (2016). Of the active of these process complexes, almost all (the ice-rock slide "Weißseespitze", the rock slide complex "Schwarze Wand" and the DGSD "Fernergries") are located either in the proglacial areas or above a glacier tongue (see section 6.1.4). This fact is attributed to rock wall debuttressing after the LIA. The same spatial pattern can be identified concerning fossil rock slides and DGSDs in the study area: Vehling (2016) states that these (most notably the fossil part of the "Vorderer Nörderberg" DGSG complex) are located in comparable positions in reference to the glacier extents during the Egesen stadial.
Increased sediment transport in hill slope channels in the proglacial area has also been measured. Riehl (2015) reports that the two sediment traps showing the highest values are both located in (vegetated) 1855 lateral moraines and attributes the increased values to the reworking of LIA sediment stores.
The importance of fluvial erosion of the main channels in the proglacial areas is very high (cf. above). Warburton (1990) noted that circa 95 % of the sediment eroded in the proglacial zone he studied were mobilized by a melt water flood event that lasted only three days. The extreme event 2012 in the study area can be seen in the same light. The amount of sediment mobilized from the banks and (probably) also flushed from below the glacier display the great importance of these processes in the Upper Kauner Valley between 2012 and 2014.

7.3 Overall average lowering rate for the catchment

The average lowering rate of the whole basin (L) can be easily calculated from the sediment mass exported at the catchment outlet and the average bedrock density (after Dietrich and Dunne (1978)):

$$L = \frac{Q_S + Q_D}{d_b} \tag{7.3.1}$$

with Q_S being the fluvial solid load sediment discharge at the catchment outlet, Q_D the fluvial dissolved load sediment discharge at the outlet and d_b the average bedrock density in the catchment. Given a total export of solids of circa $0.55\,\mathrm{kg\,m^{-2}\,yr^{-1}}$ (cf. figure 7.1.4) and a average bedrock density of $2.7\,\mathrm{t\,m^{-3}}$ and neglecting dissolved export (as no values are available), a lowering rate for the Upper Kauner Valley of about $0.2\,\mathrm{mm\,yr^{-1}}$ is determined. This value is above the average reported by Hinderer (2001) for catchments in the Alps and of same magnitude of surface lowering and denudation rates reported for different catchments in the European Alps (cf. table 7.3.1, (Otto et al., 2009)). Also Norton et al. (2011) report average surface lowering rates for Alpine catchments of 0.17 to $1.4\,\mathrm{mm\,yr^{-1}}$. Given that average surface lowering rates of partially glaciated alpine catchments have often been reported as being comparatively high, the (low?) value for the Upper Kauner Valley is surprising at first. However, it has already been stated above that probably not much sediment is leaving the sub-catchment of the Riffler river because of extensive sedimentation areas in the floodplains upstream. If the denudation rate is calculated in reference to the sub-catchment of the Fagge river alone (which also contains the lion's share of glaciated terrain in the Upper Kauner Valley), a value of circa $0.3\,\mathrm{mm\,yr^{-1}}$ results. Another possible explanation for the rather low denudation rate is the fact that many of the sub-catchments are decoupled from the main fluvial system, either by rock glaciers blocking the upper part of the valley (Riffl Valley, Innere Ölgrube) or by fluvial sedimentation areas (Krummgampen Valley). Some of the hanging valleys in the Upper Kauner Valley are covered by coarse sediment, preventing channel formation and are stabilized by vegetation (Kühgrube, Äußere Ölgrube) with only very small and clear rivers draining from them. The decoupled sub-catchments cover roughly one third of the whole study area. Considering this circumstance, the rate for all of the Upper Kauner Valley seems to be realistic. An extremely high denudation rate ($4.6\,\mathrm{mm\,yr^{-1}}$) has been reported by Carrivick et al. (2013) from Ödenwinkelkees catchment. This is about double the amount of what has been maximally reported in studies elsewhere. They suspect both the high amount of unconsolidated material in their study area as well as a relatively short observation period as possible reasons for this very high value. Their data, however, are not strictly comparable. As Carrivick and colleagues admit, it could be the fact that their value incorporates also catchment-internal sediment transport. Their value is therefore not comparable to the ones reported in table 7.3.1. Carrivick et al. (2013) suggest that their denudation rate should be comparable to values

Location	**Denudation rate [mm yr^{-1}]**	**Time period**	**Method**	**Source**
Walensee, Switzerland	> 1.5	15×10^3 yr	Lake archive	Müller (1999)
Himalaya catchments	2	last 6×10^3 yr	Fan volume	Shroder et al. (1999)
Upper Rhone Valley, Switzerland	0.95	Late + postglacial	Lake archive	Hinderer (2001)
Alps (mean)	0.62	Late + postglacial	Tectonic basin archives	Hinderer (2001)
Bündner Rhine, Switzerland	0.58	Quaternary	Export measurements	Jäckli (1957)
British Columbia, Canada			Lake archive	Owens and Slaymaker (1992)
Alps (mean)	0.13	Present day	Export measurements	Hinderer (2001)
Rhone/Brig, Switzerland	0.35	Present day	Export measurements	Schlunegger and Hinderer (2003)
Rhone/Port de Scex, Switzerland	0.15	Present day	Export measurements	Schlunegger and Hinderer (2003)
Vispa/Visp, Switzerland	0.72	Present day	Export measurements	Schlunegger and Hinderer (2003)

Table 7.3.1: Export based average surface lowering rates for entire alpine catchments found in the scientific literature.

of 1 to 10 mm yr^{-1} obtained by Hallet et al. (1996) using suspended sediment discharge in proglacial streams.

7.4 Conclusion and outlook

Fostered by the new possibilities in catchment-wide sediment transport quantification, the effectiveness of sediment transport in whole catchments, i.e. "the sediment delivery problem" (Walling, 1983) has attracted more notice again. While sediment transport quantification via LiDAR is relatively easy, an identification of process link areas and, ultimately, modeling the whole sediment transport system of a catchment or even only on a single slope is still very diffi-

cult. Research on this topic is, therefore, very important. Quite some research has been undertaken, although under a new catch phrase that emphasizes the focus on the transport system inherent to the scientific work being undertaken: "connectivity".
While scientific work on hydrological and biologic connectivity has a relatively long tradition in their respective fields (e.g. Schreiber, 1988, Schumaker, 1996), work on sediment connectivity, especially in high mountain areas, has seen a rise only a few years ago. Examples of relevant work include Caine and Swanson (1989), Borselli et al. (2008), Chiverrell et al. (2009), Thiel (2013), Heckmann and Schwanghart (2013), Messenzehl et al. (2014). Many of the recent studies on connectivity, however, focus on a topological, qualitative analysis of the sediment transport system, i.e. only the structural connectivity is being looked at and a validation is omitted. In addition, many geomorphological studies on connectivity honor only fluvial transport while transport by other processes is being dropped (Bracken et al., 2015).
In general, slope and fluvial systems are not well coupled in the study area. This implies that only a small amount of material is transported directly from sediment storages on the slope to the main channels. A look at the sediment budget (which also gives internal sediment transfer/mobilization rates) reveals that while about $34\,160\,\mathrm{t\,yr^{-1}}$ have left the catchment between 2012 and 2014, about $50\,000\,\mathrm{t\,yr^{-1}}$ were mobilized but did not reach either the glacier or the main fluvial system. If the fact that this export value is much higher than the historic average (due to the August 2012 extreme event), and that an addition $120\,000\,\mathrm{t\,yr^{-1}}$ of rock fall being deposited on glacier ice, often far from the main fluvial system, it becomes evident how disconnected the sediment transport system in the Upper Kauner Valley really is. If all sediment mobilized is summed (almost $180\,000\,\mathrm{t\,yr^{-1}}$) and an export rate of about $7000\,\mathrm{t\,yr^{-1}}$ (educated guess based on the long term average, excluding the 2012 extreme event) is assumed it becomes evient that only about 4 % of all moved sediment in the study area reach the outlet. This is not untypical for glacial valleys, as their broad valley bottoms often lead to an uncoupling of the main fluvial and hill slope subsystems. Similar results are reported by Beylich et al. (2011) from Erdalen, Norway or Austdalur, Iceland. Not many studies have tried to establish a sediment budget for meso-scale catchments or have even quantified more than one sediment transferring process in such a catchment. In addition to the ones discussed in chapter 7.1, Vorndran (1979) (cited in Becht 1995b) has established a mass balance for the Sextner river catchment in Southern Tyrol but has not differentiated between different processes. Becht (1995b) has quantified different geomorphic processes in the Eastern Alps.
Even less sediment budgets have been established using LiDAR data as a main source and as there is no calibration curve facilitating a comparison of remote sensing budgets and hydrological monitoring budgets makes a comparison of the results obtained in the PROSA project to previous work difficult.
Several research gaps had been identified from the current state of sediment budget research at the beginning of this thesis (cf. 2.4) and corresponding research goals had been developed. Looking back at these research goals, several statements can be made and research gaps for the future are identified. In addition, recommendations for future research concerned with sediment transfer in high mountain areas can be made:

To show that spatially and temporally highly resolved catchment-wide LiDAR data can be successfully applied as a main source to establish a sediment budget of a meso-scale high mountain catchment.

It could be demonstrated that spatially and temporally highly resolved catchment wide LiDAR can be used as a main source to establish a sediment budget of the size of the Upper Kauner Valley. The massive data base, however, could only be processed and evaluated by applying partially automatic work flows as much as possible and by investing large amounts of computing time and manpower. The management, administration processing and evaluation of umpteen different TLS scans from almost 40 different monitoring stations and billions ALS measurement points could only be accomplished using data management on a dedicated server with a server-client interface that could be addressed in scripts. Point cloud classification (see subsection 5.4.4) took several months of calculating time and over 500 single man hours of correction work. It is the opinion of the author that the qualitative performance of automatic vegetation classification will not improve significantly in the near future, which means that the total classification time could only be reduced by speeding up the automatic part of the work flow, which can be done by applying more powerful CPUs. The DEMs obtained from the catchment-wide ALS point cloud data, independent of their origin, was precise enough to measure geomorphic processes directly all over the study area (e.g. debris flows (5.7.1.2.1) or large magnitude rock falls). This allowed to reduce the amount of geomorphic processes that had to be measured on the plot scale and regionalized to the catchment scale. Nevertheless, it could also be demonstrated that ALS data is not precise enough to measure processes operating at low magnitudes but quasi-continuously over a time scale of a few years. These processes include fluvial hill slope erosion on shallow soil slip scars, deposition of debris fall on talus landforms or avalanche deposits. It might be possible to detect the former two with very high resolution TLS data. This, however, is only possible on the test plot scale and not at the scale of a meso-scale catchment. TLS data served as a measurement basis for debris fall in sub-project one (cf. subsubsection 5.7.1.1.1) and the obtained intermediary results were used as one of two data bases for debris fall regionalization. Due to the large target distances, however, the resulting DoDs are often geomorphologically not very convincing, which is why the author regards the measurements obtained in sub-project two as more reliable. The quality of TLS data could be improved by choosing scanner positions much closer to the rock walls. This, however, would reduce the area of rock walls surveyed, hence the data basis, but results would certainly be more convincing.

SfM has proven to be a powerful tool to generate point clouds even if the user has no formal education in photogrammetry. Point clouds and their derivatives could be obtained from historical images and long-term sediment movements could be detected. A decisive weakness of photogrammetry-derived point clouds remains that no points can be obtained below forests or other vegetated areas. This makes a vegetation classification/removal based on point neighborhood statistics difficult. Vegetation removal based on color is no help with black-white historical images. Similar problems occur when using color images for photogrammetry-based point cloud generation as not all vegetation or objects that prevent the calculation of a DTM are of the same (green) color. This is why the author would always favor high-density LiDAR data over photogrammetry-

derived data, an opinion that is shared by Wichmann (personal communication Wichmann, October 2014). This strength of ALS data could be used to obtain spatially highly resolved DTMs of the whole study area as a basis for process modeling and mapping. DTMs from ALS data served as input for modeling debris fall (see section 5.7.1.1.1), permafrost (5.6.3), which served as a data basis for geomorphological mapping (5.6.1) and served as an input for modeling fluvial hill slope erosion using the SCA model (5.7.3.2). To sum up, it is evident that the point cloud data of various origins served as the main source for the construction of the Upper Kauner Valley sediment budget.
One recurring factor for the scientific work in this thesis was the large size of the study area. The combination of methods and size of the study area has given the PROSA project and also this thesis a unique position, but this also meant that the processing and generation of all data bases has taken a large amount of time. The preparation of the geomorphological-geological map, the (almost finished) preparation of the land cover map, both at a scale matching the spatially highly resolved LiDAR data, and the processing of point cloud data alone (without acquisition and georeferencing work) required a lot of work before a combination and evaluation of the data could be started. A second factor impeding the sediment budget research in the Upper Kauner Valley has been the significant anthropogenic impact. 1.3 % of the planimetric study area have been modified by human interventions. This may not sound much, but the affected areas are often geomorphologically highly active (e.g. the proglacial area of the Weißsee Glacier) and human interventions even include sediment transport (see chapter 7.1). Regarding the usage of point cloud data for sediment transfer measurement, the melt-out of permafrost and dead ice below the surface and the spatially and temporally irregular occurrence of snow (patches) has been a recurring challenge. To prevent topographic surface changes related to these processes, areas usable for balancing had to be chosen very carefully and masks had to be prepared to exclude negative values on the DoDs stemming from ice or snow melt for sediment budgeting. Given a 62 km^2 large catchment and a very large point measurement data base, this was a time consuming task.

To quantify sediment transport rates of all relevant sediment transporting processes in close collaboration with the relevant working groups from the PROSA project.
Transport rates on permafrost creep, debris flows, rock fall of different magnitudes and fluvial slope erosion have successfully been determined in this thesis, often using input data from other sub-projects. Quantification was accomplished methodologically in a diverse manner: Depending on the process under investigation, methods/techniques included, among others, test plots (5.7.2.3), spatial modeling (5.7.1.1.1), regression analysis (5.7.1.2.1) and differencing of DTMs of various origins (5.7.1.2.1, 5.7.3). Sometimes, (intermediary) results from other sub-projects were reviewed and used. These were also of diverse methodological origin, ranging from test plot or sediment trap data (e.g. 5.7.1.1.1) to finished rates (6.1.1.2).

To use the results of the quantification efforts of the other working groups in PROSA as a basis for a (model-based) regionalization of sediment transport rates to the catchment scale to obtain a sediment budget.
Most of the measurements obtained by own work or in the other sub-projects could be used for a regionalization. Strategies differed among processes: While it was not necessary to regionalize debris flows transport rates (subsubsection 5.7.1.2.1, as virtually all debris flows could be measured directly), regionalization of debris fall rates was completed following two very different strategies. In some cases, not transport measurements from other sub-projects were used as an input, but mapping results or creep velocities, while rates to be regionalized to the mapped areas were determined by the author (e.g. 5.7.1.3).

To use methods for an identification of process coupling to establish an analyzable representation of the landsystem or fragmented high mountain landscape with landforms or process areas as system elements and quantified sediment pathways as links between system elements and combine this with transport rates to establish a sediment budget.
Locations of sediment transfer from one landform or subsystem to another were identified using different approaches, depending on the acting process. All of these assessments made use of the geomorphological-geological map prepared for this purpose (section 5.6.1): Coupling of landsystem elements via debris fall, for example, could be investigated very closely via rock fall particle trajectory modeling and subsequent analysis using graph theory-based tools (5.7.1.1.1). Sediment transfer from the hill slopes to the main fluvial system was localized and quantified by debris flow mapping and net balancing of topographic point measurements (table 6.1.4). The same holds true for fluvial hill slope erosion (5.7.3).

To investigate whether the landscape inherited by the LIA has affected process rates since its deglaciation.
It could clearly be shown that process rates are generally higher in the proglacial areas of the Upper Kauner Valley (chapter 7.2). Parametrization of a sediment exhaustion model for the true right 1855 lateral moraine of Gepatsch Glacier has proven to be difficult, mainly due to the relative complexity of the proglacial area.

To identify changes of process rates over sub-recent and present-day time scales.
While most processes were quantified using the time period 2012–2014 as a reference, process rates were also quantified for longer time periods, where possible. This involved data obtained from historical aerial images, which formed the basis for point cloud generation (SfM, 5.4.2.2) or mapping of historical events (e.g. debris flows (5.7.1.2.1), shallow soil slips (5.7.1.3), rock falls of high magnitude (5.7.1.1.2), development of Krummgampen Valley rock glacier (5.7.1.5.2). Results indicate that process rates have been changing since AD 1953. Such analyzes, however, are hampered by the fact that the quality of the historical data is often sub-optimal (mostly low spatial resolution of images), which results in incomplete inventories.

The thesis submitted herewith constitutes a small step towards the goal of establishing a sediment budget of entire alpine catchments honoring multiple processes and with sediment transfer rates quantified at a temporal resolution that enables the estimation of magnitude-frequency distributions and a spatial resolution good enough to detect sediment transport processes of magnitudes of a few cubic meters. Work in the PROSA project has also identified persisting methodological research gaps: For example, quantification of low magnitude fluvial processes on hill slopes or shallow soil slip scars using remote sensing techniques has proven to be very difficult and valid sediment transport estimation by many rock glaciers within one catchments remains a challenging task.
It is evident that a lot of future research is necessary until the sediment budget of a meso-scale alpine catchment that does not require comprehensive discussions of transport rates after the construction of the budget. While some difficulties have arisen from the fact that necessary data was not available (e.g. bank erosion by the main channel or data for regionalization of fluvial hill slope erosion), the fact that sediment transport measurements are often dependent on the spatial and temporal resolution of successive measurements remains a problem as both can have an impact on the obtained rates. Further research is also necessary concerning the (automatic) mapping of interaction points of different processes in a meso-scale catchment. While the methodological focus in the PROSA project is balancing topographic measurements from irregular intervals, it is desirable to model sediment transport using continuous functions of time as had also been postulated by Arthur N. Strahler in 1952 (Strahler, 1952, cited in Gärtner-Roer 2012):

> ...geomorphology will achieve its fullest development only when the forms and processes are related in terms of dynamic systems and the transformations of mass and energy are considered as functions of time...

Another problem of sediment budget studies in high mountain areas remains the short duration of many measurement programs. The sediment budget presented in this thesis is based on measurements spanning a time period of three years. Given the long recurrence intervals of high-magnitude sediment transport events, the quality the conclusion drawn from the investigations could be significantly improved by monitoring the same catchment for a much longer time period, or as Becht (1995b, p. 4) puts it:

> Eine Schwierigkeit prozeßorientierter Arbeiten auch im dicht besiedelten Hochgebirge der Alpen liegt im Fehlen von Vergleichsuntersuchungen an Typlokalitäten.

Maybe the Upper Kauner Valley can become one of these type localities. It is believed that work in the PROSA project and the data and results obtained in this thesis represent a valuable cornerstone for future research, at least.

8 Acknowledgements

This thesis would have never been completed without the help, advice and (financial) support of many people. At his point, I want to thank all of them.

- First and foremost, my PhD adviser Prof. Dr. Michael Becht has to be named. He had offered me the PhD position and he has also been the driving force behind the application and successive administration of the whole PROSA project. I want to thank him for his trust and his continued efforts in financing my work. He has also granted me freedom in processing and analyzing the data in all phases of the project. Especially in the last phases of my work, his admonitory words have helped to keep me on track.

- Special thanks goes to PD Dr. Tobias Heckmann. He was the second proposer of PROSA's sub-project five, the operational supervisor of my PhD work and has been serving as a role model both professionally and personally. It was as early as fall 2007 that I got to know him when I started to serve as a tutor in the undergraduate statistics course. This had been the beginning of an almost continuous collaboration, whether in the context of my tutorships in graduate statistics and GIS courses or in my work as a student research assistant in the SediCouple project. I thank him for a countless fruitful discussions which not only helped me in my work but also shaped my scientific world view. He always encouraged my work and found time to answer questions. His constant advice helped me to negotiate my way through the different phases of the project and his ideas and data analysis tools were central to the becoming of this thesis.

- The thesis would not have been possible without the data provided by sub-project one. Jana-Marie Dusik not only shared an office with me for the past three years but also acquired the lion's share of the TLS data. Together, we have experienced both sunny and rainy days in the Upper Kauner Valley, be it during TLS campaigns, total station and dGPS measurements or ulterior field work. In office, we had many fruitful discussions and she not only was a moral support in all phases of the thesis but even provided me with candy if nothing else helped. PD Dr. Florian Haas was not only Jana's operative supervisor and the second proposer of sub-project one, but also was ready if I had questions. Shortly before the finishing of this thesis, he quickly registered the TLS data from the delta surveys when I noticed that the results by the student assistant were unsatisfactorily. His optimism helped to ground and encourage me when I lost track or considered some obstacles too high from time to time.

- I am much obliged to the team of sub-project five from the working group of Prof. Dr. Norbert Pfeifer of the Technical University of Vienna. Prof. Dr. Pfeifer, Dr. Camillo Ressel, Dr. Christian Briese and, most importantly, Philipp Glira. They have hosted and taught me during my several weeks visit in spring 2013. They organized the ALS surveys, georeferenced and radiometrically calibrated the ALS point data. Philipp has

been a constant support during the last four years. He not only provided surface reference marks in the study area and pointed out suitable photogrammetry software for usage in Eichstätt, but also has most patiently answered all of my questions. I have learned much from him.

- Prof. Dr. Joachim Rohn of sub-project two had the quality and benevolence to employ me for two months in spring 2015. His PhD student Lucas Vehling provided measurements and data sets for the regionalization of debris fall and all data for both rock fall of higher magnitudes and slow moving mass movements in the study area. He was always ready to share his deep knowledge of the study area and provided valuable impulses.

- Prof. Dr. Michael Kuhn and Martin Stocker-Waldhuber of sub-project four provided me with values on the sediment transport by the glaciers in the study area that were used in the overall sediment budget. Extents of the glaciers in the study area compiled by them were very helpful in my mapping efforts and Martin's correction of the study area boundaries was very important to obtain a correct spatial study area definition.

- PROSA's sub-project three, i.e. the Halle working group with Dr. David Morche and PhD student Henning Baewert conducted a countless number of sediment transport measurements in the study area, the results of which are an important part in the sediment budget. With them or their student assistants Anne Schuchardt, Matthias Faust, Martin Weber and Eric Rascher being present in the Kauner Valley almost all summer, they were always a source for information on processes and conditions in the study area. As they shared their vacation home with all PROSA affiliates, the Eichstätt working group saved a lot of organizational work and I was always thankful for both scientific and private discussions in the evenings. The ever changing interns of the Halle working group coming from all over the world to the Kauner Valley added an international flair to our field work and rendered my stays in the valley much more enjoyable. Special thanks to Halle's student Karolin Dubberke who differentiated the geomorphological map in the floodplain areas.

- Dr. David Morche was not only the driving force in sub-project three but also co-organized the Kauner Valley geomorphological summer school I was allowed to participate. My stay there was a very motivating experience and I also want to thank the other organizers for inviting me. Especially Dr. Jan Blöthe and Dr. Sabine Kraushaar were very encouraging conversational partners, not only during the summer school week, but also at various conferences.

- There is no way that this thesis could have been finished without the help in data acquisition and processing by both my and Jana's student assistants. In this context, I want to thank Hendrik Hövel, Arnt Luthart, Kerstin Schlobies, Sebastian Wiggenhauser and Stefan Löser. They were enjoyable field work companions and conducted field work on their own. Research assistants Philip Neugirg, Sarah Betz, Florian Riehl, Martin Näher and Philipp Rumohr need special mention as their BSc or MSc theses yielded (intermediary) results that could and were used directly in

the construction or discussion of the sediment budget, the primary goal for the whole PROSA project and this PhD thesis.

- The processing and management of the enormous amount of point data would not have been possible without the software acquired from Laserdata GmbH. The team of this company, especially Dr. Christian Georges and Dr. Volker Wichmann, was an indispensable support in my efforts of data management and point classification. They regularly updated and maintained the software on the PROSA server and were always ready to answer my questions concerning processing automation in Python and Linux bash or even check my code when I had become blind for errors. Dr. Volker Wichmann gave the LIS workshop in Innsbruck and answered all my noob questions concerning C++ very very fast. Additionally, he was always very respondent when I (thought) to have found bugs in SAGA GIS, a software he maintains.

- Before actually writing this thesis, I had virtually no experience in TEX. Peter Zimmermann has both taught a TEX course and was always available to ask my TEX questions, often even checking my script sections for errors and providing me with corrected versions or example scripts. Claudia Pietsch has been a great support on both deciding on the layout of the figures prepared for this thesis. Her experience in Adobe CS and printing in general made it possible to prepare figures in the right size and resolution from the beginning.

- Writing a PhD thesis requires patience and persistence. I like to thank all the fellow PhD students who were working on their PhDs in Physical Geography in Eichstätt at the same time. They were very important in sharing thoughts on the "meta-level" of writing a PhD thesis, at the same time spiriting me up in my own work. Kerstin Wegner, Judith Abel, Alena Huber (thanks for the Chili plant!), Manuel Stark, Peter Fischer, Kathrin Umstädter, Florian Betz, Tayierjiang Aishan and Fabian Neugirg made the working environment much more enjoyable. They also always encouraged me by honoring my work.

- I would also like to thank Prof. Dr. Achim Beylich (Geological Survey of Norway) who was always very supportive, friendly and encouraging during all our meetings, during our co-authorship for the PROSA book publication and his visit in Eichstätt in 2015. He most willingly discussed the outline of this thesis with me in detail and, in doing so, gave important and motivating remarks for its completion.

- An important data source for me and the project was the TIWAG as it provided both meteorological and hydrological data and remote sensing (products), mainly for the lower part of the catchment and the reservoir area. I personally thank Christine Fey, Heiner Rett and Anja Klebelsberg.

- I thank Prof. Dr. Günther Wirsching and Dr. Hans Fischer from our university's mathematics department who showed me how to select appropriate theoretical distributions for modeling sediment production.

- Dr. Gottfried Thaler and the team of EPOSA (Echtzeit Positionierung Austria) have generously provided me with a free account for their Post-Processing services. Thank you.

- I also want to thank Klaus Meissl and the team of IDC EDV GmbH (http://www.idc-edv.at/geosi-software/), who provided me with a free version of their GEOSI software, which I used in processing the total station and dGPS data after the TLS reflector measurement campaign.

- During my field work stays in the Kauner Valley, Barbara Mark and team of the vacation house Karlspitze in Feichten were always more than friendly and always supportive if anything was needed.

- During the last four years I have taught a number of courses in statistics, GIS and cartography. I always enjoyed teaching, so I thank all students who had taken these courses for. Especially warm memories will always be associated with the two U.S. field trips in 2013 (together with PD Dr. Martin Trappe) and 2016 (with Prof. Dr. Susanne Jochner).

- The working groups of the PROSA consortium were partially financed by grants of the German Research Foundation (Deutsche Forschungsgemeinschaft, DFG) and Austria's Science fond (Der Wissenschaftsfonds, FWF) to Tobias Heckmann (HE5747 / 2-2), Michael Becht (BE1118 / 27-1 and -2), Michael Moser (MO2068 / 3-1) and Joachim Rohn (RO2211 / 5-1 and RO2211 / 5-2). This is why I also thank the DFG and FWF for originally providing the funds for my work.

- A special thanks also to the lecturers of my university's English department (Elizabeth Rogans and Bobbi Reimann) for answering some questions concerning geographical proper nouns during the writing of this thesis.

- Thanks to my uncle Clemens Hilger has provided me with a license for Adobe Creative Suite CS6, a software I often used for figure construction. He has also given valuable advice on print space and colors.

- I would also like to thank all of my friends, many of which have been or were also working on their PhDs in a variety of scientific areas, for sharing their thoughts on PhD student life. Another "thank you" the UT community for providing me with an opportunity to forget my thesis if I wanted to.

- My parents have always supported me, before and after the start of my PhD work. My family provided a social background I knew was always there, not matter what. I decidedly want to thank for their support and love I have experienced all of my life.

- Since the start of my work in the PROSA project, my then-girlfriend-now-wife Christine has been at my side. I thank her for her patience with a mute boyfriend during dinner meals, her understanding for sometimes odd working hours and her willingness to include office stops in our evening walks. And of course: For everything else!

Appendix

Appendix 1

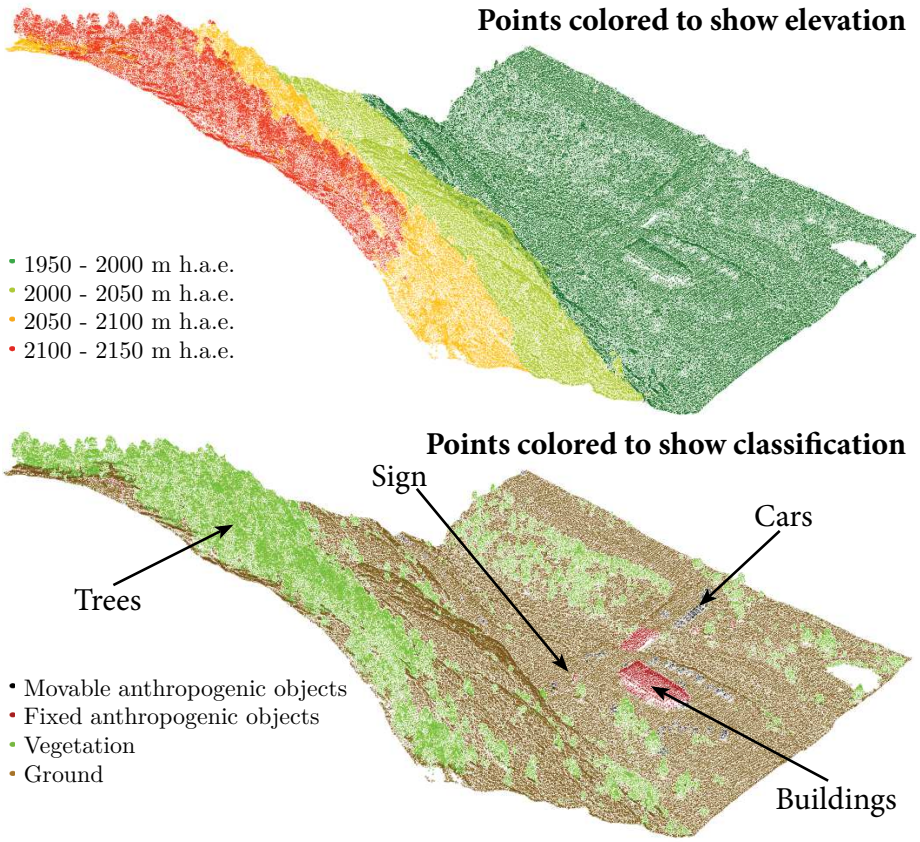

Fernergries area point cloud classification result (see also figure 5.4.8).

Appendix 2

Map on the opposite page.

Appendix 3

Table of TLS scans acquired on the next but one and the five following pages.

Appendix 4

Table of rock fall production rates obtained in other studies on page 238 (the last page before the bibliography).

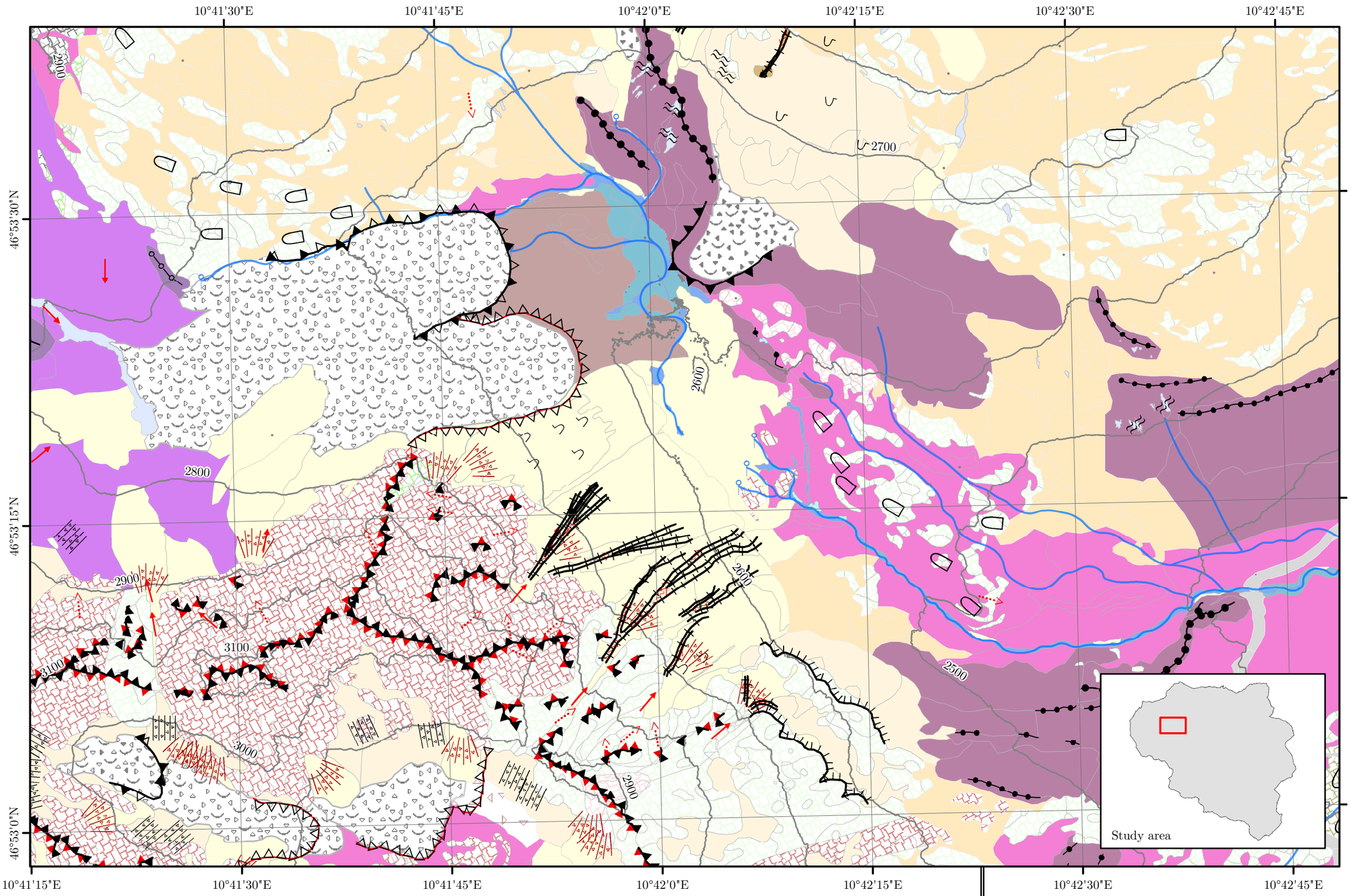

"Classical" line and point signatures:

Landforms & processes:
- Scree slope
- Alluvial fan
- Debris flow cone
- Rock fall
- Debris Flows
- Land slide
- Avalanche
- Solifluction lobe (bound)

Linear morphological features:
- Step < 2 m
- Step 2 - 10 m
- Step > 20 m
- Crest
- Ridge
- Levee
- Gorge
- Rock glacier front (active)
- Rock glacier front (inactive)
- Rock glacier front (relictic)
- Moraine ridge < 10 m (formation A.D. 1855 or later)
- Moraine ridge > 10 m (formation A.D. 1855 or later)
- Moraine ridge < 10 m (formation before A.D. 1855)
- Moraine Ridge > 10 m (formation before A.D. 1855)

0 87,5 175 350 525 m

Other:
- Striations
- Glaciated knob
- Source
- Wetland
- Stream
- Contour lines (equidistance 100 m)

Polygon features (landforms):

Anthropogenic:
- Anthropogenic

Bedrock:
- Bedrock: Amphibolite
- Bedrock: Alternating amphibolite-paragneiss
- Bedrock: Augen gneiss
- Bedrock: Biotite-plagioclase-gneiss
- Bedrock: Mostly Biotite-plagioclase-gneiss
- Bedrock: Mica shist
- Bedrock: Granitic orthogneiss
- Bedrock: Granitic porphyry
- Bedrock: Quarzite
- Bedrock: Flaky Biotite-gneiss

Fluvial:
- Fluvial, unspecified
- Fluvial, active main channel
- Fluvial, active with gravel bars
- Fluvial, gravel bar
- Mix glaciofluvial and fluvial sediments
- Mix glacial and fluvial sediments
- Old fluvial storage

Glacial:
- Moraine, not specified (pre A.D. 1855)
- Lateral or terminal moraine (pre A.D. 1855)
- Ground moraine (pre A.D. 1855)
- Lateral or terminal moraine (A.D.1855 or younger)
- Ground moraine (A.D. 1855 or younger)

Periglacial:
- Rock glacier, relict
- Rock glacier, inactive
- Rock glacier, active
- Rock glacier, not specified
- Block slope

Glacier:
- Glacier ice

Other:
- Standing water body
- Large boulder in floodplain
- Lacustrine sediment
- Slope wash areas
- Perennial snow patches
- Not specified

Gravitational:
- Talus sheets
- Talus cone
- Bergsturz deposits
- Debris cone

Appendix 3

Scan position	Acquisition dates	TLS device	Nr. of reflectors	CRS	Geomorphological situation	General exposition of scanned area	Geodetic coordinates and elevation of scan position
1	07/04/2012 08/28/2012 09/21/2012 07/05/2013 09/06/2013	LMS-Z420i LMS-Z420i LMS-Z420i VZ-4000 VZ-4000	0	local	recently exposed lateral moraine/rock wall (granite gneiss/ biotite-plagioclase gneiss) above glacier tongue	SSE	46°52.566' N, 10°45.186' E (2235.92 m h.a.e.)
2	09/24/2011 07/04/2012 08/28/2012 09/21/2012 07/04/2013 08/15/2013 09/06/2013 09/28/2013 05/28/2014 07/10/2014 09/23/2014 07/10/2015 09/22/2015	LMS-Z420i LMS-Z420i LMS-Z420i LMS-Z420i LMS-Z420i VZ-4000 VZ-4000 VZ-4000 VZ-4000 VZ-4000 VZ-4000 VZ-4000 VZ-4000	5	global	recently exposed lateral moraine/rock wall (granite gneiss/biotite-plagioclase gneiss) above glacier tongue	SSE	46°52.534' N, 10°45.104 E (2205.50 m h.a.e.)
3	8/25/2010 09/24/2011 07/05/2012 08/28/2012 09/21/2012 07/04/2013 05/28/2014 07/10/2014 09/23/2014 07/10/2015 09/22/2015	LMS-Z420i LMS-Z420i LMS-Z420i LMS-Z420i LMS-Z420i LMS-Z420i VZ-4000 VZ-4000 VZ-4000 VZ-4000 VZ-4000	8	global	1855 lateral moraine with outcrops of bitotite-plagioclase gneiss	SW	46°52.660' N, 10°44.835' E (2215.19 m h.a.e.)
4	07/13/2010 08/25/2010 09/24/2011 07/05/2012 08/27/2012 09/20/2012 07/01/2013 09/28/2013 05/28/2014 07/10/2014 09/23/2014	LMS-Z420i LMS-Z420i LMS-Z420i LMS-Z420i LMS-Z420i VZ-4000 VZ-4000 VZ-4000 VZ-4000 VZ-4000 VZ-4000	ca. 8	global	1855 lateral moraine with outcrops of biotite-plagioclase gneiss	WSW	46°52.768' N, 10°44.525' E (2136.52 m h.a.e.)

Continued on next page

Table 1 – continued from previous page

Scan position nr.	Acquisition dates	TLS device used	Number of reflectors	CRS	Geomorphological situation	General exposition of scanned area	Geodetic coordinates and elevation of scan position
	10/20/2014	VZ-4000					
	07/10/2015	VZ-4000					
	09/22/2015	VZ-4000					
5	07/13/2010	LMS-Z420i	ca. 7	global	1855 lateral moraine with outcrops of biotite-plagioclase gneiss	W	46°52.817' N, 10°44.469' E (2161.53 m h.a.e.)
	07/25/2010	LMS-Z420i					
	09/24/2011	LMS-Z420i					
	07/05/2012	LMS-Z420i					
	08/27/2012	LMS-Z420i					
	09/20/2012	LMS-Z420i					
	07/01/2013	VZ-4000					
	09/28/2013	VZ-4000					
	07/10/2014	VZ-4000					
	09/23/2014	VZ-4000					
	10/20/2014	VZ-4000					
	08/10/2015	VZ-4000					
	09/22/2015	VZ-4000					
6	07/13/2010	LMS-Z420i	ca. 5	global	1855 lateral moraine with outcrops of biotite-plagioclase gneiss	W	46°52.924' N, 10°44.448' E (2158.05 m h.a.e.)
	09/24/2011	LMS-Z420i					
	08/24/2012	LMS-Z420i					
	09/20/2012	LMS-Z420i					
	07/01/2013	VZ-4000					
	07/08/2014	VZ-4000					
	09/23/2014	VZ-4000					
	10/20/2014	VZ-4000					
	07/10/2015	VZ-4000					
	09/22/2015	VZ-4000					
7	08/21/2012	LMS-Z420i	0	local	accumulation area of old debris flow below talus slope/lower part of position 14	SW	46°53.629' N, 10°42.033' E (2701.76 m h.a.e.)
	09/07/2013	VZ-4000					
	07/15/2014	VZ-4000					
	07/30/2015	VZ-4000					
8	09/25/2011	LMS-Z420i	0	local	biotite-plagiogneiss rock wall with talus slope	WSW	46°53.119' N, 10°44.406' E (2057.89 m h.a.e.)
	07/16/2012	LMS-Z420i					
	08/25/2012	LMS-Z420i					
	07/01/2013	VZ-4000					
	09/04/2013	VZ-4000					
	07/17/2014	VZ-4000					
	09/25/2014	VZ-4000					
	07/11/2015	VZ-4000					

Continued on next page

Table 1 – continued from previous page

Scan position nr.	Acquisition dates	TLS device used	Number of reflectors	CRS	Geomorphological situation	General exposition of scanned area	Geodetic coordinates and elevation of scan position
9	09/25/2011 08/24/2012 07/02/2013 07/17/2014 09/23/2014 07/29/2015 09/22/2015	LMS-Z420i LMS-Z420i VZ-4000 VZ-4000 VZ-4000 VZ-4000 VZ-4000	0	local	biotite-plagiogneiss rock wall/paragneiss/slate gneiss rock wall	W	46°53.170' N, 10°44.284' E (2013.22 m h.a.e.)
10	09/25/2011 08/23/2012 07/01/2013 09/04/2013 05/28/2013 07/08/2014 09/23/2014 07/29/2015	LMS-Z420i LMS-Z420i VZ-4000 VZ-4000 VZ-4000 VZ-4000 VZ-4000 VZ-4000	0	local	paragneiss (i.e. slate gneiss) rock wall (mostly biotite-plagioclase gneiss)	ESE	46°53.311' N, 10°44.126' E (1979.17 m h.a.e.)
11	07/14/2011 08/27/2012 09/06/2013 07/19/2014 09/25/2014 07/11/2015 09/22/2015	LMS-Z420i LMS-Z420i VZ-4000 VZ-4000 VZ-4000 VZ-4000 VZ-4000	0	local	young lateral moraine and massive fine-grained paragneiss rock wall (mostly biotite-plagioclase gneiss)	N	46°52.389' N, 10°44.880' E (2237.02 m h.a.e.)
12	07/18/2012 08/21/2012 07/03/2013 07/15/2014 10/21/2014 07/31/2015	LMS-Z420i LMS-Z420i VZ-4000 VZ-4000 VZ-4000 VZ-4000	4	global	Riffltal rock glacier front	E	46°53.479' N, 10°41.875' E (2618.15 m h.a.e.)
13	08/21/2012 07/05/2013 09/07/2013 07/15/2014 10/21/2014 07/30/2015	LMS-Z420i VZ-4000 VZ-4000 VZ-4000 VZ-4000 VZ-4000	6	global	Blaike	SW	46°53.546' N, 10°41.991' E (2631.99 m h.a.e.)
14	08/21/2012 09/07/2013 07/15/2014 07/31/2015	LMS-Z420i VZ-4000 VZ-4000 VZ-4000	none	local	paragneiss rock wall (mostly biotite-plagioclase gneiss) with talus slope, modified by torrent-type debris flow	SW	46°53.639' N, 10°42.017' E (2711.16 m h.a.e.)
15	08/21/2012 07/03/2013 07/18/2014 10/21/2014 07/30/2015	LMS-Z420i LMS-Z420i VZ-4000 VZ-4000 VZ-4000	none	local	amphibolite/phyllite rock wall with small talus slope	N	46°53.327' N, 10°41.717' E (2735.79 m h.a.e.)

Continued on next page

Table 1 – continued from previous page

Scan position nr.	Acquisition dates	TLS device used	Number of reflectors	CRS	Geomorphological situation	General exposition of scanned area	Geodetic coordinates and elevation of scan position
15b	07/03/2013 07/18/2014 10/21/2014 07/30/2015	VZ-4000 VZ-4000 VZ-4000 VZ-4000	none	local	amphibolite/phyllite rock wall with small talus slope	N	46°53.327' N, 10°41.734' E (2731.99 m h.a.e.)
16	08/23/2012 08/15/2013 07/16/2014 09/24/2014 07/28/2015 09/21/2015	LMS-Z420i VZ-4000 VZ-4000 VZ-4000 VZ-4000 VZ-4000	7	global	AD 1855 lateral moraine	W	46°52.371' N, 10°42.995' E (2503.04 m h.a.e.)
17	08/23/2012 08/15/2013 07/16/2014 09/24/2014 07/28/2015 09/21/2015	LMS-Z420i VZ-4000 VZ-4000 VZ-4000 VZ-4000 VZ-4000	5	global	AD 1855 lateral moraine	W	46°52.247' N, 10°43.088' E (2608.06 m h.a.e.)
18	08/22/2012 08/16/2013 07/16/2014 09/24/2014 07/28/2015 09/21/2015	LMS-Z420i VZ-4000 VZ-4000 VZ-4000 VZ-4000 VZ-4000	4	global	AD 1855 lateral moraine	W	46°52.161' N, 10°43.107' E (2615.80 m h.a.e.)
19	08/22/2012 09/05/2013 09/24/2014 07/28/2015	LMS-Z420i VZ-4000 VZ-4000 VZ-4000	none	global	granitic gneiss rock wall above active glacier	W	46°51.834' N, 10°43.307' E (2770.70 m h.a.e.)
20	08/22/2012 09/05/2013 09/24/2014 07/28/2015	LMS-Z420i VZ-4000 VZ-4000 VZ-4000	none	local	granitic gneiss and biotite-plagioglas gneiss rock wall plus accumulation zone	W	46°51.746' N, 10°43.232' E (2781.99 m h.a.e.)
21	08/22/2012 09/05/2013 09/24/2014 07/28/2015	LMS-Z420i VZ-4000 VZ-4000 VZ-4000	none	local	granitic gneiss and biotite-plagioglas gneiss rock wall plus accumulation zone	W	46°51.645' N, 10°43.181' E (2830.47 m h.a.e.)
22	09/28/2013 07/19/2014 09/25/2014 09/22/2015	VZ-4000 VZ-4000 VZ-4000 VZ-4000	ca. 5, but not surveyed	local	potential slope wash area, post-1855 ground/lateral moraine	S	46°52.493' N, 10°44.893' E (2178.23 m h.a.e.)
23	07/18/2014 09/24/2014 07/29/2015	VZ-4000 VZ-4000 VZ-4000	none	local	potential slope wash area on unvegetated pre-1855 lateral or terminal moraine, bank of small stream	NNW	46°52.264' N, 10°42.406' E(2628.56 m h.a.e.)

Continued on next page

Table 1 – continued from previous page

Scan position nr.	Acquisition dates	TLS device used	Number of reflectors	CRS	Geomorphological situation	General exposition of scanned area	Geodetic coordinates and elevation of scan position
24	never	-	none	local	scan position of sub-project three. Never surveyed, but archived as many of sub-project three were surveyed by sub-project one and five to establish global coordinates. Large braidplain.	-	ca. 46°53.441' N, 10°44.093' E
25	05/11/2012 05/18/2013 05/10/2014 05/04/2015	LMS-Z420i VZ-4000 VZ-4000 VZ-4000	ca. 6, but not surveyed	local	one of five scan positions for the survey of the Gepatsch reservoir delta	ininW	46°55.023 N, 10°44.201' E (1818.55 m h.a.e.)
26	05/11/2012 05/18/2013 05/10/2014 05/04/2015	LMS-Z420i VZ-4000 VZ-4000 VZ-4000	none	local	one of five scan positions for the survey of the Gepatsch reservoir delta	WNW	46°54.630' N, 10°44.213' E (1816.60 m h.a.e.)
27	05/11/2012 05/18/2013 05/10/2014 05/04/2015	LMS-Z420i VZ-4000 VZ-4000 VZ-4000	ca. 6, but not surveyed	local	one of five scan positions for the survey of the Gepatsch reservoir delta	ESE	46°54.50' N, 10°44.419'E (1826.60 m h.a.e.)
28	05/11/2012 05/18/2013 05/10/2014 05/04/2015	LMS-Z420i VZ-4000 VZ-4000 VZ-4000	ca. 4, but not surveyed	local	one of five scan positions for the survey of the Gepatsch reservoir delta	E	46°55.129' N, 10°44.489' E (1838.86 m h.a.e.)
29	08/23/2012 09/20/2012 07/01/2013 07/17/2014 09/23/2014 07/11/2015 09/22/2015	LMS-Z420i LMS-Z420i LMS-Z420i LMS-Z420i VZ-4000 VZ-4000 VZ-4000	none	local	biotite-plagiogneiss rock wall	SW	46°53.232' N, 10°44.292' E (2014.85 m h.a.e.)
29b	07/17/2014 07/11/2015 09/22/2015	VZ-4000 VZ-4000 VZ-4000	none	local	biotite-plagiogneiss rock wall, same area as scan position 29, used to minimize shadowing effects	SW	46°53.237' N, 10°44.271' E (2006.69 m h.a.e.)
30	09/21/2012	LMS-Z420i	yes	global	section of the fluvial system / Faggenbach, scanned only once for sub-project three	mainly W	46°52.640' N, 10°44.607'E (2148.42 m h.a.e.)
31	08/25/2010 07/13/2010 09/20/2012	LMS-Z420i LMS-Z420i LMS-Z420i	yes	global	section of the fluvial system / Faggenbach (braidplain "Graichengries", scanned only once for sub-project three)	W/SW (floodplain is flat)	46°52.823' N, 10°44.467' E (2161.19 m h.a.e.)

Continued on next page

Table 1 – continued from previous page

Scan position nr.	Acquisition dates	TLS device used	Number of reflectors	CRS	Geomorphological situation	General exposition of scanned area	Geodetic coordinates and elevation of scan position
32	07/17/2014	VZ-4000	5	global	section of the fluvial system / Faggenbach, scanned only once for sub-project three, upper part of braidplain "Fernergries"	flat	46°53.161' N, 10°44.185' E (1998.21 m h.a.e.)
33	07/17/2014	VZ-4000	5	global	scanned only once for sub-project three, middle part of braidplain "Fernergries"	flat	46°53.213' N, 10°44.065' E (2013.54 m h.a.e.)
34	never		none	-	scan position of sub-project three. Never surveyed, but archived as many of sub-project three were surveyed by sub-project one and five to establish global coordinates.	-	-
35	05/18/2013 05/10/2014	VZ-4000 VZ-4000	at least 5, but not surveyed	local	one of five scan positions for the survey of the Gepatsch reservoir delta	W	46°55.157' N, 10°44.142' E (1821.59 m h.a.e.)
36	08/14/2013	VZ-4000	at least 5	global	section of the fluvial system / Faggenbach, scanned only once for sub-project three	N/A	-
37	08/14/2013	VZ-4000	at least 5	global	section of the fluvial system / Faggenbach, scanned only once for sub-project three	N/A	-
38	08/15/2013	VZ-4000	at least five	global	section of the fluvial system / Faggenbach, scanned only once for sub-project three	N/A	-
39	08/15/2013	VZ-4000	at least five	global	section of the fluvial system / Faggenbach, scanned only once for sub-project three	N/A	-
41	07/19/2014 09/23/2014 07/10/2015 09/22/2015	VZ-4000 VZ-4000 VZ-4000 VZ-4000	none		recently exposed lateral moraine/rock wall (granite gneiss/biotite-plagioclase gneiss) above glacier tongue, replacement for positon one	SSE	46°52.251' N, 10°45.174' E (2236.84 m h.a.e.)
42	05/04/2015	VZ-4000	none	local	an alternative for position 28	E	46°55.020' N, 10°44.470' E (1839.49 m h.a.e.)
43	07/18/2014 09/25/2014 07/09/2015 09/21/2015	VZ-4000 VZ-4000 VZ-4000 VZ-4000	none		old fluvial storage, high river bank above Faggenbach, slope wash area	E	46°53.828' N, 10°44.164' E (1934.56 m h.a.e.)
44	05/04/2015	VZ-4000	none	local	an alternative for position 28	E	46°54.865' N, 10°44.445' E (1829.81 m h.a.e.)

A3: TLS monitoring stations maintained by the Eichstätt working groups (as of February 15, 2016)

Appendix 4

Study	**Location**	**Reference period and method**	**Obtained value(s) in kg · m^{-2}· yr^{-1}**
Poser, 1954	Zemmgrund, Austria	Holocene, N/A	1.89–2.7
Rapp (1960)	Karkevagge, Norway	8 years, (e)	0.108, 0.162, 0.405
Rapp (1964)	Scandinavia	10000 years, N/A	0.918–1.35
Rapp (1964)	Scandinavia	9000 years, N/A	0–2.43
Galibert (1965)	N/A	N/A	0.351–0.972
Young (1969)	N/A,N/A	0–2.7	no
Höllermann (unpublished)		N/A,N/A	2.16–5.13
Souchez (1971)	Ellesmere Island, Canada	8000 years, N/A	1.35–3.51
Gray (1972)	Canadian cordillera, Canada	10000 years, N/A	0.0189–0.27
Gray (1972)	Canadian cordillera, Canada	10000 years, N/A	0.054–0.189
Caine (1974), cited in Hollermann (1983)	N/A	N/A, N/A	1.91–2.86
Soderman (1980)	Northern Finland	9500 years, N/A	0.1–2.53
Soderman (1980)	Northern Finland	”recent”	0–0.729
Douglas (1980)	Co. Antrim, Northern Ireland	2 years, (e)	3.24
Barsch (1981b)	Ellesmere Island, Canada	Holocene, N/A	2.7–8.1
Frich (1985)	West Greenland	7000 years, N/A	1.35–4.05
Andre (1986)	Northwest Spitsbergen, Norway	Late Holocene, (a)	0–1.89
Fahey (1988)	Bruce Peninsula, Southern Ontario, Canada	5 months, (e)	0.27
Francou (1988)	Roc Noir du Combeynot Alps, France	10 years, (e)	8.1
Coultard (1989)	Roc Noir du Combeynot and Crête de Vars, Alps, France	10 years, (e)	0.135–1.35
Hall (1990)	Juneau Icefield, Alaska, USA	1000 years	0.0135–0.054
Becht (1995c)	N/A	N/A	0.135–0.27
Barsch (1996)	N/A	10000 years	2.16–4.05
Barsch (1996)	N/A	10000 years	4.05–9.18
Andre (1997)	Svalbard, Norway	Holocene	0.0054, 0.189, 0.432, 1.89
Jonasson (1997)	N/A		0.594–1.188
Jonasson (1997)	N/A		0.081–0.27
Sass (1998)	Karwendel mountains, Germany	a few years, (e)	0.27
Matsuoka (1999)	Hosozawa Cirque, Japanese Alps, Japan	3 years, (e)	0.027–0.81
Beylich (2000)	Austdalur, Austfirðir, Iceland	10000–12000 years, (b)	0.21–0.27
Beylich (2000)	Austdalur, Austfirðir, Iceland	2 years, (e)	0.08–0.54
OFarrell (2009)	Matanuska glacier, Alaska	N/A, (c)	0.135–0.405
Krautblatter (2012)	Reintal, Germany	4 years, (e)	0.783

A4: Literature on rockfall rates from other cold regions reviewed for this study. Most of these values were given in mm yr^{-1} and were therefore converted to kg m^{-2} yr^{-1} using a constant density of 2.7 t m^{-3}. Where a range is given, it represents the minimum and maximum values. Where only one value or multiple values are given separated by commas, it represents mean values.

Bibliography

Abellán, A., Calvet, J., Vilaplana, J. M., Blanchard, J., 2010. Detection and spatial prediction of rockfalls by means of terrestrial laser scanner monitoring. Geomorphology 119 (3–4), 162–171.

Abellán, A., Oppikofer, T., Jaboyedoff, M., Rosser, N. J., Lim, M., Lato, M. J., 2014. Terrestrial laser scanning of rock slope instabilities. Earth Surface Processes and Landforms 39 (1), 80–97.

Abellán, A., Vilaplana, J. M., Calvet, J., García-Sellés, D., Asensio, E., 2011. Rockfall monitoring by Terrestrial Laser Scanning – case study of the basaltic rock face at Castellfollit de la Roca (Catalonia, Spain). Natural Hazards & Earth System Science 11 (3), 829–841.

Abellán, A., Vilaplana, J. M., Martínez, J., 2006. Application of a long-range Terrestrial Laser Scanner to a detailed rockfall study at Vall de Núria (Eastern Pyrenees, Spain). Engineering Geology 88 (3-4), 136–148.

Abermann, J., Lambrecht, A., Fischer, A., Kuhn, M., 2009. Quantifying changes and trends in glacier area and volume in the Austrian Ötztal Alps (1969-1997-2006). The Cryosphere 3 (2), 205–215.

Ackroyd, P., 1986. Debris Transport by Avalanche, Torlesse Range, New Zealand. Zeitschrift für Geomorphologie N.F. 30 (1), 1–14.

Ackroyd, P., 1987. Erosion by Snow Avalanche and Implications for Geomorphic Stability, Torlesse Range, New Zealand. Arctic, Antarctic, and Alpine Research 19 (1), 65–70.

Ahnert, F., 2003. Einführung in die Geomorphologie, 3rd Edition. Ulmer, Stuttgart.

Allix, A., 1924. Avalanches. Geographical Review 14 (4), 519–560.

American Society for Photogrammetry and Remote Sensing, 07.03.2005. LAS Specification Version 1.1.

Anders, N. S., Seijmonsbergen, A. C., Bouten, W., 2009. Multi-scale and object-oriented image analysis of high-res LiDAR data for geomorphological mapping in Alpine mountains. In: Proceedings of Geomorphometry. pp. 61–65.

Anderson, S., Pitlick, J., 2014. Using repeat LiDAR to estimate sediment transport in a steep stream. Journal of Geophysical Research 119 (3), 621–643.

André, M.-F., 1986. Dating slope deposits and estimating rates of rock wall retreat in northwest Spitsbergen by lichenometry. Geografiska Annaler. Series A, Physical Geography 68, 65–75.

André, M.-F., 1990a. Frequency of debris flows and slush avalanches in Spitsbergen: a tentative evaluation from lichenometry. Polish Polar Research 11 (3-4), 345–363.

André, M.-F., 1990b. Geomorphic Impact of Spring Avalanches in Northwest Spitsbergen (79Â° N). Permafrost and Periglacial Processes 1, 97–110.

André, M.-F., 1997. Holocene Rockwall Retreat in Svalbard: A Triple-Rate Evolution. Earth Surface Processes and Landforms 22 (5), 423–440.

Arbeitsgemeinschaft österreichischer Lawinenwarndienste, 2014. Saisonbericht der österreichischen Lawinenwarndienste 2013/14.

Arenson, L. U., Hoelzle, M., Springman, S., 2002. Borehole deformation measurements and internal structure of some rock glaciers in Switzerland. Permafrost and Periglacial Processes 13 (2), 117–135.

Aryal, A., Brooks, B. A., Reid, M. E., Bawden, G. W., Pawlak, G. R., 2012. Displacement fields from point cloud data: Application of particle imaging velocimetry to landslide geodesy. Journal of Geophysical Research: Earth Surface (2003–2012) 117 (F1).

Avian, M., Kellerer-Pirklbauer, A., Bauer, A., 2009. LiDAR for monitoring mass movements in permafrost environments at the cirque Hinteres Langtal, Austria, between 2000 and 2008. Natural Hazards & Earth System Science 9 (4), 1087–1094.

Azzoni, A., Freitas, M. H., 1995. Experimentally gained parameters, decisive for rock fall analysis. Rock Mechanics and Rock Engineering 28 (2), 111–124.

Bader, H.-P., Weilenmann, P., 1992. Modeling temperature distribution, energy and mass flow in a (phase-changing) snowpack. I. Model and case studies. Cold Regions Science and Technology 20 (2), 157–181.

Baewert, H., Morche, D., 2014. Coarse sediment dynamics in a proglacial fluvial system (Fagge River, Tyrol). Geomorphology 218, 88–97.

Baewert, H., Schmidt, K.-H., Morche, D., 2012. Sediment budget and roughness parameters of an alpine proglacial environment (Gepatschferner, Austria). Towards an integrated analysis of environmental drivers and rates of contemporary solute and sedimentary fluxes in changing cold climate environments, 49.

Baewert, H., Vehling, L., Glira, P., Stocker-Waldhuber, M., 2014. How much does a very active rockslope contribute to the sediment budget of an alpine glacier. In: European Geosciences Union (Ed.), Geophysical Research Abstracts. Geophysical Research Abstracts. Copernicus GmbH (Copernicus Publications), Göttingen.

Baggi, S., Schweizer, J., 2009. Characteristics of wet-snow avalanche activity: 20 years of observations from a high alpine valley (Dischma, Switzerland). Natural Hazards 50 (1), 97–108.

Ballantyne, C. K., 2002a. A general model of paraglacial landscape response. The Holocene 12 (3), 371–376.

Ballantyne, C. K., 2002b. Paraglacial geomorphology. Quaternary Science Reviews 21, 1935–2017.

Ballantyne, C. K., Harris, C., 1994. The periglaciation of Great Britain, 1st Edition. Cambridge University Press, Cambridge [u.a.].

Baltsavias, E. P., 1999. Airborne laser scanning: basic relations and formulas. ISPRS Journal of Photogrammetry and Remote Sensing 54 (2–3), 199–214.

Baptista, P., Bastos, L., Bernardes, C., Cunha, T., Dias, J., 2008. Monitoring Sandy Shores Morphologies by DGPS—A Practical Tool to Generate Digital Elevation Models. Journal of Coastal Research, 1516–1528.

Barbolini, M., Biancardi, A., Cappabianca, F., Natale, L., Pagliardi, M., 2005. Laboratory study of erosion processes in snow avalanches. Cold Regions Science and Technology 43 (1–2), 1–9.

Barsch, D., 1977. Nature and importance of mass–wasting by rock glaciers in alpine permafrost environments. Earth Surface Processes 2 (2–3), 231–245.

Barsch, D., 1981. Studien zur gegenwärtigen Geomorphodynamik im Bereich der Oobloyah Bay, N-Ellesmere Island, N.W.T., Kanada. In: Barsch, D., King, L. (Eds.), Ergebnisse der Heidelberg Ellesmere Island Expedition. Vol. 69. Selbstverlag des Geographischen Institutes der Universität Heidelberg, Heidelberg, pp. 123–161.

Barsch, D., 1996. Rockglaciers: Indicators for the present and former geoecology in high mountain environments. Springer, Berlin.

Barsch, D., Fierz, H., Haeberli, W., 1979. Shallow core drilling and borehole measurements in the permafrost of an active rock glacier near the Grubengletscher, Wallis, Swiss Alps. Arctic and Alpine Research 11 (2), 215–228.

Bartsch, A., Gude, M., Jonasson, C., Scherer, D., 2002. Identification of Geomorphic Process Units in Kärkevagge, Northern Sweden, by Remote Sensing and Digital Terrain Analysis. Geografiska Annaler. Series A, Physical Geography 84 (3-4), 171–178.

Bauer, A., Paar, G., Kaufmann, V., 2003. Terrestrial laser scanning for rock glacier monitoring. In: Phillips, M., Springman, S. M., Arenson, L. U. (Eds.), Proceedings of the 8th International Conference on Permafrost. Swets & Zeitlinger, Lisse, pp. 55–60.

Becht, M., 1995a. Slope erosion processes in the Alps. In: Slaymaker, O. (Ed.), Steepland geomorphology. Vol. 3 of International Association of Geomorphologists: Publication. Wiley, Chichester, pp. 45–61.

Becht, M., 1995b. Untersuchungen zur aktuellen Reliefentwicklung in alpinen Einzugsgebieten: Postdoctoral dissertation. Vol. 47 of Münchener Geographische Abhandlungen A. Geobuch, München.

Becht, M., Haas, F., Heckmann, T., Wichmann, V., 2005. Investigating sediment cascades using field measurements and spatial modelling. In: Des Walling, E., Horowitz, A. J. (Eds.), Sediment budgets. Vol. 291 of IAHS publication. Internat. Assoc. of Hydrological Sciences, Wallingford, pp. 206–213.

Becht, M., Heckmann, T., Mittelsten Scheid, T., Wichmann, V., 2003. Relief und Prozesse im Alpenraum. In: Liedtke, H., Leibniz-Institut für Länderkunde, Mäusbacher, R., Schmidt, K.-H. (Eds.), Bundesrepublik Deutschland. Nationalatlas. Spektrum Akademischer Verlag, pp. 96–97.

Bell, D. F., 2012. Creating DEMs from Survey Data: Interpolation Methods and Determination of Accuracy. In: Clarke, L. E. (Ed.), Geomorphological Techniques (Online Edition). British Society for Geomorphology, London, pp. 131–139.

Bell, I., Gardner, J. S., deScally, F. A., 1990. An Estimate of Snow Avalanche Debris Transport, Kaghan Valley, Himalaya, Pakistan. Arctic, Antarctic, and Alpine Research 22 (3), 317–321.

Beniston, M., 2000. Environmental change in mountains and uplands. Key issues in environmental change. Arnold [u.a.], London.

Beniston, M., 2003. Climatic change in mountain regions: a review of possible impacts. Climatic Change 59, 5–31.

Beniston, M., 2005. Mountain climates and climatic change: an overview of processes focusing on the European Alps. Pure and Applied Geophysics 162 (8-9), 1587–1606.

Beniston, M., Stoffel, M., Hill, M., 2011. Impacts of climatic change on water and natural hazards in the Alps: Can current water governance cope with future challenges? Examples from the European "ACQWA" project. Adapting to Climate Change: Reducing Water-related Risks in Europe 14 (7), 734–743.

Bennett, G. L., Molnar, P., Eisenbeiss, H., McArdell, B. W., 2012. Erosional power in the Swiss Alps: characterization of slope failure in the Illgraben. Earth Surface Processes and Landforms 37 (15), 1627–1640.

Beraldin, J.-A., Blais, F., Lohr, U., 2010. Laser Scanning Technology. In: Vosselman, G. (Ed.), Airborne and terrestrial laser scanning. Whittles Publishing, Dunbeath and Caithness, pp. 1–42.

Berger, J., 2002. Aufbau und Dynamik aktiver Blockgletscher am Beispiel der Blockgletscher in der Inneren Ölgrube und dem Kaiserbergtal (Ötztaler Alpen/Tirol). Ph.D. thesis, Ernst-Moritz-Arndt-Universität, Greifswald.

Berger, J., Krainer, K., Mostler, W., 2004. Dynamics of an active rock glacier (Ötztal Alps, Austria). Quaternary Research 62 (3), 233–242.

Bertoldi, W., Zanoni, L., Tubino, M., 2010. Assessment of morphological changes induced by flow and flood pulses in a gravel bed braided river: the Tagliamento River (Italy). Geomorphology 114 (3), 348–360.

Betz, S. K., 2016. Entwicklung flachgründiger Abtragsphänomene (Blaiken) an Berghängen im hinteren Kaunertal (Tirol) – Analyse von Geofaktoren und multitemporalen Luftbildern sowie Quantifizierung des Abtrags durch die Auswertung von Photogrammetrie- und LiDAR-Daten: Master thesis.

Beylich, A. A., 2000. Geomorphology, Sediment Budget, and Relief Development in Austdalur, Ausfirdir, East Iceland. Arctic, Antarctic, and Alpine Research 32 (4), 466–477.

Beylich, A. A., 2016. Controls and variability of solute and sedimentary fluxes in alpine/mountain environments. In: Beylich, A. A., Dixon, J. C., Zwolinski, Z. (Eds.), Source-to-Sink fluxes in Undisturbed Cold Environments. Cambridge University Press, pp. 376–379.

Beylich, A. A., Kneisel, C., 2009. Sediment Budget and Relief Development in Hrafndalur, Subarctic Oceanic Eastern Iceland: Arctic, Antarctic, and Alpine Research. Arctic, Antarctic, and Alpine Research 41 (1), 3–17.

Beylich, A. A., Lamoureux, S. F., Decaulne, A., 2011. Developing frameworks for studies on sedimentary fluxes and budgets in changing cold environments. Quaestiones Geographicae 30 (1), 5–18.

Beylich, A. A., Laute, K., 2015. Sediment sources, spatiotemporal variability and rates of fluvial bedload transport in glacier-connected steep mountain valleys in western Norway (Erdalen and Bødalen drainage basins). Geomorphology 228, 552–567.

Beylich, A. A., Laute, K., Storms, Joep E. A., 2015. Contemporary suspended sediment dynamics within two partly glacierized mountain drainage basins in western Norway (Erdalen and Bødalen, inner Nordfjord). Geomorphology.

Bezinge, A., Clark, M. J., Am Gurnell, Warburton, J., 1989. The management of sediment transported by glacial melt-water streams and its significance for the estimation of sediment yield. Annals of Glaciology 13, 1–5.

Bivand, R. S., Keitt, T., Rowlingson, B., Pebesma, E., Sumner, M., Hijmans, R., Rouault, E., 2016. rgdal: Bindings for the Geospatial Data Abstraction Library.

Blöschl, G., Grayson, R., 2001. Spatial Observations and Interpolation. In: Grayson, R., Blöschl, G. (Eds.), Spatial patterns in catchment hydrology. Cambridge University Press, Cambridge and New York, pp. 17–50.

Blöschl, G., Sivapalan, M., 1995. Scale issues in hydrological modelling: a review. Hydrological Processes 9 (3–4), 251–290.

Blöthe, J. H., Korup, O., 2013. Millennial lag times in the Himalayan sediment routing system. Earth and Planetary Science Letters 382 (0), 38–46.

Bögel, H., Schmidt, K., 1976. Kleine Geologie der Ostalpen: Allgmein verständliche Einführung in den Bau der Ostalpen unter Berücksichtigung der angrenzenden Südalpen. Ott, Thun.

Bogen, J., 1989. Glacial sediment production and development of hydro-electric power in glacierized areas. Annals of Glaciology 13, 6–11.

Borselli, L., Cassi, P., Torri, D., 2008. Prolegomena to sediment and flow connectivity in the landscape: A GIS and field numerical assessment. Catena 75 (3), 268–277.

Bourrier, F., Dorren, L. K. A., Hungr, O., 2013. The use of ballistic trajectory and granular flow models in predicting rockfall propagation. Earth Surface Processes and Landforms 38 (4), 435–440.

Bracken, L. J., Turnbull, L., Wainwright, J., Bogaart, P., 2015. Sediment connectivity: a framework for understanding sediment transfer at multiple scales. Earth Surface Processes and Landforms 40 (2), 177–188.

Brandlmeier, B., 2011. Untersuchungen zu geomorphometrischen Veränderungen auf Ufermoränen im Vorfeld des Gepatschferners mittels hochauflösender digitaler Geländemodelle (terrestrisches Laserscanning). Ph.D. thesis, Catholic University of Eichstätt-Ingolstadt, Eichstätt.

Brasington, J., Rumsby, B. T., McVey, R. A., 2000. Monitoring and modelling morphological change in a braided gravel-bed river using high resolution GPS-based survey. Earth Surface Processes and Landforms 25 (9), 973–990.

Bremer, M., Rutzinger, M., Wichmann, V., 2013. Segment based shape matching in terrestrial laser scanning point clouds. In: European Geosciences Union (Ed.), Geophysical Research Abstracts. Vol. 15 of Geophysical Research Abstracts. Copernicus GmbH (Copernicus Publications), Göttingen, p. 11968.

Bremer, M., Sass, O., 2012. Combining airborne and terrestrial laser scanning for quantifying erosion and deposition by a debris flow event. Geomorphology 138 (1), 49–60.

Brenning, A., Bangs, D., 2016. Package "RSAGA".

Brewer, P. A., Passmore, D. G., 2002. Sediment budgeting techniques in gravel-bed rivers. In: Jones, S. J. (Ed.), Sediment flux to basins. Vol. 191 of Geological Society special publication. Geological Soc, London, pp. 97–113.

Briese, C., Höfle, B., Lehner, H., Wagner, W., Pfennigbauer, M., Ullrich, A., 2008. Calibration of fullwaveform airborne laser scanning data for object classification. In: Turner, M. D., Kamerman, G. W. (Eds.), Proceedings. pp. 69500H–69500H–8.

Brocklehurst, S. H., Whipple, K. X., 2002. Glacial erosion and relief production in the Eastern Sierra Nevada, California. Geomorphology 42 (1), 1–24.

Brown, M., Lowe, D. G., 2005. Unsupervised 3D object recognition and reconstruction in unordered datasets. In: Fifth International Conference on 3-D Digital Imaging and Modeling (3DIM'05). IEEE, pp. 56–63.

Brunner, K., 1978. Zur neuen Karte Gepatschferner 1971, Maßstab 1:10000. Zeitschrift für Gletscherkunde und Glazialgeologie 14 (2), 133–151.

Brunner, K., 1987. Hundert Jahre Gletschervermessung am Gepatschferner (Tirol). Zeitschrift für Vermessungswesen 112, 47–60.

Brunner, K., 1988. Maps of Gepatschferner. In: Haeberli, W. (Ed.), Fluctuations of glaciers 1980 - 1985: Prepared by the World Glacier Monitoring Service. Vol. 5. International Association of Hydrological Sciences, pp. 77–78.

Bull, J. M., Miller, H., Gravley, D. M., Costello, D., Hikuroa, D. C. H., Dix, J. K., 2010. Assessing debris flows using LIDAR differencing: 18 May 2005 Matata event, New Zealand. Geomorphology 124 (1–2), 75–84.

Burger, K. C., Degenhardt, J. J., Giardino, J. R., 1999. Engineering geomorphology of rock glaciers. Geomorphology 31 (1-4), 93–132.

Burt, T. P., Allison, R. J. (Eds.), 2010. Sediment Cascades. John Wiley & Sons, Chichester and UK.

Cadell, W., 2002. Report on the generation and analysis of DEMs for spatial modelling.

Caine, N., 1974. The geomorphic processes of the alpine environment. In: Ives, J. D., Alford, D. (Eds.), Arctic and alpine environments. Methuen, London, pp. 721–748.

Caine, N., 1986. Sediment movement and storage on alpine slopes in the Colorado Rocky mountains. In: Abrahams, A. D. (Ed.), Hillslope Processes. Allen & Unwin, pp. 115–137.

Caine, N., Swanson, F. J., 1989. Geomorphic coupling of hillslope and channel systems in two small mountain basins. Zeitschrift für Geomorphologie N.F. 33 (2), 189–203.

Canty, A., Ripley, B. D., 2016. Package "boot".

Capps, S. R., 1910. Rock Glaciers in Alaska. The Journal of Geology 18 (4).

Carrivick, J. L., Geilhausen, M., Warburton, J., Dickson, N. E., Carver, S. J., 2013. Contemporary geomorphological activity throughout the proglacial area of an alpine catchment. Geomorphology 188, 83–95.

Carrivick, J. L., Rushmer, E. L., 2009. Inter-and intra-catchment variations in proglacial geomorphology: an example from Franz Josef Glacier and Fox Glacier, New Zealand. Arctic, Antarctic, and Alpine Research 41 (1), 18–36.

Carson, M. A., Kirkby, M. J., 1972. Hillslope form and process. Vol. 3 of Cambridge geographical studies. Univ. Press, Cambridge.

Ceaglio, E., Freppaz, M., Maggioni, M., Filippa, G., Godone, D., Zanini, E., 2010. Full-depth avalanches and soil erosion: an experimental site in NW Italy. In: European Geosciences Union (Ed.), Geophysical Research Abstracts. Copernicus GmbH (Copernicus Publications), Göttingen, p. 15565.

Ceaglio, E., Meusburger, K., Freppaz, M., Zanini, E., Alewell, C., 2012. Estimation of soil redistribution rates due to snow cover related processes in a mountainous area (Valle d'Aosta, NW Italy). Hydrology and Earth System Sciences 16 (2), 517–528.

Chassereau, J. E., Bell, J. M., Torres, R., 2011. A comparison of GPS and lidar salt marsh DEMs. Earth Surface Processes and Landforms 36 (13), 1770–1775.

Chiarle, M., Mortara, G., 2008. Geomorphological Impact of Climate Change on Alpine Glacial and Periglacial Areas – Examples of Processes and Research. In: Proceedings of the Interpraevent Conference. Forschungsgemeinschaft Interpraevent, pp. 111–122.

Chiessi, V., D'Orefice, M., Scarascia Mugnozza, G., Vitale, V., Cannese, C., 2010. Geological, geomechanical and geostatistical assessment of rockfall hazard in San Quirico Village (Abruzzo, Italy). Geomorphology 119 (3-4), 147–161.

Chiverrell, R. C., Foster, G. C., Marshall, P., Harvey, A. M., Thomas, G. S. P., 2009. Coupling relationships: Hillslope-fluvial linkages in the Hodder catchment, NW England. Geomorphology 109 (3-4), 222–235.

Chorley, R. J., Kennedy, B. A., 1971. Physical Geography: A Systems Approach. Prentice-Hall, London.

Church, M., 1972. Baffin Island Sandurs: a study of Arctic fluvial Processes. Geological Survey of Canada Bulletin 216. 208 pp., 99 figs (28 in pocket), 40 tables. Ottawa. Price $6.00. Geological Magazine 110 (05), 487.

Church, M. A., 2010. Mountains and Montane Channels. In: Burt, T. P., Allison, R. J. (Eds.), Sediment Cascades. John Wiley & Sons, Chichester and UK, pp. 17–53.

Clague, J. J., Evans, S. G., 2000. A review of catastrophic drainage of moraine-dammed lakes in British Columbia. Quaternary Science Reviews 19 (17), 1763–1783.

Coe, J. A., Harp, E. L., 2007. Influence of tectonic folding on rockfall susceptibility, American Fork Canyon, Utah, USA. Natural Hazards & Earth System Science 7 (1), 1–14.

Confortola, G., Maggioni, M., Freppaz, M., Bocchiola, D., 2012. Modelling soil removal from snow avalanches: A case study in the North-Western Italian Alps. Cold Regions Science and Technology 70 (0), 43–52.

Conrad, O., Bechtel, B., Bock, M., Dietrich, H., Fischer, E., Gerlitz, L., Wehberg, J., Wichmann, V., Böhner, J., 2015. System for Automated Geoscientific Analyses (SAGA) v. 2.1.4. Geosci. Model Dev. 8 (7), 1991–2007.

Conway, H., Carran, W., Carran, A., 2009. Rain in snow avalanches: forecasting the return to stability. In: Proceedings of the International Snow Science Workshop. pp. 267–270.

Cooke, R. U., Doornkamp, J. C., 1993. Geomorphology in environmental management, 2nd Edition. a new introduction. Clarendon Press, Oxford.

Corner, G. D., 1980. Avalanche Impact Landforms in Troms, North Norway. Geografiska Annaler. Series A, Physical Geography 62 (1-2), 1–10.

Coultard, J.-P., Francou, B., 1989. Rock temperature measurement in two alpine environments: implications for frost shattering. Arc. Alp. Res. 21, 399–416.

Coussot, P., Meunier, M., 1996. Recognition, classification and mechanical description of debris flows. Earth-Science Reviews 40 (3-4), 209–227.

Cruden, D. M., Hu, X. Q., 1993. Exhaustion and steady state models for predicting landslide hazards in the Canadian Rocky Mountains. Geomorphology 8 (4), 279–285.

Csardi, G., 2014. Package "igraph".

Curry, A. M., Cleasby, V., Zukowskyj, P., 2006. Paraglacial response of steep, sediment-mantled slopes to post-Little Ice Age glacier recession in the central Swiss Alps. Journal of Quaternary Science 21 (3), 211–225.

Curry, A. M., Morris, C. J., 2004. Lateglacial and Holocene talus slope development and rockwall retreat on Mynydd Du, UK. Geomorphology 58 (1-4), 85–106.

De Quervain, 1966. On avalanche classification: a further contribution.

Dedkov, A. P., Moszherin, V. I., 1992. Erosion and sediment yield in mountain regions of the world. In: International Association of Hydrological Sciences (Ed.), Erosion, Debris Flows and Environment in Mountainous Regions. Vol. 209. pp. 29–36.

Diaz, H. F., Bradley, R. S., 1997. Temperature variations during the last century at high elevation sites. In: Climatic Change at High Elevation Sites. Springer, pp. 21–47.

Dietrich, W. E., Dunne, T., 1978. Sediment budget for a small catchment in mountainous terrain. Zeitschrift für Geomorphologie N.F. Suppl. 29, 191–206.

Dietrich, W. E., Dunne, T., Humphrey, N. F., Reid, L. M., 1982. Construction of sediment budgets for drainage basins. In: Swanson, F. J., Janda, R. J., Dunne, T., Swanston, D. N. (Eds.), Sediment Budgets and Routing in Forested Drainage Basins. Pacific Northwest Forest and Range Experiment Station, Forest Service, U.S. Department of Agriculture, Portland, pp. 5–23.

Dorren, L. K. A., Seijmonsbergen, A. C., 2003. Comparison of three GIS-based models for predicting rockfall runout zones at a regional scale. Geomorphology 56 (1–2), 49–64.

Douglas, G. R., 1980. Magnitude frequency study of rockfall in Co. Antrim, N. Ireland. Earth Surface Processes and Landforms 5, 123–129.

Dubberke, K., 2014. Multitemporale Untersuchungen der Gerinnemobilität eines proglazialen Fließgewässers am Beispiel der Fagge in Tirol. Ph.D. thesis, Martin-Luther-Universität Halle-Wittenberg, Halle.

Dunne, T., 1979. Field studies of hillslope flow processes. In: Kirkby, M. J. (Ed.), Hillslope hydrology. Landscape systemsA Wiley-Interscience publication. Wiley, Chichester [u.a.], pp. 227–294.

Dunning, S. A., Massey, C. I., Rosser, N. J., 2009. Structural and geomorphological features of landslides in the Bhutan Himalaya derived from Terrestrial Laser Scanning: Dating, triggering, modelling, and hazard assessment of large landslides. Geomorphology 103 (1), 17–29.

Dusik, J.-M., 2013. Vergleichende Untersuchungen zur rezenten Dynamik von Blockgletschern im Kaunertal dargestellt an Beispielen aus dem Riffeltal und der Inneren Ölgrube: Msc Thesis.

Dusik, J.-M., 2016. no title yet. Ph.D. thesis, Catholic University of Eichstätt-Ingolstadt, Eichstätt.

Dusik, J.-M., Leopold, M., Heckmann, T., Haas, F., Hilger, L., David Morche, Neugirg, F., Becht, M., 2015. Influence of glacier advance on the development of the multipart Riffeltal rock glacier, Central Austrian Alps. Earth Surface Processes and Landforms.

Dussauge-Peisser, C., Helmstetter, A. A., Grasso, J.-R., Hantz, D., Desvarreux, P., Jeannin, M., Giraud, A., 2002. Probabilistic approach to rock fall hazard assessment: potential of historical data analysis. Natural Hazards & Earth System Science, 15–26.

Ebster, F., 1951. Blatt Weißkugel: Geleitwort des Kartographen. In: Jahrbuch des Deutschen Alpenvereins. Vol. 76. Deutscher Alpenverein, pp. 5–8.

Eckerstorfer, M., Christiansen, H. H., 2012. Meteorology, Topography and Snowpack Conditions causing Two Extreme Mid-Winter Slush and Wet Slab Avalanche Periods in High Arctic Maritime Svalbard. Permafrost and Periglacial Processes 23 (1), 15–25.

Eckerstorfer, M., Christiansen, H. H., Rubensdotter, L., Vogel, S., 2012. The role of cornice fall avalanche sedimentation in the valley Longyeardalen, Central Svalbard. The Cryosphere Discussions 6 (6), 4999–5036.

Ellenberg, H., Leuschner, C., 2010. Vegetation Mitteleuropas mit den Alpen in ökologischer, dynamischer und historischer Sicht, 6th Edition. Vol. 8104 of UTB. Ulmer, Stuttgart.

Embleton-Hamann, C., Slaymaker, O., 2012. The austrian alps and paraglaciation. Geografiska Annaler. Series A, Physical Geography.

Emmett, W., 1975. Basic data report on Clearwater and Snake River.

Erdmann, H., 2009. GIS-basierte, geodätische Massenbilanzierung des Gepatschferners, Ötztaler Alpen, 1872 – 2003: Bilanzierung des Volumens, der Fläche und der Masse mit GIS unter Zuhilfenahme digitaler Geländemodelle, erstellt aus topographischen Karteninformationen. Ph.D. thesis, Justus-Liebig-Universität Giessen, Giessen.

Erskine, R. H., Green, T. R., Ramirez, J. A., MacDonald, L. H., 2006. Comparison of grid–based algorithms for computing upslope contributing area. Water Resources Research 42 (9).

Evans, S. G., Clague, J. J., 1994. Recent climatic change and catastrophic geomorphic processes in mountain environments. Geomorphology 10 (1–4), 107–128.

Fahey, B. D., Lefebure, T. H., 1988. The freeze-thaw weathering regime at a section of the Niagara escarpment on the Bruce Peninsula, Southern Ontario, Canada. Earth Surface Processes and Landforms 13 (4), 293–304.

Fahnestock, M. A., Scambos, T. A., Bindschadler, R. A., 1992. Semi-automated ice velocity determination from satellite imagery. Eos 73, 493.

Fenn, C. R., 1983. Proglacial Streamflow Series: measurement analysis and interpretation. Ph.D. thesis, Southampton University.

Fenn, C. R., 1987. Sediment transfer processes in Alpine glacier basins. In: Gurnell, A. M., Clark, M. J. (Eds.), Glacio-fluvial sediment transfer. Wiley, Chichester, pp. 111–145.

Finsterwalder, R., 1951. Die Geschichte der Gepatschfernervermessung. In: Jahrbuch des Deutschen Alpenvereins. Vol. 76. Deutscher Alpenverein, pp. 9–16.

Finsterwalder, R., 1953. Die zahlenmäßige Erfassung des Gletscherrückgangs an Ostalpengletschern. Zeitschrift für Gletscherkunde und Glazialgeologie 2 (2), 189–239.

Finsterwalder, R., 1978. Beiträge zur Gepatschfernervermessung. Zeitschrift für Gletscherkunde und Glazialgeologie 14 (2), 153–159.

Finsterwalder, R., Pillewizer, W., 1939. Photogrammetric studies of glaciers in high asia. The Himalayan journal 11.

Finsterwalder, R., Rentsch, H., 1976. Die Erfassung der Höhenänderung von Ostalpengletschern in den Zeiträumen 1950-1959-1969. Zeitschrift für Gletscherkunde und Glazialgeologie 12 (1), 29–35.

Finsterwalder, R., Rentsch, H., 1980. Zur Höhenänderung von Ostalpengletschern im Zeitraum 1969-1979.

Finsterwalder, R., Rentsch, H., 1991/92. Zur Höhenänderung von Ostalpengletschern im Zeitraum 1979-1989. Zeitschrift für Gletscherkunde und Glazialgeologie 27/28, 165–172.

Finsterwalder, S., 1897. IX. Vom Gepatsch-. Weisssee- und Langtauferer-Ferner. Mittheilungen des Deutschen und Oesterreichischen Alpenvereins 23, 94–95.

Finsterwalder, S., 1928. Begleitworte zur Karte des Gepatschferners. Zeitschrift für Gletscherkunde und Glazialgeologie 16, 20–41.

Finsterwalder, S., Schunck, H., 1888. Der Gepatschferner. Zeitschrift des Deutschen und Österreichischen Alpenvereins, 50–57.

Fischer, K., 1984. Erläuterungen zur geomorphologischen Karte 1 : 25.000 der Bundesrepublik Deutschland: GMK 25, Blatt 16, 8443 Königssee.

Fischler, M. A., Bolles, R. C., 1981. Random sample consensus: a paradigm for model fitting with applications to image analysis and automated cartography. Communications of the ACM 24 (6), 381–395.

Fliri, F., 1975. Das Klima der Alpen im Raume von Tirol. Wagner, Innsbruck.

Francou, B., 1988. L'eboulisation en Haute Montagne (Alpes, Andes). Contribution iJ l'etude du systeme corniche-eboulis en milieu periglaciaire. Ph.D. thesis, Editec, Caen.

Frattini, P., Crosta, G. B., Carrara, A., Agliardi, F., 2008. Assessment of rockfall susceptibility by integrating statistical and physically-based approaches. GIS technology and models for assessing landslide hazard and risk 94 (3–4), 419–437.

Frauenfelder, R., 2004. Regional-scale modelling of the occurence and dynamics of rockglaciers and the distribution of paleopermafrost. Ph.D. thesis, Universität Zürich, Zürich.

Freeman, G. T., 1991. Calculating catchment area with divergent flow based on a regular grid. Computers and Geosciences 17 (3), 413–422.

Freppaz, M., Godone, D., Filippa, G., Maggioni, M., Lunardi S., Williams, M. W., Zanini, E., 2010. Soil Erosion Caused by Snow Avalanches: a Case Study in the Aosta Valley (NW Italy). Arctic, Antarctic, and Alpine Research 42 (4), 412–421.

Frich, P., Brandt, E., 1985. Holocene talus accumulation rates,—and their influence on rock glacier growth. A case study from Igpik, Disko—West Greenland. Geografisk Tidsskrift-Danish Journal of Geography 85 (1), 32–43.

Fryirs, K. A., 2013. (Dis)Connectivity in catchment sediment cascades: a fresh look at the sediment delivery problem. Earth Surface Processes and Landforms 38 (1), 30–46.

Fuller, I. C., Large, A. R. G., Charlton, M. E., Heritage, G. L., Milan, D. J., 2003. Reach-scale sediment transfers: an evaluation of two morphological budgeting approaches. Earth Surface Processes and Landforms 28 (8), 889–903.

Funk, D., Krautblatter, M., 2010. Diminishing friction of joint surfaces as initiating factor for destabilising permafrost rocks. Geophysical Research Abstracts 12.

Gabet, E. J., 2007. A theoretical model coupling chemical weathering and physical erosion in landslide-dominated landscapes. Earth and Planetary Science Letters 264 (1–2), 259–265.

Galibert, G. M., 1965. La Haute Montagne Alpine: L'évolution actuelle des formes dans les hauts massifs des Alpes et dans certains reliefs de comparaison (à l'exception des montagnes désertiques). Ph.D. thesis, Sciences humaines de Toulouse, Toulouse.

Gamma, P., 2000. dfwalk - Ein Murgang-Simulationsprogramm zur Gefahrenzonierung. Ph.D. thesis, Universität Bern, Bern and Schweiz.

Garbrecht, J., Martz, L. W., 1999. Digital Elevation Model Issues in Water Resources Modeling. In: Maidment, D., Djokic, D. (Eds.), Hydrologic and hydraulic modeling support with geographic information system. ESRI Press, Redlands ,California, USA, pp. 1–28.

Gardner, J., 1970a. Rockfall: a geomorphic process in high mountain terrain. The Albertan Geographer 6, 15–20.

Gardner, J. S., 1970b. Geomorphic Significance of Avalanches in the Lake Louise Area, Alberta, Canada. Arctic, Antarctic, and Alpine Research 2 (2), 135–144.

Gardner, J. S., 1983a. Accretion Rates on Some Debris Slopes in the Mount Rae Area, Canadian Rocky Mountains. Earth Surface Processes and Landforms 8, 347–355.

Gardner, J. S., 1983b. Observations on Erosion by Wet Snow Avalanches, Mount Rae Area, Alberta, Canada. Arctic, Antarctic, and Alpine Research 15 (2), 271–274.

Gärtner-Roer, I., 2012. Sediment transfer rates of two active rockglaciers in the Swiss Alps. Geomorphology 167-168, 45–50.

Gärtner-ÂRoer, I., Nyenhuis, M., 2010. Volume Estimation, Kinematics and Sediment Transfer Rates of Active Rockglaciers in the Turtmann Valley, Switzerland. In: Otto, J.-C., Dikau, R. (Eds.), Landform - Structure, Evolution, Process Control: Proceedings of the International Symposium on Landform organised by the Research Training Group 437. Springer Berlin Heidelberg, Berlin, Heidelberg, pp. 185–198.

Gegg, K., 2010. Erstellung und Validierung eines statistischen Dispositionsmodells für Hangmuren in zwei zentral-alpinen Einzugsgebieten. Ph.D. thesis, Catholic University of Eichstätt-Ingolstadt, Eichstätt.

Geilhausen, M., Otto, J.-C., Schrott, L., 2012. Spatial distribution of sediment storage types in two glacier landsystems (Pasterze & Obersulzbachkees, Hohe Tauern, Austria). Journal of Maps 8 (3), 242–259.

Gerhold, N., 1963. Zwei berühmte Blockgletscher in der Umgebung des Gepatschhauses.

Gerhold, N., 1967. Zur Glazialgeologie der westlichen Ötztaler Alpen. Veröffentlichungen des Museum Ferdinandeum 47, 5–50.

Gerhold, N., 1969. Zur Glazialgeologie der westlichen Ötztaler Alpen. Veröffentlichungen des Museum Ferdinandeum 49, 45–78.

Giardino, J. R., Vick, S. G., 1987. Geologic engineering aspects of rock glaciers. In: Giardino, J. R., Shroder, J. F., Jr., Vitek, J. D. (Eds.), Rock glaciers. Allen & Unwin, Boston [u.a.], pp. 265–287.

Giese, P., 1963. Some results of seismic refraction work at the Gepatsch glacier in the Oetztal Alps. In: IAHS Publication. Vol. 61. pp. 154–161.

Gillespie, C. S., 2014. The powRlaw package: Examples.

Girstmair, A., Mitterer-Hoinkes, S., Bollmann, E., Krainer, K., Sailer, R., Stötter, J., 2013. Rock glacier analyses in the Tyrolean Central Alps based on airborne lidar-data. In: European Geosciences Union (Ed.), Geophysical Research Abstracts. Vol. 15 of Geophysical Research Abstracts. Copernicus GmbH (Copernicus Publications), Göttingen, p. 4235.

Glira, P., Briese, C., Pfeifer, N., Dusik, J.-M., Hilger, L., Neugirg, F., Baewert, H., 2014. Accuracy analysis of height difference models derived from terrestrial laser scanning point clouds. In: European Geosciences Union (Ed.), Geophysical Research Abstracts. Geophysical Research Abstracts. Copernicus GmbH (Copernicus Publications), Göttingen, p. 15987.

Glira, P., Pfeifer, N., Briese, C., Ressl, C., 2015a. Rigorous strip adjustment of airborne laserscanning data based on the ICP algorithm. ISPRS Ann. Photogramm. Remote Sens. Spatial Inf. Sci. II-3/W5, 73–80.

Glira, P., Pfeifer, N., Ressl, C., Briese, C., 2015b. A correspondence framework for ALS strip adjustments based on variants of the ICP algorithm. Journal for Photogrammetry, Remote Sensing and Geoinformation Science.

Godt, J. W., Coe, J. A., 2007. Alpine debris flows triggered by a 28 July 1999 thunderstorm in the central Front Range, Colorado. Geomorphology 84 (1-2), 80–97.

Gray, J. T., 1972. Debris accumulation on talus slopes in central Yukon Territory. In: Slaymaker, O., MacPherson, H. J. (Eds.), Mountain geomorphology. Vol. 14 of BC geographical series. Tantalus Research, Vancouver and Canada, pp. 5–84.

Gross, G., 1987. Der Flächenverlust der Gletscher in Österreich 1850-1920-1969. Zeitschrift für Gletscherkunde und Glazialgeologie 23, 131–141.

Gruen, A., Akca, D., 2005. Least squares 3D surface and curve matching. ISPRS Journal of Photogrammetry and Remote Sensing 59 (3), 151–174.

Grunder, M., Kienholz, H., 1986. Gefahrenkartierung. In: Wildi, O., Ewald, K. (Eds.), Der Naturraum und dessen Nutzung im alpinen Tourismusgebiet von Davos. Vol. 289 of Berichte / Eidgenössische Anstalt für das Forstliche Versuchswesen. Eidgenössische Anstalt für das Forstliche Versuchswesen, Birmensdorf, pp. 67–85.

Guijarro, J. A., 2014. User's Guide to climatol.

Gurnell, A. M., Clark, M. J. (Eds.), 1987. Glacio-fluvial sediment transfer: An alpine perspective. Wiley, Chichester.

Guzzetti, F., Ardizzone, F., Cardinali, M., Rossi, M., Valigi, D., 2009. Landslide volumes and landslide mobilization rates in Umbria, central Italy. Earth and Planetary Science Letters 279 (3), 222–229.

Guzzetti, F., Malamud, B. D., Turcotte, D. L., Reichenbach, P., 2002. Power-law correlations of landslide areas in central Italy. Earth and Planetary Science Letters 195 (3-4), 169–183.

Guzzetti, F., Reichenbach, P., Wieczorek, G. F., 2003. Rockfall hazard and risk assessment in the Yosemite Valley, California, USA. Natural Hazards & Earth System Science 3 (6), 491–503.

Haas, F., 2008. Fluviale Hangprozesse in Alpinen Einzugsgebieten der Nördlichen Kalkalpen: Quantifizierung und Modellierungsansätze. Ph.D. thesis, Catholic University of Eichstätt-Ingolstadt, Eichstätt.

Haas, F., Heckmann, T., Becht, M., Cyffka, B., 2011a. Ground-based laserscanning - a new method for measuring fluvial erosion on steep slopes? In: Hafeez, M. M. (Ed.), GRACE, remote sensing and ground-based methods in multi-scale hydrology. Vol. 343 of IAHS publication. IAHS Press, Wallingford, pp. 163–168.

Haas, F., Heckmann, T., Hilger, L., Becht, M., 2012a. Quantification and modelling of debris flows in the proglacial area of the Gepatschferner, Austria, using ground-based LiDAR. In: International Association of Hydrological Sciences (Ed.), Erosion and Sediment Yields in the Changing Environment. Vol. 356 of IAHS publication. IAHS Press, Wallingford, pp. 293–302.

Haas, F., Heckmann, T., Klein, T., Becht, M., 2009. Rockfall Measurements in Alpine Catchments (Germany, Austria, Italy) by Terrestrial Laserscanning: First Results. Geophysical Research Abstracts 11.

Haas, F., Heckmann, T., Wichmann, V., Becht, M., 2004. Change of Fluvial Sediment Transport Rates after a High Magnitude Debris Flow Event in a Drainage Basin in the Northern Limestone Alps, Germany. IAHS Publication 288, 37–43.

Haas, F., Heckmann, T., Wichmann, V., Becht, M., 2011b. Quantification and Modeling of Fluvial Bedload Discharge from Hillslope Channels in two Alpine Catchments (Bavarian Alps, Germany). Zeitschrift für Geomorphologie N.F. Suppl. 55 (3), 147–168.

Haas, F., Heckmann, T., Wichmann, V., Becht, M., 2012b. Runout analysis of a large rockfall in the Dolomites/Italian Alps using LIDAR derived particle sizes and shapes. Earth Surface Processes and Landforms 37 (13), 1444–1455.

Haeberli, W., 1985. Creep of mountain permafrost: Internal structure and flow of alpine rock glaciers.

Haeberli, W., 1992. Zur Stabilität von Moränenstauseen in hochalpinen Gletschergebieten. Wasser, Energie, Luft 84, 361–364.

Haeberli, W., 1996a. Die "Permafrost-Faustregeln" der VAW/ETHZ - einige grundsätzliche Bemerkungen. In: Haeberli, W. (Ed.), Simulation der Permafrostverbreitung in den Alpen mit geographischen Informationssystemen. Arbeitsbericht NFP 31. vdf, Hochsch.-Verl. an der ETH, Zürich, pp. 13–18.

Haeberli, W. (Ed.), 1996b. Simulation der Permafrostverbreitung in den Alpen mit geographischen Informationssystemen: [Arbeitsbericht im Rahmen des Nationalen Forschungsprogrammes "Klimaänderungen und Naturkatastrophen", NFP 31]. Arbeitsbericht NFP 31. vdf, Hochsch.-Verl. an der ETH, Zürich.

Haeberli, W., Paul, F., Zemp, M., 2013. Vanishing glaciers in the European Alps. Fate of Mountain glaciers in the anthropocene. Pontifical Academy of Sciences, Scripta Varia 118, 1–9.

Hagg, W., Becht, M., 2000. Einflüsse von Niederschlag und Substrat auf die Auslösung von Hangmuren in Beispielgebieten der Ostalpen. In: Becht, M.,

Schmidt, K.-H. (Eds.), Angewandte und vernetzte geomorphologische Prozeßforschung. Vol. 123 of Zeitschrift für Geomorphologie - Supplementbände. Bornträger, Berlin, pp. 79–92.

Hales, T. C., Roering, J. J., 2007. Climatic controls on frost cracking and implications for the evolution of bedrock landscapes. Journal of Geophysical Research: Earth Surface (2003–2012) 112 (F2).

Hall, K., Otte, W., 1990. A note on biological weathering on nunataks of the Juneau Icefield, Alaska. Permafrost and Periglacial Processes 1 (2), 189–196.

Hallet, B., Hunter, L., Bogen, J., 1996. Rates of erosion and sediment evacuation by glaciers: A review of field data and their implications: Impact of Glaciations on Basin Evolution: Data and Models from the Norwegian Margin and Adjacent Areas. Global and Planetary Change 12 (1–4), 213–235.

Hamilton, S. J., Whalley, W. B., 1995. Rock glacier nomenclature: A reassessment. Geomorphology 14 (1), 73–80.

Hammer, K. M., Smith, N. D., 1983. Sediment production and transport in a proglacial stream: Hilda Glacier, Alberta, Canada. Boreas 12 (2), 91–106.

Haralick, B. M., Lee, C.-N., Ottenberg, K., Nölle, M., 1994. Review and analysis of solutions of the three point perspective pose estimation problem. International journal of computer vision 13 (3), 331–356.

Harbor, J., Warburton, J., 1992. Glaciation and denudation rates. Nature 356, 751.

Harbor, J. M., Warburton, J., 1993. Relative rates of glacial and nonglacial erosion in alpine environments. Arctic, Antarctic, and Alpine Research 25 (1), 1–7.

Harlaar, P., 2015. Soil evolution analysis on a geomorphologically active glacial forefield using a high resolution DEM. Ph.D. thesis, Wageningen University, Wageningen.

Hartl, L., 2010. The Gepatschferner from 1850-2006: Changes in Length, Area and Volume in Relation to Climate. Ph.D. thesis, University of Innsbruck, Innsbruck.

Hartmann, D. L., Klein Tank, A. M., Rusicucci, M., Alexander, L. V., Broenniman, B., Charabi, Y., Dentener, F. J., Dlugokencky, E. J., Easterling, Kaplan, A., 2013. Observations: atmosphere and surface. In: Climate Change 2013 the Physical Science Basis: Working Group I Contribution to the Fifth Assessment Report of the Intergovernmental Panel on Climate Change. Cambridge University Press, pp. 159–254.

Hastings, B. E., Kampf, S. K., 2014. Evaluation of digital channel network derivation methods in a glaciated subalpine catchment. Earth Surface Processes and Landforms 39 (13), 1790–1802.

Hattanji, T., Onda, Y., 2004. Coupling of runoff processes and sediment transport in mountainous watersheds underlain by different sedimentary rocks. Hydrological Processes 18 (4), 623–636.

Hausmann, H., Krainer, K., Brückl, E., Blöschl, G., 2008. Geophysical investigations of alpine permafrost in the Ötztal Alps of Austria. In: European Geosciences Union (Ed.), Geophysical Research Abstracts. Vol. 10 of Geophysical Research Abstracts. Copernicus GmbH (Copernicus Publications), Göttingen.

Hausmann, H., Krainer, K., Brückl, E., Blöschl, G., Chirico, G. B., Komma, J., Illnar, R., Eipeldauer, S., 2010. Sediment quantification and ground water storage in an alpine permafrost catchment. In: Third European Conference on Permafrost.

Hausmann, H., Krainer, K., Brückl, E., Mostler, W., 2007. Creep of two alpine rock glaciers: Observation and modelling (Ötztal- and Stubai Alps, Austria). Grazer Schriften der Geographie und Raumforschung 43, 145–150.

Hausmann, H., Krainer, K., Brückl, E., Roger, M., Chirico, G. B., Blöschl, G., 2013. Sediment and water storage in an Alpine permafrost catchment area, Krummgampen Valley, Ötztal Alps, Austria.

Hausmann, H., Krainer, K., Brückl, E., Ullrich, C., 2012. Internal structure, ice content and dynamics of Ölgrube and Kaiserberg Rock glaciers (Ötztal Alps, Austria) determined from geophysical surveys. Austrian Journal of Earth Sciences 105 (2), 12–31.

Hausmann, H., Krainer, K., Staudinger, M., Brückl, E., 2009. Continuous recording of seismic signals in Alpine permafrost. In: European Geosciences Union (Ed.), Geophysical Research Abstracts. Copernicus GmbH (Copernicus Publications), Göttingen, p. 10330.

Heckmann, T., 2006a. Statistical disposition modelling of mass movements. In: Böhner, J., McCloy, K. R., Strobl, J. (Eds.), SAGA - Analysis and Modelling Applications. Vol. 115 of Göttinger Geographische Abhandlungen. Goltze, Göttingen, pp. 61–73.

Heckmann, T., 2006b. Untersuchungen zum Sedimenttransport durch Grundlawinen in zwei Einzugsgebieten der Nördlichen Kalkalpen: Quantifizierung, Analyse und Ansätze zur Modellierung der geomorphologischen Aktivität. Ph.D. thesis, Catholic University of Eichstätt-Ingolstadt, Eichstätt.

Heckmann, T., 2013a. CutFill, a SAGA GIS module to calculate a sediment balance from pre- and post-event digital elevation models.

Heckmann, T., 2013b. From rasters to networks - Spatial modelling for the analysis of geomorphic systems and sediment cascades. Ph.D. thesis, Catholic University of Eichstätt-Ingolstadt, Eichstätt.

Heckmann, T., Bimböse, M., Krautblatter, M., Haas, F., Becht, M., Morche, D., 2012a. From geotechnical analysis to quantification and modelling using LiDAR data: a study on rockfall in the Reintal catchment, Bavarian Alps, Germany. Earth Surface Processes and Landforms 37 (1), 119–133.

Heckmann, T., Haas, F., Morche, D., Schmidt, K.-H., Rohn, J., Moser, M., Leopold, M., Kuhn, M., Briese, C., Pfeifer, N., Becht, M., 2012b. Quantifying proglacial morphodynamics and sediment budgets - the PROSA approach. Geophysical Research Abstracts 14.

Heckmann, T., Hilger, L., Vehling, L., Becht, M., 2016. Integrating field measurements, a geomorphological map and stochastic modelling to estimate the spatially distributed rockfall sediment budget of the Upper Kaunertal, Austrian Central Alps. Geomorphology (260), 16–31.

Heckmann, T., Schwanghart, W., 2013. Geomorphic coupling and sediment connectivity in an alpine catchment — Exploring sediment cascades using graph theory. Geomorphology 182 (0), 89–103.

Heckmann, T., Wichmann, V., Becht, M., 2002. Quantifying Sediment Transport by Avalanches in the Bavarian Alps - First Results. Zeitschrift für Geomorphologie N.F. Suppl. 127, 137–152.

Heckmann, T., Wichmann, V., Becht, M., 2005. Sediment Transport by Avalanches in the Bavarian Alps Revisited - a Perspective on Modelling. Zeitschrift für Geomorphologie N.F. Suppl. 138, 11–25.

Heinimann, H. R., Hollenstein, K., Kienholz, H., Krummenacher, B., Mani, P., 1998. Methoden zur Analyse und Bewertung von Naturgefahren: Eine risikoorientierte Betrachtungsweise.

Heißel, G., Weber, C., 2000. Die Massenbewegungen an der "Weissseespitze" in den Jahren 1996-1999 im Gletschergebiet Kaunertal / Tirol. In: Internationale Forschungsgesellschaft Interpraevent (Ed.), Changes within the natural and cultural habitat and consequences. Vol. 1. Krainer Druck, pp. 227–237.

Henninger, R., 1985. Darstellung der Veränderungen des Gepatschferners. Ph.D. thesis, Fachhochschule Karlsruhe, Karlsruhe.

Hergarten, S., 2002. Landslides, Sandpiles, and Self-Organized Criticality. Natural Hazards & Earth System Science 3, 505–514.

Heuberger, H., 1966. Gletschergeschichtliche Untersuchungen in den Zentralalpen zwischen Sellrain- und Ötztal. Vol. 20 of Wissenschaftliche Alpenvereinshefte. Universitätsverlag Wagner, Innsbruck.

Hicks, D. M., McSaveney, M. J., Chinn, T. J. H., 1990. Sedimentation in proglacial Ivory Lake, Southern Alps, New Zealand. Arctic, Antarctic, and Alpine Research 22 (1), 26–42.

Hilger, L., Dusik, J.-M., Heckmann, T., Haas, F., Glira, P., Becht, M., 2015a. Quantification of debris flow events in the upper Kauner valley (Ötztal Alps) for the years of 1953-2012. In: European Geosciences Union (Ed.), Geophysical Research Abstracts. Vol. 17. Copernicus GmbH (Copernicus Publications), Göttingen.

Hilger, L., Haas, F., Heckmann, T., Wichmann, V., Trappe, M., Becht, M., 2015b. Reconstruction of historic soil erosion rates in a small lake catchment of the Melrakkaslétta peninsula of northeast Iceland using tephrochronology and ground-based LiDAR data. Zeitschrift für Geomorphologie 59 (2), 243–263.

Hilger, L., Heckmann, T., 2014. Cut & Fill (prob. thresholding with spatial dist. error): - a SAGA GIS tool.

Hinchliffe, S., Ballantyne, C. K., 1999. Talus accumulation and rockwall retreat, Trotternish, Isle of Skye, Scotland. The Scottish Geographical Magazine 115 (1), 53–70.

Hinderer, M., 2001. Late Quaternary denudation of the Alps, valley and lake fillings and modern river loads. Geodinamica Acta 14 (4), 231–263.

Hoffmann, T., Schrott, L., 2002. Modelling sediment thickness and rockwall retreat in an Alpine valley using 2D-seismic refraction (Reintal, Bavarian Alps). Zeitschrift für Geomorphologie, Supplementary Issues 127, 175–196.

Hofle, B., Vetter, M., Pfeifer, N., Mandlburger, G., Stotter, J., 2009. Water surface mapping from airborne laser scanning using signal intensity and elevation data. Earth Surface Processes and Landforms 34 (12), 1635.

Hoinkes, H., 1954. Beiträge zur Kenntnis des Gletscherwindes. Theoretical and Applied Climatology 6 (1), 36–53.

Höllermann, P., 1964. Rezente Verwitterung, Abtragung und Formenschatz im oberen Suldental, Ortlergruppe. Zeitschrift für Geomorphologie N.F. Suppl. 4.

Höllermann, P., 1983a. Blockgletscher als Mesoformen der Periglazialstufe: Studien aus europäischen und nordamerikanischen Hochgebirgen. Vol. 67Dümmlerbuch ; 7617 of Bonner geographische Abhandlungen. Dümmler, Bonn.

Höllermann, P., 1983b. Verbreitung und Typisierung von Glatthängen, Mesoformen des Reliefs im heutigen Periglazialraum.

Holloway, S. L., 2003. Key concepts in geography, 1st Edition. Sage, London [u.a.].

Hölzle, M., 1994. Permafrost und Gletscher im Oberengadin: Grundlagen und Anwendungsbeispiele für automatisierte Schätzverfahren. Ph.D. thesis, Eidgenössische Technische Hochschule Zürich, Zürich.

Hölzle, M., Wagner, S., Kääb, A., Vonder Mühll, D. S., 1998. Surface Movement and Internal Deformation of Ice-Rock Mixtures within Rock Glaciers at Pontresina-Schafberg, Upper Engadin, Switzerland. In: Lewkowicz, A. G., Allard, M. (Eds.), Proceedings of the 7th International Conference on Permafrost. Yellowknife, pp. 465–471.

Hovius, N., Stark, C. P., Allen, P. A., 1997. Sediment flux from a mountain belt derived by landslide mapping. Geology 25 (3), 231–234.

Hovius, N., Stark, C. P., Hao-Tsu, C., Jiun-Chuan, L., 2000. Supply and removal of sediment in a landslide–dominated mountain belt: Central Range, Taiwan. The Journal of Geology 108 (1), 73–89.

Hubbard, B., Glasser, N. F., 2005. Field techniques in glaciology and glacial geomorphology. John Wiley & Sons, Chichester and West Sussex and England and Hoboken, NJ.

Huggel, C., Kääb, A., Haeberli, W., Teysseire, P., Paul, F., 2002. Remote sensing based assessment of hazards from glacier lake outbursts: a case study in the Swiss Alps. Canadian Geotechnical Journal 39 (2), 316–330.

Humlum, O., 2000. The geomorphic significance of rock glaciers: estimates of rock glacier debris volumes and headwall recession rates in West Greenland. Geomorphology 35 (1-2), 41–67.

Hungr, O., Evans, S. G., Hazzard, J., 1999. Magnitude and frequency of rock falls and rock slides along the main transportation corridors of southwestern British Columbia. Canadian Geotechnical Journal 36 (2), 224–238.

Hutchinson, J. N., 1988. Morphological and geotechnical parameters of landslides in relation to geology and hydrology: General report. In: Bonnard, C. (Ed.), Landslides: Proceedings of the Fifth International Symposium on Landslides. Balkema, Rotterdam, pp. 3–35.

Imhof, M., 1996. PERM - ein Programm für die automatisierte Kartierung von Permafrost in den Schweizer Alpen. In: Haeberli, W. (Ed.), Simulation der Permafrostverbreitung in den Alpen mit geographischen Informationssystemen. Arbeitsbericht NFP 31. vdf, Hochsch.-Verl. an der ETH, Zürich, pp. 25–34.

International Association of Oil & Gas Producers, 2015. EPSG Geodetic Parameter Registry.

Irvine-Fynn, T. D. L., Barrand, N. E., Porter, P. R., Hodson, A. J., Murray, T., 2011. Recent High-Arctic glacial sediment redistribution: A process perspective using airborne lidar. Geomorphology 125 (1), 27–39.

Iwahashi, J., Pike, R. J., 2007. Automated classifications of topography from DEMs by an unsupervised nested-means algorithm and a three-part geometric signature. Geomorphology 86 (3–4), 409–440.

Jaboyedoff, M., Demers, D., Locat, J., Locat, A., Locat, P., Oppikofer, T., Robitaille, D., Turmel, D., 2009. Use of terrestrial laser scanning for the characterization of retrogressive landslides in sensitive clay and rotational landslides in river banks. Canadian Geotechnical Journal 46 (12), 1379–1390.

Jaboyedoff, M., Labiouse, V., 2011. Technical Note: Preliminary estimation of rockfall runout zones. Natural Hazards & Earth System Science 11 (3), 819–828.

Jäckli, H., 1957. Gegenwartsgeologie des bündnerischen Rheingebietes: Ein Beitrag zur exogenen Dynamik alpiner Gebirgslandschaften. Vol. 36 of Beiträge zur Geologie der Schweiz : Geotechnische Serie. Kümmerly & Frey, Bern.

Jenness, J. S., 2004. Calculating landscape surface area from digital elevation models. Wildlife Society Bulletin 32 (3), 829–839.

Johnson, A. L., Smith, D. J. A. N., 2010. Geomorphology of snow avalanche impact landforms in the southern Canadian Cordillera. Canadian Geographer / Le Géographe canadien 54 (1), 87–103.

Johnson, A. M., Rodine, J. R., 1984. Debris flow. In: Brunsden, D., Prior, D. B. (Eds.), Slope instability. John Wiley & Sons, Chichester, pp. 257–361.

Johnson, P. G., 1974. Mass Movement of Ablation Complexes and Their Relationship to Rock Glaciers. Geografiska Annaler. Series A, Physical Geography 56 (1/2), 93–101.

Johnson, R. M., Warburton, J., 2002. Annual sediment budget of a UK mountain torrent. Geografiska Annaler: Series A, Physical Geography 84 (2), 73–88.

Jomelli, V., 1999. Les Effets de la Fonte sur la Sedimentation de Depots d'Avalanche de Neige Chargee dans le Massif des Ecrins (Alpes Francaises). Géomorphologie: relief, processus, environnement 5 (1), 39–58.

Jomelli, V., Bertran, P., 2001. Wet Snow Avalanche Deposits in the French Alps: Structure and Sedimentology. Geografiska Annaler. Series A, Physical Geography 83 (1-2), 15–28.

Jonasson, C., Nyberg, R., Rapp, A., 1997. Dating of rapid mass movements in Scandinavia: talus rockfalls, large rockslides, debris flows and slush avalanches. In: Matthews, J. A., Brunsden, D., Frenzel, B. G. B., Weiß, M. M. (Eds.), Rapid mass movement as a source of climatic evidence for the Holocene. Vol. 19 of Paläoklimaforschung. Gustav Fischer, Stuttgart and Jena and Lübeck and Ulm, pp. 267–282.

Kääb, A., Chiarle, M., Raup, B., Schneider, C., 2007a. Climate change impacts on mountain glaciers and permafrost. Global and Planetary Change 56, 7.

Kääb, A., Frauenfelder, R., Roer, I., 2007b. On the response of rockglacier creep to surface temperature increase. Global and Planetary Change 56 (1-2), 172–187.

Kager, H., 2004. Discrepancies between overlapping laser scanner strips - simutaneous fitting of aerial laser scanner strips. In: International Archives of Photogrammetry, Remote Sensing and Spatial Information Sciences. Vol. 1. pp. 555–560.

Kaufmann, V., Ladstädter, R., 2003. Quantitative analysis of rock glacier creep by means of digital photogrammetry using multi-temporal aerial photographs: two case studies in the Austrian Alps. In: Phillips, M., Springman, S. M., Arenson, L. U. (Eds.), Proceedings of the 8th International Conference on Permafrost. Swets & Zeitlinger, Lisse, pp. 525–530.

Keiler, M., Knight, J., Harrison, S., 2010. Climate change and geomorphological hazards in the eastern European Alps. Philosophical Transactions of the Royal Society A: Mathematical, Physical and Engineering Sciences 368 (1919), 2461–2479.

Keller, D., Moser, M., 2002. Assessment of Field Methods for Rock Fall and Soil Slip Modelling. Zeitschrift für Geomorphologie N.F. Suppl. 127, 127–135.

Keller, F., 1992. Automated mapping of mountain permafrost using the program PERMAKART within the geographical information system ARC/INFO. Permafrost and Periglacial Processes 3 (2), 133–138.

Kellerer-Pirklbauer, A., Proske, H., Strasser, V., 2010. Paraglacial slope adjustment since the end of the Last Glacial Maximum and its long-lasting effects on secondary mass wasting processes: Hauser Kaibling, Austria: Landslide geomorphology in a changing environment. Geomorphology 120 (1–2), 65–76.

Kerschensteiner, G., 1892. Die zweite Vermessung des Gepatschferners. Mittheilungen des Deutschen und Oesterreichischen Alpenvereins 18 (13), 148–150.

Kerschner, H., 1979. Spätglaziale Getscherstände im inneren Kaunertal (Ötztaler Alpen). In: Keller, W. (Ed.), Studien zur Landeskunde Tirols und angrenzender Gebiete. Vol. 6Leidlmair-Festschrift ; 2 of Innsbrucker geographische Studien. Inst. für Geographie der Univ. Innsbruck, Innsbruck, pp. 235–248.

Keutterling, A., Thomas, A., 2006a. Bemerkungen zur Orthophotokarte Gepatschferner 1990. Zeitschrift für Gletscherkunde und Glazialgeologie.

Keutterling, A., Thomas, A., 2006b. Monitoring glacier elevation and volume changes with digital photogrammetry and GIS at Gepatschferner glacier, Austria. International Journal of Remote Sensing 27 (19), 4371–4380.

Kienzle, S., 2004. The effect of DEM raster resolution on first order, second order and compound terrain derivatives. Transactions in GIS 8 (1), 83–111.

Kilian, W., Müller, F., Starlinger, F., 1994. Die forstlichen Wuchsgebiete Österreichs: Eine Naturraumgliederung nach waldökologischen Gesichtspunkten ; FDK:182.3:188(436). Vol. 82 of FBVA-Berichte. Forstliche Bundesversuchsanst., Waldforschungszentrum, Wien.

Kinzl, H., 1929. Beiträge zur Geschichte der Gletscherschwankungen in den Ostalpen. Zeitschrift für Gletscherkunde und Glazialgeologie 17, 66–121.

Kinzl, H., 1966. Die Gletscher der österreichischen Alpen 1963/64 und 1964/1965. In: Mitteilungen des Osterreichischen Alpenvereins. Vol. 21 of Mitteilungen des Osterreichischen Alpenvereins. Österreichischer Alpenverein, Innsbruck, pp. 61–62.

Kirchner, J. W., 2001. Data Analysis Toolkits.

Kirchner, J. W., Finkel, R. C., Clifford, R. S., Granger, D. E., Clayton, J. L., King, J. G., Megahan, W. F., 2001. Mountain erosion over 10-year, 10000-year, and 10000000-year timescales. Geology 29, 591–594.

Klebelsberg, R. v., 1964. Die Gletscher der österreichischen Alpen 1962/63. In: Hensler, E. (Ed.), Mitteilungen des Österreichischen Alpenvereins. Österreichischer Alpenverein, Innsbruck, p. 5.

Kneisel, C., 1998. Legende für geomorphologische Kartierungen in Hochgebirgen (GMK Hochgebirge). Vol. 18 of Trierer Geographische Studien. Geographische Ges, Trier.

Knight, J., 2011. Chapter Twenty-One - Uses and Limitations of Field Mapping of Lowland Glaciated Landscapes. In: Smith, M. J., Paron, P., Griffiths, J. S. (Eds.), Developments in Earth Surface Processes : Geomorphological Mapping Methods and Applications. Vol. 15. Elsevier, pp. 533–550.

Knight, J., Harrison, S., 2014. Mountain Glacial and Paraglacial Environments under Global Climate Change: Lessons from the Past, Future Directions and Policy Implications. Geografiska Annaler: Series A, Physical Geography 96 (3), 245–264.

Knight, J., Mitchell, W. A., Rose, J., 2011. Chapter Six - Geomorphological Field Mapping. In: Smith, M. J., Paron, P., Griffiths, J. S. (Eds.), Developments in Earth Surface Processes : Geomorphological Mapping Methods and Applications. Vol. 15. Elsevier, pp. 151–187.

Kohl, B., Brauner, M., Habersack, H., Markart, G., 2001. Soil Erosion due to Avalanches - Measurements on an Avalanche Cone. In: International Symposium on Snowmelt and Related Problems. pp. 28–30.

Kondolf, G. M., Piegay, H. (Eds.), 2003. Tools in fluvial geomorphology. Wiley, Chichester [u.a.].

Konz, N., Baenninger, D., Konz, M., Nearing, M., Alewell, C., 2010. Process identification of soil erosion in steep mountain regions. Hydrology & Earth System Sciences 14 (4), 675–686.

Korup, O., Rixen, C., 2014. Soil erosion and organic carbon export by wet snow avalanches. The Cryosphere 8 (2), 651–658.

Krainer, K., 2010. Geologie und Geomorphologie von Obergurgl und Umgebung. In: Koch, E.-M. (Ed.), Glaziale und periglaziale Lebensräume im Raum Obergurgl. Vol. 1 of Series / Alpine Forschungsstelle Obergurgl. Innsbruck University Press, Innsbruck, pp. 31–52.

Krainer, K., Mostler, W., 2006. Flow velocities of active rock glaciers in the austrian Alps. Geografiska Annaler 88A (4), 267–280.

Krainer, K., Mostler, W., Spötl, C., 2007. Discharge from active rock glaciers, Austrian Alps: a stable isotope approach. Austrian Journal of Earth Sciences 100, 102–112.

Krainer, K., Ribis, M., 2012. A rock glacier inventory of the tyrolean Alps (Austria). Austrian Journal of Earth Sciences 105 (2), 32–47.

Krapf, V., 2001. Palynologische Untersuchungen zur Klima- und Vegetationsgeschichte im Kauner- und Langtauferertal. Ph.D. thesis, University of Innsbruck, Innsbruck.

Kraus, K., Pfeifer, N., 1998. Determination of terrain models in wooded areas with airborne laser scanner data. ISPRS Journal of Photogrammetry and Remote Sensing 53 (4), 193–203.

Kraushaar, S., Blöthe, J., Baewert, H., Dubberke, K., Culha, C., Knöller, K., Morche, D., 2014. Supportive methods for sediment budgeting: Stable isotope measurements of perennial springs in the Kaunertal valley. In: Sedibud Conference. unpublished.

Krautblatter, M., 2004. The Impact of Rainfall Intensity and other External Factors on Primary and Secondary Rockfall (Reintal, Bavarian Alps). Ph.D. thesis, Geographisches Institut, Universität Erlangen-Nürnberg.

Krautblatter, M., Dikau, R., 2007. Towards a uniform concept for the comparison and extrapolation of rockwall retreat and rockfall supply. Geografiska Annaler 89 (1), 21–40.

Krautblatter, M., Moser, M., 2009. A nonlinear model coupling rockfall and rainfall intensity based on a four year measurement in a high Alpine rock wall (Reintal, German Alps). Natural Hazards & Earth System Science 9 (4), 1425–1432.

Krautblatter, M., Moser, M., Schrott, L., Wolf, J., Morche, D., 2012. Significance of rockfall magnitude and carbonate dissolution for rock slope erosion and geomorphic work on Alpine limestone cliffs (Reintal, German Alps). Geomorphology 167-168, 21–34.

Krigström, A., 1962. Geomorphological Studies of Sandur Plains and Their Braided Rivers in Iceland. Geografiska Annaler 44 (3/4), 328–346.

Kutta, W., 1901. Der Gepatschferner im Jahre 1896. Mittheilungen des Deutschen und Oesterreichischen Alpenvereins 27 (11), 133–135.

Laatsch, W., Grottenthaler, W., 1972. Typen der Massenverlagerung in den Alpen und ihre Klassifikation. European Journal of Forest Research 91 (6), 309–339.

Lackinger, B., Gabl, K., 2000. Lawinenhandbuch, 7th Edition. Tyrolia, Innsbruck.

Lamoureux, S. F., McDonald, D. M., Cockburn, J. M. H., Lafrenière, M. J., Atkinson, D. M., Treitz, P., 2006. An Incidence of Multi-Year Sediment Storage on Channel Snowpack in the Canadian High Arctic. Arctic 59 (4).

Lan, H., Martin, C. D., Zhou, C., Lim, C. H., 2010. Rockfall hazard analysis using LiDAR and spatial modeling. Geomorphology 118 (1–2), 213–223.

Lane, S. N., Westaway, R. M., Murray Hicks, D., 2003. Estimation of erosion and deposition volumes in a large, gravel-bed, braided river using synoptic remote sensing. Earth Surface Processes and Landforms 28 (3), 249–271.

Langham, E. J., 1981. Physics and Properties of Snowcover: 7. In: Gray, D. M., Male, D. H. (Eds.), Handbook of Snow. Principles, Processes, Management & Use. Pergamon Press, Toronto, pp. 275–337.

Lari, S., Frattini, P., Crosta, G. B., 2014. A probabilistic approach for landslide hazard analysis. Advances in Engineering Geology for Landslides and Slope Stability Problems: Part 1 182, Part A, 3–14.

Larsen, I. J., Montgomery, D. R., Korup, O., 2010. Landslide erosion controlled by hillslope material. Nature Geoscience 3 (4), 247–251.

Lauffer, H., Sommer, N., 1982. Studies on Sediment Transport in Mountain Streams of the Eastern Alps.

Lavé, J., Burbank, D. W., 2004. Denudation processes and rates in the Transverse Ranges, southern California: Erosional response of a transitional landscape to external and anthropogenic forcing. Journal of Geophysical Research: Earth Surface 109 (F1), F01006.

Leser, H., 1977. Feld- und Labormethoden der Geomorphologie, 1st Edition. De-Gruyter-Lehrbuch. de Gruyter, Berlin [u.a.].

Leser, H., Schaub, D., 1987. Geomorphologische Kartierung im Hochgebirge: ein Anwendungsbeispiel der "Grünen Legende" im Maßstab 1:10 000. In: 100 Jahre Geographisches Institut der Berliner Universität - Jubiläumskonferenz der Sektion Geographie der Humboldt. Vol. 42 of Berliner geographische Abhandlungen. Geographisches Institut der Humboldt-Universität zu Berlin, Berlin, pp. 31–37.

Leser, H., Stäblein, G., 1978. Legende der Geomorphologischen Karte 1 : 25000: 3. Fassung im GMK-Schwerpunktprogramm. In: Berliner geographische Arbeiten. Vol. 30. Geographisches Institut, Universität Berlin, Berlin, pp. 91–100.

Leser, H., Stäblein, G., Göbel, P., 1975. Geomorphologische Kartierung: Richtlinien zur Herstellung geomorphologischer Karten 1:25000. Institut für Physische Geographie der Freien Universität Berlin, Berlin.

Levermann, A., Bamber, J. L., Drijfhout, S., Ganopolski, A., Haeberli, W., Harris, N. R. P., Huss, M., Krüger, K., Lenton, T. M., Lindsay, R. W., 2012. Potential climatic transitions with profound impact on Europe. Climatic Change 110 (3-4), 845–878.

Lewkowicz, A. G., Harris, C., 2005. Frequency and magnitude of active-layer detachment failures in discontinuous and continuous permafrost, northern Canada. Permafrost and Periglacial Processes 16 (1), 115–130.

Lim, M., Rosser, N. J., Allison, R. J., Petley, D. N., 2010. Erosional processes in the hard rock coastal cliffs at Staithes, North Yorkshire. Geomorphology In Press, Corrected Proof.

Lindsay, J. B., Ashmore, P. E., 2002. The effects of survey frequency on estimates of scour and fill in a braided river model. Earth Surface Processes and Landforms 27 (1), 27–43.

Lourakis, M., Argyros, A., 2004. The design and implementation of a generic sparse bundle adjustment software package based on the levenberg-marquardt algorithm.

Lowe, D. G., 2004. Distinctive image features from scale-invariant keypoints. International journal of computer vision 60 (2), 91–110.

Loye, A., Jaboyedoff, M., Pedrazzini, A., 2009. Identification of potential rockfall source areas at a regional scale using a DEM-based geomorphometric analysis. Natural Hazards & Earth System Science 9 (5), 1643–1653.

Luckman, B. H., 1977. The Geomorphic Activity of Snow Avalanches. Geografiska Annaler. Series A, Physical Geography 59 (1-2), 31–48.

Luckman, B. H., 1978. Geomorphic Work of Snow Avalanches in the Canadian Rocky Mountains. Arctic, Antarctic, and Alpine Research 10 (2), 261–276.

Luckman, B. H., 1988. Debris accumulation patterns on talus slopes in Surprise Valley, Alberta. Géographie physique et Quaternaire 42 (3), 247–278.

Luckman, B. H., Matthews, J. A., Smith, D. J., McCarroll, D., McCarthy, D. P., 1994. Snow-Avalanche Impact Landforms: A Brief Discussion of Terminology. Arctic, Antarctic, and Alpine Research 26 (2), 128–129.

Maizels, J. K., 1979. Proglacial aggradation and changes in braided channel patterns during a period of glacier advance: an Alpine example. Geografiska Annaler. Series A. Physical Geography, 87–101.

Malamud, B. D., Turcotte, D. L., Guzzetti, F., Reichenbach, P., 2004. Landslide Inventories and Their Statistical Properties. Earth Surface Processes and Landforms 29, 687–711.

Massimo, M., 1997. Eisdicke des Gepatschferners: Messungen mit dem Radioecholot. Ph.D. thesis, Universität Innsbruck, Innsbruck.

Matsuoka, N., Murton, J. B., 2008. Frost weathering: recent advances and future directions. Permafrost and Periglacial Processes 19 (2), 195–210.

Matsuoka, N., Sakai, H., 1999. Rockfall activity from an alpine cliff during thawing periods. Geomorphology 28 (3–4), 309–328.

Matthes, F., 1938. Avalanche sculpture in the Sierra Nevada of California. Association of Scientific Hydrology Bulletin 23, 631–637.

Matthews, J. A., Shakesby, R. A., 2004. A twentieth-century neoparaglacial rock topple on a glacier foreland, Ötztal Alps, Austria. The Holocene 14 (3), 454–458.

McCann, T. (Ed.), 2008. The geology of Central Europe. Mesozoic and Cenozoic. Geological Society Pub House, Bath.

McClung, D. M., 1975. Creep and the Snow-Earth Interface Condition in the Seasonal Alpine Snowpack. IAHS Publication 114, 236–248.

McClung, D. M., Schärer, P., 1993. The Avalanche handbook. Mountaineers, Seattle.

McColl, S. T., 2012. Paraglacial rock-slope stability. Geomorphology 153–154 (0), 1–16.

McColl, S. T., Davies, T. R. H., McSaveney, M. J., 2010. Glacier retreat and rock-slope stability: debunking debuttressing. In: 11th Congress of the International Association for Engineering Geology and the Environment. pp. 467–474.

Meißl, G., 1998. Modellierung der Reichweite von Felsstürzen: Fallbeispiele zur GIS-gestützten Gefahrenbeurteilung aus dem Bayerischen und Tiroler Alpenraum ; mit 24 Tab. Vol. 28 of Innsbrucker geographische Studien. Inst. für Geographie der Univ. Innsbruck, Innsbruck.

Menéndez Duarte, R., Marquínez, J., 2002. The influence of environmental and lithologic factors on rockfall at a regional scale: an evaluation using GIS. Geomorphology 43 (1–2), 117–136.

Meng, X.-L., Rubin, D. B., 1993. Maximum likelihood estimation via the ECM algorithm: A general framework. Biometrika 80 (2), 267–278.

Mercier, D., 2008a. Paraglacial and paraperiglacial landsystems: concepts, temporal scales and spatial distribution. Géomorphologie: relief, processus, environnement 4.

Mercier, D., 2008b. Paraglacial geomorphology: Conceptual and methodological revival 4, 219–222.

Messenzehl, K., Hoffmann, T., Dikau, R., 2014. Sediment connectivity in the high-alpine valley of Val Müschauns, Swiss National Park — linking geomorphic field mapping with geomorphometric modelling. Geomorphology 221, 215–229.

Messerschmidt, A., 15.06.2016. LiDARgestützte Messung und Modellierung des fluvial Hangabtrages auf proglazialen Moränen im Oberen Kaunertal, Tirol. Ph.D. thesis, Catholic University of Eichstätt-Ingolstadt, Eichstätt.

Michoud, C., Derron, M.-H., Horton, P., Jaboyedoff, M., Baillifard, F.-J., Loye, A., Nicolet, P., Pedrazzini, A., Queyrel, A., 2012. Rockfall hazard and risk assessments along roads at a regional scale: example in Swiss Alps. Natural Hazards & Earth System Science 12 (3), 615–629.

Mikos, M., Vidmar, A., Brilly, M., 2005. Using a laser measurement system for monitoring morphological changes on the Strug rock fall, Slovenia. Natural Hazards & Earth System Science 5, 143–153.

Milan, D. J., Heritage, G. L., Hetherington, D., 2007. Application of a 3D laser scanner in the assessment of erosion and deposition volumes and channel change in a proglacial river. Earth Surface Processes and Landforms 32 (11), 1657–1674.

Mitas, L., Mitasova, H., 2005. Spatial Interpolation. In: Longley, P. (Ed.), Geographical information systems. John Wiley & Sons, Hoboken, NJ, pp. 481–492.

Mittelsten Scheid, Timm M., 2011. Untersuchung der naturräumlichen Rahmenbedingungen der Entstehung von Talmuren: Grundlage einer Modellierung zur Gefahrenabschätzung. Ph.D. thesis, Ludwig-Maximilians-Universität, Munich.

Monteiro, L. S., Moore, T., Hill, C., 2005. What is the accuracy of DGPS? Journal of Navigation 58 (02), 207–225.

Montgomery, D. R., Dietrich, W. E., 1989. Source areas, drainage density, and channel initiation. Water Resources Research 25 (8), 1907–1918.

Montgomery, D. R., Foufoula-Georgiou, E., 1993. Channel Network Source representation Using Digital Elevation Models. Water Resources Research 29 (12), 3925–3934.

Moore, J. R., Egloff, J., Nagelisen, J., Hunziker, M., Aerne, U., Christen, M., 2013. Sediment Transport and Bedrock Erosion by Wet Snow Avalanches in the Guggigraben, Matter Valley, Switzerland. Arctic, Antarctic, and Alpine Research 45 (3), 350–362.

Moore, J. R., Sanders, J. W., Dietrich, W. E., Glaser, S. D., 2009. Influence of rock mass strength on the erosion rate of alpine cliffs. Earth Surface Processes and Landforms 34 (10), 1339–1352.

Mora, P., Baldi, P., Casula, G., Fabris, M., Ghirotti, M., Mazzini, E., Pesci, A., 2003. Global Positioning Systems and digital photogrammetry for the monitoring of mass movements: application to the Ca' di Malta landslide (northern Apennines, Italy). Engineering Geology 68, 103–121.

Morawetz, S., 1954. Die Vergletscherung des inneren Kauner-, Pitz- und Rofentales. Zeitschrift für Gletscherkunde und Glazialgeologie 3 (1), 68–74.

Morche, D., Baewert, H., Bryk, A., 2014. Bed load transport in a proglacial river (Fagge, Gepatschferner, Tyrol). In: European Geosciences Union (Ed.), Geophysical Research Abstracts. Geophysical Research Abstracts. Copernicus GmbH (Copernicus Publications), Göttingen.

Morche, D., Haas, F., Baewert, H., Heckmann, T., Schmidt, K.-H., Becht, M., 2012. Sediment transport in the proglacial Fagge River (Kaunertal/Austria). In: International Association of Hydrological Sciences (Ed.), Erosion and Sediment Yields in the Changing Environment. Vol. 356 of IAHS publication. IAHS Press, Wallingford, pp. 72–80.

Moretto, J., Delai, F., Picco, L., Lenzi, M. A., 2013. Integration of colour bathymetry, LiDAR and dGPS surveys for assessing fluvial changes after flood events in the Tagliamento River (Italy). Special issue on water management in agriculture 4 (8A), 21–29.

Morrison, T., Spencer, P., 2014. Quantile Regression - A Statisticians Approach to the Local Ice Pressure-Area Relationship. In: Arctic Technology Conference.

Müller, B. U., 1999. Paraglacial sedimentation and denudation processes in an Alpine valley of Switzerland. An approach to the quantification of sediment budgets. Geodynamica Acta 12 (5), 291–301.

Müller, J., Gärtner-Roer, I., Kenner, R., Thee, P., Morche, D., 2014. Sediment storage and transfer on a periglacial mountain slope (Corvatsch, Switzerland). Geomorphology 218, 35–44.

Nagelisen, J., Moore, J. R., Vockenhuber, C., Ivy-Ochs, S., 2015. Post-glacial rock avalanches in the Obersee Valley, Glarner Alps, Switzerland. Geomorphology 238, 94–111.

Näher, M., 2013. Analyse des Sedimenttransports durch Grundlawinen im Kaunertal zur Quantifizierung des Sedimentbudgets mittels Verfahren aus der terrestrischen Photogrammetrie.

Neugirg, F., Dusik, J.-M., Haas, F., 2016a. 4.4. Case study: Slope wash, gully erosion and debris flows. In: Heckmann, T., Morche, D. (Eds.), Springerband.

Neugirg, F., Kaiser, A., Huber, A., Heckmann, T., Schindewolf, M., Schmidt, J., Becht, M., Haas, F., 2016b. Using terrestrial LiDAR data to analyse morphodynamics on steep unvegetated slopes driven by different geomorphic processes. Catena 142, 269–280.

Neugirg, F., Kaiser, A., Schindewolf, M., Becht, M., Schmidt, J., Haas, F., 2015. Monitoring and modeling slope dynamics in an Alpine watershed – a combined approach of soil science, remote sensing and geomorphology. Proc. IAHS 371, 181–187.

Neugirg, F., Stark, M., Kaiser, A., Vlacilova, M., Della Seta, M., Vergari, F., Schmidt, J., Becht, M., Haas, F., 2016c. Erosion processes in calanchi in the Upper Orcia Valley, Southern Tuscany, Italy based on multitemporal high-resolution terrestrial LiDAR and UAV surveys. Geomorphology (269), 8–22.

Neugirg, P., 2013. Beurteilung der Dynamik und Quantifizierung des Sedimenthaushalts von ausgewählten Blockgletschern im Gletschervorfeld des Gepatschferners (hinteres Kaunertal) auf Grundlage von multitemporalen LiDAR-Daten und Luftbildern: Bsc thesis.

Newman, M. C., 1993. Regression analysis of log–transformed data: Statistical bias and its correction. Environmental Toxicology and Chemistry 12 (6), 1129–1133.

Nicolussi, K., Kaufmann, M., Patzelt, G., van der, J., Thurner, A., 2005. Holocene tree-line variability in the Kauner Valley, Central Eastern Alps, indicated by dendrochronological analysis of living trees and subfossil logs. Vegetation History and Archaeobotany 14 (3), 221–234.

Nicolussi, K., Patzelt, G., 2000. Untersuchungen zur holozänen Gletscherentwicklung von Pasterze und Gepatschferner (Ostalpen). Zeitschrift für Gletscherkunde und Glazialgeologie 36, 1–87.

Nistér, D., 2004. An efficient solution to the five-point relative pose problem. Pattern Analysis and Machine Intelligence, IEEE Transactions on 26 (6), 756–770.

NIST/SEMATECH, 2012. e-Handbook of Statistical Methods.

Norton, K. P., Blanckenburg, F. v., DiBiase, R., Schlunegger, F., Kubik, P. W., 2011. Cosmogenic 10Be-derived denudation rates of the Eastern and Southern European Alps. International Journal of Earth Sciences 100 (5), 1163–1179.

Nyenhuis, M., 2006. Permafrost und Sedimenthaushalt in einem alpinen Geosystem. Ph.D. thesis, Rheinische Friedrich-Willhelms-Universität, Bonn.

O'Callaghan, J. F., Mark, D., 1984. The extraction of drainage networks from digital elevation data. Computer Vision, Graphics and Image Processing 28, 323–344.

O'Farrell, C. R., Heimsath, A. M., Lawson, D. E., Jorgensen, L. M., Evenson, E. B., Larson, G., Denner, J. D., 2009. Quantifying periglacial erosion: insights on a glacial sediment budget, Matanuska Glacier, Alaska. Earth Surface Processes and Landforms 34 (15), 2008–2022.

Oliensis, J., 1999. A multi-frame structure-from-motion algorithm under perspective projection. International journal of computer vision 34 (2-3), 163–192.

O'Neal, M. A., Pizzuto, J. E., 2011. The rates and spatial patterns of annual riverbank erosion revealed through terrestrial laser–scanner surveys of the South River, Virginia. Earth Surface Processes and Landforms 36 (5), 695–701.

Orwin, J. F., Lamoureux, S. F., Warburton, J., Beylich, A., 2010. A framework for characterizing fluvial sediment fluxes from source to sink in cold environments. Geografiska Annaler: Series A, Physical Geography 92 (2), 155–176.

Østrem, G., 1975. Sediment transport in glacial meltwater streams. In: Jopling, A. V., MacDonald, B. C. (Eds.), Glaciofluvial and glaciolacustrine sedimentation. Vol. 23 of Society of Economic Paleontologists and Mineralogists: Special publication. Soc. of Economic Paleontologists and Mineralogists, Tulsa and Okla, pp. 101–123.

Otto, J.-C., 2006. Paraglacial sediment storage quantification in the Turtmann Valley, Swiss Alps. Ph.D. thesis, Rheinische Friedrich-Willhelms-Universität, Bonn.

Otto, J.-C., Schrott, L., 2010. Quantifizierung von rezenten und postglazialen Sedimentspeichern und Sedimentflüssen - Konzeptionelle Ansätze und aktuelle Studien. In: Otto, J.-C., Schrott, L. (Eds.), Wuantifizierung von rezenten und postglazialen Sedimentflüssen in den Ostalpen. Vol. 46 of Salzburger Geographische Arbeiten. Salzburg, pp. 1–13.

Otto, J.-C., Schrott, L., Jaboyedoff, M., Dikau, R., 2009. Quantifying sediment storage in a high alpine valley (Turtmanntal, Switzerland). Earth Surface Processes and Landforms 34 (13), 1726–1742.

Owen, G., Matthews, J. A., Shakesby, R. A., He, X., 2006. Snow–avalanche impact landforms, deposits and effects at Urdvatnet, southern Norway: implications for avalanche style and process. Geografiska Annaler: Series A, Physical Geography 88 (4), 295–307.

Owens, P. N., Slaymaker, O., 1992. Late Holocene sediment yields in small alpine and sub-alpine drainage basins. In: Walling, D. E., Davies, J. R., Hasholt, B. (Eds.), Erosion, Debris flows and Environment in Mountain Regions. Vol. 209. International Association of Hydrological Sciences, pp. 147–154.

Parks, B., Madison, R. J., 1985. Estimation of selected flow and water-quality characteristics of Alaskan streams.

Peckham, R. J., Jordan, G. (Eds.), 2007. Digital Terrain Modelling. Lecture Notes in Geoinformation and Cartography. Springer.

Peev, C., 1966. Geomorphic Activity of Snow Avalanches. IAHS Publication 69, 357–368.

Petrie, G., Toth, C. K., 2008. Introduction to laser ranging, profiling, and scanning. In: Shan, J., Toth, C. K. (Eds.), Topographic Laser Ranging and Scanning: Principles and Processing. CRC Press, pp. 1–28.

Pfaller, V., 2011. Vegetationsgeographische Untersuchungen auf erosionsgefährdeten Ufermoränen im Vorfeld des Gepatschferners (Tirol). Ph.D. thesis, Catholic University of Eichstätt-Ingolstadt, Eichstätt.

Pfiffner, O. A., 2010. Geologie der Alpen, 2nd Edition. Vol. 8416 : Geologie of UTB. Haupt, Bern [u.a.].

Phillips, J. D., 1986. Sediment Storage, Sediment Yield, and Time Scales in Landscape Denudation Studies. Geographical Analysis 18 (2), 161–167.

Pillewizer, W., 1957. Untersuchungen an Blockströmen der Ötztaler Alpen. Geomorphologische Abhandlungen des Geograpischen Instituts der Freien Universität Berlin 5, 37–50.

Pollefeys, M., Koch, R., van Gool, L., 2002. Self-calibration and metric reconstruction in spite of varying and unknown internal camera parameters 32 (1), 7–25.

Poser, H., 1954. Die Periglazial-Erscheinungen in der Umgebung der Gletscher des Zemmgrunds (Zillertaler Alpen). In: Ebers, E. (Ed.), Studien aus dem Alpenvorland und den Alpen. Vol. Göttinger geographische Abhandlungen of Studien über die Periglazialerscheinungen in Mitteleuropa. Geographisches Inst. der Univ, Göttingen.

Prima, Oky, Dicky, Ardiansyah, Echigo, A., Yokoyama, R., Yoshida, T., 2006. Supervised landform classification of Northeast Honshu from DEM-derived thematic maps. Geomorphology 78 (3–4), 373–386.

Prokop, A., Panholzer, H., 2009. Assessing the capability of terrestrial laser scanning for monitoring slow moving landslides. Natural Hazards & Earth System Science 9 (6), 1921–1928.

Purtscheller, F., 1978. Ötztaler und Stubaier Alpen. Vol. 53 of Sammlung Geologischer Führer. Bornträger, Berlin.

R Development Core Team, 2012. R: A Language and Environment for Statistical Computing.
URL `http://www.R-project.org/`

Rabatel, A., Ravanel, L., Deline, P., Jaillet, S., 2007. The use of laserscanning and terrestrial photogrammetry to quantify rock falls/avalanches in steep high-alpine rock walls. In: European Geosciences Union (Ed.), Geophysical Research Abstracts. Vol. 9 of Geophysical Research Abstracts. Copernicus GmbH (Copernicus Publications), Göttingen.

Rapp, A., 1957. Studien über Schutthalden in Lappland und auf Spitzbergen. Zeitschrift für Geomorphologie N.F. 1, 179–200.

Rapp, A., 1959. Avalanche Boulder Tongues in Lappland. A Description of Little-Known Landforms of Periglacial Debris Accumulation. Geografiska Annaler. Series A, Physical Geography 41, 34–48.

Rapp, A., 1960. Recent Development of Mountain Slopes in Karkevagge and Surroundings, Northern Scandinavia. Geografiska Annaler. Series A, Physical Geography 42 (2/3), 65–200.

Rapp, A., Rudberg, S., 1964. Studies on periglacial phenomena in Scandinavia: 1960 - 1963. Vol. 78 of Meddelande från Göteborgs Universitets Geografiska Institution. Göteborg.

Rascher, E., Sass, O., 2016. Constructing a Sediment Budget for the Johnsbach, Styria – Adding up numbers and drawing arrows? In: European Geosciences Union (Ed.), Geophysical Research Abstracts. Vol. 18. Copernicus GmbH (Copernicus Publications), Göttingen.

Rey, F., 2003. Influence of vegetation distribution on sediment yield in forested marly gullies. Catena 50 (2), 549–562.

Rieg, L., Wichmann, V., Rutzinger, M., Sailer, R., Geist, T., Stötter, J., 2013. Data infrastructure for multitemporal airborne LiDAR point cloud analysis – Examples from physical geography in high mountain environments. Computers, Environment and Urban Systems 45, 137–146.

Riegl, J., Studnicka, N., Ullrich, A., 2003. Merging and processing of laser scan data and high-resolution digital images acquired with a hybrid 3D laser sensor. In: Proceedings of the XIX CIPA Symposium.

Riegl Laser Measurement GmbH, 2010. Datasheet: LMS-Z420i.

Riegl Laser Measurement GmbH, 2011. RiSCAN PRO: Viewer, Acquisition & Processing Software. Technical Documentation & User Instructions. Version 1.7.7.

Riegl Laser Measurement GmbH, 2014. VZ-4000.

Riehl, F., 2015. Quantifizierung und Modellierung des fluvialen Sedimentaustrags aus kleinen Hanggerinnen in zentralalpinen Einzugsgebieten des Kaunertals und Horlachtals, Tirol: Master thesis.

Roer, I., Haeberli, W., Avian, M., Kaufmann, V., Delaloye, R., Lambiel, C., Kääb, A., 2008. Observations and considerations on destabilizing active rock glaciers in the european Alps. In: Proceedings of the Ninth International Conference on Permafrost. Fairbanks, pp. 1505–1510.

Rosser, N. J., Petley, D. N., Lim, M., Dunning, S. A., Allison, R. J., 2005. Terrestrial laser scanning for monitoring the process of hard rock coastal cliff erosion. Quarterly Journal of Engineering Geology and Hydrogeology 38 (4), 363–375.

Ruiz, A., Kornus, W., Talaya, J., Colomer, J. I., 2004. Terrain modeling in an extremely steep mountain: A combination of airborne and terrestrial lidar. In: International Archives of the Photogrammetry, R. S., Sciences, S. I. (Eds.), Proceedings of 20th International Society for Photogrammetry and Remote Sensing (ISPRS) Congress on Geo-imagery Bridging Continents.

Rumohr, P., 2015. Quantifizierung des Sedimenttransports durch Grundlawinen im oberen Kaunertal mittels gravimetrischer und terrestrisch-photogrammetrischer Verfahren: Master thesis.

Rusinkiwicz, S., Levoy, M., 2001. Efficient variants of the ICP algorihtm. In: Proceedings of the Third International Conference on 3-D Digital Imaging and Modeling. IEEE, pp. 145–152.

Ryan, J. A., Ulrich, J. M., 2008. xts: Extensible Time Series.

Sæmundsson, o., Decaulne, A., Jónsson, H. P., 2008. Sediment transport associated with snow avalanche activity and its implication for natural hazard management in Iceland. In: International Sympoium on Mitigative Measures against Snow Avalanches. pp. 137–142.

Sanders, J. W., Cuffey, K. M., MacGregor, K. R., Collins, B. D., 2013. The sediment budget of an alpine cirque. Geological Society of America Bulletin 125 (1), 229–248.

Sass, O., 1998. Die Steuerung von Steinschlagmenge und -verteilung durch Mikroklima, Gesteinsfeuchte und Gesteinseigenschaften im westlichen Karwendelgebirge (Bayerische Alpen). Vol. B 29 of Münchener Geographische Abhandlungen. Geobuch, München.

Sass, O., 2005a. Rock moisture measurements: techniques, results, and implications for weathering. Earth Surface Processes and Landforms 30.

Sass, O., 2005b. Temporal variability of rockfall in the Bavarian alps, Germany. Arctic, Antarctic, and Alpine Research 37 (4), 564–573.

Sass, O., Haas, F., Schimmer, C., Heel, M., Bremer, M., Stöger, F., Wetzel, K.-F., 2012. Impact of forest fires on geomorphic processes in the tyrolean limestone alps.

Sass, O., Heel, M., Hoinkis, R., Wetzel, K.-F., 2010. A six-year record of debris transport by avalanches on a wildfire slope (Arnspitze, Tyrol). Zeitschrift für Geomorphologie N.F. 54 (2), 181–193.

Sass, O., Wollny, K., 2001. Investigations regarding Alpine talus slopes using ground-penetrating radar (GPR) in the Bavarian Alps, Germany. Earth Surface Processes and Landforms 26 (10), 1071–1086.

Sattler, K., Keiler, M., Zischg, A., Schrott, L., 2011. On the Connection between Debris Flow Activity and Permafrost Degradation: A Case Study from the Schnalstal, South Tyrolean Alps, Italy. Permafrost and Periglacial Processes 22, 254–265.

Savigear, R. A. G., 1965. A TECHNIQUE OF MORPHOLOGICAL MAPPING 1. Annals of the Association of American Geographers 55 (3), 514–538.

Scambos, T. A., Dutkiewicz, M. J., Wilson, J. C., Bindschadler, R. A., 1992. Application of image cross-correlation to the measurement of glacier velocity using satellite image data. Remote Sensing of Environment 42 (3), 177–186.

Schiefer, E., Gilbert, R., 2007. Reconstructing morphometric change in a proglacial landscape using historical aerial photography and automated DEM generation. Geomorphology 88 (1-2), 167–178.

Schlobies, K., 2016. Detektion von Oberflächenveränderungen im Bereich potenzieller Toteismilieus aus airborne LiDAR-Daten unter Anwendung der logistischen Regression in einem zentralalpinen Einzusgebiet: Master thesis.

Schlunegger, F., Hinderer, M., 2003. Pleistocene/Holocene climate change, reestablishment of fluvial drainage network and increase in relief in the Swiss Alps. Terra Nova 15, 88–95.

Schreiber, K. F. (Ed.), 1988. Connectivity in Landscape Ecology. Proceeding of the 2nd International Seminar of the " International Association for Landscape Ecology". Vol. 29 of Münstersche Geographische Arbeiten. Schöningh, Paderborn.

Schrott, L., Götz, J., Geilhausen, M., Morche, D., 2006. Spatial and temporal variability of sediment transfer and storage in an Alpine basin (Reintal valley, Bavarian Alps, Germany). Geographica Helvetica 61 (3), 191–200.

Schrott, L., Hufschmidt, G., Hankammer, M., Hoffmann, T., Dikau, R., 2003. Spatial Distribution of Sediment Storage Types and Quantification of Valley Fill Deposits in an Alpine Basin, Reintal, Bavarian Alps, Germany. Geomorphology 55, 45–63.

Schrott, L., Otto, J.-C., Keller, F., 2012. Modelling alpine Permafrost distribution in the Hohe Tauern Region, Austria. Austrian Journal of Earth Sciences 105 (2), 169–183.

Schulz, E., Dornblut, S., 2002. Herstellung von Geländemodellen und Orthophotos im Wettersteingebirge. Ph.D. thesis, Technische Fachhochschule, Berlin.

Schumaker, N. H., 1996. Using landscape idiocies to predict habitat connectivity. Ecology 77, 1210–1225.

Seijmonsbergen, A. C., Hengl, T., Anders, N. S., 2011. Chapter Ten - Semi-Automated Identification and Extraction of Geomorphological Features Using Digital Elevation Data. In: Smith, M. J., Paron, P., Griffiths, J. S. (Eds.), Developments in Earth Surface Processes : Geomorphological Mapping Methods and Applications. Vol. 15. Elsevier, pp. 297–335.

Selby, M. F., 1980. A rock mass strength classification for geomorphic purposes: with tests from Antarctica and New Zealand. Zeitschrift für Geomorphologie N.F. 24 (1), 31–51.

Shan, J., Toth, C. K. (Eds.), 2008. Topographic Laser Ranging and Scanning: Principles and Processing. CRC Press.

Sharp, G. C., Lee, S. W., Wehe, D. K., 2002. ICP registration using invariant features. Pattern Analysis and Machine Intelligence, IEEE Transactions on 24 (1), 90–102.

Shroder, J. F., Scheppy, R. A., Bishop, M. P., 1999. Denudation of Small Alpine Basins, Nanga Parbat Himalaya, Pakistan. Arctic, Antarctic, and Alpine Research 31 (2), 121–127.

Siewert, M. B., Krautblatter, M., Christiansen, H. H., Eckerstorfer, M., 2012. Arctic rockwall retreat rates estimated using laboratory-calibrated ERT measurements of talus cones in Longyeardalen, Svalbard. Earth Surface Processes and Landforms 37 (14), 1542–1555.

Simonett, D. S., 1967. Landslide distribution and earthquakes in the Bewani and Torricelli Mountains, New Guinea. In: Jennings, J. N., Mabbutt, J. A. (Eds.), Landform studies from Australia and New Guinea. Univ. Press, Cambridge, pp. 64–84.

Slaymaker, O., 1991. Mountain Geomorphology: A Theoretical Framework for Measurement Programmes. Catena 18, 427–437.

Slaymaker, O., 2008. Sediment budget and sediment flux studies under accelerating global change in cold environments. Zeitschrift für Geomorphologie, Supplementary Issues 52 (1), 123–148.

Slaymaker, O., 2009. Proglacial, periglacial or paraglacial? In: Knight, J., Harrison, S. (Eds.), Periglacial and Paraglacial Processes and Environments. Vol. 320 of Special Publications. The Geological Society Publishing House, London, pp. 71–84.

Slaymaker, O., 2011. Criteria to distinguish between periglacial, proglacial and paraglacial environments. Quaestiones Geographicae 30 (1), 85–94.

Slaymaker, O., Embleton-Hamann, C., 2009. Mountains. In: Slaymaker, O. (Ed.), Geomorphology and global environmental change. Cambridge Univ. Press, Cambridge [u.a.], pp. 27–70.

Smith, M. J., Paron, P., Griffiths, J. S. (Eds.), 2011. Developments in Earth Surface Processes : Geomorphological Mapping Methods and Applications. Elsevier.

Södermann, G., 1980. Slope processes in cold environments of northern Finland. Fennia-International Journal of Geography 158 (2), 83–152.

Sommer, N., 1980. Untersuchungen über die Geschiebe- und Schwebstofführung und den Transport von gelösten Stoffen in Gebirgsbächen. In: Internationale Forschungsgesellschaft Interpraevent (Ed.), Proceedings of the International Symposium Interpraevent. Vol. 2. pp. 69–94.

Sonklar, K. v., 1860. Die Oetzthaler Gebirgsgruppe, mit besonderer Rücksicht auf Orographie und Gletscherkunde. Perthes, Gotha.

Souchez, R., 1971. Rate of frost shattering and slope development in dolomitic limestone, southwestern Ellesmere Island (Arctic Canada). Quaternaria 14.

Spencer, P., Morrison, T., 2014. Quantile Regression as a Tool for Investigating Local and Global Ice Pressures. In: Arctic Technology Conference.

Spotila, J. A., Buscher, J. T., Meigs, A. J., Reiners, P. W., 2004. Long-term glacial erosion of active mountain belts: example of the Chugach–St. Elias Range, Alaska. Geology 32 (6), 501–504.

Stäblein, G., 1979. Geomorphologische Deteilkartierung in der Bundesrepublik Deutschland. In: Ehlers, E., Meynen, E. (Eds.), Geographisches Taschenbuch und Jahrweiser für Landeskunde. Geographisches Taschenbuch und Jahrweiser für Landeskunde. Franz Steiner Verlag, Wiesbaden.

Stäblein, G., 1990. Inventarisierung des Reliefs als eine Voraussetzung zur großräumigen geoökologischen Planung. Geogr. Rundschau 42, 613–617.

Stahr, A. R., Hartmann, T., 1999. Landschaftsformen und Landschaftselemente im Hochgebirge. Springer, Berlin [u.a.].

Staines, K. E. H., Carrivick, J. L., Tweed, F. S., Evans, A. J., Russell, A. J., Jóhannesson, T., Roberts, M., 2015. A multi-dimensional analysis of proglacial landscape change at Sólheimajökull, southern Iceland. Earth Surface Processes and Landforms 40 (6), 809–822.

Stark, C. P., Guzzetti, F., 2009. Landslide rupture and the probability distribution of mobilized debris volumes. Journal of Geophysical Research: Earth Surface 114 (F2), F00A02.

Stark, C. P., Hovius, N., 2001. The characterization of landslide size distributions. Geophysical Research Letters 28 (6), 1091–1094.

Stiny, J., 1910. Die Muren: Versuch einer Monographie mit besonderer Berücksichtigung der Verhältnisse in den Tiroler Alpen. Verlag der Wagnerschen Universitätsbuchhandlung, Innsbruck.

Stocker-Waldhuber, M., Kuhn, M., 2016. An approach to close the balances of fluxes of ice, water and sediments through the tongue of Gepatschferner. In: Heckmann, T., Morche, D. (Eds.), Springerband.

Strahler, A. N., 1952. Dynamic basis of geomorphology. Geological Society of America Bulletin 63 (9), 923–938.

Strunden, J., Ehlers, T. A., Brehm, D., Nettesheim, M., 2015. Spatial and temporal variations in rockfall determined from TLS measurements in a deglaciated valley, Switzerland. Journal of Geophysical Research: Earth Surface 120 (7), 1251–1273.

Swanson, F. J., Janda, R. J., Dunne, T., Swanston, D. N. (Eds.), 1982. Sediment Budgets and Routing in Forested Drainage Basins: Gen. Tech. Rep. PNW-141. Pacific Northwest Forest and Range Experiment Station, Forest Service, U.S. Department of Agriculture, Portland.

Takahashi, T., 1981. Estimation of potential debris flows and their hazardous zones: Soft countermeasures for a disaster. Journal of Natural disaster science 3 (1), 57–89.

Taylor, J. R., 1997. An introduction to error analysis: The study of uncertainties in physical measurements. Univ. Science Books, Sausalito and Calif.

Temme, A., Heckmann, T., Harlaar, P., 2016. Silent play in a loud theatre – dominantly time-dependent soil development in the geomorphically active proglacial area of the Gepatschferner glacier, Austria. Catena.

Thiel, M., 2013. Quantifizierung der Konnektivität von Sedimentkaskaden in alpinen Geosystemen. Ph.D. thesis, Catholic University of Eichstätt-Ingolstadt, Eichstätt.

Thomas, A., 1994. Abfluss, Temperatur und Niederschlag am Gepatschferner (Ötztaler Alpen) von 1988-1993. Zeitschrift für Gletscherkunde und Glazialgeologie 30, 119–124.

Thöny, W. F., Tropper, P., Schennach, F., Krenn, E., Finger, F., Kaindl, R., Bernhard, F., Hoinkes, G., 2008. The metamorphic evolution of migmatites from the Ötztal Complex (Tyrol, Austria) and constraints on the timing of the pre-Variscan high-T event in the Eastern Alps. Swiss Journal of Geosciences 101 (1), 111–126.

Tognacca, C., 1999. Beitrag zur Untersuchung der Entstehungsmechanismen von Murgängen. Ph.D. thesis, Eidg. Amt für Strassen- und Flussbau, Zürich.

Tollmann, A., 1977. Geologie von Österreich. Die Zentralalpen. Vol. 1. Franz Deuticke, Vienna.

Toppe, R., 1987. Terrain models-A tool for natural hazard mapping. In: Salm, B. W., Gubler, H. (Eds.), Avalanche Formation, Movement and Effects. IAHS Publications. IAHS Press, pp. 629–638.

Tschada, H., 1975. Beobachtungen über die Geschiebefracht von Hochgebirgsbächen. In: Aulitzky, H. (Ed.), Hochwasser- und Lawinenschutz in Tirol. Innsbruck, pp. 109–.

Tschada, H., Hofer, B., 1990. Total solids load from the catchment area of the Kaunertal hydroelectric power station: the results of 25 years of operation. In: Hydrology in Mountainous Regions. II - Artificial Reservoirs; Water and Slopes. Vol. 194. IAHS Press, pp. 121–128.

Umstädter, K., 2015. Bodenerosion nach Brandereignissen auf La Palma. Ph.D. thesis, Catholic University of Eichstätt-Ingolstadt, Eichstätt.

van Den Eeckhaut, M., Poesen, J., Govers, G., Verstraeten, G., Demoulin, A., 2007. Characteristics of the size distribution of recent and historical landslides in a populated hilly region. Earth and Planetary Science Letters 256 (3–4), 588–603.

van Dijke, J. J., van Westen, C. J., 1990. Rockfall hazard: A geomorphological application of neighborhood analysis with ILWIS. ITC Journal 1, 40–44.

van Steijn, H., 1996. Debris-flow magnitude - frequency relationships for mountainous regions of Central and Northwest Europe: Landslides in the European Union. Geomorphology 15 (3–4), 259–273.

Vavtar, F., 1981. Syngenetische metamorphe Kiesanreicherungen in Paragneisen des Ötztal-Kristallins (Kaunertal, Tirol). Veröffentlichungen des Tiroler Landesmuseums Ferdinandeum 61, 151–169.

Vehling, L., 2016. Gravitative Massenbewegungen an alpinen Felshängen: Quantitative Bedeutung in der Sedimentkaskade proglazialer Geosysteme (Kaunertal, Tirol). Ph.D. thesis, Friedrich-Alexander-Universität Erlangen-Nürnberg, Erlangen.

Vehling, L., Hilger, L., Dusik, J.-M., Neugirg, F., Haas, F., Heckmann, T., Rohn, J., Moser, M., Becht, M., 2013a. Integrating geomorphological and geotechnical mapping for sediment budgeting in the upper Kaunertal valley, Austrian Alps. Geophysical Research Abstracts 15.

Vehling, L., Rohn, J., Moser, M., 2013b. Gravitative Massenbewegungen in einem proglazialen Geosystem, Gepatschferner, Tirol – Quantitative Erfassung der relevanten Geofaktoren und Bilanzierungsansätze. In: Kurosch, T. (Ed.), Berichte von der 19. Tagung für Ingenieurgeologie: München 13. bis 16. März 2013. München, pp. 470–475.

Vehling, L., Rohn, J., Moser, M., 2015. Quantification of small rock fall processes in a proglacial high mountain area, Gepatsch glacier, Austria. Zeitschrift für Geomorphologie, N.F. Suppl.

Veit, H., 2002. Die Alpen - Geoökologie und Landschaftsentwicklung. Ulmer, Stuttgart.

Venables, W. N., Ripley, B. D., 2002. Modern applied statistics with S, 4th Edition. Statistics and computing. Springer, New York, NY.

Vorndran, G., 1979. Geomorphologische Massenbilanzen. Vol. 1 of Augsburger Geographische Hefte. Augsburg.

Vosselman, G. (Ed.), 2010. Airborne and terrestrial laser scanning. Whittles Publishing, Dunbeath and Caithness.

Wagner, S., 1992. Creep of alpine permafrost, investigated on the murtel rock glacier. Permafrost and Periglacial Processes 3 (2), 157–162.

Wahrhaftig, C., Cox, A., 1959. Rock glaciers in the Alaska Range. Geological Society of America Bulletin 70 (4), 383.

Walling, D. E., 1983. The sediment delivery problem: Scale Problems in Hydrology. Journal of Hydrology 65 (1–3), 209–237.

Wang, L., Liu, H., 2006. An efficient method for identifying and filling surface depressions in digital elevation models for hydrologic analysis and modelling. International Journal of Geographical Information Science 20 (2), 193–213.

Warburton, J., 1990. An Alpine Proglacial Fluvial Sediment Budget. Geografiska Annaler. Series A, Physical Geography 72 (3/4), 261–272.

Warburton, J., 1992. Observations of Bed Load Transport and Channel Bed Changes in a Proglacial Mountain Stream. Arctic and Alpine Research 24 (3), 195–203.

Wechsler, S. P., 2006. Quantifying DEM Uncertainty and its Effect on Topographic Parameters.

Wechsler, S. P., 2007. Uncertainties associated with digital elevation models for hydrologic applications: a review. Hydrology & Earth System Sciences 11 (4).

Westaway, R. M., Lane, S. N., Hicks, D. M., 2003. Remote survey of large-scale braided, gravel-bed rivers using digital photogrammetry and image analysis: International Journal of Remote Sensing. International Journal of Remote Sensing 24 (4), 795–815.

Whalley, W. B., 1974. The Mechanics of High-magnitude, Low-frequency Rock Failure and Its Importance in a Mountainous Area. University of Reading.

Whalley, W. B., 1984. Rockfalls. In: Brunsden, D., Prior, D. B. (Eds.), Slope instability. John Wiley & Sons, Chichester, pp. 217–256.

Wheaton, J. M., 2008. Uncertainty in Morphological Sediment Budgeting of Rivers. Ph.D. thesis, University of Southhampton, Southhampton (PhD Thesis).

Wheaton, J. M., Brasington, J., Darby, S. E., Sear, D. A., 2010. Accounting for uncertainty in DEMs from repeat topographic surveys: improved sediment budgets. Earth Surface Processes and Landforms, n/a.

Wichmann, V., 2006. Modellierung geomorphologischer Prozesse in einem alpinen Einzugsgebiet: Abgrenzung und Klassifizierung der Wirkungsräume von Sturzprozessen und Muren mit einem GIS. Ph.D. thesis, Catholic University of Eichstätt-Ingolstadt, Eichstätt.

Wichmann, V., Becht, M., 2005. Modeling of geomorphic processes in an alpine catchment. In: Atkinson, P. M., Foody, G. M., Darby, S. E., Wu, F. (Eds.), GeoDynamics. CRC Press, Boca Raton, pp. 151–167.

Wichmann, V., Becht, M., 2006. Rockfall modelling: Methods and model application in an alpine basin (Reintal, Germany). In: Böhner, J., McCloy, K. R., Strobl, J. (Eds.), SAGA - Analysis and Modelling Applications. Vol. 115 of Göttinger Geographische Abhandlungen. Goltze, Göttingen, pp. 105–116.

Wichmann, V., Heckmann, T., Haas, F., Becht, M., 2009. A new modelling approach to delineate the spatial extent of alpine sediment cascades: GIS and SDA applications in geomorphology. Geomorphology 111 (1-2), 70–78.

Wiegand, C., Geitner, C., 2010. Shallow erosion in grassland areas in the Alps. What we know and what we need to investigate further. In: Borsdorf, A., Grabherr, G., Heinrich, K. (Eds.), Challenges for mountain regions - tackling complexity. Böhlau, Wien.

Wiegand, C., Geitner, C., 2013. Investigations into the distribution and diversity of shallow eroded areas in steep grasslands in Tyrol (Austria). Erdkunde 67 (4), 325–343.

Wiggenhauser, S., 2015. Untersuchung zur Stauraumverlandung des Gepatsch-Stausees: Integration von LiDAR- und photogrammetrischen Daten zur Quantifizierung der Sedimentationsraten im Mündungsbereich des Faggenbaches in den Gepatsch-Stausee (Ötztaler Alpen, Österreich): Master thesis.

Wilson, J. P., Gallant, J. C., 2000. Terrain Analysis: Principles and Applications. John Wiley & Sons, New York [etc.].

Wohl, E., 2000. Mountain rivers. Vol. 14 of Water resources monograph. American Geophysical Union, Washington, DC.

Xiao, X., White, E. P., Hooten, M. B., Durham, S. L., 2011. On the use of log–transformation vs. nonlinear regression for analyzing biological power laws. Ecology 92 (10), 1887–1894.

Ying Yang, M., Förstner, W., 2010. Plane Detection in Point Cloud Data.

Yokoyama, R., Shirasawa, M., Pike, R. J., 2002. Visualizing Topography by Openness:A New Application of Image Processing to Digital Elevation Models. Photogrammetric Engineering and Remote Sensing 68 (3), 257–265.

Young, A., 1960. Soil movement by denudational processes on slopes. Nature, London 188, 120–122.

Young, A., 1969. Present Rate of Land Erosion. Nature 224 (5222), 851–852.

Young, D., Benaglia, T., Chauveau, D., Hunter, D., Elmore, R., Hettmansperger, T., Thomas, H., Xuan, F., 2009. mixtools: An R Package for Analyzing Finite Mixture Models. Journal of Statistical Software 32 (6), 1–29.

Young, E. J., 2012. dGPS. In: Clarke, L. E. (Ed.), Geomorphological Techniques (Online Edition). British Society for Geomorphology, London.

Zanon, R., Pergher, L., 2013. Geologische Evaluierung hochalpiner Speicherstandorte in Tirol/Österreich. In: 19. Tagung für Ingenieurgeologie. pp. 401–406.

Zepp, H., 2004. Geomorphologie: Eine Einführung, 3rd Edition. Vol. 2164 : GeographieGrundriß allgemeine Geographie of UTB. Schöningh, Paderborn and München [u.a.].

Zevenbergen, L. W., Thorne, C. R., 1987. Quantitative Analysis of Land Surface Topography. Earth Surface Processes and Landforms 12, 47–56.

Zimmermann, M., Haeberli, W., 1992. Climatic Change and Debris Flow Activity in High-Mountain Areas: A Case Study in the Swiss Alps. In: Boer, M. M., Koster, E. A. (Eds.), Greenhouse impact on cold climate ecosystems and landscapes: selected papers of the European Conference on Landscape Ecological Impact of Climatic Change, Lunteren, The Netherlands, December 3 - 7, 1989. Vol. 22 of Catena - Supplementband. Catena-Verlag, Cremlingen-Destedt, pp. 59–72.